

Planet Masses, Radii, and Orbits from NASA's K2 Mission

ANDREW W. HOWARD,¹ EVAN SINUKOFF,^{1,2} SARAH BLUNT,^{1,3,4,5} ERIK A. PETIGURA,⁶
IAN J. M. CROSSFIELD,⁷ HOWARD ISAACSON,⁸ MOLLY KOSIAREK,⁴ RYAN A. RUBENZAHL,¹
JOHN M. BREWER,⁹ BENJAMIN J. FULTON,^{1,10} COURTNEY D. DRESSING,⁸ LEA A. HIRSCH,¹¹
HEATHER KNUTSON,¹² JOHN H. LIVINGSTON,^{13,14,15} SEAN M. MILLS,¹ ARPITA ROY,^{16,17}
LAUREN M. WEISS,¹⁸ BJORN BENNEKE,¹⁹ DAVID R. CIARDI,¹⁰ JESSIE L. CHRISTIANSEN,¹⁰
WILLIAM D. COCHRAN,²⁰ JUSTIN R. CREPP,¹⁸ ERICA GONZALES,⁴ BRAD M. S. HANSEN,⁶
KEVIN HARDEGREE-ULLMAN,^{10,21,22} STEVE B. HOWELL,²³ SÉBASTIEN LÉPINE,²⁴
ARTURO O. MARTINEZ,^{23,25} LESLIE A. ROGERS,²⁶ JOSHUA E. SCHLIEDER,²⁷ MICHAEL WERNER,²⁸
ALEX S. POLANSKI,^{7,29} ISABEL ANGELO,⁶ COREY BEARD,^{30,31} AIDA BEHMARD,³² LUKE G. BOUMA,¹
CASEY L. BRINKMAN,² ASHLEY CHONTOS,³³ FEI DAI,² PAUL A. DALBA,⁴ STEVEN GIACALONE,¹
SAMUEL K. GRUNBLATT,³⁴ MICHELLE L. HILL,³⁵ STEPHEN R. KANE,³⁵ JACK LUBIN,⁶
ANDREW W. MAYO,³⁶ TEO MOCNIK,³⁷ JOSEPH M. AKANA MURPHY,⁴ MALENA RICE,³⁸
LEE J. ROSENTHAL,² DAKOTAH TYLER,⁶ JUDAH VAN ZANDT,⁶ AND SAMUEL W. YEE⁵

¹*Department of Astronomy, California Institute of Technology, Pasadena, California, USA*

²*Institute for Astronomy, University of Hawaii, 2680 Woodlawn Drive, Honolulu, HI, USA*

³*Center for Interdisciplinary Exploration and Research in Astrophysics (CIERA) and Department of Physics and Astronomy, Northwestern University, Evanston, IL 60208, USA*

⁴*Department of Astronomy & Astrophysics, University of California, Santa Cruz, CA, USA*

⁵*Center for Astrophysics | Harvard & Smithsonian, 60 Garden Street, Cambridge, MA 02138, USA*

⁶*Department of Physics & Astronomy, University of California Los Angeles, Los Angeles, CA, USA*

⁷*Department of Physics and Astronomy, University of Kansas, Lawrence, KS, USA*

⁸*Astronomy Department, University of California, Berkeley, CA, USA*

⁹*Department of Physics and Astronomy, San Francisco State University, 1600 Holloway Ave., San Francisco, CA 94132, USA*

¹⁰*IPAC - NASA Exoplanet Science Institute, California Institute of Technology, 770 S. Wilson Ave, Pasadena, CA, USA*

¹¹*Department of Chemical & Physical Sciences, University of Toronto Mississauga, 3359 Mississauga Road, Mississauga, Ontario L5L 1C6, Canada*

¹²*Geological and Planetary Sciences, California Institute of Technology, Pasadena, CA, USA*

¹³*Astrobiology Center, 2-21-1 Osawa, Mitaka, Tokyo 181-8588, Japan*

¹⁴*National Astronomical Observatory of Japan, 2-21-1 Osawa, Mitaka, Tokyo 181-8588, Japan*

¹⁵*Astronomical Science Program, The Graduate University for Advanced Studies, SOKENDAI, 2-21-1 Osawa, Mitaka, Tokyo 181-8588, Japan*

¹⁶*Space Telescope Science Institute, 3700 San Martin Drive, Baltimore, MD 21218, USA*

¹⁷*Astrophysics & Space Institute, Schmidt Sciences, New York, NY 10011, USA*

¹⁸*Department of Physics and Astronomy, University of Notre Dame, Notre Dame, IN 46556, USA*

¹⁹*Institut de Recherche sur les Exoplanètes, Université de Montréal, Montréal, QC, Canada*

²⁰*McDonald Observatory and Center for Planetary Systems Habitability, The University of Texas, Austin, TX, USA*

²¹*Department of Physics and Astronomy, University of Toledo, Toledo, OH, 43606, USA*

²²*Steward Observatory, The University of Arizona, Tucson, AZ 85721, USA*

²³*NASA Ames Research Center, Moffett Field, CA, USA*

²⁴*Department of Physics & Astronomy, Georgia State University, 25 Park Place NE 605, Atlanta, GA, USA*

²⁵*Bay Area Environmental Research Institute, Moffett Field, CA, USA*

²⁶*Department of Astronomy & Astrophysics, University of Chicago, 5640 S. Ellis Ave, Chicago, IL, USA*

²⁷*NASA Goddard Space Flight Center, 8800 Greenbelt Road, Greenbelt, MD, USA*

²⁸*Jet Propulsion Laboratory, California Institute of Technology, 4800 Oak Grove Drive, Pasadena, CA, USA*

²⁹*Lowell Observatory, 1400 W. Mars Hill Rd. Flagstaff, AZ. 86001. USA*

³⁰*Department of Physics & Astronomy, The University of California, Irvine, Irvine, CA 92697, USA*

³¹*NASA FINESST Fellow*

³²*Department of Astrophysics, American Museum of Natural History, 200 Central Park West, Manhattan, NY, USA*

³³*Department of Astrophysical Sciences, Princeton University, 4 Ivy Lane, Princeton, NJ 08544, USA*

³⁴*Department of Physics and Astronomy, University of Alabama, Box 870324, Tuscaloosa, AL 35487, USA*

³⁵*Department of Earth and Planetary Sciences, University of California, Riverside, CA 92521, USA*

³⁶*Centre for Star and Planet Formation, Natural History Museum of Denmark & Niels Bohr Institute, University of Copenhagen, Oster Voldgade 5-7, DK-1350 Copenhagen K., Denmark*

³⁷*Gemini Observatory/NSF NOIRLab, Hilo, HI 96720, USA*

³⁸*Department of Astronomy, Yale University, 219 Prospect Street, New Haven, CT 06511, USA*

ABSTRACT

We report the masses, sizes, and orbital properties of 86 planets orbiting 55 stars observed by NASA’s K2 Mission with follow-up Doppler measurements by the HIRES spectrometer at the W.M. Keck Observatory and the Automated Planet Finder at Lick Observatory. Eighty-one of the planets were discovered from their transits in the K2 photometry, while five were found based on subsequent Doppler measurements of transiting planet host stars. The sizes of the transiting planets range from Earth-size to larger than Jupiter (1–3 R_{\oplus} is typical), while the orbital periods range from less than a day to a few months. For 32 of the planets, the Doppler signal was detected with significance greater than 5- σ (51 were detected with >3- σ significance). An important characteristic of this catalog is the use of uniform analysis procedures to determine stellar and planetary properties. This includes the transit search and fitting procedures applied to the K2 photometry, the Doppler fitting techniques applied to the radial velocities, and the spectral modeling to determine bulk stellar parameters. Such a uniform treatment will make the catalog useful for statistical studies of the masses, densities, and system architectures of exoplanetary systems. This work also serves as a data release for all previously unpublished RVs and associated stellar activity indicators obtained by our team for these systems, along with derived stellar and planet parameters.

1. INTRODUCTION

The Kepler mission operated for four years and discovered 4000+ planets whose occurrence patterns and individual characteristics transformed exoplanet science. Analysis of the Kepler time series photometry demonstrated that small planets vastly outnumber large ones (e.g., Howard et al. 2012; Petigura et al. 2013). Results from *Kepler* showed that systems of multiple planets orbiting within 1 au (e.g., Lis-

sauer et al. 2011) are a common planetary system architecture despite their dissimilarity with the solar system. The mission also identified new planet types including circumbinary planets (Doyle et al. 2011) and low-density “super-puffs” (Masuda 2014). The population of close-in, small planets have proved particularly interesting. Variouslly called “super-Earths” and “sub-Neptunes”, these planets were known from prior Doppler discoveries (Howard et al. 2010a;

Mayor et al. 2011). However, details of their densities and planetary system architectures were not studied in detail until *Kepler* data were available. These planets are commonly in multiplanet systems with low mutual inclinations (e.g., Fang & Margot 2012) and low orbital eccentricities (Xie et al. 2016; Mills et al. 2019).¹

Measurements of the masses and radii of transiting planets provide information about their bulk densities and constrain their bulk compositions. During the *Kepler* mission, Marcy et al. (2014) measured the masses of 42 planets orbiting 22 stars. Subsequent analyses (Weiss & Marcy 2014; Rogers 2015; Wolfgang & Lopez 2015) demonstrated that planets in the size range spanning Earth to Neptune have a range of densities. High densities for planets smaller than $\sim 1.6 R_{\oplus}$ suggest that these planets are mostly composed of rock and iron (like Earth). The lower densities of the larger planets mean that these planets are (in part) composed of lower-density material (e.g., Lopez & Fortney 2014). However, the gradient from large to small planets is not smooth and uniformly populated in this domain. Fulton et al. (2017) showed that low-density sub-Neptunes are nearly distinct from high-density super-Earths. The “radius valley” separating these two types of planets (Van Eylen et al. 2018a; Fulton & Petigura 2018) has been interpreted as evidence for photoevaporation by XUV photons of tenuous planetary envelopes of hydrogen and helium (Owen & Wu 2017). Core-powered mass loss is an alternative theory in which the power for atmosphere loss comes from the interior of the planet (Ginzburg et al. 2018; Gupta & Schlichting 2019). Understanding the transition from low- to high-density planets with decreas-

ing planet size has been an area of significant study (e.g., Wolfgang & Lopez 2015; Howe & Burrows 2015; Owen & Wu 2016; Lehmer & Catling 2017; Jin & Mordasini 2018; Ning et al. 2018; Kanodia et al. 2019; Luque & Pallé 2022) and is a motivation for the work described in this paper.

The K2 mission (Howell et al. 2014) followed the *Kepler* mission using the same spacecraft, telescope, and photometer. K2 operated during 2014–2018 with twenty pointings along the ecliptic, each lasting about 80 days. Each of these “Campaigns” produced time-series photometry for bright stars in the ~ 100 square degree fields. A primary goal of the K2 mission was to broaden the sample of transiting planets, particularly those orbiting bright stars, for which follow-up measurements are more feasible. In this sense, the K2 project represented a transition from the deep, narrow (and top-down-driven) *Kepler* survey to the broad, shallower, and community-driven *TESS* survey (Ricker et al. 2016; Guerrero et al. 2021).

Our research collaboration used K2 to observe magnitude-limited samples of stars for most of the K2 fields (typically 5000–7000 GKM dwarf stars per field) through a proposal-driven process. With these observations, we planned to recreate many aspects of the original *Kepler* planet search based on new catalogs of planets. We undertook significant observational programs to validate and characterize the new planets and to measure their masses using the HIRES spectrometer on the Keck I telescope and the Levy spectrometer on the Automated Planet Finder (APF) telescope. This paper reports the Doppler measurements and planet masses for our K2 study. Subsequent follow-up papers provide statistical analyses of the ensemble planet properties from this catalog with comparisons to theoretical models of bulk planet composition.

¹ See Borucki (2017) and a special issue of *New Astronomy Reviews* (Lissauer & Eisberg 2018) for reviews of the *Kepler* mission and its major results.

The plan for this paper is as follows. Sec. 2 provides a description of our K2 project and its goals, as well as the transiting planet search and target selection. Our spectroscopic observations are described in Sec. 3 and our modeling of the spectra to determine stellar properties and planet masses are described in Sec. 4. Details of individual systems and their Keplerian models are provided in Sec. A and Sec. 5 is a concluding discussion.

2. K2 PLANET SEARCH

We conducted a search for planets orbiting stars observed by K2 with several goals. First, we sought to increase the number of *bright* stars with discovered transiting planets. Such planets are more favorable for follow-up measurements to determine planet masses. We sought to measure the masses of ~ 20 K2 planets with sizes between those of Earth and Neptune, roughly doubling the number of planets in that size range with precisely measured masses and radii. The sample at that time was dominated by *Kepler* planets and was sufficient to detect the transition from rocky to gas-dominated (by volume) planets near $1.6 R_{\oplus}$. However, the data were too sparse to disentangle other important effects that shape the size-density distribution. At that time, all of the known small planets with densities of $\gtrsim 5 \text{ g cm}^{-3}$ were in close orbits with high equilibrium temperatures. Their high bulk densities may be a reflection of photoevaporation and atmospheric loss rather than the intrinsic composition distribution of small planets (Lopez et al. 2012; Owen & Wu 2013). To disentangle these effects, we sought to preferentially observe K2 planets with equilibrium temperatures and sizes that were not explored in the *Kepler* sample due to the lack of bright systems.

Our search was also motivated by a desire to find bright targets for atmospheric transmission spectroscopy studies by the James Webb Space Telescope (*JWST*) and the Hubble Space Tele-

scope (*HST*). Mass determinations are crucial to these studies because a planet’s surface gravity affects the size of the atmospheric signatures through the atmospheric scale height (Batalha et al. 2019). Here, we sought to expand the domain of characterized atmospheres by emphasizing planets that are smaller and cooler than hot Jupiters, which were (and remain) the most well-studied to date (e.g., Sing et al. 2016; *JWST* Transiting Exoplanet Community Early Release Science Team et al. 2023).

A third significant motivation was to facilitate measurements of detailed patterns of planet occurrence in regions of the Milky Way outside of the Kepler Field. The goal is to measure variations in planet occurrence between K2 fields to establish whether our detailed measurements from Kepler can be applied directly to the solar neighborhood and to determine how much of the variation in planet occurrence correlates with stellar properties (e.g., metallicity, stellar multiplicity). This work has been explored in detail in the ‘Scaling K2’ project (Hardegree-Ullman et al. 2020; Zink et al. 2020a,b, 2021; Christiansen et al. 2022; Zink et al. 2023; Christiansen et al. 2023).

Fig. 1 is a flow chart of the elements of our K2 planet search. This paper describes target selection (Sec. 2.1), generation of time series photometry and transiting planet search (Sec. 2.2), generation of a planet catalog (Sec. 2.3), planet validation (Sec. 2.4), and planet mass measurements (Sec. 3–A). Search completeness and planet occurrence based on the catalog in this paper are not addressed in this paper and are subjects for future work.

2.1. K2 Target Selection

Our K2 search began with sets of proposals to observe FGK dwarfs and M dwarfs. We selected $\sim 10,000$ FGK dwarfs per K2 Field from the TESS Dwarf Catalog (TDC; Ricker et al. 2015). The TDC consists of 3 million F5–M5 objects selected from 2MASS and cross-matched with

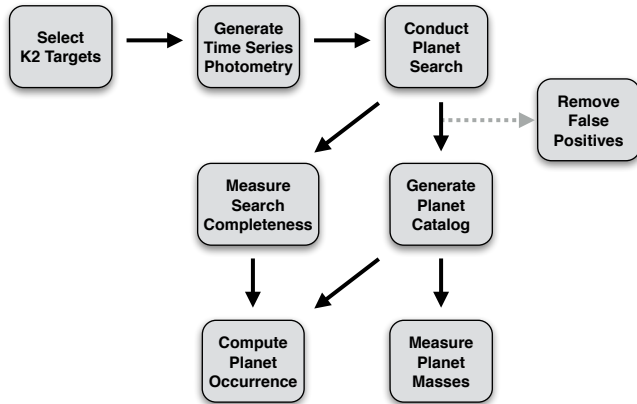


Figure 1. Flow chart of our K2 planet search. This paper describes elements of this process that culminate in the measurement of planet masses; measuring search completeness and computing planet occurrence will be described in subsequent papers. See Sec. 2 for details.

the NOMAD, Tycho-2, Hipparcos, APASS, and UCAC4 catalogs to obtain photometric colors, proper motions, and parallaxes. Giant stars were removed based on reduced proper motion vs. $J-H$ color (see Collier Cameron et al. 2007). M giants were excluded using JHK color-color cuts (Bessell & Brett 1988). The proposals for FGK dwarfs were limited to $T_{\text{eff}} = 3900-7000$ K and had magnitude cuts of $V \leq 14$. (The precise cut varied by a few tenths of a magnitude to obtain $\sim 10^4$ stars per field.) Many of these bright stars were proposed by other teams for a variety of science projects. The end result was that $\sim 4000-10,000$ FGK stars matching the above description were observed by K2 per field.

We supplemented the FGK dwarf proposals with a series of K2 proposals to observe M dwarfs drawn from the SUPERBLINK proper motion database (Lépine & Shara 2005). Targets were selected using reduced proper-motion and optical/NIR color-cuts and SED fitting to capture most nearby M dwarfs while minimizing contamination from distant giants. We estimated spectral types using several color-color relations: Eq. 2 of Rodriguez et al. (2013), Table 5 of Kraus & Hillenbrand (2007a), and Ta-

ble 6 of Pecaut & Mamajek (2013). We then converted the resulting averaged spectral types to stellar radii following Boyajian et al. (2012). Late-type targets were prioritized by comparing a nominal Earth-sized transit depth to K2’s photometric precision, requiring an expected transit $S/N \gtrsim 8$. Furthermore, we required Kepler magnitudes of < 16.5 mag to allow feasible spectroscopic follow-up.

2.2. Transiting Planet Search

Our transit search methodology used the TERRA pipeline (Petigura 2015) to identify candidates in our custom-detrended `k2phot` photometry. Our resulting planet and candidate catalogs have been presented in several previous papers (Sinukoff et al. 2016; Crossfield et al. 2016; Dressing et al. 2017; Petigura et al. 2018a; Livingston et al. 2018; Yu et al. 2018; Crossfield et al. 2018), and we refer the reader to these for details. Once candidates were identified, we fit the light curves for all of the K2 systems using `k2phot`² (Petigura et al. 2015; Aigrain et al. 2016) and `everest` (Luger et al. 2016). We performed the analysis using a methodology described in detail in Crossfield et al. (2016) and Livingston et al. (2018). In summary, we performed a Markov Chain Monte Carlo (MCMC) exploration of the parameter space using `emcee` Foreman-Mackey et al. (2013) and `batman` (Kreidberg 2015) to fit the transit parameters. We first removed any long-term trends in the photometry and isolated the individual planet transits in $3 \times T_{14}$ segments centered on the mid-transit times to reduce the computation expense (T_{14} is the transit duration from first to last contact); in multi-planet systems we fit the transits for each planet separately.

The free parameters in the transit model are: orbital period P_{orb} , mid-transit time T_0 , scaled

² <https://github.com/petigura/k2phot>

planet radius R_p/R_* , scaled semi-major axis a/R_* , impact parameter $b \equiv a \cos i/R_*$, and quadratic limb-darkening coefficients (q_1 and q_2) under the transformation of [Kipping \(2013\)](#). We additionally included the logarithm of the Gaussian errors ($\log \sigma$) and a constant out-of-transit baseline offset to allow for variation in the normalization of the light curve. We included Gaussian priors on the limb darkening coefficients informed from a Monte Carlo sampling of an interpolated grid of theoretical limb darkening coefficients ([Claret et al. 2012](#)). This allows for propagation of uncertainties in host star effective temperature T_{eff} , surface gravity $\log g$, and metallicity $[\text{Fe}/\text{H}]$.

We performed a preliminary non-linear least squares fit using `lmfit` ([Newville et al. 2014](#)). We initialized 100 “walkers” around the least squares solution and ran the MCMC for 5000 steps, discarding the first 3000 steps as “burn-in” before inspecting the chains and posteriors for convergence. We then calculated the autocorrelation time using the `acor` package in Python to check that we had a sufficient number of independent samples. The median and 68% credible intervals of the marginalized posterior distribution for the planet radius and orbital period are reported in [Table 3](#). Most of our targets have also subsequently been observed at lower precision by *TESS*, but we leave a joint analysis of *K2* and *TESS* photometry and RVs for future analysis.

2.3. Selected Stars and Planets

The targets selected for observation in our Keck/HIRES radial velocity program were taken from our *K2* transit light curve transit search efforts described above. We selected our targets manually for the list of all *K2* targets after accounting for stellar properties (brightness, activity, rotation), planet properties (inferred mass, predicted RV semi-amplitude, proximity of the orbital and stellar rotation periods), and follow-up and vetting observations (high-

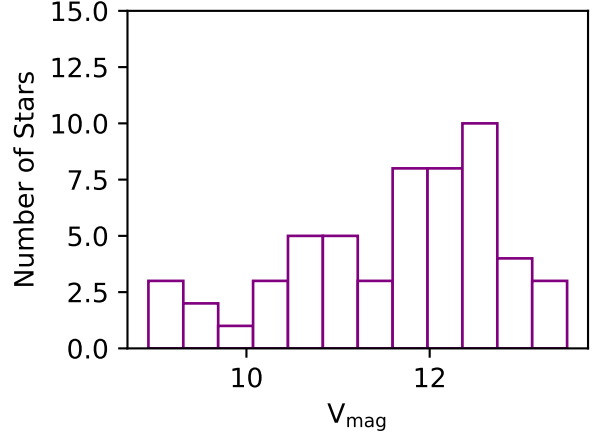


Figure 2. Distribution of planet host star brightness (V).

dispersion spectroscopy, high-resolution imaging, and *K2* photometric diagnostics) — as well as our attempt to produce an eventual mass catalog that would serve a broad range of science cases.

[Table 1](#) lists the stars observed for our HIRES program; the table notes the stars’ names, EPIC and TIC numbers, the number of RV observations N_{obs} from HIRES, the APF, and the literature used in our analysis; and the number of planets (N_p) in each system. [Fig. 2](#) shows that our stars span V magnitudes of roughly 9 to 13.5; fainter on average than many modern *TESS* targets ([Guerrero et al. 2021](#)), but significantly brighter than the average *Kepler* host star sample. The overall bulk properties of the target stars are listed in [Table 2](#). [Fig. 3](#) shows that our sample focuses predominately on stars with roughly Sun-like properties, while also including a smaller number of evolved stars and cooler dwarfs.

Finally, [Table 3](#) lists the derived properties of the planets orbiting our target stars. This includes orbital period, mid-transit time, radius, mass, density, instellation flux, and equilibrium temperature as derived from our *K2* transit light curve and Keck/HIRES radial velocity analyses.

2.4. Planet Validation

Table 1. Host star Parameters

Name	Other Name	EPIC No.	TIC No.	Field	RA	Dec.	V (mag)	N _{obs}			n _p
								HIRES	APF	Literature	
HD 3167	K2-96	220383386	318707987	8	00:34:58	+04:22:53.3	8.941 ± 0.015	60	116	76	2
HIP 41378	—	211311380	366443426	5/18	08:26:28	+10:04:49.3	8.93 ± 0.02	218	0	389	5
HD 106315	K2-109	201437844	56815340	10	12:13:53	−00:23:36.5	8.95 ± 0.02	352	125	155	2
HD 89345	K2-234	248777106	281731203	14	10:18:41	+10:07:44.0	9.38 ± 0.03	12	21	66	1
K2-222	—	220709978	257774438	8	01:05:51	+11:45:12.3	9.54 ± 0.03	55	32	0	1
K2-291	—	247418783	27039476	13	05:05:47	+21:32:55	10.01 ± 0.03	50	0	25	1
K2-236	—	211945201	243244680	5	09:06:18	+19:24:08.1	10.15 ± 0.06	36	2	19	1
K2-418	—	229004835	94924542	10	12:25:57	−01:24:16.5	10.23 ± 0.04	22	0	0	1
K2-277	—	212357477	404421005	6	13:28:04	−15:56:16.2	10.36 ± 0.05	26	0	0	1
GJ 9827	K2-135	246389858	301289516	12	23:27:05	−01:17:10.6	10.51 ± 0.069	92	0	142	3
K2-261	—	201498078	281731203	14	10:52:08	+00:29:36.1	10.61 ± 0.06	8	4	0	1
K2-100	—	211990866	307733361	5	08:38:24	+20:06:21.8	10.65 ± 0.09	33	0	0	1
K2-31	—	204129699	50171060	2	16:21:46	−23:32:52.3	10.8 ± 0.07	8	0	9	1
K2-39	—	206247743	250977648	3	22:33:28	−09:01:22.0	10.83 ± 0.07	45	0	30	1
K2-229	—	228801451	98720809	10	12:27:30	−06:43:18.7	10.98 ± 0.08	24	0	115	2
K2-111	—	210894022	14227229	4	03:59:34	+21:17:55.3	11.14 ± 0.04	54	0	18	1
K2-99	—	212803289	176966903	6	13:55:06	−05:26:32.9	11.15 ± 0.1	19	0	33	1
K2-265	—	206011496	146364192	3	22:48:08	−14:29:40.9	11.19 ± 0.1	53	0	0	1
K2-24	—	203771098	68048686	2	16:10:18	−24:59:25.0	11.28 ± 0.1	63	0	0	2
K2-38	—	204221263	12666215	2	16:00:08	−23:11:21.4	11.34 ± 0.11	65	0	0	2
K2-73	—	206245553	38354061	3	22:20:06	−09:03:21.9	11.35 ± 0.15	60	0	0	2
WASP-107	—	228724232	429302040	10	12:33:33	−10:08:46.2	11.47 ± 0.2	50	0	31	1
K2-66	—	206153219	50183101	3	22:06:06	−10:42:41.6	11.71 ± 0.19	44	0	0	1
K2-36	—	201713348	363445121	1	11:17:48	+03:51:59.0	11.73 ± 0.23	46	0	0	2
K2-105	—	211525389	6892385	5	08:21:41	+13:29:51.1	11.75 ± 0.2	31	0	0	1
K2-214	—	220376054	344657681	8	00:59:30	+04:13:40.1	11.8 ± 0.21	29	0	0	1
K2-220	—	220621788	266012991	8	00:51:05	+09:31:00.5	11.89 ± 0.02	28	0	0	1
K2-110	—	212521166	287333762	6	13:49:24	−12:17:04.2	11.91 ± 0.07	12	0	27	1
WASP-47	K2-23	206103150	102264230	3	22:04:49	−12:01:08.0	11.99 ± 0.01	76	0	143	4
K2-79	—	210402237	435339558	4	03:41:01	+13:31:09.7	12.07 ± 0.06	62	0	0	1
K2-106	—	220674823	266015990	8	00:52:19	+10:47:40.9	12.1 ± 0.21	39	0	53	2
K2-98	—	211391664	366410512	5	08:25:57	+11:30:40.1	12.17 ± 0.03	6	0	12	1
K2-3	—	201367065	173103335	1	11:29:20	−01:27:17.2	12.17 ± 0.01	74	0	360	3
EPIC 213546283	—	213546283	2670610	7	19:17:30	−29:02:57.1	12.21 ± 0.3	12	0	0	1
K2-199	—	212779596	2621213	6	13:55:36	−06:08:10.1	12.29 ± 0.02	45	0	0	2
EPIC 245991048	—	245991048	9030096	12	23:42:31	−09:42:48.8	12.3 ± 0.25	16	0	0	1
K2-32	—	205071984	437444661	2	16:49:42	−19:32:34.2	12.31 ± 0.03	64	0	0	3
K2-108	—	211736671	27635334	5	08:13:32	+16:25:11.0	12.33 ± 0.01	20	0	0	1
K2-62	—	206096602	434094657	3	22:17:27	−12:11:15.0	12.4 ± 0.04	20	0	0	1
K2-189	—	212394689	422349881	6	13:34:29	−15:02:10.9	12.4 ± 0.21	17	0	0	1
K2-10	—	201577035	363573185	1	11:28:29	+01:41:26.3	12.42 ± 0.02	22	0	25	1
EPIC 201357835	—	201357835	147677251	10	12:20:44	−01:35:17.9	12.44 ± 0.03	7	0	0	1
K2-216	—	220481411	418761354	8	00:45:55	+06:20:49.1	12.48 ± 0.05	31	0	29	1
K2-280	—	216494238	119605900	7	19:26:23	−22:14:51.6	12.54 ± 0.04	16	0	0	1
K2-37	—	203826436	68504570	2	16:13:48	−24:47:13.4	12.57 ± 0.03	19	0	0	3
K2-180	—	211319617	366411016	5	08:25:51	+10:14:49.1	12.6 ± 0.02	26	0	0	1
K2-27	—	201546283	363548415	1	11:26:04	+01:13:50.7	12.64 ± 0.02	15	0	31	1
K2-181	—	211355342	366528389	5	08:30:13	+10:54:37.1	12.75 ± 0.03	10	0	0	1
EPIC 245943455	—	245943455	49735922	12	23:30:51	−11:04:38.1	12.82 ± 0.03	9	0	0	1
K2-85	—	210707130	14160842	4	03:57:52	18:27:55.0	12.8 ± 0.5	21	0	0	1
K2-61	—	206044803	402314147	3	22:38:42	−13:33:36.1	12.99 ± 0.02	7	0	0	1
K2-121	—	211818569	7059054	5	08:27:45	+17:34:45.8	13.32 ± 0.03	18	0	0	1
K2-18	—	201912552	388804061	1	11:30:15	+07:35:18.2	13.5 ± 0.05	21	0	133	2
K2-55	—	205924614	2028887614	3	22:15:00	−17:15:02.6	13.55 ± 0.02	12	0	0	1
K2-19	—	201505350	281885301	1	11:39:50	+00:36:12.9	13 ± 0.01	51	0	0	3

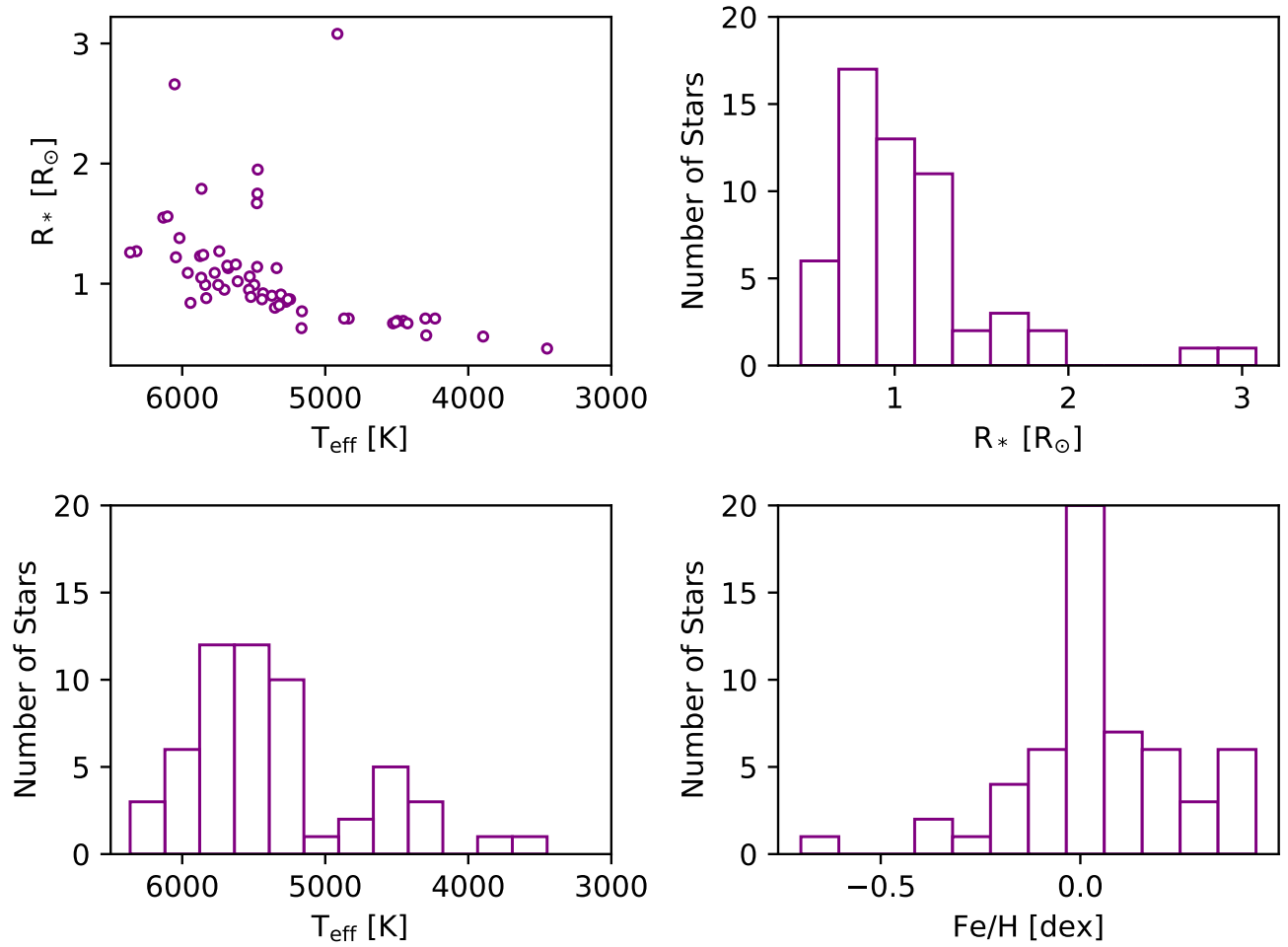


Figure 3. Properties of planet host stars showing distributions of stellar temperature, radius, and iron abundance.

Table 2. Host star Properties

Name	T_{eff} (K)	$\log g$ (dex)	[Fe/H] (dex)	S_{HK}	$\log R'_{\text{HK}}$	$V \sin i$ (km s ⁻¹)	M_{\star} (M_{\odot})	R_{\star} (R_{\odot})
HD 3167	5261 ± 60	4.47 ± 0.05	0.04 ± 0.05	—	-5.04	1.17 ± 1.1	0.866 ± 0.033	0.872 ± 0.057
HIP 41378	6320 ⁺⁶⁰ ₋₃₀	4.294 ± 0.006	-0.10 ± 0.07	—	-4.78 ± 0.03	5.6 ± 0.5	1.16 ± 0.04	1.273 ± 0.015
HD 106315	6364 ± 87	4.291 ± 0.025	-0.22 ± 0.09	0.14	—	13.2 ± 1.0	1.154 ± 0.042	1.269 ± 0.024
HD 89345	5472 ± 110	3.70 ± 0.10	0.44 ± 0.09	0.1334	-5.199	2.62 ± 1.0	1.17 ± 0.03	1.95 ± 0.18
K2-222	5961 ± 100	4.330 ± 0.080	-0.250 ± 0.044	0.1407	-5.128	1.6 ± 1.0	0.92 ± 0.04	1.093 ± 0.038
K2-291	5520 ± 60	4.50 ± 0.05	0.08 ± 0.04	—	—	< 2	0.934 ± 0.038	0.899 ^{+0.035} _{-0.033}
K2-236	6019 ± 100	4.180 ± 0.080	0.140 ± 0.044	0.1337	-5.193	0.1 ± 1.0	1.17 ± 0.07	1.387 ± 0.049
K2-418	5839 ± 100	4.420 ± 0.080	-0.110 ± 0.044	0.1616	-4.984	1.6 ± 1.0	0.95 ± 0.04	0.998 ± 0.036
K2-277	5705 ± 100	4.450 ± 0.080	0.050 ± 0.044	0.186	-4.875	2.3 ± 1.0	0.98 ± 0.04	0.952 ± 0.035
GJ 9827	4294 ± 52	4.682 ± 0.021	-0.26 ± 0.08	0.6446	—	2.43 ± 1.0	0.593 ± 0.018	0.579 ± 0.018
K2-261	5478 ± 100	4.020 ± 0.080	0.350 ± 0.043	0.1382	-5.16	3.0 ± 1.0	1.09 ± 0.07	1.679 ± 0.065
K2-100	6044 ± 100	4.400 ± 0.080	0.300 ± 0.044	0.2772	-4.526	13.3 ± 1.0	1.21 ± 0.04	1.227 ± 0.045
K2-31	5340 ± 100	4.450 ± 0.083	0.180 ± 0.046	0.2936	-4.647	2.8 ± 1.0	0.92 ± 0.04	1.138 ± 0.044
K2-39	4915 ± 100	3.580 ± 0.080	0.430 ± 0.043	0.173	-5.06	0.1 ± 1.0	1.38 ± 0.16	3.08 ± 0.14
K2-229	5163 ± 100	4.530 ± 0.080	0.040 ± 0.043	0.3516	-4.603	2.6 ± 1.0	0.84 ± 0.03	0.774 ± 0.032
K2-111	5832 ± 100	4.430 ± 0.080	-0.440 ± 0.044	0.1411	-5.133	0.1 ± 1.0	0.83 ± 0.03	0.884 ± 0.063
K2-99	6053 ± 100	3.900 ± 0.080	0.240 ± 0.044	0.119	-5.393	9.4 ± 1.0	1.48 ± 0.12	2.66 ± 0.11
K2-265	5435 ± 100	4.470 ± 0.080	0.050 ± 0.043	0.196	-4.878	1.8 ± 1.0	0.90 ± 0.04	0.924 ± 0.036
K2-24	5625 ± 60	4.29 ± 0.05	0.34 ± 0.04	0.1269	-5.2439	—	1.07 ± 0.06	1.16 ± 0.04
K2-38	5679 ± 100	4.320 ± 0.083	0.230 ± 0.046	0.1435	-5.12	1.5 ± 1.0	1.04 ± 0.05	1.131 ^{+0.123} _{-0.095}
K2-73	5867 ± 100	4.390 ± 0.081	0.040 ± 0.044	0.1586	-4.999	2.0 ± 1.0	1.02 ± 0.04	1.058 ± 0.039
WASP-107	4425 ± 70	4.633 ± 0.012	0.02 ± 0.09	—	—	< 2	0.683 ^{+0.017} _{-0.016}	0.67 ± 0.02
K2-66	5865 ± 100	3.990 ± 0.080	-0.050 ± 0.044	0.1276	-5.267	4.0 ± 1.0	1.06 ± 0.07	1.79 ± 0.10
K2-36	4836 ± 100	4.550 ± 0.084	0.000 ± 0.046	0.4628	-4.594	2.7 ± 1.0	0.76 ± 0.03	0.717 ± 0.031
K2-105	5373 ± 100	4.450 ± 0.085	0.220 ± 0.047	0.2097	-4.843	2.7 ± 1.0	0.94 ± 0.04	0.905 ± 0.035
K2-214	5875 ± 100	4.280 ± 0.081	0.040 ± 0.044	0.1432	-5.112	1.9 ± 1.0	1.03 ± 0.05	1.236 ± 0.047
K2-220	5612 ± 100	4.450 ± 0.080	-0.050 ± 0.044	0.1391	-5.155	1.1 ± 1.0	0.91 ± 0.04	1.026 ± 0.040
K2-110	4868 ± 100	4.530 ± 0.080	-0.270 ± 0.044	0.1761	-5.063	0.1 ± 1.0	0.70 ± 0.03	0.710 ± 0.030
WASP-47	5476 ± 100	4.270 ± 0.080	0.370 ± 0.044	0.1325	-5.201	2.2 ± 1.0	1.01 ± 0.05	1.144 ± 0.049
K2-79	5853 ± 100	4.180 ± 0.081	-0.000 ± 0.044	0.1414	-5.129	1.9 ± 1.0	1.01 ± 0.05	1.247 ± 0.045
K2-106	5496 ± 100	4.420 ± 0.080	0.060 ± 0.044	0.1419	-5.135	1.7 ± 1.0	0.91 ± 0.04	0.995 ± 0.039
K2-98	6103 ± 100	4.120 ± 0.081	-0.060 ± 0.044	0.1335	-5.189	5.6 ± 1.0	1.11 ^{+0.08} _{-0.06}	1.565 ± 0.065
K2-3	3896 ± 189	4.734 ± 0.062	-0.32 ± 0.13	—	—	—	0.601 ± 0.089	0.561 ± 0.068
EPIC 213546283	5685 ± 100	4.23 ± 0.10	-0.135 ± 0.060	0.1761	-4.923	0.1 ± 1.0	0.89 ± 0.04	1.154 ± 0.044
K2-199	4507 ± 110	4.6 ± 0.2	-0.04 ± 0.08	0.47	-4.735	—	0.69 ± 0.03	0.68 ± 0.03
EPIC 245991048	5773 ± 100	4.31 ± 0.10	0.038 ± 0.060	0.1432	-5.119	1.8 ± 1.0	0.99 ± 0.05	1.094 ± 0.041
K2-32	5274 ± 100	4.490 ± 0.083	-0.030 ± 0.046	0.1567	-5.061	0.7 ± 1.0	0.84 ± 0.03	0.855 ± 0.034
K2-108	5474 ± 60	3.99 ± 0.05	0.33 ± 0.04	0.1225	-5.2928	2.83 ± 1.0	1.121 ^{+0.065} _{-0.053}	1.75 ± 0.14
K2-62	4455 ± 70	4.57 ± 0.20	-0.10 ± 0.12	0.2961	-4.972	—	0.67 ± 0.03	0.696 ± 0.023
K2-189	5442 ± 100	4.510 ± 0.085	-0.100 ± 0.047	0.1663	-4.999	1.9 ± 1.0	0.85 ± 0.03	0.879 ± 0.034
K2-10	5533 ± 100	4.470 ± 0.085	-0.070 ± 0.047	0.1481	-5.093	1.5 ± 1.0	0.88 ± 0.04	0.956 ± 0.037
K2-245	5942 ± 100	4.580 ± 0.081	-0.450 ± 0.045	0.1387	-5.148	0.1 ± 1.0	0.88 ± 0.03	0.840 ^{+0.047} _{-0.034}
K2-216	4495 ± 70	4.60 ± 0.20	0.08 ± 0.12	0.612	-4.627	—	0.72 ± 0.03	0.699 ± 0.023
K2-280	5741 ± 100	4.14 ± 0.10	0.353 ± 0.060	0.127	-5.273	2.5 ± 1.0	1.17 ± 0.09	1.279 ± 0.052
K2-37	5352 ± 100	4.530 ± 0.083	-0.080 ± 0.046	0.1787	-4.957	1.3 ± 1.0	0.84 ± 0.03	0.809 ± 0.032
K2-180	5166 ± 100	4.630 ± 0.081	-0.710 ± 0.045	0.2003	-4.916	0.1 ± 1.0	0.67 ± 0.02	0.638 ± 0.020
K2-27	5246 ± 100	4.480 ± 0.081	0.120 ± 0.045	0.1627	-5.037	1.6 ± 1.0	0.88 ± 0.03	0.876 ± 0.036
K2-181	5528 ± 100	4.350 ± 0.085	0.180 ± 0.047	0.183	-4.914	2.1 ± 1.0	0.96 ± 0.04	1.060 ± 0.042
EPIC 245943455	5310 ± 100	4.420 ± 0.081	0.240 ± 0.045	0.1538	-5.073	1.9 ± 1.0	0.93 ± 0.04	0.910 ± 0.038
K2-85	4232 ± 70	4.44 ± 0.10	0.14 ± 0.09	0.7276	-4.4024	3 ± 1	0.70 ± 0.02	0.71 ± 0.10
K2-61	5748 ± 100	4.380 ± 0.085	0.030 ± 0.048	0.1433	-5.119	1.6 ± 1.0	0.97 ± 0.04	0.995 ± 0.042
K2-121	4526 ± 110	4.63 ± 0.20	0.040 ± 0.080	0.728	-4.534	—	0.71 ± 0.03	0.675 ± 0.033
K2-18	3449 ± 70	4.60 ± 0.20	0.00 ± 0.12	0.5806	-5.183	—	0.32 ± 0.06	0.468 ± 0.019
K2-55	4300 ⁺¹⁰⁷ ₋₁₀₀	4.566 ± 0.036	0.376 ± 0.095	0.78	-4.7339	2.2 ± 1.0	0.688 ± 0.069	0.715 ^{+0.043} _{-0.040}
K2-19	5322 ± 100	4.51 ± 0.08	0.06 ± 0.05	—	—	< 2	0.88 ± 0.03	0.82 ± 0.03

Table 3. Planet Properties

Name	Orbital Period (days)	Transit Time (BJD)	Radius (R_{\oplus})	Mass (M_{\oplus})	Density (g cm^{-3})	T_{eq} (K)	Flux (F_{\oplus})
HD 3167 b	$0.959641^{+0.000012}_{-0.000011}$	$2457394.37454 \pm 0.00043$	$1.70^{+0.15}_{-0.18}$	5.02 ± 0.38	$5.60^{+1.43}_{-2.15}$	1608 ± 56	1625^{+222}_{-244}
HD 3167 c	29.8454 ± 0.0012	2457394.9788 ± 0.0012	$3.01^{+0.28}_{-0.42}$	$9.80^{+1.24}_{-1.30}$	$1.97^{+0.59}_{-0.94}$	511 ± 18	$16.6^{+2.5}_{-2.3}$
HD 3167 d	8.509 ± 0.045	$2457806.07^{+0.50}_{-0.52}$	—	6.90 ± 0.71	—	776 ± 28	88.9 ± 6.2
HIP 41378 b	15.57208 ± 0.00002	2457152.2818 ± 0.0012	2.595 ± 0.036	6.89 ± 0.88	2.17 ± 0.28	959^{+9}_{-5}	140^{+5}_{-3}
HIP 41378 c	31.70603 ± 0.00006	$2457163.1609^{+0.0023}_{-0.0027}$	2.727 ± 0.060	4.4 ± 1.1	1.19 ± 0.30	757^{+7}_{-4}	54^{+2}_{-1}
HIP 41378 d	278.3618 ± 0.0005	2457166.2604 ± 0.0017	3.54 ± 0.06	< 4.6	< 0.56	367^{+3}_{-2}	$3.01^{+0.11}_{-0.06}$
HIP 41378 e	369 ± 10	2457142.0194 ± 0.0010	4.92 ± 0.09	12 ± 5	0.55 ± 0.23	335 ± 4	2.1 ± 0.1
HIP 41378 f	542.07975 ± 0.00014	$2457186.91423^{+0.00039}_{-0.00038}$	9.2 ± 0.1	12 ± 3	0.09 ± 0.02	294^{+3}_{-1}	$1.24^{+0.06}_{-0.02}$
HIP 41378 g	62.06 ± 0.32	—	—	7 ± 1.5	—	605 ± 4.7	$22.3^{+0.8}_{-0.5}$
HD 106315 b	9.55288 ± 0.00021	$2457586.5476^{+0.0024}_{-0.0025}$	2.40 ± 0.20	10.5 ± 3.1	$4.1^{+1.9}_{-1.4}$	1040 ± 18	277 ± 20
HD 106315 c	21.05652 ± 0.00012	$2457569.01767^{+0.00097}_{-0.00096}$	4.379 ± 0.086	12.0 ± 3.8	$0.78^{+0.26}_{-0.25}$	799 ± 14	97 ± 7
HD 89345 b	11.81469 ± 0.00044	2457913.8041 ± 0.0011	$7.20^{+0.42}_{-0.15}$	$34.1^{+3.4}_{-3.3}$	$0.55^{+0.12}_{-0.09}$	993 ± 29	231^{+29}_{-26}
K2-222 b	15.3863 ± 0.0014	2457399.0652 ± 0.0042	$2.41^{+0.17}_{-0.08}$	5.7 ± 2.6	2 ± 1	801 ± 20	98 ± 10
K2-291 b	$2.225177^{+0.000066}_{-0.000068}$	$2457830.06163^{+0.00099}_{-0.00104}$	$1.589^{+0.095}_{-0.072}$	6.49 ± 1.16	$8.84^{+2.50}_{-2.03}$	1278 ± 30	633^{+59}_{-56}
K2-236 b	19.4910 ± 0.0007	$2457158.82659 \pm 0.00092$	$5.50^{+0.19}_{-0.08}$	11 ± 7	$0.33^{+0.22}_{-0.21}$	809 ± 21	101^{+11}_{-10}
EPIC 229004835 b	16.1388 ± 0.0016	2457613.7661 ± 0.0019	$2.18^{+0.13}_{-0.07}$	19.3 ± 5.1	$11.9^{+4.2}_{-3.5}$	734 ± 19	$68.9^{+7.4}_{-6.9}$
K2-277 b	6.32677 ± 0.00018	2457221.2301 ± 0.0012	$2.23^{+0.14}_{-0.06}$	7.4 ± 3.3	4 ± 2	953 ± 25	195^{+22}_{-20}
GJ 9827 b	$1.2089765 \pm 2.3e - 06$	$2457738.82586 \pm 0.00026$	1.529 ± 0.05787	4.87 ± 0.37	$7.47^{+1.1}_{-0.95}$	1055 ± 21	294 ± 24
GJ 9827 c	$3.648095 \pm 2.4e - 05$	$2457742.19929^{+0.00072}_{-0.00071}$	1.201 ± 0.04586	1.92 ± 0.49	$6.1^{+1.8}_{-1.6}$	730 ± 15	67 ± 5
GJ 9827 d	$6.20183 \pm 1e - 05$	$2457740.96114^{+0.00045}_{-0.00044}$	1.955 ± 0.07535	3.42 ± 0.62	$2.51^{+0.57}_{-0.51}$	612 ± 12	33 ± 3
K2-261 b	11.63395 ± 0.00021	$2457906.84055 \pm 0.00054$	$10.32^{+0.17}_{-0.08}$	56 ± 6	$0.339^{+0.061}_{-0.052}$	973 ± 28	212^{+26}_{-23}
K2-100 b	1.673890 ± 0.000017	$2457140.71966 \pm 0.00042$	$3.57^{+0.10}_{-0.04}$	8 ± 15	0.9 ± 1.9	1720 ± 44	2100 ± 200
K2-31 b	$1.25784906 \pm 0.00000098$	$2456893.598952 \pm 0.000036$	46 ± 8	551^{+16}_{-17}	$0.032^{+0.025}_{-0.013}$	1688 ± 47	1930^{+220}_{-210}
K2-39 b	4.60547 ± 0.00047	2456985.4268 ± 0.0038	$6.40^{+0.41}_{-0.17}$	$37.6^{+5.3}_{-4.8}$	$0.93^{+0.25}_{-0.19}$	1550^{+58}_{-55}	1370^{+220}_{-180}
K2-229 b	0.584272 ± 0.000017	$2457605.08611 \pm 0.00078$	$1.260^{+0.082}_{-0.034}$	2.55 ± 0.38	$7.6^{+2.1}_{-1.7}$	1763^{+52}_{-51}	2290^{+280}_{-260}
K2-229 c	8.3262 ± 0.0015	2457611.3227 ± 0.0033	$2.04^{+0.21}_{-0.07}$	7 ± 4	$5.1^{+3.5}_{-2.9}$	727 ± 21	66^{+8}_{-7}
K2-111 b	5.35232 ± 0.00035	2457067.9628 ± 0.0024	$1.184^{+0.056}_{-0.034}$	$5.4^{+2.2}_{-2.1}$	$13.8^{+7.3}_{-5.9}$	1019^{+44}_{-45}	255^{+47}_{-42}
K2-99 b	18.24901 ± 0.00062	2457233.8255 ± 0.0012	$12.37^{+0.18}_{-0.10}$	287^{+23}_{-22}	$0.90^{+0.15}_{-0.13}$	1108^{+33}_{-34}	357^{+46}_{-41}
K2-265 b	2.36906 ± 0.00008	2456981.6450 ± 0.0014	$1.676^{+0.084}_{-0.039}$	4.6 ± 1.5	5 ± 2	1257 ± 35	592^{+69}_{-64}
K2-24 b	20.88977 ± 0.00035	2456905.88977 ± 0.0055	5.4 ± 0.2	19.0 ± 2.2	0.64 ± 0.12	686 ± 13	52 ± 4
K2-24 c	42.3391 ± 0.0012	2456915.4485 ± 0.0079	7.5 ± 0.3	15.4 ± 1.9	0.20 ± 0.04	542 ± 10	20 ± 2
K2-38 b	4.01668 ± 0.00032	2456896.8707 ± 0.0035	$1.55^{+0.11}_{-0.05}$	6 ± 2	$6.5^{+3.7}_{-2.5}$	1189^{+67}_{-69}	500 ± 100
K2-38 c	10.56104 ± 0.00059	2456900.4751 ± 0.0021	$2.18^{+0.15}_{-0.06}$	7.7 ± 2.7	$2.7^{+1.6}_{-1.1}$	862^{+48}_{-50}	131^{+32}_{-28}
K2-73 b	7.49556 ± 0.00029	2456987.6726 ± 0.0012	$2.58^{+0.13}_{-0.06}$	$9.2^{+3.8}_{-3.7}$	$2.8^{+1.3}_{-1.2}$	968 ± 25	209^{+23}_{-21}
K2-73 c	1000 ± 100	2456905^{+62}_{-99}	—	1142^{+53}_{-45}	—	$186.1^{+6.6}_{-7.2}$	0.285 ± 0.042
WASP-107 b	$5.7214742 \pm 4.3e - 7$	$2457584.329897 \pm 0.000032$	10.55 ± 0.32	30.6 ± 1.7	$0.143^{+0.016}_{-0.014}$	$525 - 820$	51 ± 4
WASP-107 c	1088^{+15}_{-16}	2458521^{+65}_{-56}	—	115^{+13}_{-14}	—	118 ± 3	0.046 ± 0.004
K2-66 b	5.06939 ± 0.00053	2456984.0075 ± 0.0037	$2.75^{+0.16}_{-0.10}$	16 ± 4	3 ± 1	1427 ± 51	980^{+150}_{-130}
K2-36 c	5.340786 ± 0.000073	$2456812.84096 \pm 0.00059$	$2.41^{+0.25}_{-0.07}$	$26.0^{+7.8}_{-7.9}$	$9.4^{+4.2}_{-3.3}$	772 ± 24	84^{+11}_{-10}
K2-36 b	1.422586 ± 0.000029	$2456827.96295 \pm 0.00068$	$1.291^{+0.081}_{-0.038}$	$5.1^{+4.5}_{-4.4}$	12^{+12}_{-10}	1200^{+37}_{-36}	492^{+64}_{-57}
K2-105 b	8.26726 ± 0.00018	$2457147.98867 \pm 0.00079$	$3.40^{+0.12}_{-0.05}$	15.4 ± 4.4	$2.24^{+0.77}_{-0.68}$	805^{+22}_{-23}	100^{+12}_{-11}
K2-214 b	8.59656 ± 0.00051	2457396.6009 ± 0.0023	$2.51^{+0.14}_{-0.07}$	2.4 ± 6.5	0.9 ± 2.4	1001 ± 27	238^{+27}_{-25}
K2-220 b	13.68186 ± 0.00095	2457401.2729 ± 0.0025	$2.37^{+0.14}_{-0.07}$	0 ± 4	0.0 ± 1.6	761 ± 21	$79.7^{+9.1}_{-8.4}$
K2-110 b	13.86368 ± 0.00019	$2457233.73861 \pm 0.00048$	$2.558^{+0.085}_{-0.037}$	17 ± 3	$5.7^{+1.4}_{-1.2}$	571 ± 17	$25.3^{+3.2}_{-2.9}$
WASP-47 b	4.159152 ± 0.000013	2456982.9772 ± 0.0001	$12.251^{+0.043}_{-0.033}$	357 ± 11	$0.97^{+0.14}_{-0.12}$	1146^{+33}_{-34}	409^{+50}_{-46}
WASP-47 c	$592.5^{+2.6}_{-2.5}$	2455993^{+6}_{-7}	—	394 ± 13	—	219.3 ± 6.4	$0.549^{+0.067}_{-0.061}$
WASP-47 d	9.03101 ± 0.00037	2456988.3079 ± 0.0011	$3.58^{+0.32}_{-0.10}$	13.3 ± 1.5	$1.44^{+0.42}_{-0.32}$	885 ± 26	145^{+18}_{-16}
WASP-47 e	0.789570 ± 0.000034	2456981.3436 ± 0.0014	$1.79^{+0.18}_{-0.06}$	$7.06^{+0.71}_{-0.68}$	$6.1^{+1.9}_{-1.4}$	1992^{+59}_{-58}	3740^{+460}_{-420}
K2-79 b	10.99497 ± 0.00045	2457070.2428 ± 0.0015	$3.99^{+0.11}_{-0.07}$	$3.8^{+4.3}_{-4.2}$	0.3 ± 0.4	925^{+25}_{-24}	174^{+20}_{-18}
K2-106 b	0.571282 ± 0.000015	2457393.4405 ± 0.0012	$1.87^{+0.11}_{-0.05}$	$8.03^{+0.88}_{-0.85}$	$7.3^{+1.7}_{-1.3}$	2115 ± 59	4740^{+550}_{-510}
K2-106 c	13.33918 ± 0.00099	2457405.7330 ± 0.0019	$3.01^{+0.15}_{-0.09}$	$5.0^{+2.8}_{-2.9}$	$1.10^{+0.67}_{-0.63}$	740^{+21}_{-20}	$71.0^{+8.2}_{-7.5}$
K2-98 b	10.13693 ± 0.00046	2457145.9796 ± 0.0016	$4.93^{+0.13}_{-0.07}$	20^{+21}_{-33}	$0.8^{+0.9}_{-1.3}$	1093 ± 31	339^{+41}_{-37}
K2-3 b	$10.054626^{+0.000009}_{-0.000010}$	$2456813.41843^{+0.00039}_{-0.00038}$	2.140 ± 0.264	$6.48^{+0.99}_{-0.93}$	$3.70^{+1.67}_{-1.08}$	463 ± 39	11 ± 4
K2-3 c	$24.646582^{+0.000039}_{-0.000039}$	$2456812.28013^{+0.00090}_{-0.00095}$	$1.72^{+0.23}_{-0.22}$	$2.14^{+1.08}_{-1.04}$	$2.98^{+1.96}_{-1.50}$	344 ± 29	3 ± 1
K2-3 d	$44.556456^{+0.000097}_{-0.000087}$	$2456826.22347^{+0.00053}_{-0.00052}$	$1.52^{+0.21}_{-0.20}$	< 2.80	< 5.62	282 ± 24	282 ± 23
EPIC 213546283 b	9.77058 ± 0.00035	2457312.1249 ± 0.0012	$3.4^{+0.2}_{-0.1}$	8 ± 9	1 ± 1	917^{+25}_{-24}	168^{+19}_{-17}
K2-199 b	3.225286 ± 0.000078	2457221.9649 ± 0.0011	$1.74^{+0.12}_{-0.05}$	7.1 ± 1.8	$6.5^{+2.5}_{-1.9}$	842^{+31}_{-30}	119^{+18}_{-16}

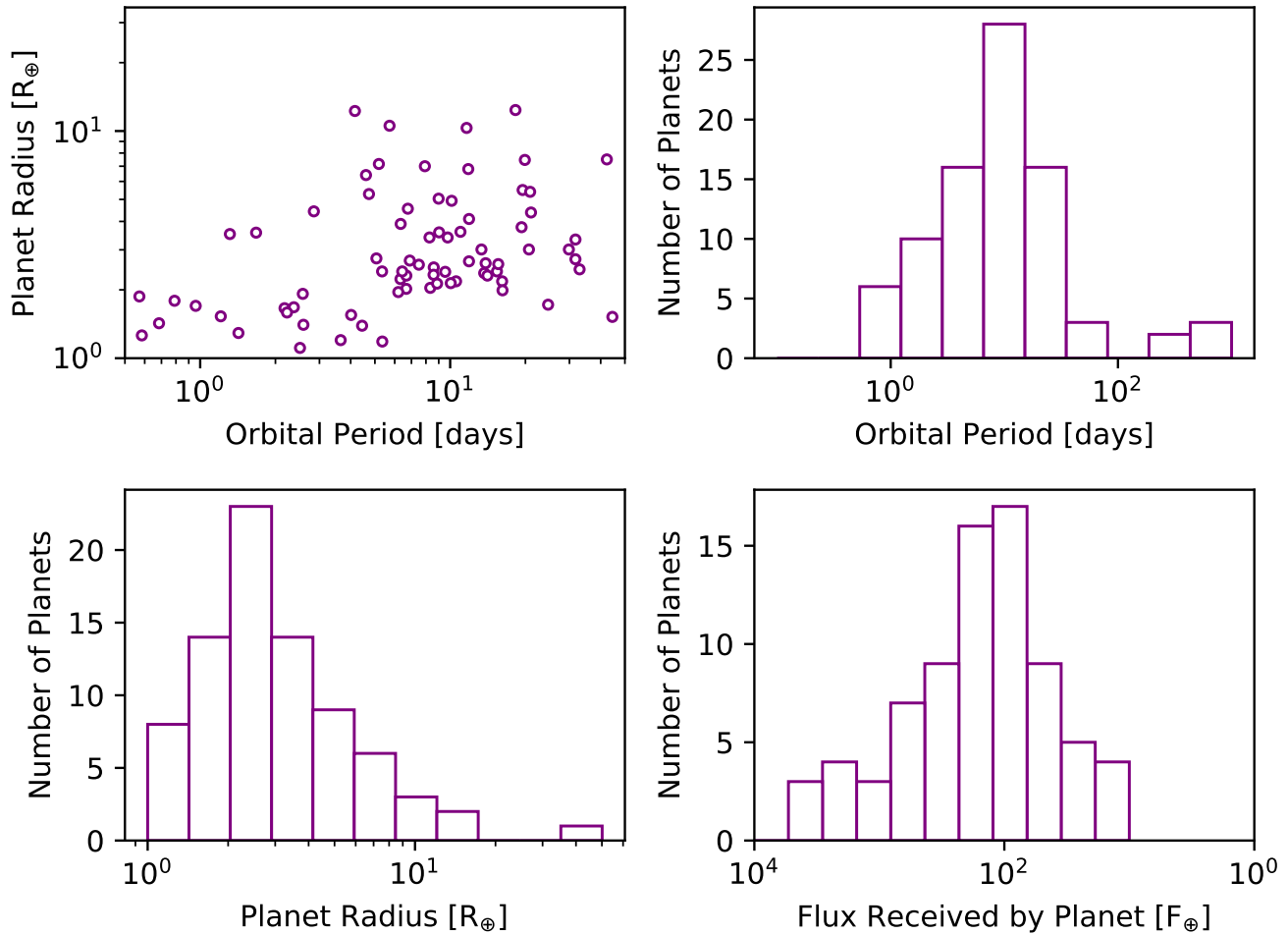


Figure 4. Distributions of planet size, orbital period, and flux received for the planets described in this paper.

Most of the planets for which we made mass measurements have been validated using statistical techniques (Montet et al. 2015; Crossfield et al. 2016; Livingston et al. 2018; Mayo et al. 2018) or through mass measurements. These systems can be identified in the tables below by their ‘K2 names’ (e.g., ‘K2-3’) or names from other common catalogs (HD, HIP, GJ). The subsections of Sec. A provides references for the papers that validate each planet. A handful of planets in this paper were not validated prior to this work and we adopt ‘EPIC names’ for these (e.g., EPIC 213546283).

3. STELLAR SPECTROSCOPY

3.1. Observations

We used the HIRES spectrometer (Vogt et al. 1994) on the Keck I telescope at the W. M. Keck Observatory to measure optical spectra of all targets presented in this paper. These spectra span 3640–7990 Å and most have a resolution of $R = 60,000$. We used the spectra to determine properties of host stars and for precise Doppler measurements to measure planets (see Sec. 3.2). Our HIRES observations followed standard procedures of the California Planet Search (CPS; Howard et al. 2010b).

The K2 targets in this paper span a range of V -band magnitudes. We therefore adopted different spectral signal-to-noise targets for each

star using the exposure meter on HIRES. These exposure meter levels ranged from 250,000 counts for the brightest stars (corresponding to $\text{SNR} = 200$ per reduced pixel on blaze near 550 nm) to 30,000 counts for the faintest stars ($\text{SNR} = 75$). Note that the exposure meter counts are in units of flux received by the photomultiplier tube in approximately V -band (in arbitrary units), which are proportional to the number of photoelectrons recorded by HIRES over an appropriate wavelength range.

For a few bright stars that are noted in Sec. A, we recorded three exposures per night. We adopted this strategy to help mitigate stellar jitter on approximately hour-long timescales due to granulation on the star’s surface or to improve the Doppler precision for stars with high $V \sin i$. The survey was designed so that each star would be observed on at least 15 nights to provide a consistent floor of Doppler detectability. In practice, we met this threshold for 42/55 stars. Some stars were observed more frequently because of sky conditions or because of interest in noteworthy systems (e.g., HD 3167). The median number of nights with an observation is 30 and 14 stars have observations of 50 or more nights.

For a few of the stars that are particularly bright, we also obtained spectra and corresponding RVs from the Levy Spectrometer on the 2.4 m Automated Planet Finder (APF) telescope (Vogt et al. 2014) with a spectral resolution of $R = 100,000$ and a similar wavelength coverage. Our APF observing procedures are described in Fulton et al. (2015). Systems with APF observations are noted in Sec. A.

3.2. Doppler Measurements

We determined precise, relative radial velocities (RVs) for Keck/HIRES and APF/Levy spectra using the iodine cell method. With this technique, the stars are observed with a glass cell of gaseous iodine mounted in front of the spectrometer entrance slit. Thousands

of narrow iodine lines in the wavelength range 5000–6200 Å are imprinted onto the stellar spectra. These molecular absorption lines provide a robust wavelength reference against which Doppler shifts are measured and strongly constrain the shape of the spectrometer instrumental profile at the time of each observation (Marcy & Butler 1992; Valenti et al. 1995).

Our procedure for determining RVs is descended from Butler et al. (1996) and is part of the standard procedures of the California Planet Search (Howard et al. 2010b). We measured the Doppler shift of each star-times-iodine spectrum by forward-modeling ~ 700 spectral chunks, each 2 Å wide. The ingredients of the forward model in each chunk are a deconvolved spectrum of the target star, a high-resolution/high-SNR spectrum of the iodine absorption cell, a description of the instrumental profile, a description of wavelength solution, and the Doppler shift. We measured stellar activity from the Mt. Wilson S_{HK} and $\log R'_{\text{HK}}$ values from the HIRES spectra using the procedures in Isaacson & Fischer (2010).

We also included RV measurements from other facilities that are in the published literature, where available for particular K2 systems. Table 4 provides a comprehensive list of HIRES, APF, and literature RVs and S_{HK} values used in this paper.

4. MODELING

4.1. Stellar Characterization

We determined stellar parameters for each system from a spectroscopic analysis from a HIRES spectrum of the host star. For stars hotter than 4700 K, we measured T_{eff} , $\log g$, $v \sin i$ and $[\text{Fe}/\text{H}]$ using Spectroscopy Made Easy (SME, Brewer et al. 2015). We followed Brewer & Fischer (2018) to estimate uncertainties as a function of spectral SNR and subsequently inflated our uncertainty on T_{eff} to 100 K to account for systematic differences between differ-

Table 4. Radial Velocity Measurements

Name	Time (BJD)	RV (m s ⁻¹)	Uncertainty (m s ⁻¹)	S_{HK} ^a	Instrument
HD 3167	2457633.77119	0.76	1.38	—	APF
HD 3167	2457600.98655	-1.74	1.09	—	APF
HD 3167	2457600.85553	-0.53	1.36	—	APF
HD 3167	2457599.99676	6.02	1.23	—	APF
HD 3167	2457599.97510	-1.77	1.34	—	APF

^aUncertainties on S_{HK} are 0.002 for all Keck-HIRES measurements.

NOTE—This table will be available in its entirety in machine-readable form in the published paper. A portion is shown here for guidance regarding its form and content. RV measurements from literature papers that we use in our analyses are also given in this table. The references for each of these points are given in the relevant subsection of Section A.

Table 5. RV Instrument Summary

Name	N_{RV}
HIRES	1988
APF	346
HARPS	475
HARPS-N	196
FIES	93
CORALIE	76
CARMENES	58
PFS	94
PARAS	19
CORPOST	6
McDonald 2.7m	6
FIES-POST	4
HDS	3

ent spectroscopic modeling tools. For some of these hot stars, the HIRES spectrum had previously been analyzed with SME by Brewer et al. (2016) and Brewer & Fischer (2018); for these we adopt the measurements shown in those catalogs. For three hot stars (EPIC 213546283, EPIC 216494238, EPIC 245991048) we used SpecMatch (Petigura et al. 2015) instead which has been shown to have good agreement with SME (Petigura et al. 2017a).

For stars cooler than 4700 K, we used SpecMatch-Emp (Yee et al. 2017) as the increase in molecular lines limits the reliabil-

ity of stellar characterization pipelines such as SME and SpecMatch. SpecMatch-EMP compares the HIRES spectra with a library of well-characterized stars to derive T_{eff} , $\log g$, $v \sin i$, and $[\text{Fe}/\text{H}]$.

Afterwards, we derived the stellar mass and radius using isoclassify (Huber 2017), see Fulton et al. (2018) for a detailed description of our procedures. All of the stellar properties are listed in Table 2.

4.2. Doppler Time Series Modeling

4.2.1. Keplerian Models

We analyzed the radial velocities for each system using RadVel, an open source Python package for fitting Keplerian orbits to radial velocity data sets (Fulton et al. 2018). The model for the radial velocity (v_r) of the star is given by a sum over contributions from its orbiting planets:

$$v_r(t) = \sum_k^{N_{\text{pl}}} v_{r,k}(t) + \gamma + \dot{\gamma}(t - t_0) + \ddot{\gamma}(t - t_0)^2,$$

$$v_{r,k}(t) = K_k [\cos(\nu_k + \omega_k) + e_k \cos \omega_k], \quad (1)$$

where the RV semi-amplitude K , orbital eccentricity e , and argument of periastron ω are free parameters, t_0 is a reference epoch, and N_{pl} is the number of planets in the model. In some models we also included $\dot{\gamma}$ and/or $\ddot{\gamma}$ as free parameters, which model a linear and quadratic

RV trend, respectively. A nonzero $\dot{\gamma}$ or $\ddot{\gamma}$ may indicate a distant planet which has only partially completed a full orbit during the observing baseline. The offset term γ is unique for each instrument, so for datasets compiled from multiple instruments we assigned a different γ term for each one. Finally, the true anomaly ν is determined from the time of observation, a reference time (e.g., the time of conjunction t_c), the orbital eccentricity, and the planet’s orbital period P from Kepler’s equation, which RadVel solves numerically (see [Fulton et al. 2018](#)).

4.2.2. Gaussian Process Modeling of Activity

For systems with $\log R'_{\text{HK}} > -4.9$ and more than 30 available RV observations, we adopted a Gaussian Process (GP) noise model to account for the effects of stellar activity on the data (see, e.g., [Kosiarek et al. 2019a](#), [López-Morales et al. 2016](#), [Grunblatt et al. 2015](#), [Haywood et al. 2014](#)). The choice of $\log R'_{\text{HK}} > -4.9$ was made to apply activity modeling to systems where the expected activity amplitude is detectable for HIRES observations which have systematic and photon-limited errors of $\sim 2 \text{ m s}^{-1}$ for the brightest stars and a little worse for fainter stars. This corresponds to a cutoff of roughly more active than the Sun, which varies between $\log R'_{\text{HK}} = -4.9$ in active periods to $\log R'_{\text{HK}} = -4.95$ in quiet parts of the cycle. The basic approach was to characterize stellar activity variations by measuring the covariance properties of photometry and then apply that model to the RVs. [Kosiarek & Crossfield \(2020\)](#) demonstrated good agreement between hyperparameter posteriors for simultaneous photometry and radial velocities of the Sun.

Our GP model for activity uses a quasi-periodic kernel in all cases; see [Grunblatt et al. 2015](#) for a definition of this kernel and a description of each parameter. An element in the covariance matrix kernel is given by

$$C_{ij} = \eta_1^2 \exp \left\{ -\frac{|t_i - t_j|^2}{\eta_2^2} - \frac{\sin^2(\pi|t_i - t_j|/\eta_3)}{2\eta_4^2} \right\}. \quad (2)$$

This kernel is physically motivated, with a free parameter representing the stellar rotation period (η_3), an exponential free parameter representing the characteristic evolution time of an activity region (η_2), a scale parameter representing the relative weights of the periodic and exponential decay components (η_4), and an amplitude (η_1).

For each system that meets the requirements for a GP fit, we initially trained the GP on non-detrended Everest photometry (rebinned to one point every 15 hours for computational tractability) to constrain the hyperparameters η_3 , η_4 , and η_2 , following [Grunblatt et al. \(2015\)](#). We imposed a Gaussian prior on η_4 centered at 0.5 and with $\sigma = 0.05$, following [López-Morales et al. \(2016\)](#), and uniform priors between 0 and the time range of the photometry (ending date minus beginning date) on the timescale parameters η_3 and η_2 . We used `george` ([Foreman-Mackey 2015](#)) and `emcee` ([Foreman-Mackey et al. 2013](#)) to produce posterior distributions of the photometric dataset modeled with GP regression. The posteriors on η_3 , η_4 , and η_2 were then used as priors on the same parameters in an orbit fit with GP regression using the same kernel, but with independent amplitude (η_1) parameters for each telescope contributing RV observations to the dataset. We use `radvel` ([Fulton et al. 2017](#)) to compute RV and GP posteriors. When performing a GP fit, we also held eccentricity for all planets fixed at 0 unless otherwise specified.

Other approaches to GP regression for RV orbit-fitting are explored in the literature (see, e.g. [Rajpaul et al. 2015](#), [Jones et al. 2017](#)). We chose to train the GPs presented in this work on photometry primarily because of the avail-

ability of complete, consistently derived photometric datasets.

4.2.3. MCMC Analyses

The procedure for fitting the above model to the observed RV data within RadVel is as follows. We first performed a maximum-a-posteriori (MAP) fit using Powell’s method (Powell 1964, as implemented in `scipy.optimize.minimize`, Virtanen et al. 2020). We then used the resulting solution to seed a Markov chain Monte Carlo (MCMC, as implemented in `emcee`, Foreman-Mackey et al. 2013) to estimate the full posterior distribution. We ran eight independent ensembles in parallel, each containing 50 walkers. We checked that the MCMC was “burned-in” by computing the Gelman-Rubin statistic (G-R, Gelman et al. 2003) and ensured that $G-R < 1.03$ for all free parameters. We saved up to 10,000 of the MCMC samples after this point or until we determined the chains were “well-mixed” ($G-R < 1.01$) and that the number of independent samples (T_z statistic, Ford 2006) is > 1000 for all free parameters for at least five consecutive checks. Once the MCMC was complete, a second MAP fit was run starting at the median values determined by the MCMC posteriors. This is the final MAP solution quoted alongside the posterior quantiles estimated from the MCMC chains.

We invoked a physical prior on the orbital eccentricity $e \in [0, 0.99]$. The RV semiamplitude is allowed to be negative, which while nonphysical eliminates the statistical bias that a $K > 0$ prior would introduce and cause us to overestimate the masses of planets detected at lower significance (Lucy & Sweeney 1971). For all transiting planets we adopted fixed values for the orbital period P and time of conjunction/time of mid-transit t_c . In all other cases we used uninformative priors.

4.2.4. Model Comparison

For each system we explored more complex models by re-running the fitting procedure with additional free parameters, namely including trends $(\gamma, \dot{\gamma})$ and eccentric orbits (e, ω) . For eccentric models we fit using the basis $(\sqrt{e} \cos \omega, \sqrt{e} \sin \omega)$ to improve the MCMC sampling efficiency and convergence (Fulton et al. 2018). For stars with high activity we also tested models that included a Gaussian Process (see Section 4.2.2 for more details). We selected between models based on the AIC statistic which estimates a goodness of fit while also penalizing models with more free parameters (Akaike 1974). We favored models with lower AIC values (better, simpler fit) to those with higher values (worse or overly-complex fit).

4.2.5. Searches for Additional Planets

For systems with more than 40 RVs, we conducted a search for additional planets using a periodogram analysis. See Fig. 12 for an example. In that figure, the black line shows the normalized difference in χ^2 for the adopted model (based on two transiting planets in this case) compared to a model with one additional planet, as a function of the orbital period of the additional planet. Model parameters for all planets not otherwise constrained were allowed to vary with each trial period for the additional planet, which was assumed to be in a circular orbit. The periodogram power $\Delta\chi^2/\chi^2$ was computed using the 2DKLS formalism of O’Toole et al. (2009). The threshold for detection of additional planets using the RVs was a 1% false alarm probability using the empirical method in Howard & Fulton (2016).

5. DISCUSSION

5.1. Summary of Results

Figure 5 shows the full distribution of planet masses and radii measured for all 81 transiting planets in our sample. These range from small, low-mass super-Earths, such as GJ 9827c (Sec. A.9) and K2-229b (Sec. A.14), to massive

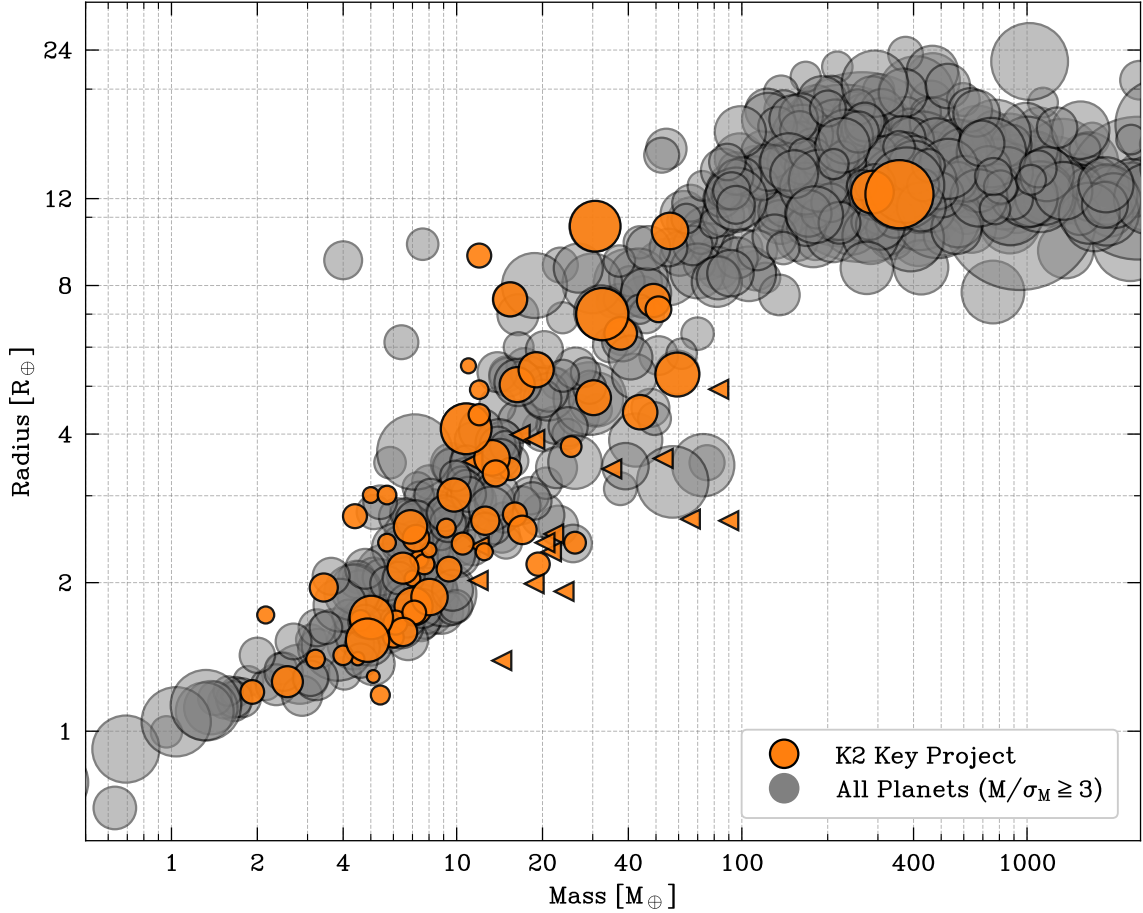


Figure 5. Mass-radius diagram for our full sample (orange circles, with triangles indicating 3σ upper mass limits) in the context of all known exoplanets with a $\geq 3\sigma$ mass measurements (NASA Exoplanet Archive, 2023/09/24). Point sizes are scaled so that more precise mass measurements have larger marker sizes. The sub-Neptune portion of this diagram is shown in Fig. 7.

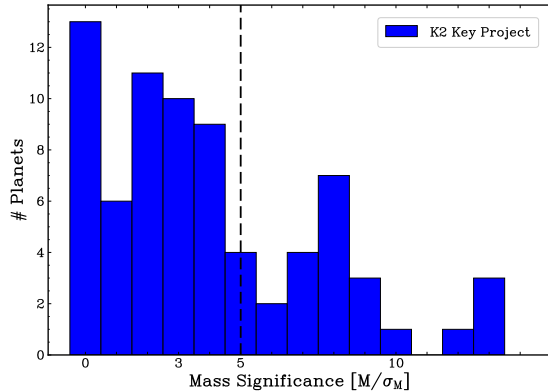


Figure 6. Mass significance (M_p/σ_{M_p}) for all planets in our sample. 32 planet masses are measured at $\geq 5\sigma$ (vertical dashed line), while 51 are measured at $\geq 3\sigma$.

WASP-47b (Sec. A.28). The masses of many of these planets are tightly constrained: from our RV analysis, 32 planet masses are measured at $\geq 5\sigma$ (vertical dashed line), while 51 are measured at $\geq 3\sigma$ (see Fig. 6).

By design, our sample mainly consists of sub-Neptune size planets. Of the 81 transiting planets in our sample with well-determined radii, 66 have $R_p < 4R_\oplus$. Fig. 7 shows the masses and radii of these small planets in the context of the known exoplanet population along with a Kernel Density Estimate (KDE) map, and reveals that our targets are generally representative of the sub-Neptune exoplanet population.

hot Jupiters, such as K2-99b (Sec. A.16) and

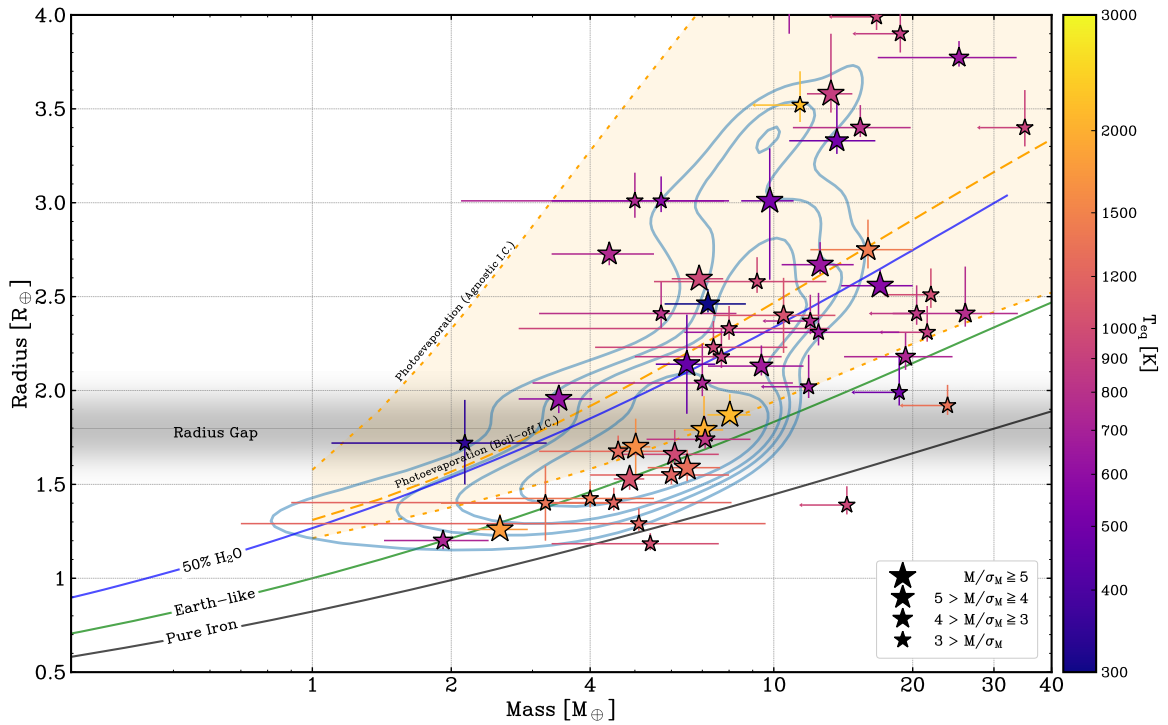


Figure 7. Our measured masses and radii for sub-Neptune-size planets. Points are color-coded based on the equilibrium temperatures of the planets, with marker size scaled so that more precise mass measurements have larger marker sizes; the lowest precision measurements are plotted as 3σ upper limits. The underlying blue contours represent a KDE analysis of all known exoplanets around FGK stars (NASA Exoplanet Archive, 2023/09/24). We also show composition tracks for three different bulk compositions (solid curves, from Zeng et al. 2019) as well as the photoevaporation limits (dashed/dotted curves) from Rogers et al. (2023).

Our final sample also includes five non-transiting planets that were thus not identified from the initial K2 photometry. These are HD 3167d (Sec. A.1), HIP 41378g (Sec. A.54), K2-73c (Sec. A.20), WASP-47c (Sec. A.28), and WASP-107c (Sec. A.21). Some systems also show evidence for likely long-term accelerations indicating additional, long-period bodies in the systems (cf. Bonomo et al. 2023a); these systems will be the subject of a follow-up paper (Rhem et al., in prep.).

5.2. Future Work

Large samples of planet masses and radii offer numerous opportunities for follow-up studies (Teske et al. 2021; Polanski et al. 2024). For example, one can attempt to measure the diversity of planet core mass and bulk composition using

interior structure models. Such efforts can attempt to measure the intrinsic spread of core compositions (and how many planet cores are approximately Earth-like), as well as to seek correlations between stellar properties such as mass or $[\text{Fe}/\text{H}]$ with estimated planet core mass.

Such data sets can also be used to examine how planet density varies with planet mass or radius (e.g. Luque & Pallé 2022), and how the super-Earth/mini-Neptune ‘radius valley’ (Fulton et al. 2017) manifests in planet mass or density. They can also be used to empirically determine parametric, probabilistic ‘mass-radius relations’ that demonstrate how planet mass can be predicted from planet radius (e.g., Wolfgang & Lopez 2015; Ning et al. 2018).

In addition, RV observations of these systems over long time baselines can reveal the presence

of massive, long-period companions on wide orbits. Since the RV observations presented here were mostly acquired from ~ 2015 – 2018 , just a few observations in the present day could reveal long-term accelerations or ‘trends.’ The detection of such RV trends can reveal new substellar companions suitable for high-contrast characterization (Crepp et al. 2014), and systematic analyses can constrain planet formation and migration via planetary system architectures (Bonomo et al. 2023b; Van Zandt et al. 2023). Though one initial study has already been done in this direction using K2 targets (Bonomo et al. 2023b), the target overlap is surprisingly small and so more work could still be done in this arena.

5.3. Conclusions

In summary, we have measured the masses, radii, and stellar & orbital properties of 86 planets orbiting 55 stars. All these targets were identified using custom transit-search analysis of data from NASA’s four-year *K2* mission, and masses were measured using Keck/HIRES radial velocity spectroscopy. Our sample includes:

- 55 targeted planetary systems, mostly around Sun-like stars but spanning a range of stellar parameters (Tables 1 and 2, and Figs. 3 and 2);
- 81 transiting planets with mass measurements (or constraints) from our analysis (Table 3, and Figs. 4 and 5);
- 5 non-transiting planets identified through our RV observations;
- 32 mass measurements at $\geq 5\sigma$ significance (51 at $>3\sigma$; Fig. 6);
- 66 planets with sizes $< 4R_{\oplus}$ (Fig. 7).

Our analysis presents newly-measured planet masses for a large sample of *K2* systems. In particular, we present mass measurements of $\geq 3\sigma$ significance for four systems that previously

lacked such measurements: K2-10 (Sec. A.40), K2-55 (Sec. A.52), K2-105 (Sec. A.24), and K2-121 (Sec. A.50). We also present other measurements that improve on the literature precision, but remain at the $2 - -3\sigma$ level, for three systems: K2-73 (Sec. A.20), K2-85 (Sec. A.3), and K2-277 (Sec. A.8). Finally, we present mass upper limits ($< 2\sigma$ mass precision), and thus conclusively rule out eclipsing-binary false-positive scenarios, for 12 systems that were candidates (or statistically validated as planets) but that lacked previous mass measurements: K2-37, K2-61, K2-62, K2-181, K2-189, K2-214, K2-220, EPIC 201357835, EPIC 202089657, EPIC 213546283, EPIC 245943455, and EPIC 245991048 (see individual sections in Appendix A).

Together with ongoing RV follow-up of transiting exoplanets discovered by *TESS* (Teske et al. 2021; Chontos et al. 2022; Crossfield et al. 2025, Armstrong et al., in review), our survey of *K2* planets continues to reveal new worlds suitable for future study. For example, multiple planets in our sample have already been observed by *HST* (GJ 9827, HD 3167, HD 106315, HIP 41378, K2-3 Roy et al. 2023; Mikal-Evans et al. 2021; Kreidberg et al. 2022; Diamond-Lowe et al. 2022) or are being observed by *JWST* (WASP-47e, GJ 9827d, HD 106315c). Between atmospheric spectroscopy, subsequent (long-term) RV monitoring, dynamical studies, and improved stellar parameters, our sample of planetary systems should enable intriguing new studies for many years to come.

The *K2* planet search described here was conducted over several years with contributions from dozens of astronomers. The target stars were selected and characterized by AOM, AWH, BB, BJF, EAP, ES, IJMC, JHL, JLC, JMB, and SL. Observing proposals were written by AWH, BB, BMSH, CDD, EAP, ES, HK, IJMC, JES, JLC, LAR, and TPG. The radial velocity ob-

serving program with HIRES was planned and coordinated by AWH, HI, and ES. HIRES observations were conducted by IA, CB, AB, SB, LGB, CLB, AC, IJMC, FD, PAD, BJF, SG, SKG, MLH, LAH, AWH, HI, MK, JAL, AWM, SMM, TM, JMAM, ASP, EAP, MR, LJR, RAR, ES, DT, JVZ, and LMW (those who observed K2 targets with HIRES for 10+ nights). High-resolution imaging and associated target vetting were done by DRC, EG, IJMC, JES, JRC, KHU, LAH, MW, and SBH. Analyses of the K2 light curves were conducted by JHL. Analyses of radial velocity measurements were conducted by SB, RAR, ES, and MK, and AWH. AWH, SB, RR, MK, IJMC, and ES wrote this paper.

The authors thank: the anonymous referee for comments that improved the quality of the paper; Dr. Thomas Greene for useful discussions during this project; and Drs. Johanna Teske and Michael Endl for help observing some of our targets.

The scope and extent of this project were enabled by NASA's Key Strategic Mission Support program that provided 40 nights at the W.M. Keck Observatory. We gratefully acknowledge their support throughout that program. We are grateful to the time assignment committees of NASA, the California Institute of Technology, the University of Hawai'i, and the University of California for their generous allocations of observing time. We thank additional observers who contributed to the RV measurements from the W.M. Keck Observatory. AWH acknowledges support for our K2 team through a NASA Astrophysics Data Analysis Program grant. AWH and IJMC acknowledge support from the K2 Guest Observer Program. LMW acknowledges support from the

NASA Exoplanet Research Program (grant no. 80NSSC23K0269). Some of the data presented in this paper were obtained from the Mikulski Archive for Space Telescopes (MAST). STScI is operated by the Association of Universities for Research in Astronomy, Inc., under NASA contract NAS5-26555. Support for MAST for non-HST data is provided by the NASA Office of Space Science via grant NNX09AF08G and by other grants and contracts. This research has also used the NASA Exoplanet Archive, operated by the California Institute of Technology, under contract with the National Aeronautics and Space Administration under the Exoplanet Exploration Program. This research has used the NASA/IPAC Infrared Science Archive, operated by the Jet Propulsion Laboratory, California Institute of Technology, under contract with the National Aeronautics and Space Administration. This research has used the NASA Exoplanet Follow-Up Observation Program website, operated by the California Institute of Technology, under contract with the National Aeronautics and Space Administration under the Exoplanet Exploration Program. Finally, we recognize and acknowledge the cultural role that the summit of Maunakea has within the indigenous Hawaiian community. We are grateful to conduct observations from this mountain.

Facility: Keck:I (HIRES), Keck:II (NIRC2), Kepler, Automated Planet Finder (Levy)

Software: RadVel (Fulton et al. 2018), emcee (Foreman-Mackey et al. 2013), isochrones (Morton 2015), acor (<https://github.com/dfm/acor>), Specmatch-Emp (Ye et al. 2017), isoclassify (Huber 2017) (Petigura et al. 2015), everest (Luger et al. 2016)

REFERENCES

- Adams, E. R., Jackson, B., & Endl, M. 2016, *AJ*, 152, 47, doi: [10.3847/0004-6256/152/2/47](https://doi.org/10.3847/0004-6256/152/2/47)
- Adams, E. R., Jackson, B., Endl, M., et al. 2017, *AJ*, 153, 82, doi: [10.3847/1538-3881/153/2/82](https://doi.org/10.3847/1538-3881/153/2/82)

- Aigrain, S., Parviainen, H., & Pope, B. J. S. 2016, *MNRAS*, 459, 2408, doi: [10.1093/mnras/stw706](https://doi.org/10.1093/mnras/stw706)
- Akaike, H. 1974, *IEEE Transactions on Automatic Control*, 19, 716, doi: [10.1109/TAC.1974.1100705](https://doi.org/10.1109/TAC.1974.1100705)
- Akana Murphy, J. M., Kosiarek, M. R., Batalha, N. M., et al. 2021, *AJ*, 162, 294, doi: [10.3847/1538-3881/ac2830](https://doi.org/10.3847/1538-3881/ac2830)
- Akinsanmi, B., Santos, N. C., Faria, J. P., et al. 2020, *A&A*, 635, L8, doi: [10.1051/0004-6361/202037618](https://doi.org/10.1051/0004-6361/202037618)
- Alam, M. K., Kirk, J., Dressing, C. D., et al. 2022, *ApJL*, 927, L5, doi: [10.3847/2041-8213/ac559d](https://doi.org/10.3847/2041-8213/ac559d)
- Almenara, J. M., Díaz, R. F., Bonfils, X., & Udry, S. 2016, *A&A*, 595, L5, doi: [10.1051/0004-6361/201629770](https://doi.org/10.1051/0004-6361/201629770)
- Almenara, J. M., Astudillo-Defru, N., Bonfils, X., et al. 2015, *A&A*, 581, L7, doi: [10.1051/0004-6361/201525918](https://doi.org/10.1051/0004-6361/201525918)
- Anderson, D. R., Collier Cameron, A., Delrez, L., et al. 2017, *A&A*, 604, A110, doi: [10.1051/0004-6361/201730439](https://doi.org/10.1051/0004-6361/201730439)
- Armstrong, D. J., Santerne, A., Veras, D., et al. 2015, *A&A*, 582, A33, doi: [10.1051/0004-6361/201526008](https://doi.org/10.1051/0004-6361/201526008)
- Barragán, O., Grziwa, S., Gandolfi, D., et al. 2016, *AJ*, 152, 193, doi: [10.3847/0004-6256/152/6/193](https://doi.org/10.3847/0004-6256/152/6/193)
- Barragán, O., Aigrain, S., Kubyskhina, D., et al. 2019, *Monthly Notices of the Royal Astronomical Society*, 490, 698, doi: [10.1093/mnras/stz2569](https://doi.org/10.1093/mnras/stz2569)
- Barros, S. C. C., Demangeon, O., & Deleuil, M. 2016, *A&A*, 594, A100, doi: [10.1051/0004-6361/201628902](https://doi.org/10.1051/0004-6361/201628902)
- Barros, S. C. C., Almenara, J. M., Demangeon, O., et al. 2015, *MNRAS*, 454, 4267, doi: [10.1093/mnras/stv2271](https://doi.org/10.1093/mnras/stv2271)
- Barros, S. C. C., Gosselin, H., Lillo-Box, J., et al. 2017, *A&A*, 608, A25, doi: [10.1051/0004-6361/201731276](https://doi.org/10.1051/0004-6361/201731276)
- Batalha, N. E., Lewis, T., Fortney, J. J., et al. 2019, *ApJL*, 885, L25, doi: [10.3847/2041-8213/ab4909](https://doi.org/10.3847/2041-8213/ab4909)
- Becker, J. C., Vanderburg, A., Adams, F. C., Rappaport, S. A., & Schwengeler, H. M. 2015, *ApJL*, 812, L18, doi: [10.1088/2041-8205/812/2/L18](https://doi.org/10.1088/2041-8205/812/2/L18)
- Becker, J. C., Vanderburg, A., Rodriguez, J. E., et al. 2018, *The Astronomical Journal*, 157, 19, doi: [10.3847/1538-3881/aaf0a2](https://doi.org/10.3847/1538-3881/aaf0a2)
- Beichman, C., Livingston, J., Werner, M., et al. 2016, *ApJ*, 822, 39, doi: [10.3847/0004-637X/822/1/39](https://doi.org/10.3847/0004-637X/822/1/39)
- Benneke, B., Werner, M., Petigura, E., et al. 2017, *ApJ*, 834, 187, doi: [10.3847/1538-4357/834/2/187](https://doi.org/10.3847/1538-4357/834/2/187)
- Benneke, B., Wong, I., Piaulet, C., et al. 2019, *ApJL*, 887, L14, doi: [10.3847/2041-8213/ab59dc](https://doi.org/10.3847/2041-8213/ab59dc)
- Berardo, D., Crossfield, I. J. M., Werner, M., et al. 2019, *The Astronomical Journal*, 157, 185, doi: [10.3847/1538-3881/ab100c](https://doi.org/10.3847/1538-3881/ab100c)
- Bessell, M. S., & Brett, J. M. 1988, *PASP*, 100, 1134, doi: [10.1086/132281](https://doi.org/10.1086/132281)
- Bonomo, A. S., Dumusque, X., Massa, A., et al. 2023a, *A&A*, 677, A33, doi: [10.1051/0004-6361/202346211](https://doi.org/10.1051/0004-6361/202346211)
- . 2023b, *A&A*, 677, A33, doi: [10.1051/0004-6361/202346211](https://doi.org/10.1051/0004-6361/202346211)
- Borsato, L., Malavolta, L., Piotto, G., et al. 2019, *Monthly Notices of the Royal Astronomical Society*, 484, 3233, doi: [10.1093/mnras/stz181](https://doi.org/10.1093/mnras/stz181)
- Borucki, W. J. 2017, *Proceedings of the American Philosophical Society*, 161, 38
- Bourrier, V., Deline, A., Krenn, A., et al. 2022, *A&A*, 668, A31, doi: [10.1051/0004-6361/202243778](https://doi.org/10.1051/0004-6361/202243778)
- Bourrier, V., Attia, O., Mallonn, M., et al. 2023, *A&A*, 669, A63, doi: [10.1051/0004-6361/202245004](https://doi.org/10.1051/0004-6361/202245004)
- Boyajian, T. S., von Braun, K., van Belle, G., et al. 2012, *ApJ*, 757, 112, doi: [10.1088/0004-637X/757/2/112](https://doi.org/10.1088/0004-637X/757/2/112)
- Brahm, R., Espinoza, N., Rabus, M., et al. 2019, *MNRAS*, 483, 1970, doi: [10.1093/mnras/sty3230](https://doi.org/10.1093/mnras/sty3230)
- Brewer, J. M., & Fischer, D. A. 2018, *ApJS*, 237, 38, doi: [10.3847/1538-4365/aad501](https://doi.org/10.3847/1538-4365/aad501)
- Brewer, J. M., Fischer, D. A., Basu, S., Valenti, J. A., & Piskunov, N. 2015, *ApJ*, 805, 126, doi: [10.1088/0004-637X/805/2/126](https://doi.org/10.1088/0004-637X/805/2/126)
- Brewer, J. M., Fischer, D. A., Valenti, J. A., & Piskunov, N. 2016, *ApJS*, 225, 32, doi: [10.3847/0067-0049/225/2/32](https://doi.org/10.3847/0067-0049/225/2/32)
- Bryant, E. M., & Bayliss, D. 2022, *AJ*, 163, 197, doi: [10.3847/1538-3881/ac58ff](https://doi.org/10.3847/1538-3881/ac58ff)
- Butler, R. P., Marcy, G. W., Williams, E., et al. 1996, *PASP*, 108, 500, doi: [10.1086/133755](https://doi.org/10.1086/133755)
- Chakraborty, A., Roy, A., Sharma, R., et al. 2018, *ArXiv e-prints*. <https://arxiv.org/abs/1805.03466>

- Chontos, A., Murphy, J. M. A., MacDougall, M. G., et al. 2022, *AJ*, 163, 297, doi: [10.3847/1538-3881/ac6266](https://doi.org/10.3847/1538-3881/ac6266)
- Christiansen, J. L., Vanderburg, A., Burt, J., et al. 2017, *AJ*, 154, 122, doi: [10.3847/1538-3881/aa832d](https://doi.org/10.3847/1538-3881/aa832d)
- Christiansen, J. L., Bhure, S., Zink, J. K., et al. 2022, *AJ*, 163, 244, doi: [10.3847/1538-3881/ac5c4c](https://doi.org/10.3847/1538-3881/ac5c4c)
- Christiansen, J. L., Zink, J. K., Hardegree-Ullman, K. K., et al. 2023, *AJ*, 166, 248, doi: [10.3847/1538-3881/acf9f9](https://doi.org/10.3847/1538-3881/acf9f9)
- Claret, A., Hauschildt, P. H., & Witte, S. 2012, *VizieR Online Data Catalog*, J/A+A/546/A14
- Cloutier, R., Astudillo-Defru, N., Doyon, R., et al. 2017, *A&A*, 608, A35, doi: [10.1051/0004-6361/201731558](https://doi.org/10.1051/0004-6361/201731558)
- . 2019, *A&A*, 621, A49, doi: [10.1051/0004-6361/201833995](https://doi.org/10.1051/0004-6361/201833995)
- Collier Cameron, A., Wilson, D. M., West, R. G., et al. 2007, *MNRAS*, 380, 1230, doi: [10.1111/j.1365-2966.2007.12195.x](https://doi.org/10.1111/j.1365-2966.2007.12195.x)
- Crepp, J. R., Johnson, J. A., Howard, A. W., et al. 2014, *ApJ*, 781, 29, doi: [10.1088/0004-637X/781/1/29](https://doi.org/10.1088/0004-637X/781/1/29)
- Crossfield, I. J. M., Petigura, E., Schlieder, J. E., et al. 2015, *ApJ*, 804, 10, doi: [10.1088/0004-637X/804/1/10](https://doi.org/10.1088/0004-637X/804/1/10)
- Crossfield, I. J. M., Ciardi, D. R., Petigura, E. A., et al. 2016, *ApJS*, 226, 7, doi: [10.3847/0067-0049/226/1/7](https://doi.org/10.3847/0067-0049/226/1/7)
- Crossfield, I. J. M., Ciardi, D. R., Isaacson, H., et al. 2017, *AJ*, 153, 255, doi: [10.3847/1538-3881/aa6e01](https://doi.org/10.3847/1538-3881/aa6e01)
- Crossfield, I. J. M., Guerrero, N., David, T., et al. 2018, *ApJS*, 239, 5, doi: [10.3847/1538-4365/aae155](https://doi.org/10.3847/1538-4365/aae155)
- Crossfield, I. J. M., Polanski, A. S., Robertson, P., et al. 2025, *AJ*, 169, 89, doi: [10.3847/1538-3881/ad9aa6](https://doi.org/10.3847/1538-3881/ad9aa6)
- Dai, F., Masuda, K., Winn, J. N., & Zeng, L. 2019, *ApJ*, 883, 79, doi: [10.3847/1538-4357/ab3a3b](https://doi.org/10.3847/1538-4357/ab3a3b)
- Dai, F., & Winn, J. N. 2017, *AJ*, 153, 205, doi: [10.3847/1538-3881/aa65d1](https://doi.org/10.3847/1538-3881/aa65d1)
- Dai, F., Winn, J. N., Arriagada, P., et al. 2015, *ApJL*, 813, L9, doi: [10.1088/2041-8205/813/1/L9](https://doi.org/10.1088/2041-8205/813/1/L9)
- Dai, F., Winn, J. N., Albrecht, S., et al. 2016, *ApJ*, 823, 115, doi: [10.3847/0004-637X/823/2/115](https://doi.org/10.3847/0004-637X/823/2/115)
- Dalal, S., Hébrard, G., Lecavelier des Étangs, A., et al. 2019, *A&A*, 631, A28, doi: [10.1051/0004-6361/201935944](https://doi.org/10.1051/0004-6361/201935944)
- Damasso, M., Bonomo, A. S., Astudillo-Defru, N., et al. 2018, *ArXiv e-prints*, <https://arxiv.org/abs/1802.08320>
- Damasso, M., Zeng, L., Malavolta, L., et al. 2019, *A&A*, 624, A38, doi: [10.1051/0004-6361/201834671](https://doi.org/10.1051/0004-6361/201834671)
- Dattilo, A., Vanderburg, A., Shallue, C. J., et al. 2019, *AJ*, 157, 169, doi: [10.3847/1538-3881/ab0e12](https://doi.org/10.3847/1538-3881/ab0e12)
- Diamond-Lowe, H., Kreidberg, L., Harman, C. E., et al. 2022, *AJ*, 164, 172, doi: [10.3847/1538-3881/ac7807](https://doi.org/10.3847/1538-3881/ac7807)
- dos Santos, L. A., Ehrenreich, D., Bourrier, V., et al. 2020, *A&A*, 634, L4, doi: [10.1051/0004-6361/201937327](https://doi.org/10.1051/0004-6361/201937327)
- Doyle, L. R., Carter, J. A., Fabrycky, D. C., et al. 2011, *Science*, 333, 1602, doi: [10.1126/science.1210923](https://doi.org/10.1126/science.1210923)
- Dressing, C. D., Newton, E. R., Schlieder, J. E., et al. 2017, *The Astrophysical Journal*, 836, 167, doi: [10.3847/1538-4357/836/2/167](https://doi.org/10.3847/1538-4357/836/2/167)
- Dressing, C. D., Sinukoff, E., Fulton, B. J., et al. 2018, *AJ*, 156, 70, doi: [10.3847/1538-3881/aacf99](https://doi.org/10.3847/1538-3881/aacf99)
- Dressing, C. D., Hardegree-Ullman, K., Schlieder, J. E., et al. 2019, *AJ*, 158, 87, doi: [10.3847/1538-3881/ab2895](https://doi.org/10.3847/1538-3881/ab2895)
- Fang, J., & Margot, J.-L. 2012, *ApJ*, 761, 92, doi: [10.1088/0004-637X/761/2/92](https://doi.org/10.1088/0004-637X/761/2/92)
- Ford, E. B. 2006, *ApJ*, 642, 505, doi: [10.1086/500802](https://doi.org/10.1086/500802)
- Foreman-Mackey, D. 2015, *George: Gaussian Process regression*. <http://ascl.net/1511.015>
- Foreman-Mackey, D., Hogg, D. W., Lang, D., & Goodman, J. 2013, *PASP*, 125, 306, doi: [10.1086/670067](https://doi.org/10.1086/670067)
- Foreman-Mackey, D., Montet, B. T., Hogg, D. W., et al. 2015, *ApJ*, 806, 215, doi: [10.1088/0004-637X/806/2/215](https://doi.org/10.1088/0004-637X/806/2/215)
- Fortney, J. J., Marley, M. S., & Barnes, J. W. 2007, *ApJ*, 659, 1661, doi: [10.1086/512120](https://doi.org/10.1086/512120)
- Fridlund, M., Gaidos, E., Barragán, O., et al. 2017, *A&A*, 604, A16, doi: [10.1051/0004-6361/201730822](https://doi.org/10.1051/0004-6361/201730822)

- Fukui, A., Livingston, J., Narita, N., et al. 2016, *AJ*, 152, 171, doi: [10.3847/0004-6256/152/6/171](https://doi.org/10.3847/0004-6256/152/6/171)
- Fulton, B. J., & Petigura, E. A. 2018, *AJ*, 156, 264, doi: [10.3847/1538-3881/aae828](https://doi.org/10.3847/1538-3881/aae828)
- Fulton, B. J., Petigura, E. A., Blunt, S., & Sinukoff, E. 2018, *PASP*, 130, 044504, doi: [10.1088/1538-3873/aaaaa8](https://doi.org/10.1088/1538-3873/aaaaa8)
- Fulton, B. J., Weiss, L. M., Sinukoff, E., et al. 2015, *ApJ*, 805, 175, doi: [10.1088/0004-637X/805/2/175](https://doi.org/10.1088/0004-637X/805/2/175)
- Fulton, B. J., Petigura, E. A., Howard, A. W., et al. 2017, *AJ*, 154, 109, doi: [10.3847/1538-3881/aa80eb](https://doi.org/10.3847/1538-3881/aa80eb)
- Gaia Collaboration, Brown, A. G. A., Vallenari, A., et al. 2018, *A&A*, 616, A1, doi: [10.1051/0004-6361/201833051](https://doi.org/10.1051/0004-6361/201833051)
- Gandolfi, D., Barragán, O., Hatzes, A. P., et al. 2017, *AJ*, 154, 123, doi: [10.3847/1538-3881/aa832a](https://doi.org/10.3847/1538-3881/aa832a)
- Gelman, A., Carlin, J. B., Stern, H. S., & Rubin, D. B. 2003, *Bayesian Data Analysis*, 2nd edn. (Chapman and Hall)
- Ginzburg, S., Schlichting, H. E., & Sari, R. 2018, *MNRAS*, 476, 759, doi: [10.1093/mnras/sty290](https://doi.org/10.1093/mnras/sty290)
- Grunblatt, S. K., Howard, A. W., & Haywood, R. D. 2015, *ApJ*, 808, 127, doi: [10.1088/0004-637X/808/2/127](https://doi.org/10.1088/0004-637X/808/2/127)
- Grzywa, S., Gandolfi, D., Csizmadia, S., et al. 2016, *AJ*, 152, 132, doi: [10.3847/0004-6256/152/5/132](https://doi.org/10.3847/0004-6256/152/5/132)
- Guenther, E. W., Goffo, E., Sebastian, D., et al. 2024, arXiv e-prints, arXiv:2402.09322, doi: [10.48550/arXiv.2402.09322](https://doi.org/10.48550/arXiv.2402.09322)
- Guenther, E. W., Barragán, O., Dai, F., et al. 2017, *A&A*, 608, A93, doi: [10.1051/0004-6361/201730885](https://doi.org/10.1051/0004-6361/201730885)
- Guerrero, N. M., Seager, S., Huang, C. X., et al. 2021, *ApJS*, 254, 39, doi: [10.3847/1538-4365/abefe1](https://doi.org/10.3847/1538-4365/abefe1)
- Guilluy, G., Bourrier, V., Jaziri, Y., et al. 2023, *A&A*, 676, A130, doi: [10.1051/0004-6361/202346419](https://doi.org/10.1051/0004-6361/202346419)
- Gupta, A., & Schlichting, H. E. 2019, *MNRAS*, 487, 24, doi: [10.1093/mnras/stz1230](https://doi.org/10.1093/mnras/stz1230)
- Hardegree-Ullman, K. K., Zink, J. K., Christiansen, J. L., et al. 2020, *ApJS*, 247, 28, doi: [10.3847/1538-4365/ab7230](https://doi.org/10.3847/1538-4365/ab7230)
- Haywood, R. D., Collier Cameron, A., Queloz, D., et al. 2014, *MNRAS*, 443, 2517, doi: [10.1093/mnras/stu1320](https://doi.org/10.1093/mnras/stu1320)
- Hejazi, N., Crossfield, I. J. M., Nordlander, T., et al. 2023, *ApJ*, 949, 79, doi: [10.3847/1538-4357/accb97](https://doi.org/10.3847/1538-4357/accb97)
- Heller, R., Rodenbeck, Kai, & Hippke, Michael. 2019, *A&A*, 625, A31, doi: [10.1051/0004-6361/201935276](https://doi.org/10.1051/0004-6361/201935276)
- Hellier, C., Anderson, D. R., Collier Cameron, A., et al. 2012, *MNRAS*, 426, 739, doi: [10.1111/j.1365-2966.2012.21780.x](https://doi.org/10.1111/j.1365-2966.2012.21780.x)
- Howard, A. W., & Fulton, B. J. 2016, *Publications of the Astronomical Society of the Pacific*, 128, 114401, doi: [10.1088/1538-3873/128/969/114401](https://doi.org/10.1088/1538-3873/128/969/114401)
- Howard, A. W., Marcy, G. W., Johnson, J. A., et al. 2010a, *Science*, 330, 653, doi: [10.1126/science.1194854](https://doi.org/10.1126/science.1194854)
- Howard, A. W., Johnson, J. A., Marcy, G. W., et al. 2010b, *ApJ*, 721, 1467, doi: [10.1088/0004-637X/721/2/1467](https://doi.org/10.1088/0004-637X/721/2/1467)
- Howard, A. W., Marcy, G. W., Bryson, S. T., et al. 2012, *ApJS*, 201, 15, doi: [10.1088/0067-0049/201/2/15](https://doi.org/10.1088/0067-0049/201/2/15)
- Howe, A. R., & Burrows, A. 2015, *ApJ*, 808, 150, doi: [10.1088/0004-637X/808/2/150](https://doi.org/10.1088/0004-637X/808/2/150)
- Howell, S. B., Sobeck, C., Haas, M., et al. 2014, *PASP*, 126, 398, doi: [10.1086/676406](https://doi.org/10.1086/676406)
- Huber, D. 2017, *Isoclassify: V1.2, v1.2*, Zenodo, doi: [10.5281/zenodo.573372](https://doi.org/10.5281/zenodo.573372)
- Isaacson, H., & Fischer, D. 2010, *ApJ*, 725, 875, doi: [10.1088/0004-637X/725/1/875](https://doi.org/10.1088/0004-637X/725/1/875)
- Jin, S., & Mordasini, C. 2018, *ApJ*, 853, 163, doi: [10.3847/1538-4357/aa9f1e](https://doi.org/10.3847/1538-4357/aa9f1e)
- Johnson, M. C., Dai, F., Justesen, A. B., et al. 2018, *MNRAS*, 481, 596, doi: [10.1093/mnras/sty2238](https://doi.org/10.1093/mnras/sty2238)
- Jones, D. E., Stenning, D. C., Ford, E. B., et al. 2017, arXiv e-prints, arXiv:1711.01318. <https://arxiv.org/abs/1711.01318>
- JWST Transiting Exoplanet Community Early Release Science Team, Ahrer, E.-M., Alderson, L., et al. 2023, *Nature*, 614, 649, doi: [10.1038/s41586-022-05269-w](https://doi.org/10.1038/s41586-022-05269-w)
- Kane, S. R., Fetherolf, T., & Hill, M. L. 2020, *AJ*, 159, 176, doi: [10.3847/1538-3881/ab7818](https://doi.org/10.3847/1538-3881/ab7818)
- Kanodia, S., Wolfgang, A., Stefansson, G. K., Ning, B., & Mahadevan, S. 2019, *ApJ*, 882, 38, doi: [10.3847/1538-4357/ab334c](https://doi.org/10.3847/1538-4357/ab334c)
- Kipping, D. M. 2013, *MNRAS*, 435, 2152, doi: [10.1093/mnras/stt1435](https://doi.org/10.1093/mnras/stt1435)

- Korth, J., Csizmadia, S., Gandolfi, D., et al. 2019, *MNRAS*, 482, 1807, doi: [10.1093/mnras/sty2760](https://doi.org/10.1093/mnras/sty2760)
- Kosiarek, M. R., & Crossfield, I. J. M. 2020, *AJ*, 159, 271, doi: [10.3847/1538-3881/ab8d3a](https://doi.org/10.3847/1538-3881/ab8d3a)
- Kosiarek, M. R., Blunt, S., López-Morales, M., et al. 2019a, *AJ*, 157, 116, doi: [10.3847/1538-3881/aafe83](https://doi.org/10.3847/1538-3881/aafe83)
- Kosiarek, M. R., Crossfield, I. J. M., Hardegree-Ullman, K. K., et al. 2019b, *AJ*, 157, 97, doi: [10.3847/1538-3881/aaf79c](https://doi.org/10.3847/1538-3881/aaf79c)
- Kosiarek, M. R., Berardo, D. A., Crossfield, I. J. M., et al. 2021, *AJ*, 161, 47, doi: [10.3847/1538-3881/abca39](https://doi.org/10.3847/1538-3881/abca39)
- Kostov, V. B., Mullally, S. E., Quintana, E. V., et al. 2019, *AJ*, 157, 124, doi: [10.3847/1538-3881/ab0110](https://doi.org/10.3847/1538-3881/ab0110)
- Kraus, A. L., & Hillenbrand, L. A. 2007a, *AJ*, 134, 2340, doi: [10.1086/522831](https://doi.org/10.1086/522831)
- . 2007b, *AJ*, 134, 2340, doi: [10.1086/522831](https://doi.org/10.1086/522831)
- Kreidberg, L. 2015, *PASP*, 127, 1161, doi: [10.1086/683602](https://doi.org/10.1086/683602)
- Kreidberg, L., Line, M. R., Thorngren, D., Morley, C. V., & Stevenson, K. B. 2018, *ApJL*, 858, L6, doi: [10.3847/2041-8213/aabf3e](https://doi.org/10.3847/2041-8213/aabf3e)
- Kreidberg, L., Mollière, P., Crossfield, I. J. M., et al. 2022, *AJ*, 164, 124, doi: [10.3847/1538-3881/ac85be](https://doi.org/10.3847/1538-3881/ac85be)
- Kruse, E., Agol, E., Luger, R., & Foreman-Mackey, D. 2019, *ApJS*, 244, 11, doi: [10.3847/1538-4365/ab346b](https://doi.org/10.3847/1538-4365/ab346b)
- Lam, K. W. F., Santerne, A., Sousa, S. G., et al. 2018, *A&A*, 620, A77, doi: [10.1051/0004-6361/201834073](https://doi.org/10.1051/0004-6361/201834073)
- Lehmer, O. R., & Catling, D. C. 2017, *ApJ*, 845, 130, doi: [10.3847/1538-4357/aa8137](https://doi.org/10.3847/1538-4357/aa8137)
- Lépine, S., & Shara, M. M. 2005, *AJ*, 129, 1483, doi: [10.1086/427854](https://doi.org/10.1086/427854)
- Lillo-Box, J., Lopez, T. A., Santerne, A., et al. 2020, *A&A*, 640, A48, doi: [10.1051/0004-6361/202037896](https://doi.org/10.1051/0004-6361/202037896)
- Lissauer, J. J., & Eisberg, J. 2018, *NewAR*, 83, 1, doi: [10.1016/j.newar.2019.04.002](https://doi.org/10.1016/j.newar.2019.04.002)
- Lissauer, J. J., Ragozzine, D., Fabrycky, D. C., et al. 2011, *ApJS*, 197, 8, doi: [10.1088/0067-0049/197/1/8](https://doi.org/10.1088/0067-0049/197/1/8)
- Livingston, J. H., Crossfield, I. J. M., Petigura, E. A., et al. 2018, *The Astronomical Journal*, 156, 277, doi: [10.3847/1538-3881/aae778](https://doi.org/10.3847/1538-3881/aae778)
- Livingston, J. H., Endl, M., Dai, F., et al. 2018, *AJ*, 156, 78, doi: [10.3847/1538-3881/aaccde](https://doi.org/10.3847/1538-3881/aaccde)
- Lopez, E. D., & Fortney, J. J. 2014, *ApJ*, 792, 1, doi: [10.1088/0004-637X/792/1/1](https://doi.org/10.1088/0004-637X/792/1/1)
- Lopez, E. D., Fortney, J. J., & Miller, N. 2012, *ApJ*, 761, 59, doi: [10.1088/0004-637X/761/1/59](https://doi.org/10.1088/0004-637X/761/1/59)
- López-Morales, M., Haywood, R. D., Coughlin, J. L., et al. 2016, *AJ*, 152, 204, doi: [10.3847/0004-6256/152/6/204](https://doi.org/10.3847/0004-6256/152/6/204)
- Lucy, L. B., & Sweeney, M. A. 1971, *AJ*, 76, 544, doi: [10.1086/111159](https://doi.org/10.1086/111159)
- Luger, R., Agol, E., Kruse, E., et al. 2016, *AJ*, 152, 100, doi: [10.3847/0004-6256/152/4/100](https://doi.org/10.3847/0004-6256/152/4/100)
- Luque, R., & Pallé, E. 2022, *Science*, 377, 1211, doi: [10.1126/science.abl7164](https://doi.org/10.1126/science.abl7164)
- Madhusudhan, N., Nixon, M. C., Welbanks, L., Piette, A. A. A., & Booth, R. A. 2020, *ApJL*, 891, L7, doi: [10.3847/2041-8213/ab7229](https://doi.org/10.3847/2041-8213/ab7229)
- Madhusudhan, N., Sarkar, S., Constantinou, S., et al. 2023, *ApJL*, 956, L13, doi: [10.3847/2041-8213/acf577](https://doi.org/10.3847/2041-8213/acf577)
- Malavolta, L., Borsato, L., Granata, V., et al. 2017, *The Astronomical Journal*, 153, 224, doi: [10.3847/1538-3881/aa6897](https://doi.org/10.3847/1538-3881/aa6897)
- Mann, A. W., Gaidos, E., Vanderburg, A., et al. 2017, *AJ*, 153, 64, doi: [10.1088/1361-6528/aa5276](https://doi.org/10.1088/1361-6528/aa5276)
- Marcy, G. W., & Butler, R. P. 1992, *PASP*, 104, 270, doi: [10.1086/132989](https://doi.org/10.1086/132989)
- Marcy, G. W., Isaacson, H., Howard, A. W., et al. 2014, *ApJS*, 210, 20, doi: [10.1088/0067-0049/210/2/20](https://doi.org/10.1088/0067-0049/210/2/20)
- Martinez, A. O., Crossfield, I. J. M., Schlieder, J. E., et al. 2017, *ApJ*, 837, 72, doi: [10.3847/1538-4357/aa56c7](https://doi.org/10.3847/1538-4357/aa56c7)
- Masuda, K. 2014, *ApJ*, 783, 53, doi: [10.1088/0004-637X/783/1/53](https://doi.org/10.1088/0004-637X/783/1/53)
- Mayo, A. W., Vanderburg, A., Latham, D. W., et al. 2018, *AJ*, 155, 136, doi: [10.3847/1538-3881/aaadff](https://doi.org/10.3847/1538-3881/aaadff)
- Mayor, M., Marmier, M., Lovis, C., et al. 2011, *arXiv e-prints*, arXiv:1109.2497. <https://arxiv.org/abs/1109.2497>
- Mikal-Evans, T., Crossfield, I. J. M., Benneke, B., et al. 2021, *AJ*, 161, 18, doi: [10.3847/1538-3881/abc874](https://doi.org/10.3847/1538-3881/abc874)
- Mills, S. M., Howard, A. W., Petigura, E. A., et al. 2019, *AJ*, 157, 198, doi: [10.3847/1538-3881/ab1009](https://doi.org/10.3847/1538-3881/ab1009)
- Montet, B. T., Morton, T. D., Foreman-Mackey, D., et al. 2015, *ApJ*, 809, 25, doi: [10.1088/0004-637X/809/1/25](https://doi.org/10.1088/0004-637X/809/1/25)

- Mortier, A., Zapatero Osorio, M. R., Malavolta, L., et al. 2020, *MNRAS*, 499, 5004, doi: [10.1093/mnras/staa3144](https://doi.org/10.1093/mnras/staa3144)
- Morton, T. D. 2015, isochrones: Stellar model grid package, Astrophysics Source Code Library. <http://ascl.net/1503.010>
- Narita, N., Hirano, T., Fukui, A., et al. 2015, *ApJ*, 815, 47, doi: [10.1088/0004-637X/815/1/47](https://doi.org/10.1088/0004-637X/815/1/47)
- . 2017, *PASJ*, 69, 29, doi: [10.1093/pasj/psx002](https://doi.org/10.1093/pasj/psx002)
- Nava, C., López-Morales, M., Mortier, A., et al. 2022, *AJ*, 163, 41, doi: [10.3847/1538-3881/ac3141](https://doi.org/10.3847/1538-3881/ac3141)
- Nespral, D., Gandolfi, D., Deeg, H. J., et al. 2017, *A&A*, 601, A128, doi: [10.1051/0004-6361/201628639](https://doi.org/10.1051/0004-6361/201628639)
- Neveu-VanMalle, M., Queloz, D., Anderson, D. R., et al. 2016, *A&A*, 586, A93, doi: [10.1051/0004-6361/201526965](https://doi.org/10.1051/0004-6361/201526965)
- Newville, M., Stensitzki, T., Allen, D. B., & Ingargiola, A. 2014, LMFIT: Non-Linear Least-Square Minimization and Curve-Fitting for Python, doi: [10.5281/zenodo.11813](https://doi.org/10.5281/zenodo.11813)
- Ning, B., Wolfgang, A., & Ghosh, S. 2018, *ApJ*, 869, 5, doi: [10.3847/1538-4357/aaeb31](https://doi.org/10.3847/1538-4357/aaeb31)
- Niraula, P., Redfield, S., Dai, F., et al. 2017, *AJ*, 154, 266, doi: [10.3847/1538-3881/aa957c](https://doi.org/10.3847/1538-3881/aa957c)
- Nowak, G., Palle, E., Gandolfi, D., et al. 2020, *MNRAS*, 497, 4423, doi: [10.1093/mnras/staa2077](https://doi.org/10.1093/mnras/staa2077)
- Osborn, H. P., Santerne, A., Barros, S. C. C., et al. 2017, *A&A*, 604, A19, doi: [10.1051/0004-6361/201628932](https://doi.org/10.1051/0004-6361/201628932)
- O’Toole, S. J., Tinney, C. G., Jones, H. R. A., et al. 2009, *MNRAS*, 392, 641, doi: [10.1111/j.1365-2966.2008.14051.x](https://doi.org/10.1111/j.1365-2966.2008.14051.x)
- Owen, J. E., & Wu, Y. 2013, *ApJ*, 775, 105, doi: [10.1088/0004-637X/775/2/105](https://doi.org/10.1088/0004-637X/775/2/105)
- . 2016, *ApJ*, 817, 107, doi: [10.3847/0004-637X/817/2/107](https://doi.org/10.3847/0004-637X/817/2/107)
- . 2017, *ApJ*, 847, 29, doi: [10.3847/1538-4357/aa890a](https://doi.org/10.3847/1538-4357/aa890a)
- Passegger, V. M., Suárez Mascareño, A., Allart, R., et al. 2024, arXiv e-prints, arXiv:2401.06276, doi: [10.48550/arXiv.2401.06276](https://doi.org/10.48550/arXiv.2401.06276)
- Pecaut, M. J., & Mamajek, E. E. 2013, *ApJS*, 208, 9, doi: [10.1088/0067-0049/208/1/9](https://doi.org/10.1088/0067-0049/208/1/9)
- Persson, C. M., Fridlund, M., Barragán, O., et al. 2018, ArXiv e-prints. <https://arxiv.org/abs/1805.04774>
- Petigura, E. A. 2015, ArXiv e-prints. <https://arxiv.org/abs/1510.03902>
- Petigura, E. A., Howard, A. W., & Marcy, G. W. 2013, *Proceedings of the National Academy of Science*, 110, 19273, doi: [10.1073/pnas.1319909110](https://doi.org/10.1073/pnas.1319909110)
- Petigura, E. A., Schlieder, J. E., Crossfield, I. J. M., et al. 2015, *ApJ*, 811, 102, doi: [10.1088/0004-637X/811/2/102](https://doi.org/10.1088/0004-637X/811/2/102)
- Petigura, E. A., Howard, A. W., Lopez, E. D., et al. 2016, *ApJ*, 818, 36, doi: [10.3847/0004-637X/818/1/36](https://doi.org/10.3847/0004-637X/818/1/36)
- Petigura, E. A., Howard, A. W., Marcy, G. W., et al. 2017a, *AJ*, 154, 107, doi: [10.3847/1538-3881/aa80de](https://doi.org/10.3847/1538-3881/aa80de)
- Petigura, E. A., Sinukoff, E., Lopez, E. D., et al. 2017b, *AJ*, 153, 142, doi: [10.3847/1538-3881/aa5ea5](https://doi.org/10.3847/1538-3881/aa5ea5)
- Petigura, E. A., Crossfield, I. J. M., Isaacson, H., et al. 2018a, *AJ*, 155, 21, doi: [10.3847/1538-3881/aa9b83](https://doi.org/10.3847/1538-3881/aa9b83)
- Petigura, E. A., Benneke, B., Batygin, K., et al. 2018b, *AJ*, 156, 89, doi: [10.3847/1538-3881/aaceac](https://doi.org/10.3847/1538-3881/aaceac)
- Petigura, E. A., Livingston, J., Batygin, K., et al. 2020, *AJ*, 159, 2, doi: [10.3847/1538-3881/ab5220](https://doi.org/10.3847/1538-3881/ab5220)
- Piaulet, C., Benneke, B., Rubenzahl, R. A., et al. 2021, *ApJ*, 161, 70, doi: [10.3847/1538-3881/abcd3c](https://doi.org/10.3847/1538-3881/abcd3c)
- Polanski, A. S., Lubin, J., Beard, C., et al. 2024, *ApJS*, 272, 32, doi: [10.3847/1538-4365/ad4484](https://doi.org/10.3847/1538-4365/ad4484)
- Pope, B. J. S., Parviainen, H., & Aigrain, S. 2016, *MNRAS*, 461, 3399, doi: [10.1093/mnras/stw1373](https://doi.org/10.1093/mnras/stw1373)
- Powell, M. J. D. 1964, *The Computer Journal*, 7, 155, doi: [10.1093/comjnl/7.2.155](https://doi.org/10.1093/comjnl/7.2.155)
- Prieto-Arranz, J., Palle, E., Gandolfi, D., et al. 2018, *A&A*, 618, A116, doi: [10.1051/0004-6361/201832872](https://doi.org/10.1051/0004-6361/201832872)
- Radica, M., Artigau, É., Lafrenière, D., et al. 2022, *MNRAS*, 517, 5050, doi: [10.1093/mnras/stac3024](https://doi.org/10.1093/mnras/stac3024)
- Rajpaul, V., Aigrain, S., Osborne, M. A., Reece, S., & Roberts, S. 2015, *MNRAS*, 452, 2269, doi: [10.1093/mnras/stv1428](https://doi.org/10.1093/mnras/stv1428)
- Rice, K., Malavolta, L., Mayo, A., et al. 2019, *MNRAS*, 484, 3731, doi: [10.1093/mnras/stz130](https://doi.org/10.1093/mnras/stz130)

- Ricker, G. R., Winn, J. N., Vanderspek, R., et al. 2015, *Journal of Astronomical Telescopes, Instruments, and Systems*, 1, 014003, doi: [10.1117/1.JATIS.1.1.014003](https://doi.org/10.1117/1.JATIS.1.1.014003)
- Ricker, G. R., Vanderspek, R., Winn, J., et al. 2016, in *Society of Photo-Optical Instrumentation Engineers (SPIE) Conference Series*, Vol. 9904, *Space Telescopes and Instrumentation 2016: Optical, Infrared, and Millimeter Wave*, ed. H. A. MacEwen, G. G. Fazio, M. Lystrup, N. Batalha, N. Siegler, & E. C. Tong, 99042B, doi: [10.1117/12.2232071](https://doi.org/10.1117/12.2232071)
- Rizzuto, A. C., Mann, A. W., Vanderburg, A., Kraus, A. L., & Covey, K. R. 2017, *AJ*, 154, 224, doi: [10.3847/1538-3881/aa9070](https://doi.org/10.3847/1538-3881/aa9070)
- Rodriguez, D. R., Zuckerman, B., Kastner, J. H., et al. 2013, *ApJ*, 774, 101, doi: [10.1088/0004-637X/774/2/101](https://doi.org/10.1088/0004-637X/774/2/101)
- Rodriguez, J. E., Vanderburg, A., Eastman, J. D., et al. 2018, *AJ*, 155, 72, doi: [10.3847/1538-3881/aaa292](https://doi.org/10.3847/1538-3881/aaa292)
- Rodriguez, J. E., Zhou, G., Vanderburg, A., et al. 2017, *AJ*, 153, 256, doi: [10.3847/1538-3881/aa6dfb](https://doi.org/10.3847/1538-3881/aa6dfb)
- Rodríguez Martínez, R., Gaudi, B. S., Schulze, J. G., et al. 2023, *AJ*, 165, 97, doi: [10.3847/1538-3881/acb04b](https://doi.org/10.3847/1538-3881/acb04b)
- Rogers, J. G., Owen, J. E., & Schlichting, H. E. 2023, arXiv e-prints, arXiv:2311.12295, doi: [10.48550/arXiv.2311.12295](https://doi.org/10.48550/arXiv.2311.12295)
- Rogers, L. A. 2015, *ApJ*, 801, 41, doi: [10.1088/0004-637X/801/1/41](https://doi.org/10.1088/0004-637X/801/1/41)
- Roy, P.-A., Benneke, B., Piaulet, C., et al. 2023, *ApJL*, 954, L52, doi: [10.3847/2041-8213/acebf0](https://doi.org/10.3847/2041-8213/acebf0)
- Rubenzahl, R. A., Dai, F., Howard, A. W., et al. 2021, *ApJ*, 161, 119, doi: [10.3847/1538-3881/abd177](https://doi.org/10.3847/1538-3881/abd177)
- Sanchis-Ojeda, R., Winn, J. N., Dai, F., et al. 2015, *ApJL*, 812, L11, doi: [10.1088/2041-8205/812/1/L11](https://doi.org/10.1088/2041-8205/812/1/L11)
- Santerne, A., Brugger, B., Armstrong, D. J., et al. 2018, *Nature Astronomy*, doi: [10.1038/s41550-018-0420-5UNREFEREED](https://doi.org/10.1038/s41550-018-0420-5UNREFEREED):
- Santerne, A., Malavolta, L., Kosiarek, M. R., et al. 2019, arXiv e-prints, arXiv:1911.07355, doi: [10.48550/arXiv.1911.07355](https://doi.org/10.48550/arXiv.1911.07355)
- Sarkis, P., Henning, T., Kürster, M., et al. 2018, *AJ*, 155, 257, doi: [10.3847/1538-3881/aac108](https://doi.org/10.3847/1538-3881/aac108)
- Schmitt, J. R., Tokovinin, A., Wang, J., et al. 2016, *AJ*, 151, 159, doi: [10.3847/0004-6256/151/6/159](https://doi.org/10.3847/0004-6256/151/6/159)
- Sing, D. K., Fortney, J. J., Nikolov, N., et al. 2016, *Nature*, 529, 59, doi: [10.1038/nature16068](https://doi.org/10.1038/nature16068)
- Sinukoff, E., Howard, A. W., Petigura, E. A., et al. 2016, *ApJ*, 827, 78, doi: [10.3847/0004-637X/827/1/78](https://doi.org/10.3847/0004-637X/827/1/78)
- . 2017a, *AJ*, 153, 271, doi: [10.3847/1538-3881/aa725f](https://doi.org/10.3847/1538-3881/aa725f)
- . 2017b, *AJ*, 153, 70, doi: [10.3847/1538-3881/153/2/70](https://doi.org/10.3847/1538-3881/153/2/70)
- Smith, A. M. S., Gandolfi, D., Barragán, O., et al. 2017, *MNRAS*, 464, 2708, doi: [10.1093/mnras/stw2487](https://doi.org/10.1093/mnras/stw2487)
- Smith, A. M. S., Breton, S. N., Csizmadia, S., et al. 2022, *MNRAS*, 510, 5035, doi: [10.1093/mnras/stab3497](https://doi.org/10.1093/mnras/stab3497)
- Spake, J. J., Sing, D. K., Evans, T. M., et al. 2018, *Nature*, 557, 68, doi: [10.1038/s41586-018-0067-5](https://doi.org/10.1038/s41586-018-0067-5)
- Teske, J., Wang, S. X., Wolfgang, A., et al. 2021, *ApJS*, 256, 33, doi: [10.3847/1538-4365/ac0f0a](https://doi.org/10.3847/1538-4365/ac0f0a)
- Teske, J. K., Wang, S., Wolfgang, A., et al. 2018, *AJ*, 155, 148, doi: [10.3847/1538-3881/aaab56](https://doi.org/10.3847/1538-3881/aaab56)
- Toledo-Padrón, B., Lovis, C., Suárez Mascareño, A., et al. 2020, *A&A*, 641, A92, doi: [10.1051/0004-6361/202038187](https://doi.org/10.1051/0004-6361/202038187)
- Tsiaras, A., Waldmann, I. P., Tinetti, G., Tennyson, J., & Yurchenko, S. N. 2019, *Nature Astronomy*, 3, 1086, doi: [10.1038/s41550-019-0878-9](https://doi.org/10.1038/s41550-019-0878-9)
- Valenti, J. A., Butler, R. P., & Marcy, G. W. 1995, *PASP*, 107, 966, doi: [10.1086/133645](https://doi.org/10.1086/133645)
- Van Eylen, V., Agentoft, C., Lundkvist, M. S., et al. 2018a, *MNRAS*, 479, 4786, doi: [10.1093/mnras/sty1783](https://doi.org/10.1093/mnras/sty1783)
- Van Eylen, V., Albrecht, S., Gandolfi, D., et al. 2016a, *AJ*, 152, 143, doi: [10.3847/0004-6256/152/5/143](https://doi.org/10.3847/0004-6256/152/5/143)
- Van Eylen, V., Nowak, G., Albrecht, S., et al. 2016b, *ApJ*, 820, 56, doi: [10.3847/0004-637X/820/1/56](https://doi.org/10.3847/0004-637X/820/1/56)
- Van Eylen, V., Dai, F., Mathur, S., et al. 2018b, *MNRAS*, 478, 4866, doi: [10.1093/mnras/sty1390](https://doi.org/10.1093/mnras/sty1390)
- Van Zandt, J., Petigura, E. A., MacDougall, M., et al. 2023, *AJ*, 165, 60, doi: [10.3847/1538-3881/aca6ef](https://doi.org/10.3847/1538-3881/aca6ef)
- Vanderburg, A., Bieryla, A., Duev, D. A., et al. 2016a, *ApJL*, 829, L9, doi: [10.3847/2041-8205/829/1/L9](https://doi.org/10.3847/2041-8205/829/1/L9)

- Vanderburg, A., Latham, D. W., Buchhave, L. A., et al. 2016b, *ApJS*, 222, 14, doi: [10.3847/0067-0049/222/1/14](https://doi.org/10.3847/0067-0049/222/1/14)
- Vanderburg, A., Becker, J. C., Kristiansen, M. H., et al. 2016, *The Astrophysical Journal*, 827, L10, doi: [10.3847/2041-8205/827/1/110](https://doi.org/10.3847/2041-8205/827/1/110)
- Vanderburg, A., Becker, J. C., Buchhave, L. A., et al. 2017, *AJ*, 154, 237, doi: [10.3847/1538-3881/aa918b](https://doi.org/10.3847/1538-3881/aa918b)
- Virtanen, P., Gommers, R., Oliphant, T. E., et al. 2020, *Nature Methods*, 17, 261, doi: [10.1038/s41592-019-0686-2](https://doi.org/10.1038/s41592-019-0686-2)
- Vogt, S. S., Allen, S. L., Bigelow, B. C., et al. 1994, *Society of Photo-Optical Instrumentation Engineers (SPIE) Conference Series*, Vol. 2198, HIRES: the high-resolution echelle spectrometer on the Keck 10-m Telescope (Crawford, David L. and Craine, Eric R.), 362, doi: [10.1117/12.176725](https://doi.org/10.1117/12.176725)
- Vogt, S. S., Radovan, M., Kibrick, R., et al. 2014, *PASP*, 126, 359, doi: [10.1086/676120](https://doi.org/10.1086/676120)
- Weiss, L. M., & Marcy, G. W. 2014, *ApJL*, 783, L6, doi: [10.1088/2041-8205/783/1/L6](https://doi.org/10.1088/2041-8205/783/1/L6)
- Weiss, L. M., Deck, K. M., Sinukoff, E., et al. 2017, *AJ*, 153, 265, doi: [10.3847/1538-3881/aa6c29](https://doi.org/10.3847/1538-3881/aa6c29)
- Wittenmyer, R. A., Sharma, S., Stello, D., et al. 2018, *AJ*, 155, 84, doi: [10.3847/1538-3881/aaa3e4](https://doi.org/10.3847/1538-3881/aaa3e4)
- Wittenmyer, R. A., Clark, J. T., Sharma, S., et al. 2020, *MNRAS*, 496, 851, doi: [10.1093/mnras/staa1528](https://doi.org/10.1093/mnras/staa1528)
- Wolfgang, A., & Lopez, E. 2015, *ApJ*, 806, 183, doi: [10.1088/0004-637X/806/2/183](https://doi.org/10.1088/0004-637X/806/2/183)
- Xie, J.-W., Dong, S., Zhu, Z., et al. 2016, *Proceedings of the National Academy of Science*, 113, 11431, doi: [10.1073/pnas.1604692113](https://doi.org/10.1073/pnas.1604692113)
- Yee, S. W., Petigura, E. A., & von Braun, K. 2017, *ApJ*, 836, 77, doi: [10.3847/1538-4357/836/1/77](https://doi.org/10.3847/1538-4357/836/1/77)
- Yu, L., Crossfield, I. J. M., Schlieder, J. E., et al. 2018, *AJ*, 156, 22, doi: [10.3847/1538-3881/aac6e6](https://doi.org/10.3847/1538-3881/aac6e6)
- Zeng, L., Jacobsen, S. B., Sasselov, D. D., et al. 2019, *Proceedings of the National Academy of Science*, 116, 9723, doi: [10.1073/pnas.1812905116](https://doi.org/10.1073/pnas.1812905116)
- Zink, J. K., Hardegree-Ullman, K. K., Christiansen, J. L., et al. 2020a, *AJ*, 159, 154, doi: [10.3847/1538-3881/ab7448](https://doi.org/10.3847/1538-3881/ab7448)
- . 2020b, *AJ*, 160, 94, doi: [10.3847/1538-3881/aba123](https://doi.org/10.3847/1538-3881/aba123)
- . 2021, *AJ*, 162, 259, doi: [10.3847/1538-3881/ac2309](https://doi.org/10.3847/1538-3881/ac2309)
- . 2023, *AJ*, 165, 262, doi: [10.3847/1538-3881/acd24c](https://doi.org/10.3847/1538-3881/acd24c)

APPENDIX

A. INDIVIDUAL SECTIONS

This appendix describes each planetary system considered in this paper and our analysis of its photometry and RVs. Individual subsections provide details of each analysis, tables of system parameters, and figures with results. The entire set of planetary properties is listed in Table 3 and is plotted in Fig. 4, as well as in Figs. 5 and 7.

A.1. *HD 3167*

HD 3167 (K2-96, EPIC 220383386) is a bright late G dwarf from Campaign 8. [Vanderburg et al. \(2016a\)](#) discovered two transiting planets with radii of $1.6 R_{\oplus}$ (planet b) and $2.9 R_{\oplus}$ (planet c) and orbital periods of 0.96 days and 29.8 days, respectively. [Christiansen et al. \(2017\)](#) found masses of $5.02 \pm 0.38 M_{\oplus}$ and $9.80^{+1.30}_{-1.24} M_{\oplus}$ for the two planets using RVs from HIRES (60 measurements), APF (116), and HARPS-N (76). They also discovered a third nontransiting planet with a period of 8.5 days and a mass of $6.90 \pm 0.71 M_{\oplus}$. Subsequently, [Gandolfi et al. \(2017\)](#) characterized by the system using new RVs from FIES (37 measurements), HARPS (45), and HARPS-N (32). They did not detect planet d, but found masses of $5.69 \pm 0.44 M_{\oplus}$ and $8.33^{+1.79}_{-1.85} M_{\oplus}$ for planets b and c, respectively. A later analysis including CHEOPS transits and additional RVs reported a second nontransiting planet, with masses (or minimum masses) of 4.7 ± 0.3 , 10.7 ± 0.8 , 5.0 ± 0.5 , and $9.7 \pm 1.2 M_{\oplus}$ for planets b, c, d, and e, respectively ([Bourrier et al. 2022](#)), largely consistent with previous results.

Planet c was revealed to be in a near-polar orbit via Rossiter-McLaughlin measurements at HARPS-N ([Dalal et al. 2019](#)), and H₂O vapor was detected in its atmosphere by *HST* transmission spectroscopy ([Mikal-Evans et al. 2021](#)).

We adopt the stellar and planet parameters from [Christiansen et al. \(2017\)](#). The full set of adopted parameters are listed in Tables 1, 2 and 3.

A.2. *HD 106315*

HD 106315 (K2-109, EPIC 201437844) is a bright ($V = 8.951 \pm 0.018$) F5 dwarf observed in Campaign 10. [Crossfield et al. \(2017\)](#) and [Rodriguez et al. \(2017\)](#) concurrently announced the discovery of two small transiting planets with orbital periods of 9.5 days (planet b) and 21 days (planet c) and sizes of $2.4 R_{\oplus}$ and $4.3 R_{\oplus}$. The star is rapidly rotating with $V \sin i = 13.2 \pm 1.0$ km s⁻¹, consistent with its early spectral type, making the system a challenging target for Doppler measurements. The two planets orbiting HD 106315 were also noted in the [Mayo et al. \(2018\)](#) catalog.

[Barros et al. \(2017\)](#) collected 130 RVs from HARPS from which they measured a mass of $12.6 \pm 3.2 M_{\oplus}$ and density of 4.7 ± 1.7 g cm⁻³ for planet b and a mass of $15.2 \pm 3.7 M_{\oplus}$ and a density of 1.01 ± 0.29 g cm⁻³ for planet c.

[Kosiarek et al. \(2021\)](#) followed with an analysis based on 352 HIRES observations and 25 PFS observations, in addition to the HARPS RVs. They additionally updated the stellar parameters from Gaia DR2 ([Gaia Collaboration et al. 2018](#)) and propagated these forward to calculate updated planet radii. They found that a circular 2-planet fit without a Gaussian process best fits the data based on the AIC statistic, resulting in planet masses of $10.5 \pm 3.1 M_{\oplus}$ for planet b and $12.0 \pm 3.8 M_{\oplus}$ for planet c. HD 106315 b is a super-Earth with a small volatile mass that increases its radius and HD 106315 c is a Neptune-sized planet consistent with having a rocky core and a 10% H/He envelope. A tentative hint of H₂O was seen in planet c’s atmosphere via *HST*/WFC3 transmission spectroscopy

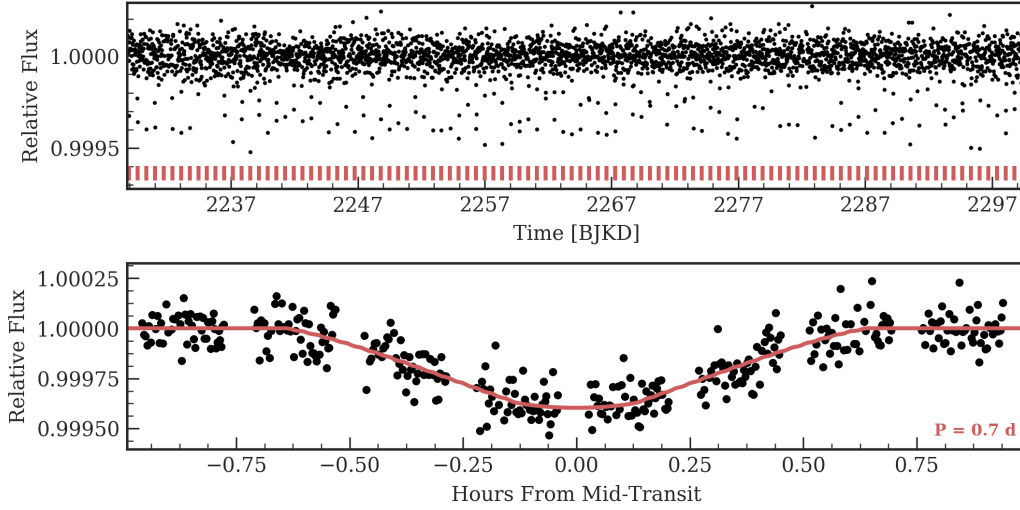


Figure 8. Time series (top) and phase-folded (bottom) light curve for the planet orbiting K2-85. Plot formatting is the same as in Fig. 10.

(Kreidberg et al. 2022), and the planet is being targeted with *JWST* MIRI/LRS spectroscopy in GO-2950. For our analysis, we adopt the Kosiarek et al. (2021) solution. See Tables 1 and 2 for stellar properties and Table 3 for planet parameters.

A.3. K2-85

K2-85 (EPIC 210707130) is a late K dwarf with elevated chromospheric activity ($\log R'_{\text{HK}} = -4.67$) from Campaign 4 that hosts an ultra-short period planet ($P = 0.7$ days) with a radius of $1.4 R_{\oplus}$. See Tables 1 and 2 for stellar properties and Table 3 for precise planet parameters. Dressing et al. (2017) used near-infrared spectroscopy to measure a stellar radius of $0.68 \pm 0.03 R_{\odot}$. Barros et al. (2016) designated the object as a planet candidate. It is validated and appears in the Crossfield et al. (2016), Adams et al. (2016), and Mayo et al. (2018) catalogs. Our HIRES measurements reveal a planet mass of $4.0 \pm 1.5 M_{\oplus}$, as listed in Table 3.

A.4. K2-222

K2-222 (EPIC 220709978) is a G0 dwarf observed by K2 in Campaign 8 with one detected transiting planet with an orbital period of 15 days and a size of $2.4 R_{\oplus}$. See Tables 1 and 2 for stellar properties and Table 3 for precise planet parameters. Petigura et al. (2018a) lists this object as a planet candidates and Mayo et al. (2018) validated it as a planet. Our fit of the EVEREST light curve of the K2 photometry for K2-222 is shown in Fig. 10.

We acquired 55 RVs of K2-222 with HIRES (exposure meter setting of 250,000) and 32 with the APF. We modeled the system as a single planet in a circular orbit, with the orbital period and phase fixed to the transit ephemeris. Our model did not include any explicit priors, and RVs within one night from a particular telescope were binned. We considered more complicated models with orbital eccentricity and/or a linear RV trend, but rejected these because of insufficient evidence based on the AICc statistic. The results of this analysis are listed in Table 6 and the best-fit model is shown in Fig. 11. Our analysis finds a low jitter for the HIRES RVs and a high value for the APF data

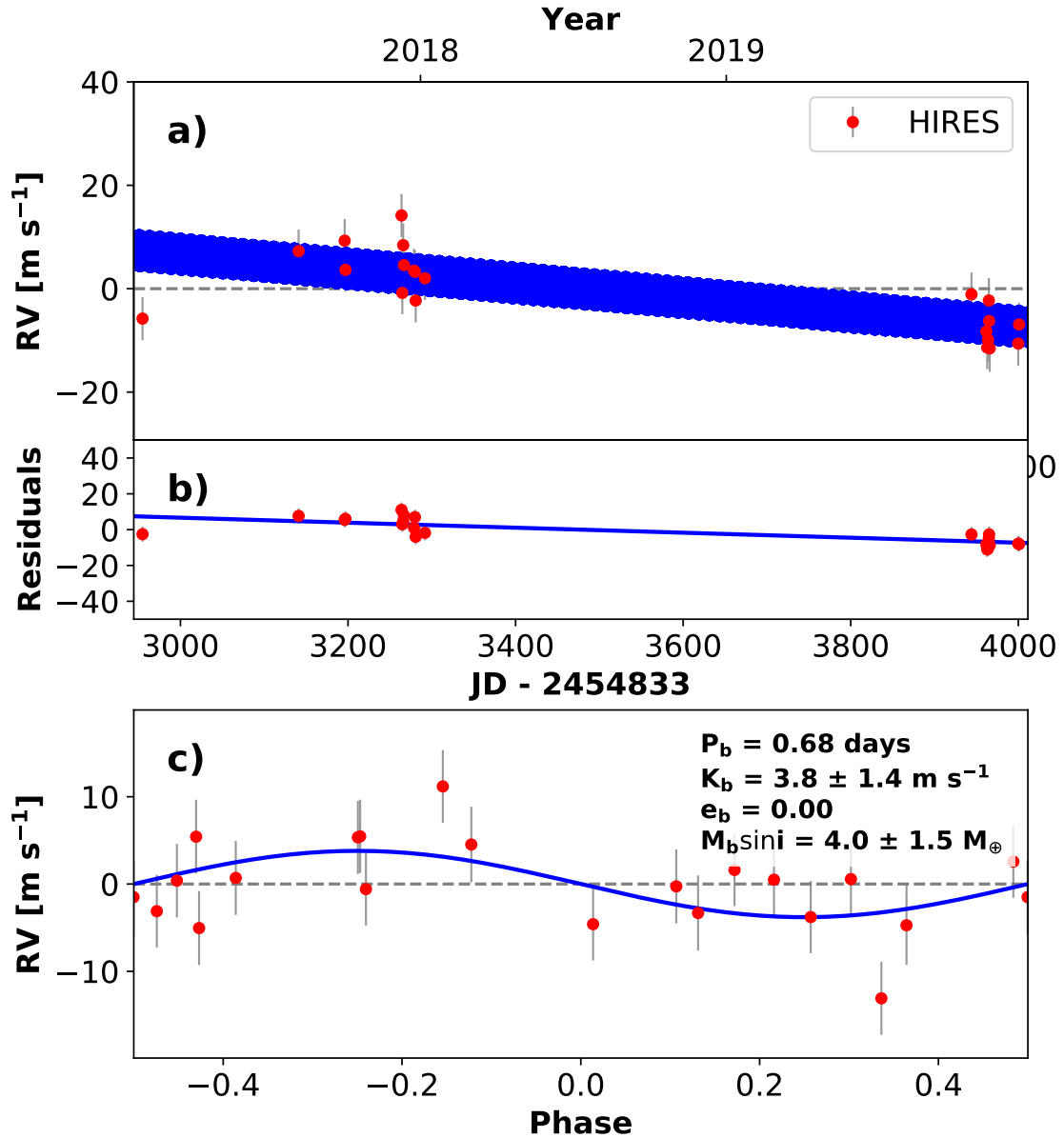


Figure 9. RVs and Keplerian model for K2-85. Symbols, lines, and annotations are similar to those in Fig. 11.

(see Table 6), suggesting underestimated errors on the latter. Using the method in Sec. 4.2.5, we also searched the RVs for additional planets, but we found no compelling signals (Fig. 12). Although the star is bright, we only detected the planet’s signal at $2.4\text{-}\sigma$. Subsequent analysis by other teams securely measured the planet to be $8\text{--}9 M_\oplus$ (Nava et al. 2022; Bonomo et al. 2023b).

A.5. K2-291

K2-291 (EPIC 247418783) is a G0 dwarf star observed in Campaign 13 that hosts one super-Earth transiting planet ($R_p = 1.5 R_\oplus$) in a short-period orbit ($P = 2.23$ d). The host star has elevated activity with $\log R'_{\text{HK}} = -4.79$ dex.

K2-291b was discovered, confirmed, and characterized by Kosiarek et al. (2019a). They discovered the planet in the K2 Campaign 13 data and measured the mass using a combination of HIRES and

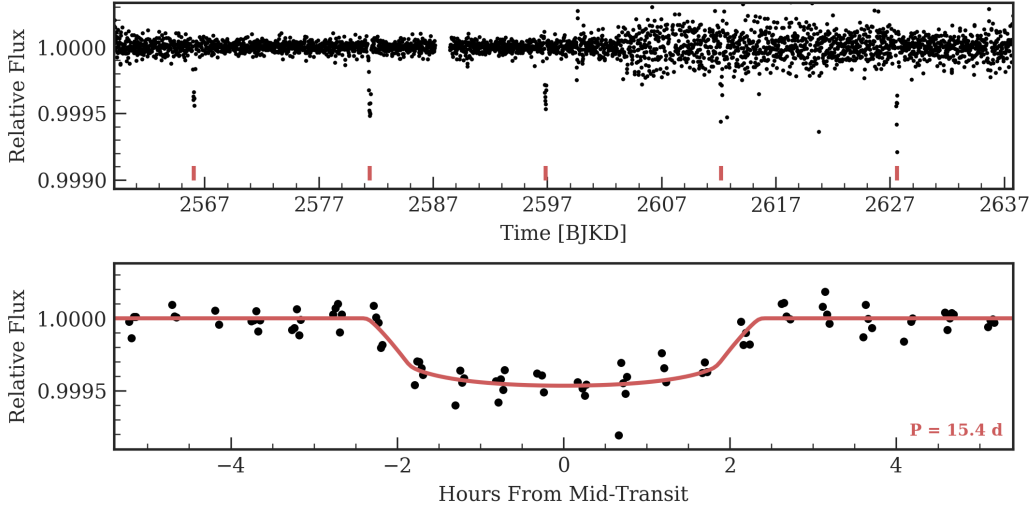


Figure 10. De-trended, time series (top) and phase-folded (middle and bottom) light curve for K2-222. Transit epochs are marked by vertical ticks in the time series, and the maximum a posteriori transit model is shown as a colored line in the phase-folded panel. Gray points are not included in the light curve fit. Different color ticks indicate the planets in the time series, and there are separate phase-folded panels for each planet in the middle and lower rows. In the top panel, time is expressed in units of days with BKJD = $\text{BJD}_{\text{TBD}} - 2,545,833$.

HARPS-N RVs. [Kosiarek et al. \(2019a\)](#) used a Gaussian process to characterize stellar activity and found that a circular, 1-planet model with a GP characterizes the data best, resulting in a mass of $M_b = 6.5 M_{\oplus}$. We adopt their solution; see see Tables 1 and 2 for stellar properties and Table 3 for the planet parameters.

A.6. *K2-236*

K2-236 is a nearly solar-type star from Campaign 5 with slightly elevated T_{eff} , $[\text{Fe}/\text{H}]$, and R_{\star} compared to the Sun. The star was re-observed in Campaign 16, although we only analyzed the photometry from Field 5. We detected one transiting planet with a size of $5.7 R_{\oplus}$ and an orbital period of 19.5 days. See Tables 1 and 2 for stellar properties and Table 3 for precise planet parameters. The planet is noted in the catalogs by [Barros et al. \(2016\)](#), [Petigura et al. \(2018a\)](#), and [Mayo et al. \(2018\)](#) as a candidate. Our fit of the EVEREST light curve of the K2 photometry for K2-236 is shown in Fig. 13.

[Chakraborty et al. \(2018\)](#) studied this system using the PARAS spectrometer and found a mass of $27_{-13}^{+14} M_{\oplus}$ and a density of $0.65_{-0.30}^{+0.34} \text{ g cm}^{-3}$ based on 19 RVs. They also validated the planet using VESPA, finding a false positive probability of 2%.

We acquired 36 RVs of K2-236 with HIRES, typically with an exposure meter setting of 60,000 counts. We also acquired 2 RVs from the APF. We modeled the system as a single planet in a circular orbit with the orbital period and phase fixed to the transit ephemeris. RVs from PARAS, HIRES, and APF were included, with binning applied per night and per telescope. The results of this analysis are listed in Table 7 and the best-fit model is shown in Fig. 14. We considered more complicated models with eccentricity and/or an RV slope, but rejected these because of insufficient evidence using

Table 6. K2-222 System Parameters

Parameter	Credible Interval	Maximum Likelihood	Units
RV Analysis – MCMC Step Parameters			
P_b	$\equiv 15.3863$	$\equiv 15.3863$	days
$T_{\text{conj},b}$	$\equiv 2457399.0652$	$\equiv 2457399.0652$	BJD _{TBD}
$\sqrt{e} \cos \omega_b$	$\equiv 0.0$	$\equiv 0.0$	
$\sqrt{e} \sin \omega_b$	$\equiv 0.0$	$\equiv 0.0$	
K_b	$1.6^{+0.7}_{-0.7}$	1.6	m s^{-1}
γ_{HIRES}	$-1.22^{+0.54}_{-0.55}$	-1.21	m s^{-1}
γ_{APF}	1.2 ± 2.2	1.2	m s^{-1}
$\dot{\gamma}$	$\equiv 0.0$	$\equiv 0.0$	$\text{m s}^{-1} \text{ day}^{-1}$
$\ddot{\gamma}$	$\equiv 0.0$	$\equiv 0.0$	$\text{m s}^{-1} \text{ day}^{-2}$
σ_{HIRES}	$2.83^{+0.62}_{-0.24}$	2.68	m s^{-1}
σ_{APF}	4^{+2}_{-13}	6	m s^{-1}
Orbital & Physical Parameters			
P_b	$\equiv 15.3863$	$\equiv 15.3863$	days
$T_{\text{conj},b}$	$\equiv 2457399.0652$	$\equiv 2457399.0652$	BJD _{TBD}
e_b	$\equiv 0.0$	$\equiv 0.0$	
ω_b	$\equiv 0.0$	$\equiv 0.0$	radians
K_b	$1.6^{+0.7}_{-0.7}$	1.6	m s^{-1}
M_b	$5.7^{+2.5}_{-2.7}$	5.8	M_{\oplus}
R_b/R_*	$0.0202^{+0.0013}_{-0.0008}$	0.0203	
ρ_b	2 ± 1	2	g cm^{-3}
R_b	$2.41^{+0.15}_{-0.09}$	2.42	R_{\oplus}
Priors			
Parameter	Prior		
None			

the AICc statistic. Our combined analysis of PARAS, HIRES, and APF data finds a lower mass and density for the planet than [Chakraborty et al. \(2018\)](#), although neither analysis detects the planet signal with high confidence. We conclude that K2-236 b is a sub-Saturn-size planet with low density.

A.7. K2-418 (EPIC 229004835)

K2-418(EPIC-229004835) is a solar-type star observed in Campaign 10 that has one transiting planet with an orbital period of 16 days and a size of $2.1 R_{\oplus}$. The object was identified by our pipeline ([Livingston et al. 2018](#)) and in [Mayo et al. \(2018\)](#) as a planet candidate. See Tables 1 and 2 for stellar properties and Table 3 for precise planet parameters. Our fit of the EVEREST light curve of the K2 photometry for K2-418 is shown in Fig. 15. Our observations described below are sufficient to validate the planet candidate according to the criteria listed in Section 2.4.

We acquired 22 RVs of K2-418 with HIRES, typically with an exposure meter setting of 250,000. We modeled the system as a single planet in a circular orbit, with no additional priors. The results of this analysis are listed in Table 8 and the best fit model is shown in Fig. 16. We considered more

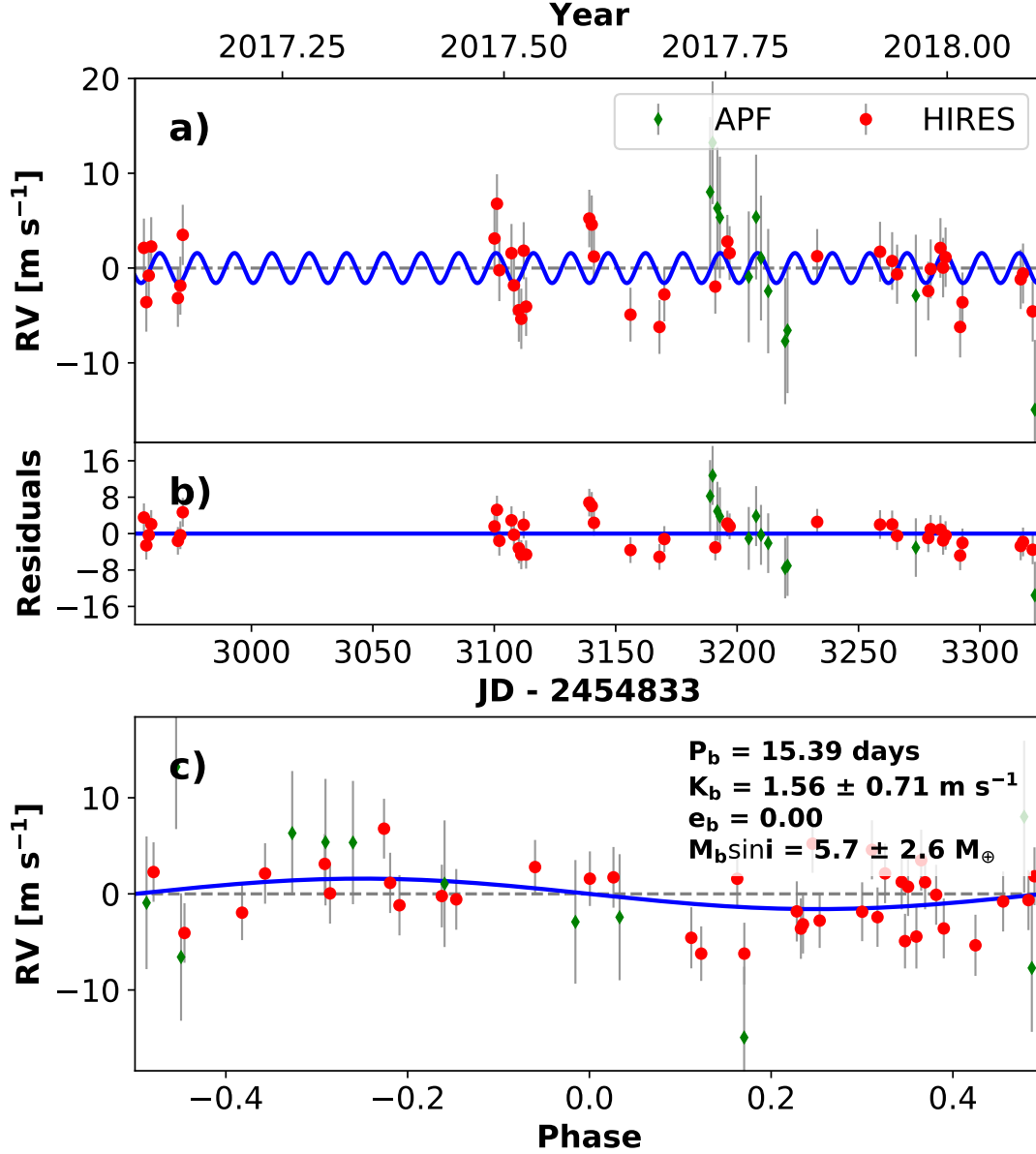


Figure 11. RVs and Keplerian model for K2-222. Panel a shows the time series RVs from HIRES and HARPS with the best-fit Keplerian model in blue. The residuals to this model are shown in panel b. Panels c and d show the same RVs phased to the orbital periods of the planets with annotations indicating parameters of the model. This paper contains many similar plots for other systems, each showing the time-series RVs and residuals on the top and one panel each for the phased RVs for each planet. Data from the instrument (or segment of data from an instrument needing a separate zero point in the analysis) are labeled with separate symbols.

complicated models, but found insufficient evidence to justify inclusion of orbital eccentricity or a linear RV trend based on the AICc statistic.

The size of K2-418 b ($2.18^{+0.13}_{-0.07} R_{\oplus}$) places it on the sub-Neptune side of the radius valley (Fulton et al. 2017). However, the density we measured of $11.9^{+4.2}_{-3.5} \text{ g cm}^{-3}$ suggests a rocky composition. This may be driven in part by sparse phase coverage and a possible outlier RV at upper quadrature (see Fig. 16). The star has $\log R'_{\text{HK}} = -4.984$ so an outlier RV cannot be explained

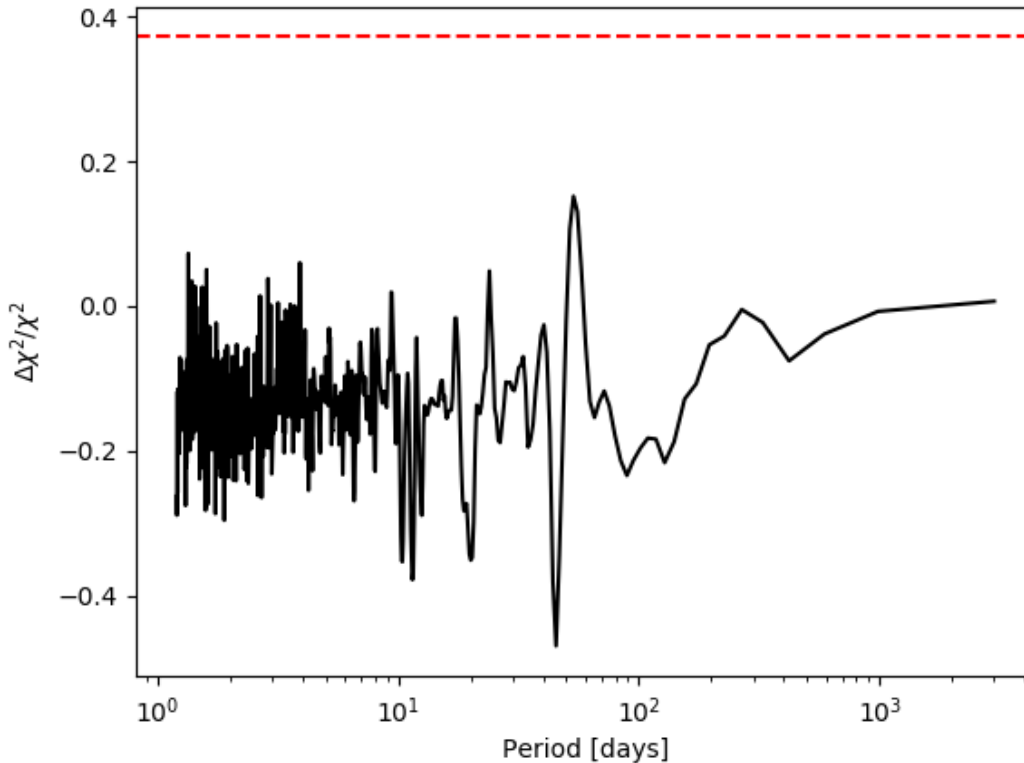


Figure 12. Periodogram search of the RVs for a third planet orbiting K2-222. The black line shows the normalized difference in χ^2 for the adopted two-planet model (Table 6) compared to a model with one additional planet, as a function of the orbital period of the additional planet. The parameters not listed as fixed in Table 6 were allowed to vary with each trial period for the third planet, which is assumed to be in a circular orbit. The periodogram power $\Delta\chi^2/\chi^2$ was calculated using the 2DKLS formalism of O’Toole et al. (2009). The dashed red line denotes the 1% false alarm probability level computed using the empirical method in Howard & Fulton (2016). In this case, we did not find a compelling period for a prospective third planet.

by elevated stellar activity. Subsequent observations and analysis reveal a mass of $10.4 \pm 1.5M_{\oplus}$ (Bonomo et al. 2023b), broadly consistent with, but more precise than our measurement.

A.8. K2-277

K2-277 is a solar-type star from Campaign 6 with one transiting planet with a radius of $2.1 R_{\oplus}$ and an orbital period of 6.3 days. The planet was listed as a candidate in Petigura et al. (2018a) and was subsequently validated by Livingston et al. (2018). It was not listed in Mayo et al. (2018) even though Campaign 6 was covered in that catalog. See Tables 1 and 2 for stellar properties and Table 3 for precise planet parameters. Our fit of the EVEREST light curve of the K2 photometry for K2-277 is shown in Fig. 17.

We acquired 26 RVs of K2-277 with HIRES, typically with an exposure meter setting of 250,000 counts. We modeled the system as a single planet in a circular orbit with the orbital period and phase fixed to the values from the transit ephemeris. The results of this analysis are listed in Table

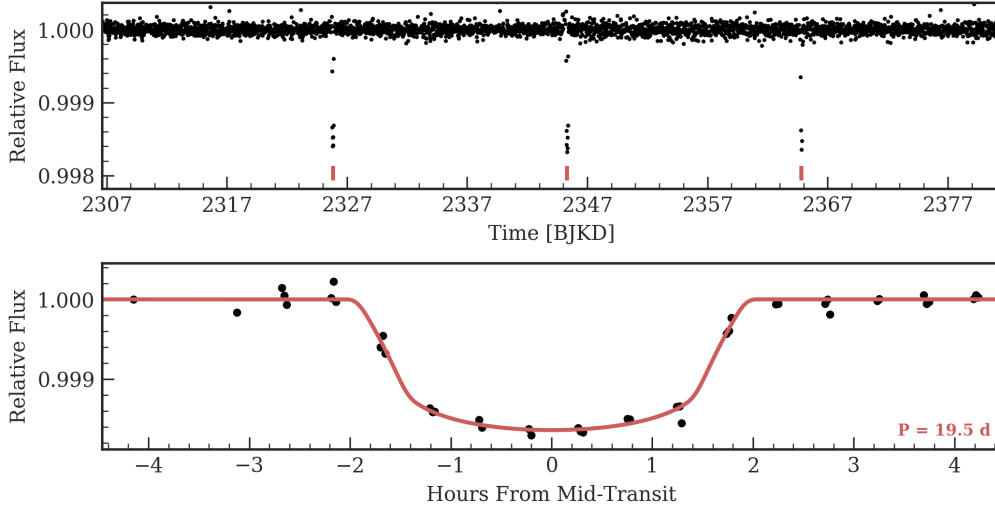


Figure 13. Time series (top) and phase-folded (bottom) light curve for the planet orbiting K2-236. Plot formatting is the same as in Fig. 10.

9 and the best fit model is shown in Fig. 18. Note that our model includes a linear RV trend that is strongly favored compared to a model without a trend based on the AICc statistic. We rejected models with an eccentric orbit based on similar AICc comparisons. K2-277 b is detected with only $\sim 2\text{-}\sigma$ significance based on the HIRES RVs. As a result, this sub-Neptune’s bulk density of $4 \pm 2 \text{ g cm}^{-3}$ is consistent with a rocky composition or a significant gas envelope.

A.9. GJ 9827

GJ9827 is a relatively bright ($V = 10.4$) K6V star in Campaign 12. Niraula et al. (2017) and Rodriguez et al. (2018) discovered three transiting planets with sizes and orbital periods of 1.8, 1.4, and 2.1 R_{\oplus} , and 1.21, 3.65, and 6.20 days, respectively.

Over the last few years, this system has had considerable follow-up. Teske et al. (2018) measured the mass of planet b ($M_b \approx 8 M_{\oplus}$) and the upper limits on planets c and d ($M_c < 2.5 M_{\oplus}$, $M_d < 5.6 M_{\oplus}$) based on RVs from PFS. Prieto-Arranz et al. (2018) added RVs from HARPS and HARPS-N to determine the masses of all three planets ($M_b = 3.74 \pm 0.50 M_{\oplus}$, $M_c = 1.47 \pm 0.59 M_{\oplus}$, and $M_d = 2.38 \pm 0.71 M_{\oplus}$). Rice et al. (2019) refined these measurements with additional HARPS-N data and a Gaussian process fit informed from the K2 light curve ($M_b = 4.91 \pm 0.49 M_{\oplus}$ and $M_d = 4.04 \pm 0.84 M_{\oplus}$). Passegger et al. (2024) recently reported an analysis also consistent with these previous studies.

Kosiarek et al. (2021) followed with 92 HIRES measurements and performed an analysis that included all previously published data. They additionally updated the stellar parameters from Gaia DR2 information and propagated these to update the planet radii. We adopt their solution; see Tables 1 and 2 for stellar properties and Table 3 for the planet parameters. They find a circular 3-planet fit that includes a Gaussian process informed from the S_{HK} best fits the data based on the AICc statistic, resulting in planet masses of $M_b = 4.87 \pm 0.37 M_{\oplus}$, $M_c = 1.92 \pm 0.49 M_{\oplus}$, and $M_d = 3.42 \pm 0.62 M_{\oplus}$. GJ 9827 b and c are both rocky super-Earths consistent with an Earth-like composition. GJ 9827 d is a super-Earth that requires a small amount of volatiles to explain

Table 7. K2-236 System Parameters

Parameter	Credible Interval	Maximum Likelihood	Units
RV Analysis – MCMC Step Parameters			
P_b	$\equiv 19.491$	$\equiv 19.491$	days
$T_{\text{conj},b}$	$\equiv 2457158.8266$	$\equiv 2457158.8266$	BJD _{TBD}
$\sqrt{e} \cos \omega_b$	$\equiv 0.0$	$\equiv 0.0$	
$\sqrt{e} \sin \omega_b$	$\equiv 0.0$	$\equiv 0.0$	
K_b	$2.3^{+1.6}_{-1.4}$	2.3	m s^{-1}
γ_{PARAS}	$1260.7^{+2.6}_{-2.5}$	1260.6	m s^{-1}
γ_{HIRES}	-1.0 ± 1.3	-1.0	m s^{-1}
γ_{APF}	0^{+7100}_{-5200}	0	m s^{-1}
$\dot{\gamma}$	$\equiv 0.0$	$\equiv 0.0$	$\text{m s}^{-1} \text{ day}^{-1}$
$\ddot{\gamma}$	$\equiv 0.0$	$\equiv 0.0$	$\text{m s}^{-1} \text{ day}^{-2}$
σ_{PARAS}	$-0.0^{+3.3}_{-3.5}$	-0.0	m s^{-1}
σ_{HIRES}	$5^{+1.8}_{-0.5}$	4.4	m s^{-1}
σ_{APF}	0^{+22000}_{-11000}	0	m s^{-1}
Orbital & Physical Parameters			
P_b	$\equiv 19.491$	$\equiv 19.491$	days
$T_{\text{conj},b}$	$\equiv 2457158.8266$	$\equiv 2457158.8266$	BJD _{TBD}
e_b	$\equiv 0.0$	$\equiv 0.0$	
ω_b	$\equiv 0.0$	$\equiv 0.0$	radians
K_b	$2.3^{+1.6}_{-1.4}$	2.3	m s^{-1}
M_b	$11^{+7.2}_{-6.7}$	10.8	M_{\oplus}
R_b/R_*	$0.0375^{+0.0004}_{-0.0015}$	0.0384	
ρ_b	$0.35^{+0.29}_{-0.18}$	0.30	g cm^{-3}
R_b	$\equiv 5.4972$	$\equiv 5.4972$	R_{\oplus}
Priors			
Parameter	Prior		
None			

its radius. This volatile envelope was confirmed by the detection of H₂O in planet d’s atmosphere through *HST*/WFC3 transmission spectroscopy (Roy et al. 2023).

A.10. K2-261

K2-261 is a G7 star in Field 14 with one transiting planet with a radius of $9.7 R_{\oplus}$ and an orbital period of 11.6 days. The planet was discovered and characterized independently by Johnson et al. (2018) and Brahm et al. (2019). Johnson et al. (2018) found K2-261b to be a warm Saturn with a mass of $70.9 \pm 9.9 M_{\oplus}$ in an eccentric orbit ($e = 0.39 \pm 0.15$) based on RVs from FIES, HARPS-N, and HARPS. Brahm et al. (2019) found a lower mass for this eccentric planet ($M_b = 56.9 \pm 6.7 M_{\oplus}$, $e = 0.42 \pm 0.03$) based on RVs from Coralie, FEROS, and HARPS.

We acquired 8 RVs of K2-261 with HIRES, typically with an exposure meter setting of 50,000, and 4 RVs with the APF. We fit all of the data with a model of a single planet in an eccentric orbit with the orbital period and phase fixed to the transit ephemeris. We find a mass of $56 \pm 6 M_{\oplus}$, which is consistent with previous results, and a lower eccentricity of $e = 0.179 \pm 0.067$ based on the

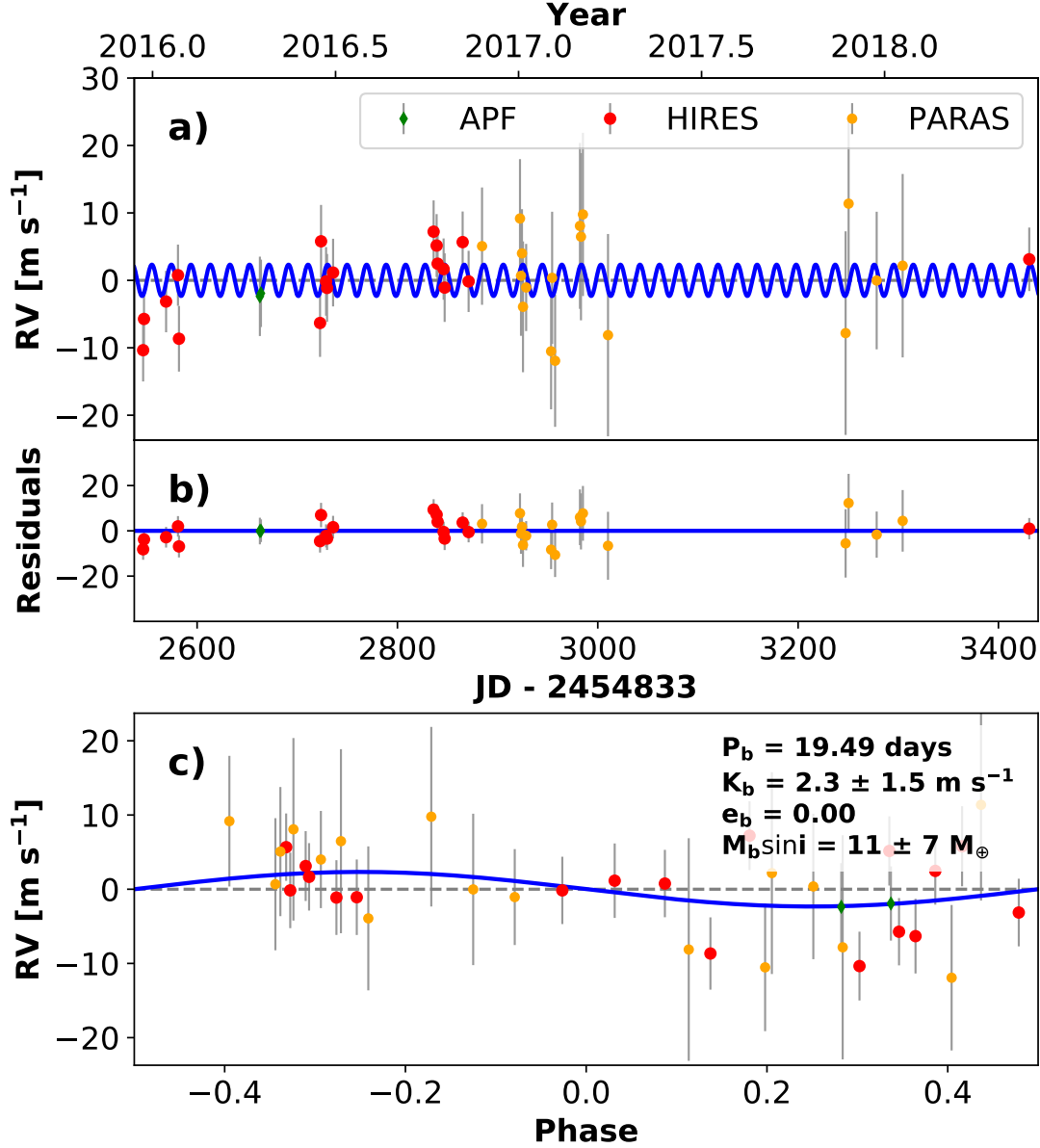


Figure 14. RVs and Keplerian model for K2-236. Symbols, lines, and annotations are similar to those in Fig. 11.

global analysis. An eccentric orbit is clearly favored over a circular one in a model comparison test ($\Delta\text{AICc} = 24.24$), and a linear trend is not warranted based on an AICc comparison. The results of this analysis are listed in Table 10 and the best fit model is shown in Fig. 20. K2-261 b is a low-density warm-Saturn planet. See Tables 1 and 2 for stellar properties and Table 3 for precise planet parameters.

A.11. K2-100

K2-100 is a relatively young dwarf star with $T_{\text{eff}} = 6044 \pm 100$ K. Evidence for youth includes elevated stellar activity ($\log R'_{\text{HK}} = -4.526$), membership in the Praesepe cluster (e.g., Kraus & Hillenbrand 2007b) that has an age of ~ 600 Myr, $\sim 1\%$ spot modulation in K2 photometry with a rotational period of 4.3 days (Mann et al. 2017), and $V \sin i = 13.3 \pm 1.0$ km s $^{-1}$. The transiting planet has an

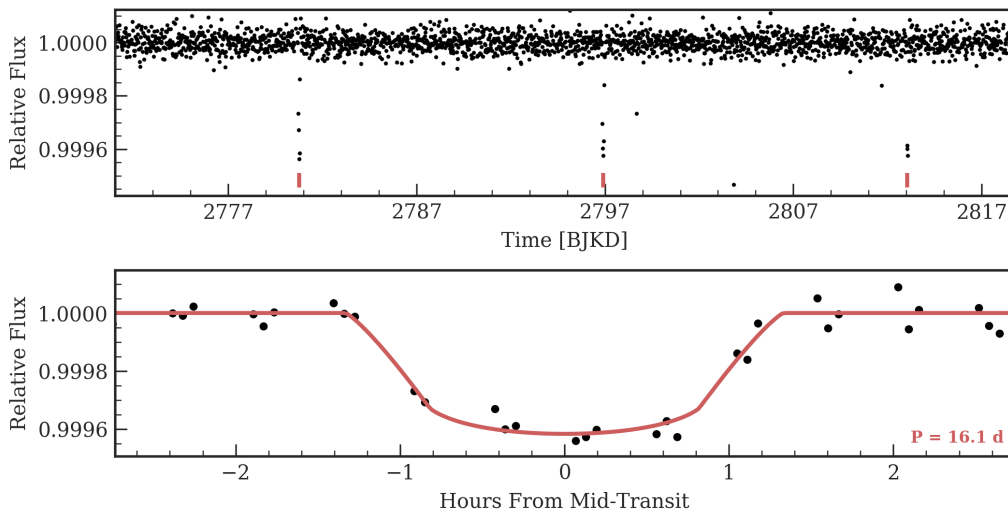


Figure 15. Time series (top) and phase-folded (bottom) light curve for the planet orbiting K2-418. Plot formatting is the same as in Fig. 10.

orbital period of 1.7 days and a radius of $3.7 R_{\oplus}$, apparently inflated for the short orbital period. See Tables 1 and 2 for stellar properties and Table 3 for precise planet parameters.

K2-100 b was noted the catalog of seven planets in Praesepe by Mann et al. (2017), who also validated the planet with a false positive analysis. The system was noted in the uniform search for planets in clusters by Rizzuto et al. (2017). Pope et al. (2016) and Petigura et al. (2018a) list K2-100 b as a planet candidate, although these papers did not attempt statistical validation. Our fit of the EVEREST light curve of the K2 photometry for K2-100 is shown in Fig. 21.

Barragán et al. (2019) gathered 78 RVs of this star using HARPS. Their analysis of the RVs using a Gaussian process model trained on activity indices gives a planet mass of $10.6 \pm 3.0 M_{\oplus}$ and a density of $2.04^{+0.66}_{-0.61} \text{ g cm}^{-3}$.

We acquired 33 RVs of K2-100 with HIRES, typically with an exposure meter setting of 125,000. Due to the high $V \sin i$, we collected three exposures per night separated by an hour or more each (when possible). We also adopted a strategy of observing the star on consecutive nights that partially freezes out the stellar activity on rotational timescales, giving greater sensitivity to the planet’s signal on orbital timescales.

We modeled the system as a single planet in a circular orbit with the orbital period and phase fixed to the transit ephemeris. We included our HIRES RVs and the HARPS measurements from Barragán et al. (2019). HIRES RVs were binned within one night. The results are listed in Table 11 and the best-fit model is shown in Fig. 22. We considered more complicated models with free eccentricity and/or a linear RV trend, but rejected those based on model comparison using the AICc statistic. K2-100 is a good candidate for a Gaussian process model due to the high activity ($\log R'_{\text{HK}} = -4.526$). Combining our HIRES RVs with observations from HARPS-N satisfies our criteria for attempting a Gaussian process model. However, the photometry for this system is not particularly constraining, and hence we adopted an untrained GP.

The high stellar flux received by K2-100 b ($2100 \pm 200 F_{\oplus}$), combined with its approximately Neptune size and relative youth, suggests that it is inflated. We do not detect the Doppler signal

Table 8. EPIC 229004835 System Parameters

Parameter	Credible Interval	Maximum Likelihood	Units
RV Analysis – MCMC Step Parameters			
P_b	$\equiv 16.1388$	$\equiv 16.1388$	days
$T_{\text{conj},b}$	$\equiv 2457613.7661$	$\equiv 2457613.7661$	BJD _{TBD}
$\sqrt{e} \cos \omega_b$	$\equiv 0.0$	$\equiv 0.0$	
$\sqrt{e} \sin \omega_b$	$\equiv 0.0$	$\equiv 0.0$	
K_b	$5.1^{+1.3}_{-1.4}$	5.1	m s^{-1}
γ_{HIRES}	-1 ± 1.0	-1.0	m s^{-1}
$\dot{\gamma}$	$\equiv 0.0$	$\equiv 0.0$	$\text{m s}^{-1} \text{ day}^{-1}$
$\ddot{\gamma}$	$\equiv 0.0$	$\equiv 0.0$	$\text{m s}^{-1} \text{ day}^{-2}$
σ_{HIRES}	$4.27^{+1.30}_{-0.30}$	3.80	m s^{-1}
Orbital & Physical Parameters			
P_b	$\equiv 16.1388$	$\equiv 16.1388$	days
$T_{\text{conj},b}$	$\equiv 2457613.7661$	$\equiv 2457613.7661$	BJD _{TBD}
e_b	$\equiv 0.0$	$\equiv 0.0$	
ω_b	$\equiv 0.0$	$\equiv 0.0$	radians
K_b	$5.1^{+1.3}_{-1.4}$	5.1	m s^{-1}
M_b	19.3 ± 5.0	19.0	M_{\oplus}
R_b/R_*	$0.0190^{+0.0016}_{-0.0002}$	0.0185	
ρ_b	$9.9^{+0.1}_{-6.1}$	13.0	g cm^{-3}
R_b	$\equiv 2.1832$	$\equiv 2.1832$	R_{\oplus}
Priors			
Parameter	Prior		
None			

from K2-100 b, likely due to the high stellar jitter (see Table 11), but we rule out a high density for this planet. Our constraint on the Doppler semiamplitude is consistent with the value $K_b = 10.6 \pm 3.0 \text{ m s}^{-1}$ obtained by Barragán et al. (2019), who used a GP trained on activity indices to obtain a detection. We elected not to train the GP on activity indices for consistency with our analysis of other systems in this paper. K2-100 may be a good target for IR Doppler spectrometers that may be less affected by spot-related activity. Such measurements would still need to contend with the reduced information content of stellar spectra given the elevated $V \sin i$.

A.12. K2-31

K2-31 is a late G dwarf with a close-in, transiting sub-Saturn size planet ($R_P = 46 \pm 8 R_{\oplus}$, $P = 1.3$ days). See Tables 1 and 2 for stellar properties and Table 3 for precise planet parameters determined by our analysis. The planet was noted the catalogs of Barros et al. (2016), Crossfield et al. (2016), Vanderburg et al. (2016b), and Schmitt et al. (2016), and has been validated. Our fit of the EVEREST light curve of the K2 photometry for K2-31 is shown in Fig. 23. The V shape of the transit is due to the high impact parameter (grazing transit) and the short K2 sampling rate (30 min) compared to the transit duration (1 hr).

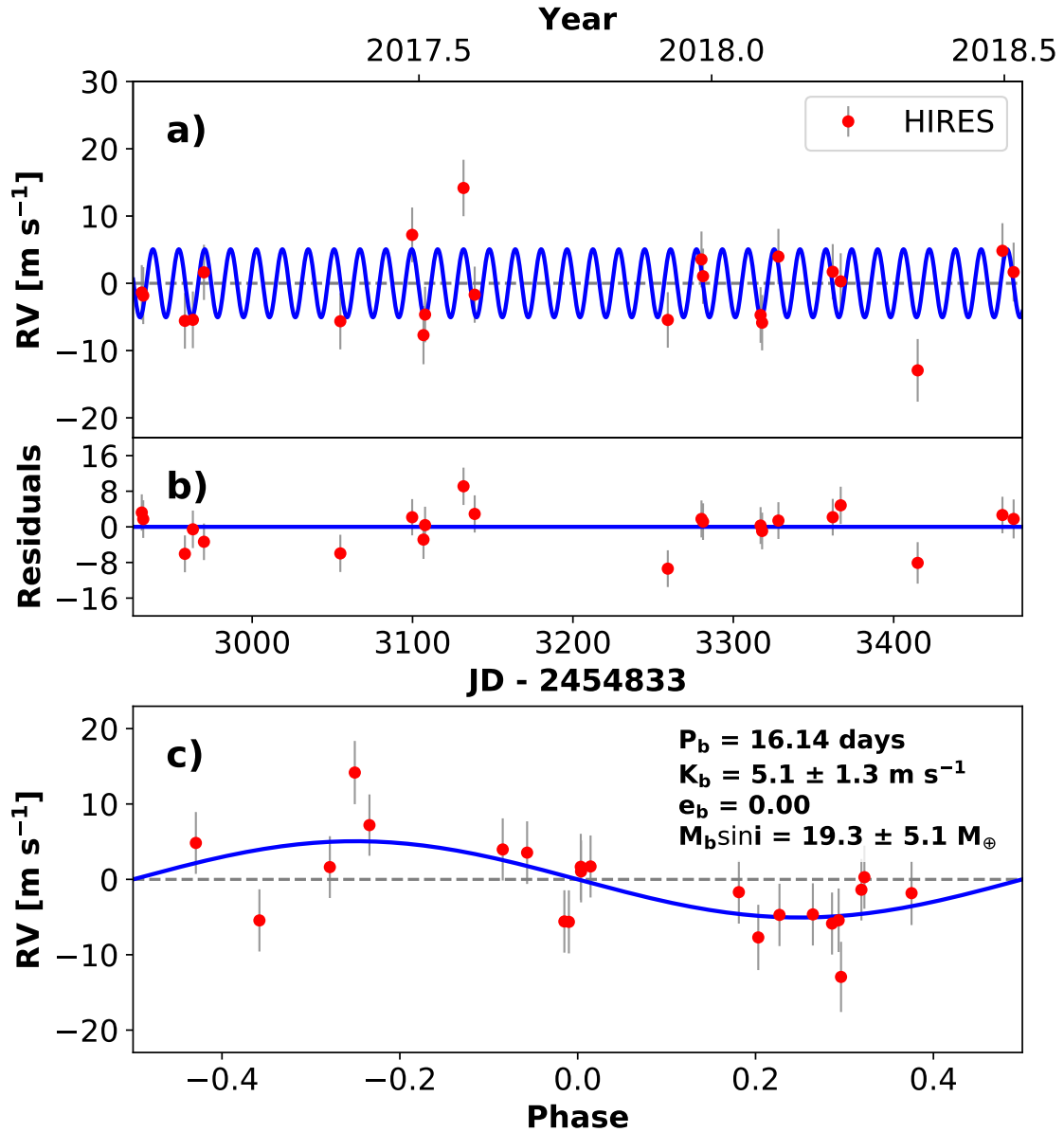


Figure 16. RVs and Keplerian model for K2-418. Symbols, lines, and annotations are similar to those in Fig. 11.

Grziwa et al. (2016) characterized the system using 6 FIES RVs and 3 HARPS RVs and measured a planet mass of $563.8 \pm 25.1 M_\oplus$. Due to the grazing transit ($b = 0.90\text{--}1.05$), its measured $R_P = 8.0\text{--}15.7 R_\oplus$ is highly uncertain. Dai et al. (2016) added seven RVs from PFS RVs and 10 from TRES. They modeled all available RVs and found a mass of $564.2_{-8.3}^{+9.5} M_\oplus$ with $e < 0.027$ (95% confidence).

We acquired 8 RVs of K2-31 with HIRES, typically with an exposure meter setting of 50,000 counts. The star is outside of our target sample and was mostly observed in poor conditions because it is bright and the Doppler signal was expected to be large. The star has somewhat elevated stellar activity ($\log R'_{\text{HK}} = -4.647$). We modeled the system as a single planet in a circular orbit with the orbital period and phase fixed to the transit ephemeris, without additional priors. The results are listed in Table 12 and the best-fit model is shown in Fig. 24. We find a mass of $551_{-17}^{+16} M_\oplus$, consistent

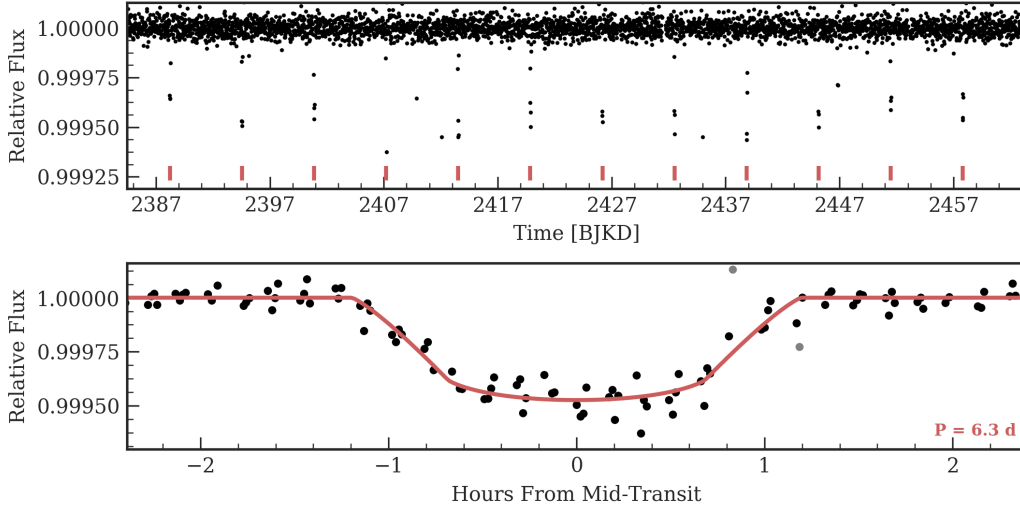


Figure 17. Time series (top) and phase-folded (bottom) light curve for the planet orbiting K2-277. Plot formatting is the same as in Fig. 10.

with previous studies. We considered more complicated models but found insufficient evidence to justify inclusion of orbital eccentricity or a linear RV trend based on the AICc statistic.

A.13. K2-39

K2-39 is a metal-rich ($[\text{Fe}/\text{H}] = 0.430 \pm 0.043$ dex) K-type subgiant with one transiting planet with a radius of $6.5 R_{\oplus}$ and an orbital period of 4.6 days. The planet is validated and appears in the Crossfield et al. (2016), Vanderburg et al. (2016b), and Schmitt et al. (2016) catalogs. See Tables 1 and 2 for stellar properties and Table 3 for precise planet parameters.

Van Eylen et al. (2016a) measured a mass of $50.3^{+9.7}_{-9.4} M_{\oplus}$ for K2-39 b using RVs from HARPS (7 measurements), FIES (17), and PFS (6). Their model also includes a long-term RV trend with curvature. Petigura et al. (2017b) also measured a mass of $30.9 \pm 4.6 M_{\oplus}$, using data from Van Eylen et al. (2016a) and 42 new HIRES RVs.

We attempted to reduce the data using EVEREST, but found unusually high photometric noise. Instead, we adopted a light curve of the K2 photometry produced using K2phot. The photometry is shown in Fig. 25. Petigura et al. (2017b) noted the discrepancy in R_P/R_{\star} between the adopted values from Crossfield et al. (2016) and Van Eylen et al. (2016a), reexamined the photometry using multiple pipelines, and adopted a value of 0.0179 ± 0.0013 (closer to the Van Eylen et al. (2016a) result). Our adopted value of $R_P/R_{\star} = 0.0180 \pm 0.0008$ is consistent with this.

We acquired a total of 45 RVs of K2-39 with HIRES, typically with an exposure meter setting of 80,000. We modeled the system as a single planet in a circular orbit with the orbital period and phase from the transit ephemerides. Our model does not include a linear trend as in Van Eylen et al. (2016a), or orbital eccentricity, based on model comparison using the AICc statistic. Since this system meets our N_{obs} and activity thresholds (Sec. 4.2.2), we include a GP trained on the photometry to model the stellar variability. The results of this analysis are listed in Table 13 and the best-fit model is shown in Fig. 26. K2-39 b is giant planet with a radius and density similar to Saturn’s.

Table 9. K2-277 System Parameters

Parameter	Credible Interval	Maximum Likelihood	Units
RV Analysis – MCMC Step Parameters			
P_b	$\equiv 6.3268$	$\equiv 6.3268$	days
$T_{\text{conj},b}$	$\equiv 2457221.2301$	$\equiv 2457221.2301$	BJD _{TBD}
$\sqrt{e} \cos \omega_b$	$\equiv 0.0$	$\equiv 0.0$	
$\sqrt{e} \sin \omega_b$	$\equiv 0.0$	$\equiv 0.0$	
K_b	2.6 ± 1.2	2.6	m s^{-1}
γ_{HIRES}	$-1.57^{+0.95}_{-0.97}$	-1.56	m s^{-1}
$\dot{\gamma}$	$0.0308^{+0.0088}_{-0.0087}$	0.0307	$\text{m s}^{-1} \text{ day}^{-1}$
$\ddot{\gamma}$	$\equiv 0.0$	$\equiv 0.0$	$\text{m s}^{-1} \text{ day}^{-2}$
σ_{HIRES}	$4.24^{+1.20}_{-0.20}$	3.80	m s^{-1}
Orbital & Physical Parameters			
P_b	$\equiv 6.3268$	$\equiv 6.3268$	days
$T_{\text{conj},b}$	$\equiv 2457221.2301$	$\equiv 2457221.2301$	BJD _{TBD}
e_b	$\equiv 0.0$	$\equiv 0.0$	
ω_b	$\equiv 0.0$	$\equiv 0.0$	radians
K_b	2.6 ± 1.2	2.6	m s^{-1}
M_b	$7.4^{+3.4}_{-3.3}$	7.4	M_{\oplus}
R_b/R_*	$0.0202^{+0.0017}_{-0.0001}$	0.0198	
ρ_b	$3.5^{+0.5}_{-2.8}$	4.7	g cm^{-3}
R_b	$\equiv 2.2324$	$\equiv 2.2324$	R_{\oplus}
Priors			
Parameter	Prior		
None			

NOTE—

 Reference epoch for $\dot{\gamma}, \ddot{\gamma}$: 2457728.9046480004

We searched for additional planets in the system using Keplerian models without a Gaussian process. First, we searched for two-planet solutions with circular orbits, as shown in Fig. 27. No candidate period was identified that exceeded the 1% false alarm threshold. We do see excess power in a series of peaks near 30 days and at ~ 1 year, both of which correspond to patterns in our observing cadence. We performed a deeper search by fitting for the most significant period in Fig. 27 at 24 days and a third trial period. This periodogram (not shown) did not reveal any convincing candidate periods.

A.14. K2-229

K2-229 is a K0 dwarf with two transiting planets that have sizes $1.2 R_{\oplus}$ and $2.0 R_{\oplus}$ and orbital periods of 14 hr and 8 days. See Tables 1 and 2 for stellar properties and Table 3 for precise planet parameters.

The planets were first noted in Mayo et al. (2018), where they were validated. Santerne et al. (2018) followed up with 104 high-cadence RVs from HARPS that provided precise mass estimates. Their model included a GP constrained to the rotational period of 18.1 ± 0.3 days. They found masses of

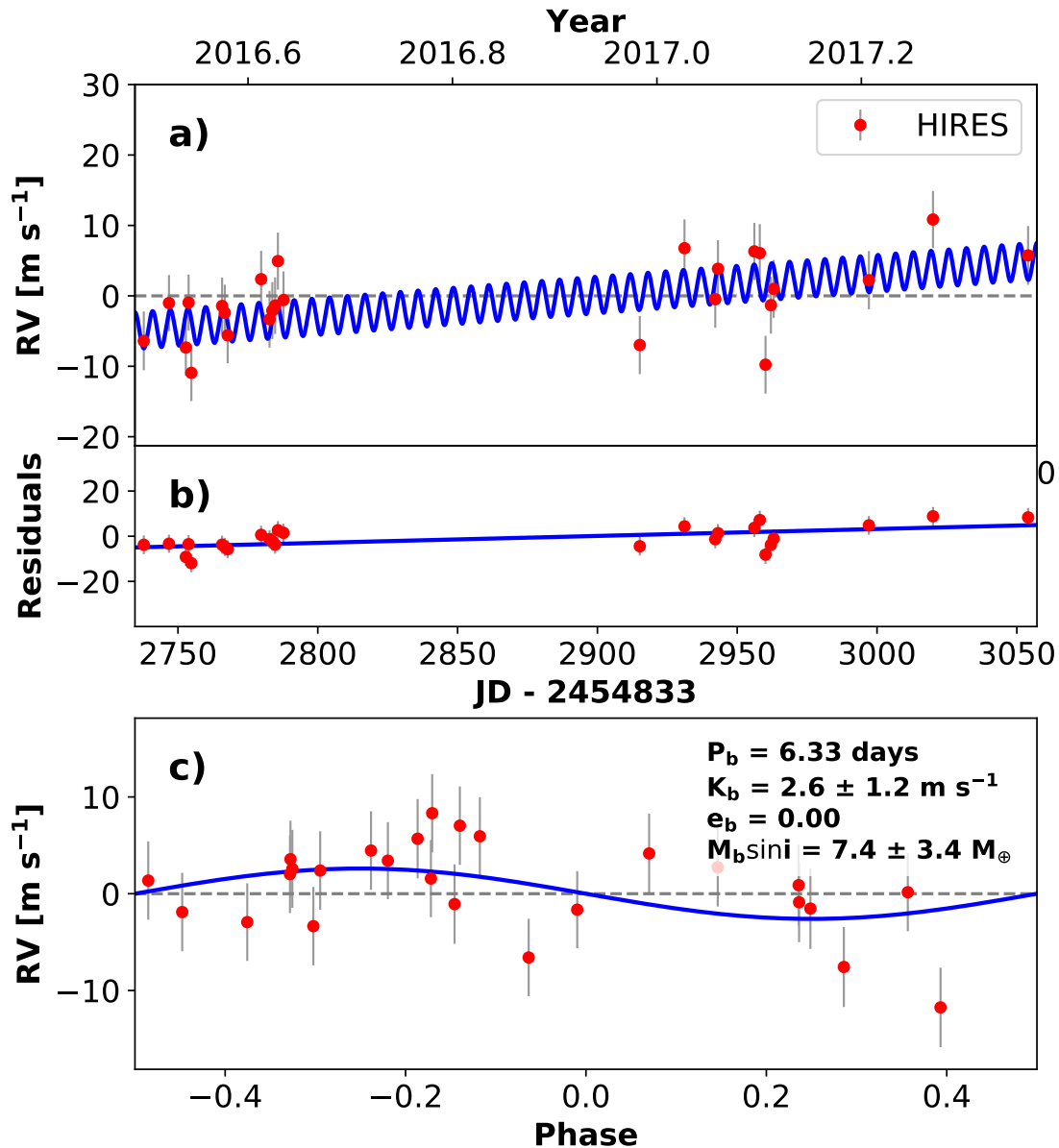


Figure 18. RVs and Keplerian model for K2-277. Symbols, lines, and annotations are similar to those in Fig. 11.

$2.59 \pm 0.43 M_\oplus$ and $< 21.3 M_\oplus$ (95% confidence), with corresponding densities of 8.9 ± 2.1 g cm⁻³ and < 12.8 g cm⁻³, for planets b and c respectively. They concluded that planet b has a 30%/70% mass fraction for rock/iron composition, i.e., closer to Mercury than Earth. The [Santerne et al. \(2018\)](#) analysis also included a nontransiting planet with $P = 31.0 \pm 0.1$ days and a mass of $< 25.1 M_\oplus$.

Our fit of the EVEREST light curve of the K2 photometry for K2-229 is shown in Fig. 28. We acquired 24 RVs of K2-229 with HIRES, typically with an exposure meter setting of 125,000 counts. The host star has significant activity, with $\log R'_{\text{HK}} = -4.603$. We modeled the system as a two-planet fit, including a Gaussian process to account for the stellar activity. We considered adding additional parameters to the model including an RV trend, planet eccentricities, and a third non-transiting

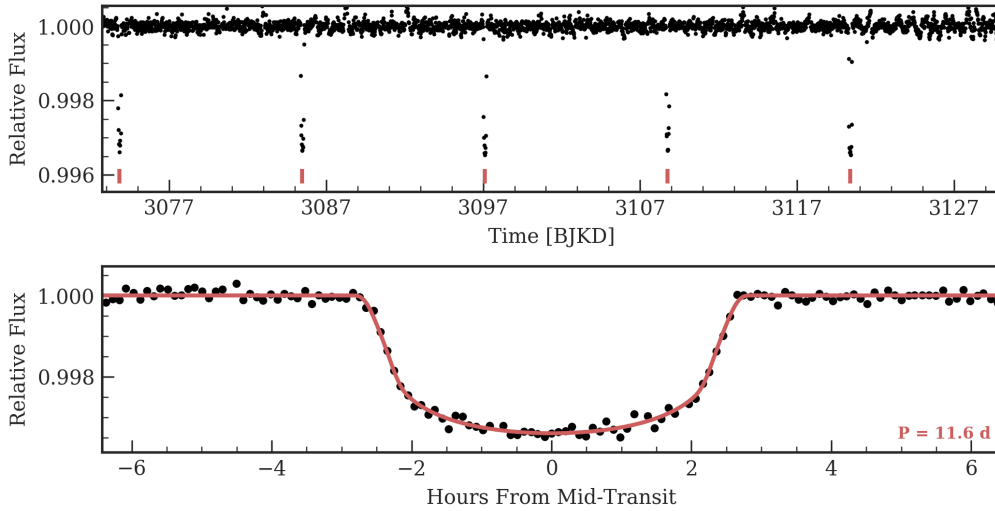


Figure 19. Time series (top) and phase-folded (bottom) light curve for the planet orbiting K2-261. Plot formatting is the same as in Fig. 10.

planet, but rejected those based on model comparison using the AICc statistic. The results of this analysis are listed in Table 14 and the best-fit model is shown in Fig. 29.

The primary result of Santerne et al. (2018) is that K2-229 b has a high density ($8.9 \pm 2.1 \text{ g cm}^{-3}$), which implies a large iron fraction (70%). Density depends on R_P , R_P/R_* , R_* , and M_P . Our mass measurement is consistent with that from Santerne et al. (2018); however we measure a larger R_P/R_* resulting in a smaller density ($7.5^{+2.05}_{-1.61} \text{ g cm}^{-3}$), requiring a smaller iron fraction (0–30%) based on the Fortney et al. (2007) mass-radius models.

A.15. K2-111

K2-111 is a solar-type star from Field 4 with low metallicity ($[\text{Fe}/\text{H}] = -0.440 \pm 0.044$). It has one transiting planet with a radius of $1.3 R_\oplus$ and an orbital period of 5.3 days. See Tables 1 and 2 for stellar properties and Table 3 for precise planet parameters.

The planet was initially listed as a false positive in Crossfield et al. (2016). Fridlund et al. (2017) validated the system and measured a mass of $8.6 \pm 3.9 M_\oplus$ using six FIES and 12 HARPS-N RVs. They also determined that the star is in the background of the Hyades cluster, at four times the distance. A subsequent analysis with more data reveal a lower and more precise mass of $5.6 \pm 0.7 M_\oplus$ and a second, non-transiting planet Mortier et al. (2020); Bonomo et al. (2023b). Our fit of the EVEREST light curve of the K2 photometry for K2-111 is shown in Fig. 30. We find a radius that is consistent with, but more precise than, the value from Mayo et al. (2018).

We acquired 54 RVs of K2-111 with HIRES, typically with an exposure meter setting of 125,000. Using the RVs from HIRES, HARPS-N, and FIES, we modeled the system as a single planet with the orbital period and phase fixed to the transit ephemeris. The results of this analysis are listed in Table 15 and the best-fit model is shown in Fig. 31. Fridlund et al. (2017) noted a trend in the residual RVs to their one-planet fit. We found weak evidence for this trend in the HIRES RVs; however, a model with a trend yielded a posterior for $\dot{\gamma}$ consistent with zero. We thus adopted the simpler model with no trend. We also ruled out a eccentric orbit based on an AICc comparison. Our mass of $5.4^{+2.2}_{-2.1}$

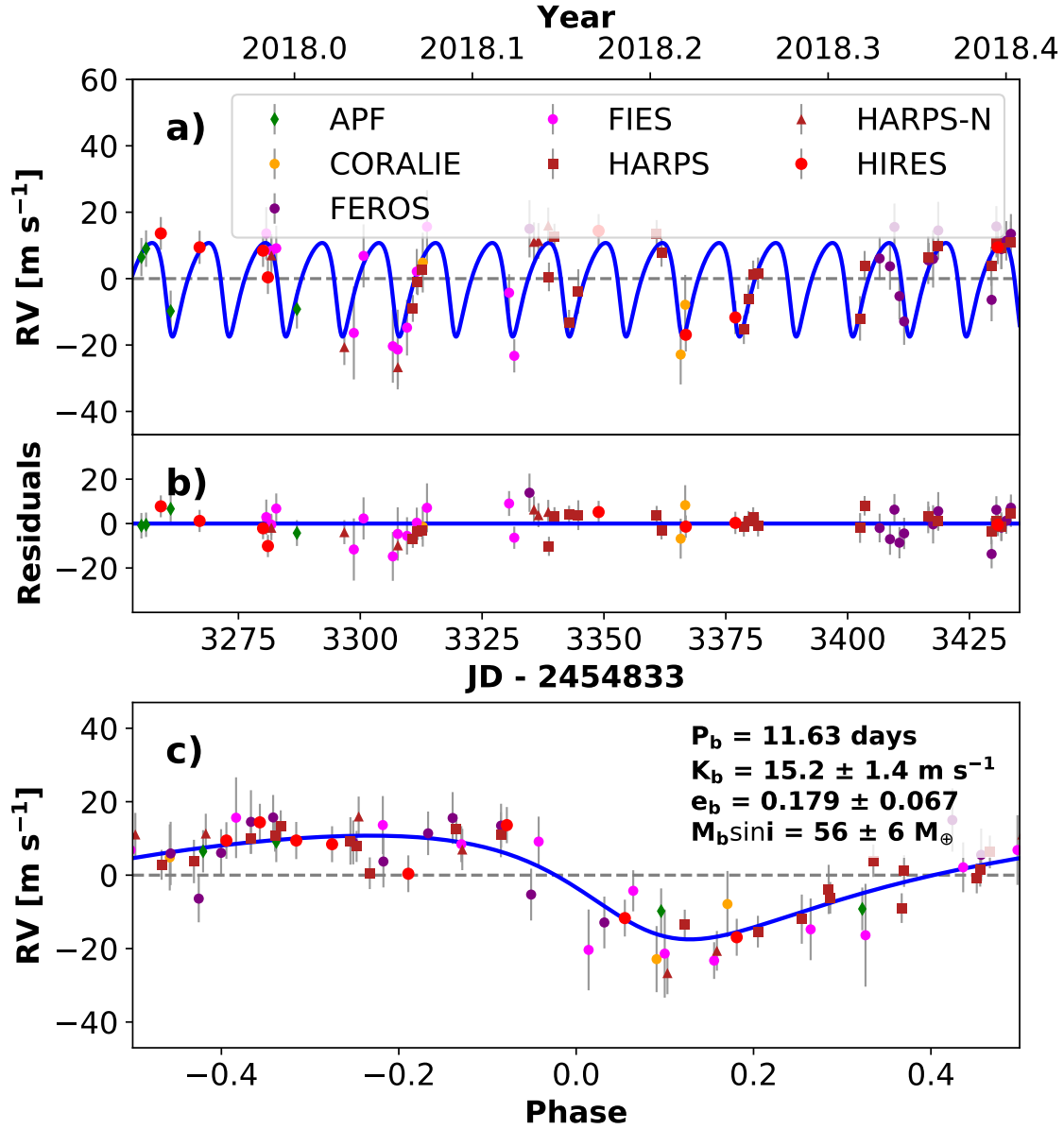


Figure 20. RVs and Keplerian model for K2-261. Symbols, lines, and annotations are similar to those in Fig. 11.

M_{\oplus} is consistent with the literature values (Fridlund et al. 2017; Mortier et al. 2020; Bonomo et al. 2023b). Our improved mass and radius estimates yield a high density ($13.8^{+7.3}_{-5.9}$ g cm $^{-3}$) consistent with a rocky composition, more confidently placing K2-111 b in the super-Earth category.

A.16. K2-99

K2-99 is subgiant from Campaign 6 and 17 that hosts one transiting sub-Saturn-size planet with an orbital period of 18 days. See Tables 1 and 2 for stellar properties and Table 3 for precise planet parameters. Smith et al. (2017) first noted the planet and measured a mass of $308 \pm 29 M_{\oplus}$ based on 14 FIES RVs, 5 HARPS-N RVs, 6 McDonald 2.7m RVs, and 8 HARPS RVs. Their model included a free eccentricity ($e = 0.19 \pm 0.04$) and linear RV trend (-2.12 ± 0.04 m s $^{-1}$ yr $^{-1}$). The planet is also listed in the catalogs by Pope et al. (2016), Crossfield et al. (2018), Petigura et al. (2018a), and Mayo

Table 10. K2-261 System Parameters

Parameter	Credible Interval	Maximum Likelihood	Units
RV Analysis – MCMC Step Parameters			
P_b	$\equiv 11.634$	$\equiv 11.634$	days
$T_{\text{conj},b}$	$\equiv 2457906.8406$	$\equiv 2457906.8406$	BJD _{TBD}
$\sqrt{e} \cos \omega_b$	$-0.33^{+0.11}_{-0.08}$	-0.34	
$\sqrt{e} \sin \omega_b$	$0.22^{+0.17}_{-0.23}$	0.30	
K_b	$15.2^{+1.6}_{-1.5}$	14.7	m s^{-1}
γ_{HIRES}	$-7.0^{+2.6}_{-2.7}$	-7.0	m s^{-1}
$\gamma_{\text{HARPS-N}}$	3334 ± 4	3333.5	
γ_{HARPS}	$3341.5^{+1.4}_{-1.5}$	3341.6	m s^{-1}
γ_{FIES}	-14.1 ± 2.4	-14.1	m s^{-1}
γ_{FEROS}	$\equiv 3319.9914$	$\equiv 3319.9914$	m s^{-1}
γ_{CORALIE}	$\equiv 3327.3724$	$\equiv 3327.3724$	m s^{-1}
γ_{APF}	$-5.9^{+3.3}_{-3.5}$	-7.9	m s^{-1}
$\dot{\gamma}$	$\equiv 0.0$	$\equiv 0.0$	$\text{m s}^{-1} \text{ day}^{-1}$
$\ddot{\gamma}$	$\equiv 0.0$	$\equiv 0.0$	$\text{m s}^{-1} \text{ day}^{-2}$
σ_{HIRES}	$6.5^{+3.1}_{-1.8}$	5.4	m s^{-1}
$\sigma_{\text{HARPS-N}}$	$8.4^{+5.8}_{-3.1}$	6.3	
σ_{HARPS}	$3.6^{+1.8}_{-1.2}$	3.2	m s^{-1}
σ_{FIES}	$0.6^{+3.5}_{-0.6}$	0.0	m s^{-1}
σ_{FEROS}	$\equiv 5.0302$	$\equiv 5.0302$	m s^{-1}
σ_{CORALIE}	$\equiv 0.0$	$\equiv 0.0$	m s^{-1}
σ_{APF}	$0.1^{+5.5}_{-0.1}$	0.0	m s^{-1}
Orbital & Physical Parameters			
P_b	$\equiv 11.634$	$\equiv 11.634$	days
$T_{\text{conj},b}$	$\equiv 2457906.8406$	$\equiv 2457906.8406$	BJD _{TBD}
e_b	$0.179^{+0.074}_{-0.056}$	0.161	
ω_b	$2.6^{+0.6}_{-0.4}$	2.4	radians
K_b	$15.2^{+1.6}_{-1.5}$	14.7	m s^{-1}
M_b	56^{+7}_{-6}	56	M_{\oplus}
ρ_b	$0.277^{+0.034}_{-0.032}$	0.320	g cm^{-3}
Priors			
Parameter	Prior		
e_b	< 0.99		
$j_{\text{it}}^{\text{HIRES}}$	$\mathcal{U}(0, 1e + 100)$		
$j_{\text{it}}^{\text{APF}}$	$\mathcal{U}(0, 1e + 100)$		
$j_{\text{it}}^{\text{CORALIE}}$	$\mathcal{U}(0, 1e + 100)$		
$j_{\text{it}}^{\text{FEROS}}$	$\mathcal{U}(0, 1e + 100)$		
$j_{\text{it}}^{\text{HARPS}}$	$\mathcal{U}(0, 1e + 100)$		
$j_{\text{it}}^{\text{FIES}}$	$\mathcal{U}(0, 1e + 100)$		
$j_{\text{it}}^{\text{HARPS-N}}$	$\mathcal{U}(0, 1e + 100)$		

et al. (2018). A more recent RV analysis updates the sizes of the host star and planet to $2.55 R_{\odot}$ and $1.06 R_{\text{Jup}}$, respectively, and identifies an outer planet c with a 522-day period and mass of $8.4 M_{\text{Jup}}$ (Smith et al. 2022).

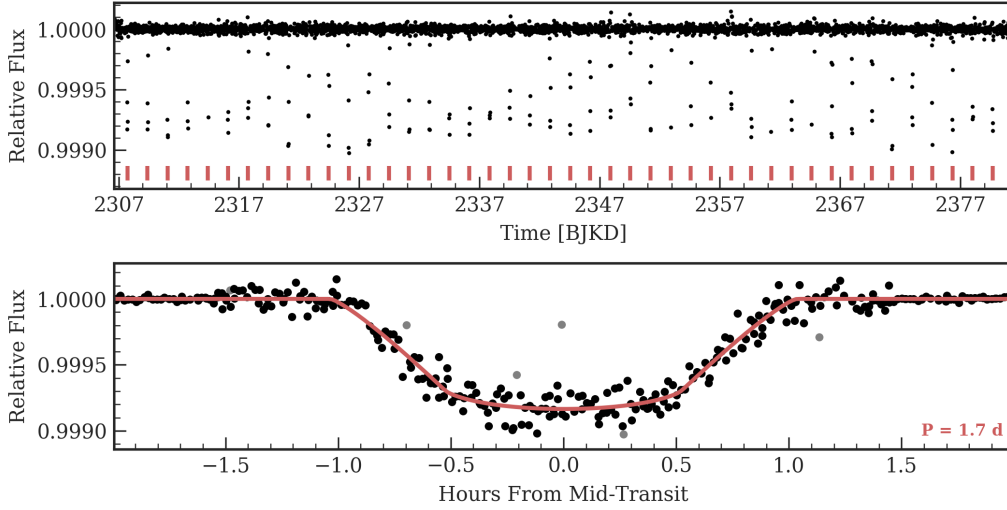


Figure 21. Time series (top) and phase-folded (bottom) light curve for the planet orbiting K2-100. Plot formatting is the same as in Fig. 10.

Our fit of the EVEREST light curve of the K2 photometry for K2-99 is shown in Fig. 33. We acquired 19 RVs of K2-99 with HIRES, typically with an exposure meter setting of 60,000. We modeled the system as a single planet with free eccentricity and a linear RV trend. The results of this analysis are listed in Table 16 and the best-fit model is shown in Fig. 34. The next-best model had a circular orbit and a linear trend and ΔAICc of 17 compared to the selected model. K2-99 b is a giant planet in a moderately eccentric orbit.

A.17. K2-265

K2-265 is a late G dwarf with one transiting planet with a radius of $1.7 R_{\oplus}$ and an orbital period of 2.4 days. See Tables 1 and 2 for stellar properties and Table 3 for planet parameters. The planet was listed as a candidate in Crossfield et al. (2016), who noted an imaged companion with a separation of $\sim 1''$ and $\Delta K = 2.8$ mag. The transit duration is consistent with the planet orbiting the brighter star. Vanderburg et al. (2016b) and Mayo et al. (2018) also list the object as a planet candidate. Lam et al. (2018) validated the system using K2 photometry and measured a mass of $6.54 \pm 0.84 M_{\oplus}$ and a density of $7.1 \pm 1.8 \text{ g cm}^{-3}$ based on 153 HARPS RVs. Our fit of the EVEREST light curve of the K2 photometry for K2-265 is shown in Fig. 35.

We acquired 53 RVs of K2-265 with HIRES, typically with an exposure meter setting of 125,000. With $\log R'_{\text{HK}} = -4.878$ and 53 RVs from HIRES, K2-265 is an excellent candidate for GP regression. As described in Sec. 4.2.2, we trained the GP hyperparameters on non-detrended Everest photometry before using computing RV orbit posteriors. For comparison, we also performed an RV orbit fit using an untrained GP. The trained and the untrained GP models produce semi-amplitudes values for planet b that are consistent within 1σ (2.4 ± 0.8 and 2.1 ± 0.8 , respectively), but the trained GP produces a median value 15% higher. The median value of K_b returned by the trained GP fit is identical to that produced by a non-GP fit, but the uncertainty on K_b is almost halved. Note that the apparent correlated noise features in the RVs near 2017.5 and 2018.0 are also seen in the S_{HK}

Table 11. K2-100 System Parameters

Parameter	Credible Interval	Maximum Likelihood	Units
RV Analysis – MCMC Step Parameters			
P_b	$\equiv 1.6739$	$\equiv 1.6739$	days
$T_{\text{conj},b}$	$\equiv 2457140.7197$	$\equiv 2457140.7197$	BJD _{TBD}
$\sqrt{e} \cos \omega_b$	$\equiv 0.0$	$\equiv 0.0$	
$\sqrt{e} \sin \omega_b$	$\equiv 0.0$	$\equiv 0.0$	
K_b	3.7 ± 7.3	8.0	m s^{-1}
γ_{HIRES}	-1^{+20}_{-22}	-1	m s^{-1}
$\gamma_{\text{HARPS-N}}$	34342^{+65}_{-69}	34380	m s^{-1}
$\dot{\gamma}$	$\equiv 0.0$	$\equiv 0.0$	$\text{m s}^{-1} \text{ day}^{-1}$
$\ddot{\gamma}$	$\equiv 0.0$	$\equiv 0.0$	$\text{m s}^{-1} \text{ day}^{-2}$
σ_{HIRES}	24^{+8}_{-11}	10	m s^{-1}
$\sigma_{\text{HARPS-N}}$	44^{+9}_{-15}	10	m s^{-1}
η_3	13^{+28}_{-5}	4	days
η_2	60^{+5}_{-12}	5	days
η_4	$0.492^{+0.063}_{-0.058}$	0.500	
$\eta_{1,\text{HIRES}}$	28^{+47}_{-20}	25	m s^{-1}
$\eta_{1,\text{HARPS-N}}$	145^{+57}_{-36}	90	m s^{-1}
Orbital & Physical Parameters			
P_b	$\equiv 1.6739$	$\equiv 1.6739$	days
$T_{\text{conj},b}$	$\equiv 2457140.7197$	$\equiv 2457140.7197$	BJD _{TBD}
e_b	$\equiv 0.0$	$\equiv 0.0$	
ω_b	$\equiv 0.0$	$\equiv 0.0$	radians
K_b	3.7 ± 7.3	8.0	m s^{-1}
M_b	8 ± 15	17	M_{\oplus}
R_b/R_*	$0.0267^{+0.0007}_{-0.0003}$	0.0267	
ρ_b	0.9 ± 1.8	2.0	g cm^{-3}
R_b	$3.57^{+0.10}_{-0.04}$	3.57	R_{\oplus}
Priors			
Parameter	Prior		
$\eta_{1,\text{HIRES}}$	$\mathcal{U}(0, 100)$		
$\eta_{1,\text{HARPS-N}}$	$\mathcal{U}(0, 100)$		
η_2	$\mathcal{U}(0, 67.019839)$		
η_3	$\mathcal{U}(0, 67.019839)$		
η_4	$\mathcal{N}(0.5, 0.05)$		
σ_{HIRES}	$\mathcal{U}(0, 10)$		
$\sigma_{\text{HARPS-N}}$	$\mathcal{U}(0, 10)$		

time series and are modeled by the GP. This system illustrates the power of GP regression to improve the precision of orbit fitting analyses.

A.18. K2-24

K2-24 is a metal-rich G dwarf with two transiting planets that have sizes $5.4 R_{\oplus}$ and $7.5 R_{\oplus}$, between that of Uranus and Saturn. The orbital periods (20.9 days and 42.4 days) are within 1% of a 2:1

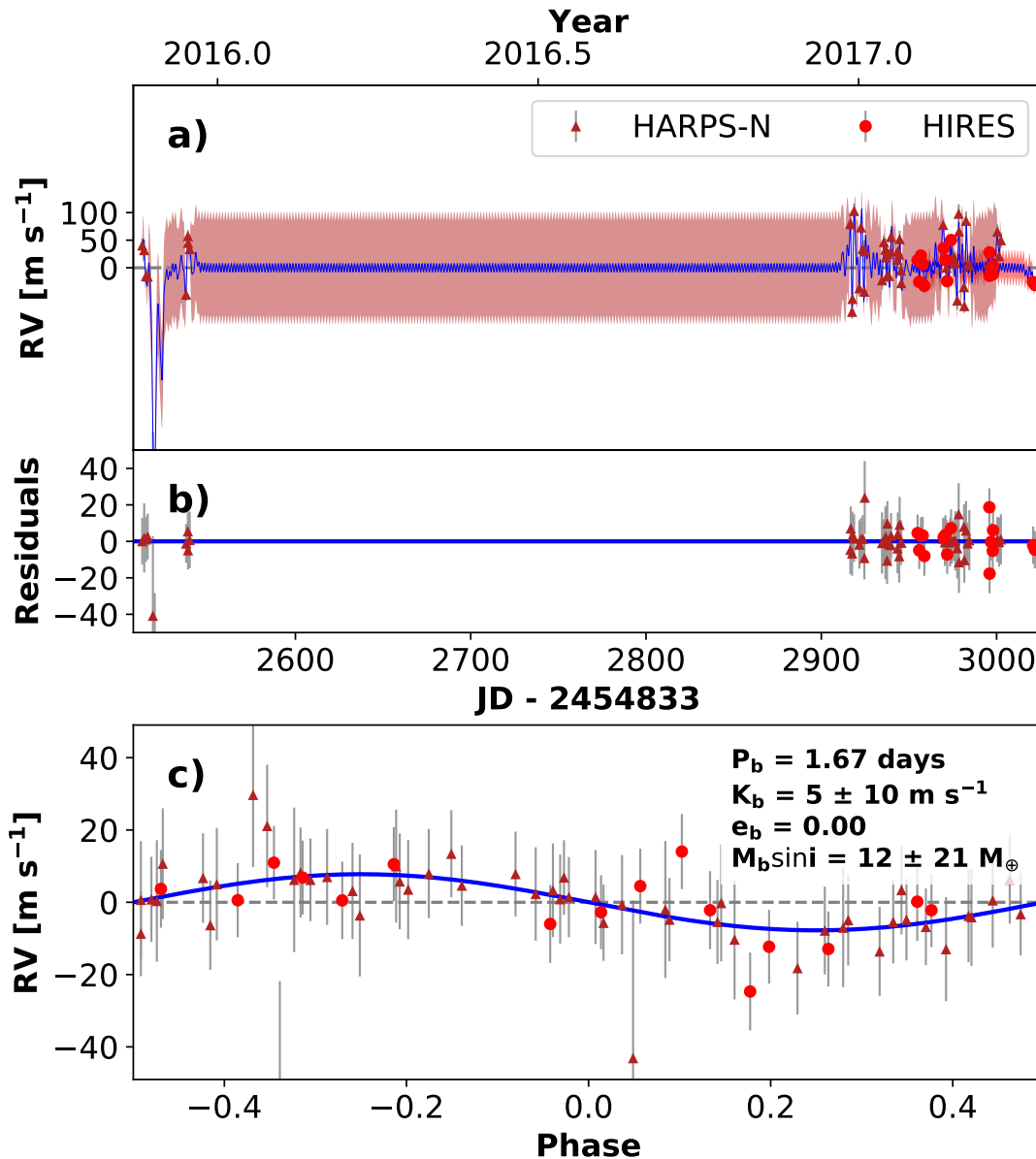


Figure 22. RVs and Keplerian model for K2-100. Symbols, lines, and annotations are similar to those in Fig. 11.

ratio. The system is noted in the catalogs of [Crossfield et al. \(2016\)](#), [Vanderburg et al. \(2016b\)](#), [Sinukoff et al. \(2016\)](#), [Wittenmyer et al. \(2018\)](#).

[Petigura et al. \(2016\)](#) validated the planets and measured masses of $21.0 \pm 5.4 M_{\oplus}$ and (planet b) $27.0 \pm 6.9 M_{\oplus}$ (planet c) based on 32 RVs from HIRES. The bulk densities of $0.63 \pm 0.25 \text{ g cm}^{-3}$ and $0.31 \pm 0.12 \text{ g cm}^{-3}$, respectively, are low for planets of that size, and modeling suggested that thick envelopes of H/He to needed to account for the masses and radii. [Dai et al. \(2016\)](#) measured 16 PFS RVs and 10 HARPS RVs. Their model of the PFS, HARPS, and HIRES RVs gave masses of $19.8^{+4.5}_{-4.4} M_{\oplus}$ and $26.0^{+5.8}_{-6.1} M_{\oplus}$, respectively. [Petigura et al. \(2018b\)](#) reported on additional HIRES RVs taken this project (63 RVs total). Their analysis included transit times from K2 photometry as well as four transit epochs from Spitzer. The additional RVs over a longer baseline revealed a

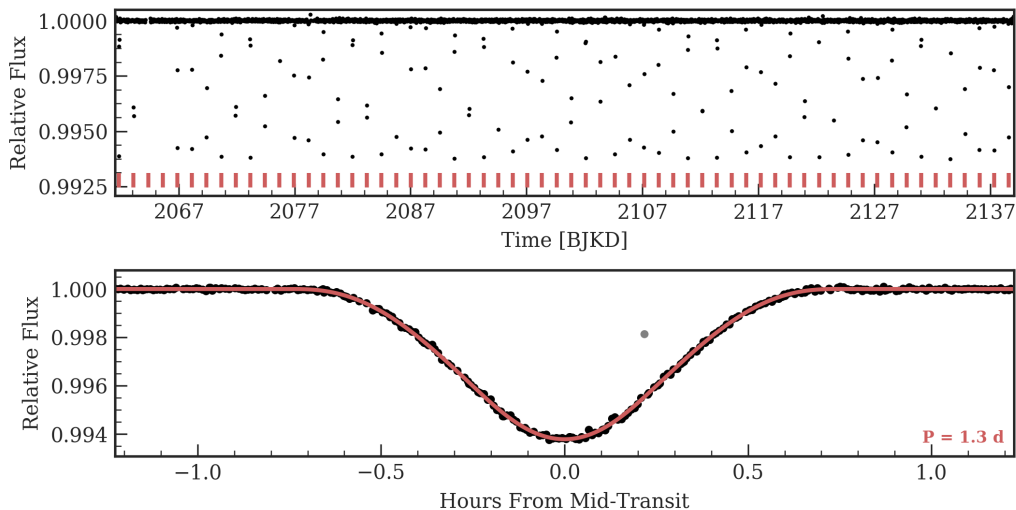


Figure 23. Time series (top) and phase-folded (bottom) light curve for the planet orbiting K2-31. Plot formatting is the same as in Fig. 10.

non-transiting planet (K2-24d) with an orbital period of 428 days. Modeling the RVs and TTVs simultaneously gave much tighter constraints for the planet masses ($19.0^{+2.2}_{-2.1} M_{\oplus}$ and $15.4^{+1.9}_{-1.8} M_{\oplus}$, respectively) and eccentricities ($e \sim 0.08$ for both planets). Interestingly, K2-24b is 20% less massive than K2-24c despite being 40% larger. We adopt the planet parameters from [Petigura et al. \(2018b\)](#). The full set of adopted parameters (stellar and planetary) is listed in Tables 1, 2 and 3.

A.19. K2-38

K2-38 is a metal-rich, solar-type star in Field 2 with two detected transiting planets. The planets have sizes $1.6 R_{\oplus}$ and $2.4 R_{\oplus}$ and periods of 4 days and 10 days, respectively. See Tables 1 and 2 for stellar properties and Table 3 for precise planet parameters.

The planets orbiting K2-38 were first identified and validated in [Sinukoff et al. \(2016\)](#), who measured preliminary masses using 14 RVs from HIRES. They modeled the system as two planets in circular orbits and found masses of $12.0 \pm 2.9 M_{\oplus}$ and $9.9 \pm 4.6 M_{\oplus}$, corresponding to densities of $17.5^{+8.5}_{-6.2} \text{ g cm}^{-3}$ and $3.6^{+2.7}_{-1.9} \text{ g cm}^{-3}$, respectively. Their model also included a linear trend of $-37 \pm 11 \text{ m s}^{-1} \text{ yr}^{-1}$; this model was favored over a flat model with $\Delta \text{BIC} = 5.6$. This analysis suggests that the inner planet has an implausibly high bulk density, while the outer planet was detected with $\sim 2\text{-}\sigma$ significance and a density intermediate between that of rocky and gas-dominated planets. The two planets also appear in catalogs by [Crossfield et al. \(2016\)](#) and [Wittenmyer et al. \(2018\)](#). More recently, [Bonomo et al. \(2023b\)](#) report planet masses of $7.7 \pm 1.2 M_{\oplus}$ and $7.4 \pm 1.4 M_{\oplus}$ for planets b and c, respectively; consistent with the values we report below.

Our fit of the EVEREST light curve of the K2 photometry for K2-38 is shown in Fig. 38. We acquired 65 RVs of K2-38 with HIRES (including the 14 RVs from [Sinukoff et al. \(2016\)](#)), typically with an exposure meter setting of 125,000 counts. We also acquired three template exposures using the B3 decker on HIRES and an exposure meter setting of 250,000 to correct for a spurious 1 yr signal present in the RV time series generated using the first two templates. The amplitude of this signal ($\sim 2\text{--}4 \text{ m s}^{-1}$) varied depending on the template used. The signal is nearly absent in the final

Table 12. K2-31 System Parameters

Parameter	Credible Interval	Maximum Likelihood	Units
RV Analysis – MCMC Step Parameters			
P_b	$\equiv 1.2578$	$\equiv 1.2578$	days
$T_{\text{conj},b}$	$\equiv 2456893.599$	$\equiv 2456893.599$	BJD _{TBD}
$\sqrt{e} \cos \omega_b$	$\equiv 0.0$	$\equiv 0.0$	
$\sqrt{e} \sin \omega_b$	$\equiv 0.0$	$\equiv 0.0$	
K_b	$346.7^{+3.7}_{-4.8}$	349.7	m s ⁻¹
γ_{TRES}	-147 ± 10	-147	m s ⁻¹
γ_{PFS}	$53.4^{+5.5}_{-5.7}$	53.6	m s ⁻¹
γ_{HIRES}	69 ± 5	69.9	m s ⁻¹
γ_{HARPS}	-4752^{+7}_{-10}	-4751	m s ⁻¹
γ_{FIES}	$-4947.9^{+3.8}_{-4.1}$	-4946.0	m s ⁻¹
$\dot{\gamma}$	$\equiv 0.0$	$\equiv 0.0$	m s ⁻¹ day ⁻¹
$\ddot{\gamma}$	$\equiv 0.0$	$\equiv 0.0$	m s ⁻¹ day ⁻²
σ_{TRES}	28^{+11}_{-8}	24	m s ⁻¹
σ_{PFS}	$14.3^{+6.7}_{-3.9}$	11.1	m s ⁻¹
σ_{HIRES}	$13.2^{+6.1}_{-3.9}$	12.0	m s ⁻¹
σ_{HARPS}	11^{+30}_{-7}	2	m s ⁻¹
σ_{FIES}	$2.9^{+5.2}_{-2.5}$	0.0	m s ⁻¹
Orbital & Physical Parameters			
P_b	$\equiv 1.2578$	$\equiv 1.2578$	days
$T_{\text{conj},b}$	$\equiv 2456893.599$	$\equiv 2456893.599$	BJD _{TBD}
e_b	$\equiv 0.0$	$\equiv 0.0$	
ω_b	$\equiv 0.0$	$\equiv 0.0$	radians
K_b	$346.7^{+3.7}_{-4.8}$	349.7	m s ⁻¹
M_b	551^{+16}_{-17}	557	M_{\oplus}
R_b/R_*	$0.366^{+0.061}_{-0.064}$	0.429	
ρ_b	$0.032^{+0.025}_{-0.012}$	0.020	g cm ⁻³
R_b	46 ± 8	53.2	R_{\oplus}
Priors			
Parameter	Prior		
jit_{HIRES}	$\mathcal{U}(0, 1e + 100)$		
jit_{FIES}	$\mathcal{U}(0, 1e + 100)$		
jit_{HARPS}	$\mathcal{U}(0, 1e + 100)$		
jit_{PFS}	$\mathcal{U}(0, 1e + 100)$		
jit_{TRES}	$\mathcal{U}(0, 1e + 100)$		

template (from which the RVs in Table 4 were computed). It appears that poor selection of the B stars (used for template deconvolution) is responsible for the systematic errors in the previous reductions.

We modeled the system as two planets in circular orbits with periods and phases fixed to the values from the K2 ephemerides. We found that an eccentric fit is significantly favored (from an AICc comparison), however the best-fit eccentricity is at unphysically high values ($e_b \sim 0.8$) for the short period and compact nature of the two planets. As a result, we adopt fits with circular orbits. The

Table 13. K2-39 System Parameters

Parameter	Credible Interval	Maximum Likelihood	Units
RV Analysis – MCMC Step Parameters			
P_b	$\equiv 4.6055$	$\equiv 4.6055$	days
$T_{\text{conj},b}$	$\equiv 2456985.4268$	$\equiv 2456985.4268$	BJD _{TBD}
$\sqrt{e} \cos \omega_b$	$\equiv 0.0$	$\equiv 0.0$	
$\sqrt{e} \sin \omega_b$	$\equiv 0.0$	$\equiv 0.0$	
K_b	11.7 ± 1.3	11.8	m s^{-1}
γ_{PFS}	$-1^{+4.2}_{-3.9}$	-1.0	m s^{-1}
γ_{HIRES}	$-1.4^{+2.8}_{-3.4}$	-1.1	m s^{-1}
γ_{HARPS}	$24490^{+4.9}_{-4.7}$	24489.7	m s^{-1}
γ_{FIES}	24569^{+11}_{-12}	24569	m s^{-1}
γ_{APF}	3^{+9}_{-11}	3	m s^{-1}
$\dot{\gamma}$	$\equiv 0.0$	$\equiv 0.0$	$\text{m s}^{-1} \text{ day}^{-1}$
$\ddot{\gamma}$	$\equiv 0.0$	$\equiv 0.0$	$\text{m s}^{-1} \text{ day}^{-2}$
σ_{PFS}	6^{+6}_{-16}	6	m s^{-1}
σ_{HIRES}	$4.6^{+1.7}_{-0.3}$	4.0	m s^{-1}
σ_{HARPS}	7^{+6}_{-20}	8	m s^{-1}
σ_{FIES}	$-0.00^{+0.39}_{-0.65}$	-0.00	m s^{-1}
σ_{APF}	$-0.00^{+0.22}_{-0.54}$	-0.00	m s^{-1}
η_3	32^{+18}_{-2}	27	days
η_2	18^{+16}_{-5}	15	days
η_4	$0.500^{+0.050}_{-0.060}$	0.510	
$\eta_{1,\text{HIRES}}$	$10.1^{+3.7}_{-0.9}$	9.2	m s^{-1}
$\eta_{1,\text{APF}}$	$12^{+23.9}_{-0.3}$	5.0	m s^{-1}
$\eta_{1,\text{HARPS}}$	$\equiv 0.0056$	$\equiv 0.0056$	m s^{-1}
$\eta_{1,\text{FIES}}$	21^{+19}_{-1}	15	m s^{-1}
$\eta_{1,\text{PFS}}$	$\equiv 0.0011$	$\equiv 0.0011$	m s^{-1}
Orbital & Physical Parameters			
P_b	$\equiv 4.6055$	$\equiv 4.6055$	days
$T_{\text{conj},b}$	$\equiv 2456985.4268$	$\equiv 2456985.4268$	BJD _{TBD}
e_b	$\equiv 0.0$	$\equiv 0.0$	
ω_b	$\equiv 0.0$	$\equiv 0.0$	radians
K_b	11.7 ± 1.3	11.8	m s^{-1}
M_b	$37.6^{+4.9}_{-5.3}$	38.0	M_{\oplus}
R_b/R_*	$0.0180^{+0.0014}_{-0.0002}$	0.0177	
ρ_b	$\equiv 0.7652$	$\equiv 0.7652$	g cm^{-3}
R_b	$\equiv 6.4017$	$\equiv 6.4017$	R_{\oplus}
Priors			
Parameter	Prior		
$\eta_{1,\text{APF}}$	$\mathcal{U}(0, 1e + 100)$		
$\eta_{1,\text{FIES}}$	$\mathcal{U}(0, 1e + 100)$		
$\eta_{1,\text{HARPS}}$	$\mathcal{U}(0, 1e + 100)$		
$\eta_{1,\text{HIRES}}$	$\mathcal{U}(0, 1e + 100)$		
$\eta_{1,\text{PFS}}$	$\mathcal{U}(0, 1e + 100)$		
Numerical prior from photom. training on η_2, η_3, η_4			

Table 14. K2-229 System Parameters

Parameter	Credible Interval	Maximum Likelihood	Units
RV Analysis – MCMC Step Parameters			
P_b	$\equiv 0.5843$	$\equiv 0.5843$	days
$T_{\text{conj},b}$	$\equiv 2457605.0861$	$\equiv 2457605.0861$	BJD _{TBD}
$\sqrt{e} \cos \omega_b$	$\equiv 0.0$	$\equiv 0.0$	
$\sqrt{e} \sin \omega_b$	$\equiv 0.0$	$\equiv 0.0$	
K_b	2.19 ± 0.30	2.20	m s^{-1}
P_c	$\equiv 8.3262$	$\equiv 8.3262$	days
$T_{\text{conj},c}$	$\equiv 2457611.3227$	$\equiv 2457611.3227$	BJD _{TBD}
$\sqrt{e} \cos \omega_c$	$\equiv 0.0$	$\equiv 0.0$	
$\sqrt{e} \sin \omega_c$	$\equiv 0.0$	$\equiv 0.0$	
K_c	2.6 ± 1.4	2.6	m s^{-1}
γ_{HIRES}	$-0.2^{+6.7}_{-7.2}$	-0.2	m s^{-1}
γ_{HARPS}	$22980.5^{+5.8}_{-5.6}$	22980.3	m s^{-1}
$\dot{\gamma}$	$\equiv 0.0$	$\equiv 0.0$	$\text{m s}^{-1} \text{ day}^{-1}$
$\ddot{\gamma}$	$\equiv 0.0$	$\equiv 0.0$	$\text{m s}^{-1} \text{ day}^{-2}$
σ_{HIRES}	$2.0^{+1.0}_{-0.4}$	1.8	m s^{-1}
σ_{HARPS}	$1.18^{+0.37}_{-0.38}$	1.16	m s^{-1}
η_3	$19.25^{+0.35}_{-0.59}$	19.35	days
η_2	$27.6^{+2.6}_{-3.5}$	28.0	days
η_4	$0.430^{+0.052}_{-0.017}$	0.415	
$\eta_{1,\text{HIRES}}$	$13.4^{+6.8}_{-1.1}$	11.4	m s^{-1}
$\eta_{1,\text{HARPS}}$	$14.8^{+4.2}_{-0.9}$	13.5	m s^{-1}
Orbital & Physical Parameters			
P_b	$\equiv 0.5843$	$\equiv 0.5843$	days
$T_{\text{conj},b}$	$\equiv 2457605.0861$	$\equiv 2457605.0861$	BJD _{TBD}
e_b	$\equiv 0.0$	$\equiv 0.0$	
ω_b	$\equiv 0.0$	$\equiv 0.0$	radians
K_b	2.19 ± 0.30	2.20	m s^{-1}
M_b	$2.55^{+0.41}_{-0.36}$	2.52	M_{\oplus}
R_b/R_*	$0.0145^{+0.0010}_{-0.0003}$	0.0144	
ρ_b	$6.7^{+0.4}_{-2.3}$	7.7	g cm^{-3}
R_b	$\equiv 1.2603$	$\equiv 1.2603$	R_{\oplus}
P_c	$\equiv 8.3262$	$\equiv 8.3262$	days
$T_{\text{conj},c}$	$\equiv 2457611.3227$	$\equiv 2457611.3227$	BJD _{TBD}
e_c	$\equiv 0.0$	$\equiv 0.0$	
ω_c	$\equiv 0.0$	$\equiv 0.0$	radians
K_c	2.6 ± 1.4	2.6	m s^{-1}
M_c	$7^{+3.9}_{-4.1}$	7.3	M_{\oplus}
R_c/R_*	$\equiv 0.0235$	$\equiv 0.0235$	
ρ_c	$4.3^{+5.1}_{-0.3}$	2.0	g cm^{-3}
R_c	$\equiv 2.0379$	$\equiv 2.0379$	R_{\oplus}
Priors			
Parameter	Prior		
$\eta_{1,\text{HARPS}}$	$\mathcal{U}(0, 1e + 100)$		
$\eta_{1,\text{HIRES}}$	$\mathcal{U}(0, 1e + 100)$		
σ_{HIRES}	$\mathcal{U}(0, 1e + 100)$		
σ_{HARPS}	$\mathcal{U}(0, 1e + 100)$		

Numerical prior from photom. training on η_2, η_3, η_4

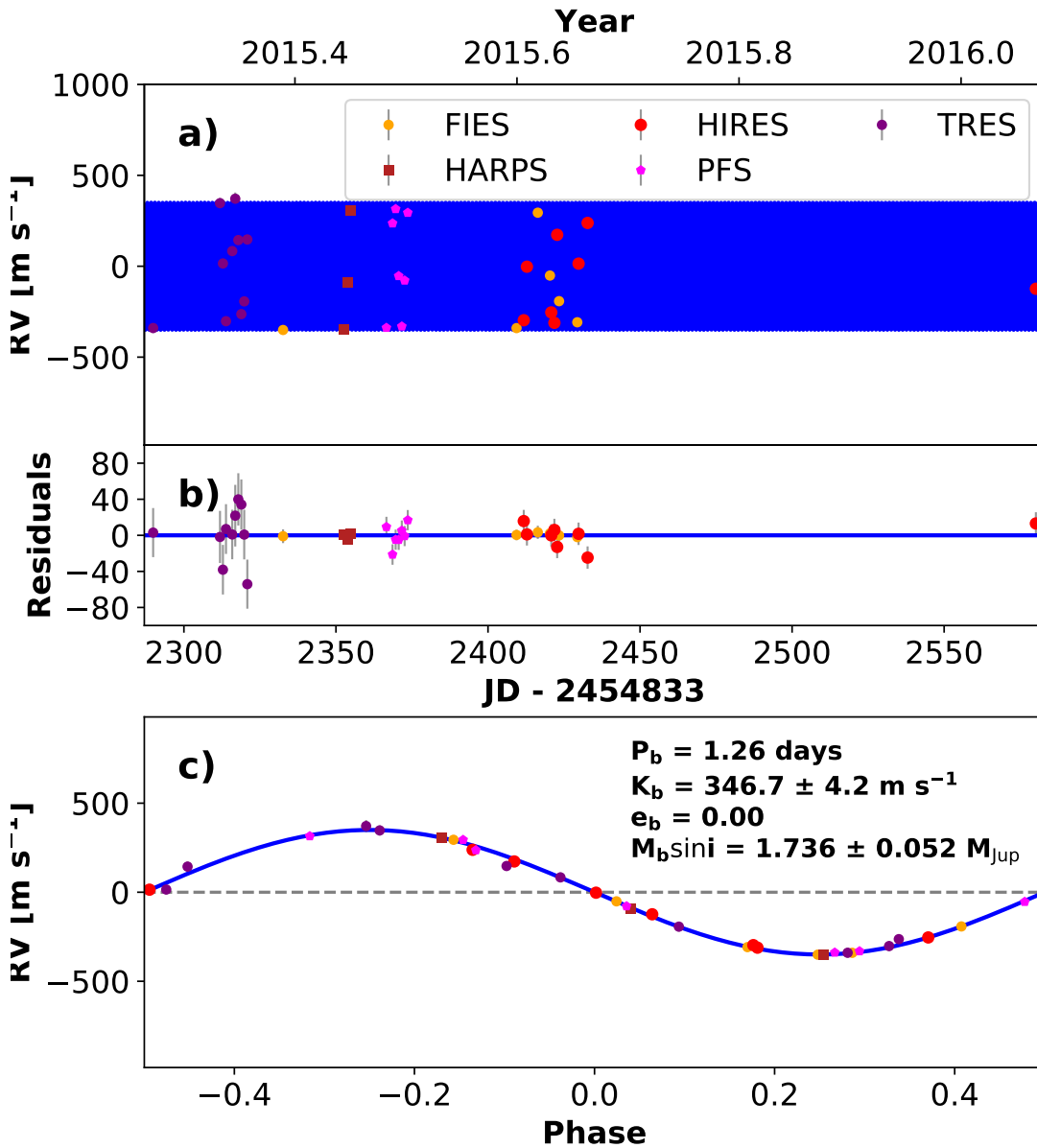


Figure 24. RVs and Keplerian model for K2-31. Symbols, lines, and annotations are similar to those in Fig. 11.

results of this analysis are listed in Table 18 and the best-fit model is shown in Fig. 39. We found no evidence for an additional planet based on a periodogram search of the RVs (Fig. 40).

We confirm with significantly higher precision the determinations in Sinukoff et al. (2016) that K2-38 b is a dense ($6.5^{+3.7}_{-2.5}$ g cm⁻³), rocky planet, while the density of K2-38 c ($2.7^{+1.6}_{-1.1}$ g cm⁻³) is intermediate between that of a solid planet and one dominated by gas.

During the preparations of this paper, Toledo-Padrón et al. (2020) published a Doppler analysis of 43 new ESPRESSO RVs and the 14 HIRES RVs from Sinukoff et al. (2016). They found masses of $7.3 \pm 1.1 M_{\oplus}$ and $8.3 \pm 1.3 M_{\oplus}$ and densities of $11.0^{+4.1}_{-2.8}$ g cm⁻³ and $3.8^{+1.8}_{-1.1}$ g cm⁻³, respectively for the two planets. We did not perform a global analysis that includes the ESPRESSO data.

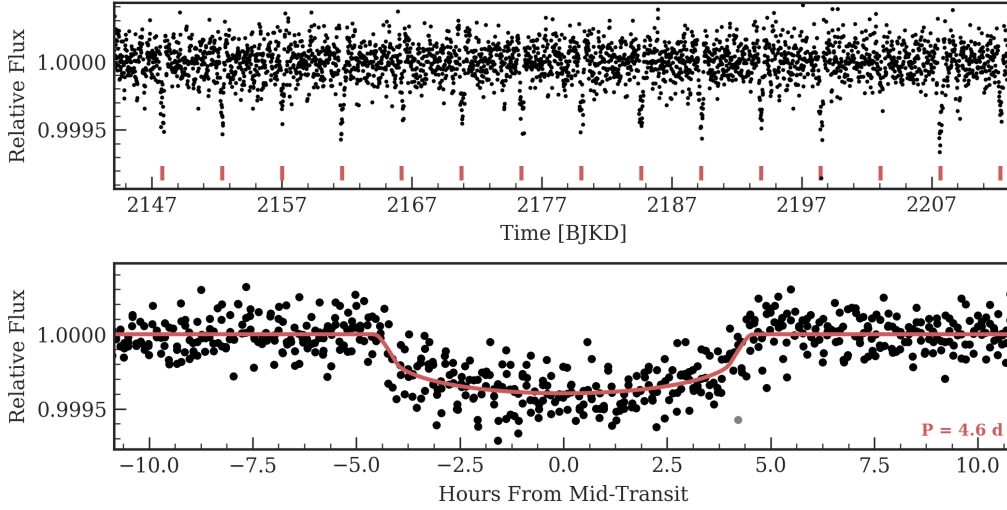


Figure 25. Time series (top) and phase-folded (bottom) light curve for the planet orbiting K2-39. Plot formatting is the same as in Fig. 10. Photometry was generated using K2phot, instead of EVEREST as with other stars.

A.20. *K2-73*

K2-73 is a solar-type star in Field 3 with one transiting planet with a size of $2.3 R_{\oplus}$ and an orbital period of 7.5 days. See Tables 1 and 2 for stellar properties and Table 3 for precise planet parameters. The planet was validated in the Crossfield et al. (2016) catalog and also noted in the catalogs of Vanderburg et al. (2016b), Schmitt et al. (2016), Barros et al. (2016), Mayo et al. (2018), and Wittenmyer et al. (2018).

Our fit of the EVEREST light curve of the K2 photometry for K2-73 is shown in Fig. 41. We acquired 60 RVs of K2-73 with HIRES, typically with an exposure meter setting of 80,000 counts. The time series RVs are dominated by a large amplitude signal with a timescale of longer than one year. We modeled the system as a transiting planet in a circular orbit with the orbital period and phase fixed to the transit ephemeris and a second, non-transiting planet with a long orbital period. The results of this analysis are listed in Table 19 and the best-fit model is shown in Fig. 42. K2-73 b is a short-period sub-Neptune with a density intermediate between those expected for gas-dominated and rocky planets ($\rho_b = 2.8_{-1.2}^{+1.3} \text{ g cm}^{-3}$). K2-73 c is a giant planet with a 2.7-year orbital period and $M_P \sin i = 1142_{-45}^{+53} M_{\oplus}$. We also find a significant eccentricity for planet c (see Table Fig. 42). Planet c has a predicted astrometric motion of $24 \mu\text{as}$ and should be detectable by Gaia. Such a detection would measure the orbital inclination and determine if that planet is coplanar with the inner transiting planet b.

A.21. *WASP-107*

WASP-107 was known to host a very low-density, short-period planet prior to observations by K2 in Campaign 10. Anderson et al. (2017) discovered WASP-107 b prior to K2 observations based on photometry from the WASP survey. They followed up the planet with 32 RVs from CORALIE and measured a mass of $38 \pm 3 M_{\oplus}$. With a mass only 2.2 times that of Neptune (0.40 times that of Saturn), but a radius 0.94 times that of Jupiter, WASP-107b is among the lowest density gas giant

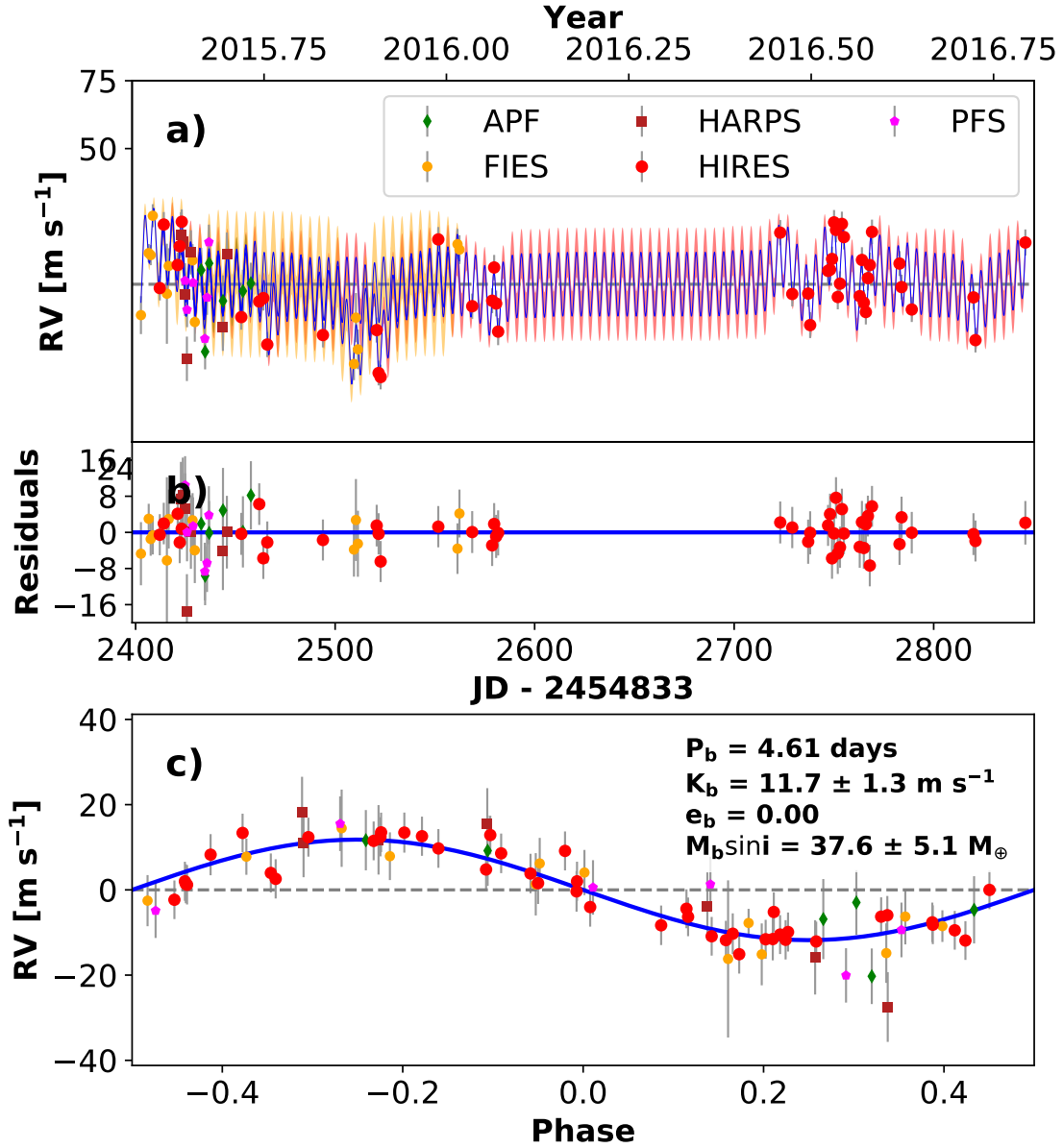


Figure 26. RVs and Keplerian model for K2-39. Symbols, lines, and annotations are similar to those in Fig. 11.

planets. It is a compelling target for transit spectroscopy because of the deep transit depth and large scale height of the planetary atmosphere. The host star is a late K dwarf with $T_{\text{eff}} = 4425 \pm 70$ K. WASP-107b also resides in a highly misaligned orbit, as predicted by spot-crossing anomalies (Dai & Winn 2017) and later confirmed by Rossiter-McLaughlin measurements (Rubenzahl et al. 2021). This may be due to the dynamical influence of the outer companion as discussed in Rubenzahl et al. (2021). The planet is notable as the first exoplanet with a detected Helium outflow in the metastable 1083 nm line (Spake et al. 2018) and is an excellent target for transmission spectroscopy with *HST* (Kreidberg et al. 2018) and JWST. Our adopted stellar parameters are in Tables 1, 2 and 3. Unusually for a cool host star, a detailed set of elemental abundances has also been measured (Hejazi et al. 2023).

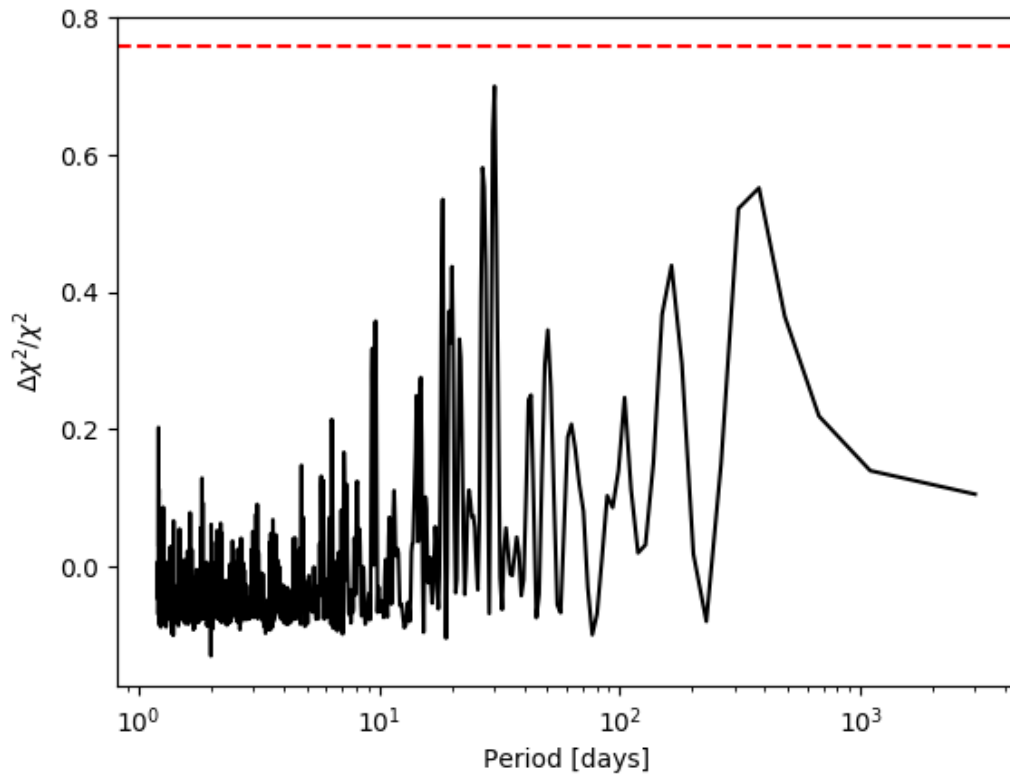


Figure 27. Periodogram search of the RVs showing no evidence for a second planet orbiting K2-39. Lines and annotations are similar to those in Fig. 12.

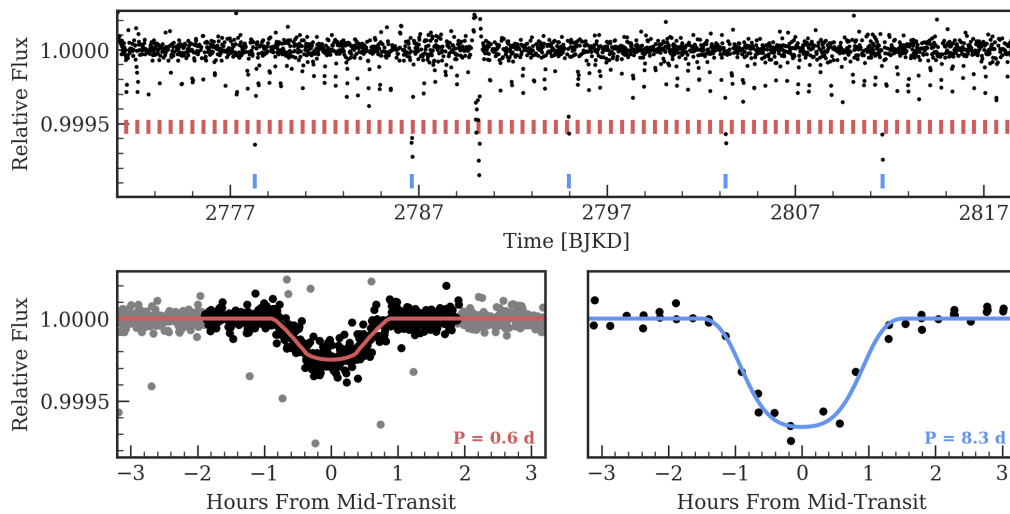


Figure 28. Time series (top) and phase-folded (bottom) light curve for the planet orbiting K2-229. Plot formatting is the same as in Fig. 10.

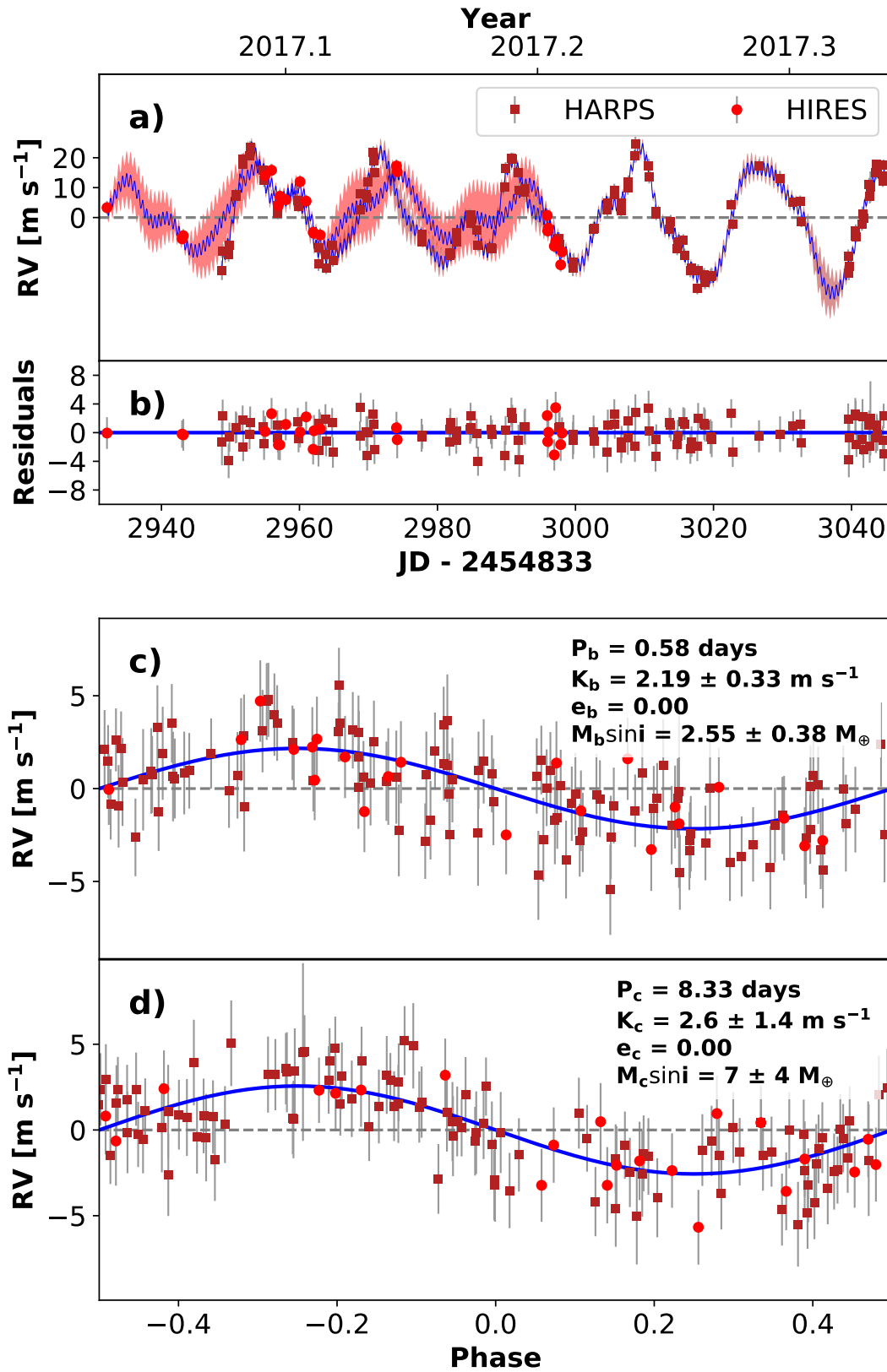


Figure 29. RVs and Keplerian model for K2-229. Symbols, lines, and annotations are similar to those in Fig. 11.

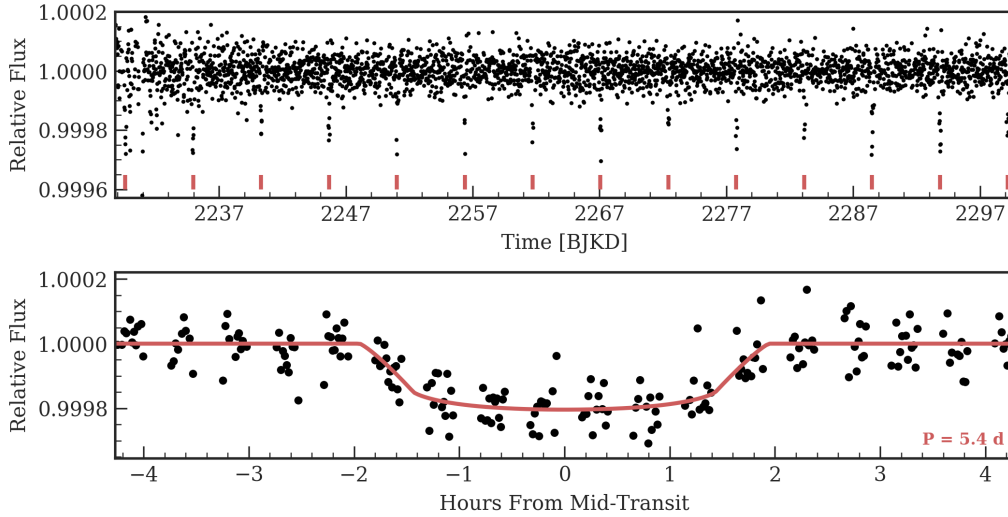


Figure 30. Time series (top) and phase-folded (bottom) light curve for the planet orbiting K2-111. Plot formatting is the same as in Fig. 10.

We adopt the Keplerian solution of Piaulet et al. (2021), who jointly fit our HIRES observations with the RVs from Anderson et al. (2017) and found a smaller and more precise mass for planet b ($30.5 \pm 1.7 M_{\oplus}$). The HIRES RVs show a significant long-period signature which Piaulet et al. (2021) found is best modeled by a second planet with $M_c \sin i = 0.36 M_J$ on a wide ~ 1090 day eccentric $e_c = 0.28$ orbit. An AICc comparison between circular and eccentric fits for planet b showed a significant preference for the circular model, consistent with the small eccentricity (0.06 ± 0.04) reported by Piaulet et al. (2021) and the expected bias for e given a prior bounded below at 0.

A.22. K2-66

K2-66 is a slightly evolved solar-temperature star from Campaign 3 with one transiting planet with a size of $2.4 R_{\oplus}$ and an orbital period of 5 days. See Tables 1 and 2 for stellar properties and Table 3 for precise planet parameters. K2-66 was first reported in Vanderburg et al. (2016b) and was later statistically validated by Crossfield et al. (2016). Sinukoff et al. (2017a) measured the mass of $21.3 \pm 3.6 M_{\oplus}$ using 38 HIRES RVs. We provide an update to that measurement here.

Our fit of the EVEREST light curve of the K2 photometry for K2-66 is shown in Fig. 45. We acquired 44 RVs with HIRES (38 of which were reported in Sinukoff et al. (2017a)), typically with an exposure meter setting of 50,000 counts. We modeled the system as a single planet in a circular orbit with orbital period and phase fixed to transit ephemeris. The results of this analysis are listed in Table 20 and the best-fit model is shown in Fig. 46. We considered other models including ones with an eccentric orbit and/or a linear RV trend. The model with a linear trend had a slightly lower AICc statistic, but the difference ($\Delta\text{AICc} = 1.7$) was insufficient to justify the additional complexity of the model. K2-66 b is a massive sub-Neptune ($16 \pm 4 M_{\oplus}$).

A.23. K2-36

K2-36 is a late-K dwarf with two transiting planets that have sizes of $1.4 R_{\oplus}$ and $2.6 R_{\oplus}$ and orbital periods of 1.4 days and 5.3 days. See Tables 1 and 2 for stellar properties and Table 3 for precise

Table 15. K2-111 System Parameters

Parameter	Credible Interval	Maximum Likelihood	Units
RV Analysis – MCMC Step Parameters			
P_b	$\equiv 5.3523$	$\equiv 5.3523$	days
$T_{\text{conj},b}$	$\equiv 2457067.9628$	$\equiv 2457067.9628$	BJD _{TBD}
$\sqrt{e} \cos \omega_b$	$\equiv 0.0$	$\equiv 0.0$	
$\sqrt{e} \sin \omega_b$	$\equiv 0.0$	$\equiv 0.0$	
K_b	2.23 ± 0.89	2.10	m s^{-1}
γ_{HIRES}	$-1.24^{+0.70}_{-0.71}$	-1.19	m s^{-1}
$\gamma_{\text{HARPS-N}}$	$-1.1^{+1.8}_{-1.7}$	-1.5	m s^{-1}
γ_{FIES}	$\equiv -16397.5644$	$\equiv -16397.5644$	m s^{-1}
$\dot{\gamma}$	$\equiv 0.0$	$\equiv 0.0$	$\text{m s}^{-1} \text{ day}^{-1}$
$\ddot{\gamma}$	$\equiv 0.0$	$\equiv 0.0$	$\text{m s}^{-1} \text{ day}^{-2}$
σ_{HIRES}	$4.66^{+0.61}_{-0.52}$	4.61	m s^{-1}
$\sigma_{\text{HARPS-N}}$	$14.1^{+1.4}_{-1.2}$	14.0	m s^{-1}
σ_{FIES}	$\equiv 0.0$	$\equiv 0.0$	m s^{-1}
Orbital & Physical Parameters			
P_b	$\equiv 5.3523$	$\equiv 5.3523$	days
$T_{\text{conj},b}$	$\equiv 2457067.9628$	$\equiv 2457067.9628$	BJD _{TBD}
e_b	$\equiv 0.0$	$\equiv 0.0$	
ω_b	$\equiv 0.0$	$\equiv 0.0$	radians
K_b	2.23 ± 0.89	2.10	m s^{-1}
M_b	5.4 ± 2.2	5.4	M_{\oplus}
ρ_b	$17.3^{+7.5}_{-7.1}$	12.0	g cm^{-3}
Priors			
Parameter	Prior		
σ_{HIRES}	$\mathcal{U}(0, 1e + 100)$		
$\sigma_{\text{HARPS-N}}$	$\mathcal{U}(0, 1e + 100)$		
σ_{FIES}	$\mathcal{U}(0, 1e + 100)$		

planet parameters. The planets were statistically validated in [Crossfield et al. \(2016\)](#) and also noted in [Vanderburg et al. \(2016b\)](#) and [Sinukoff et al. \(2016\)](#). Our fit of the EVEREST light curve of the K2 photometry for K2-36 is shown in Fig. 47. [Damasso, M. et al. \(2019\)](#) characterized the system using 81 RVs obtained with HARPS-N and found masses of $3.9 \pm 1.1 M_{\oplus}$ and $7.8 \pm 2.3 M_{\oplus}$ for planets b and c, respectively, consistent with the values subsequently reported by [Bonomo et al. \(2023b\)](#) of $4.3 \pm 1.4 M_{\oplus}$ and $7.9 \pm 2.8 M_{\oplus}$, respectively.

We acquired 46 RVs of K2-36 with HIRES, typically with an exposure meter setting of 80,000 counts. The star is moderately active with $\log R'_{\text{HK}} = -4.594$, which, combined with our $N_{\text{obs,HIRES}} = 46$, satisfies our prerequisites for a GP regression analysis. As described in Sec. 4.2.2, we trained the GP hyperparameters on non-detrended Everest photometry before using computing RV orbit posteriors. For comparison purposes, we also performed an RV orbit fit using an untrained GP. The trained hyperparameters are clearly peaked and constrained to a portion of the parameter space allowed by the priors, whereas the untrained hyperparameter posteriors extend over the entire allowable parameter space. Without training, λ is peaked at ≈ 2 days, between the orbital period values of

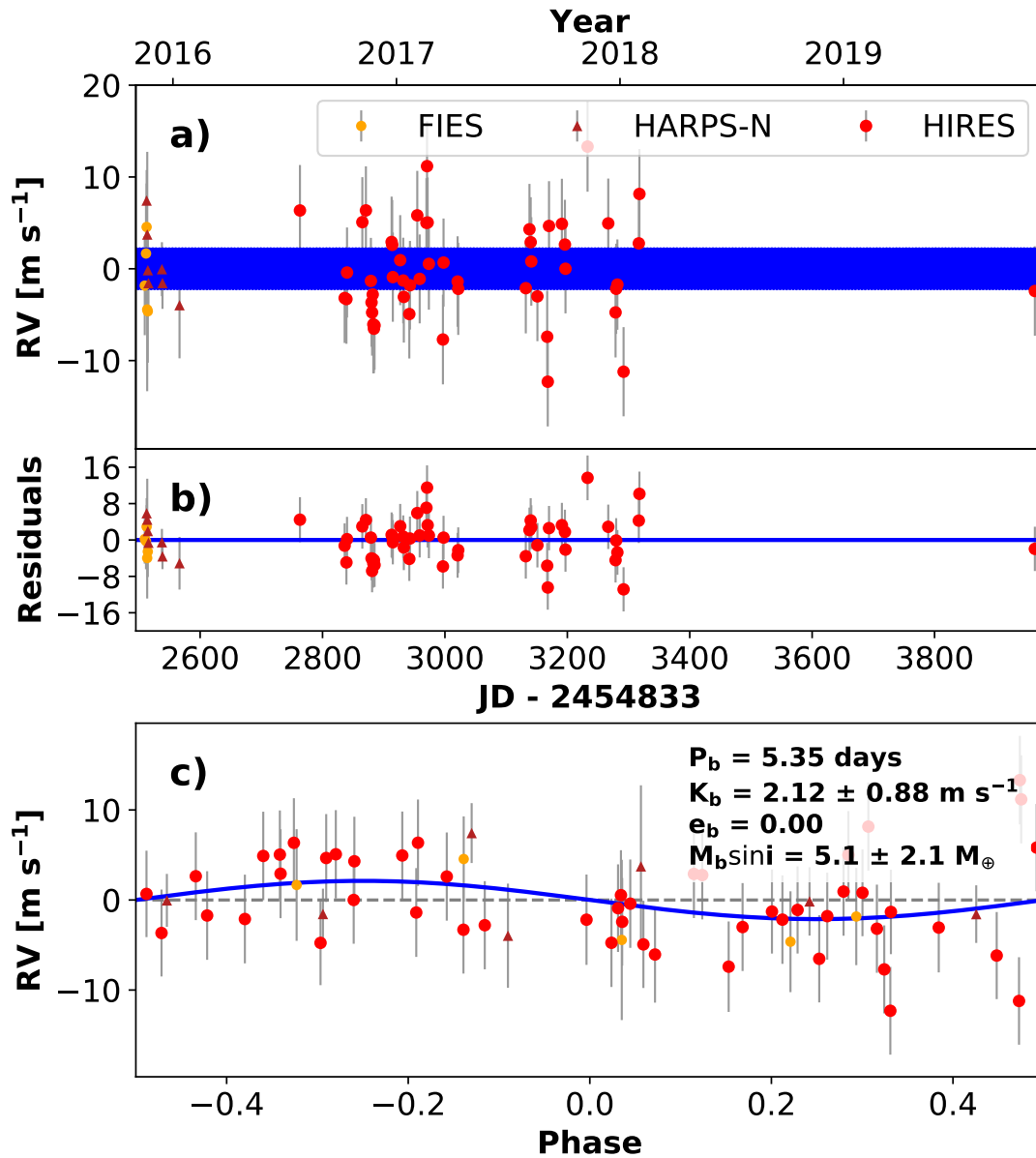


Figure 31. RVs and Keplerian model for K2-111. Symbols, lines, and annotations are similar to those in Fig. 11.

the two planets, and near half the value of the period of planet b. With training, however, the values of both timescale parameters are significantly larger than either planet period. For both planets, a trained GP reduces the uncertainties on semiamplitudes by more than 50% and favors higher median semiamplitude values, as compared with a non-GP model. This highlights not only a case where using GP regression cuts down on orbital parameter uncertainty, but also one where GP training provides a well-motivated prior keeping the timescale parameters away from the planet orbital periods.

Our GP analysis, combined with the higher-precision HIRES RVs, yields larger mass determinations for both planets than previous work (Damasso, M. et al. 2019; Bonomo et al. 2023b). A model with a circular orbit and no trend is preferred based on an AICc comparison. The results of this analysis are listed in Table 21 and the best-fit model is shown in Fig. 48. K2-36 b is a short-period super-Earth

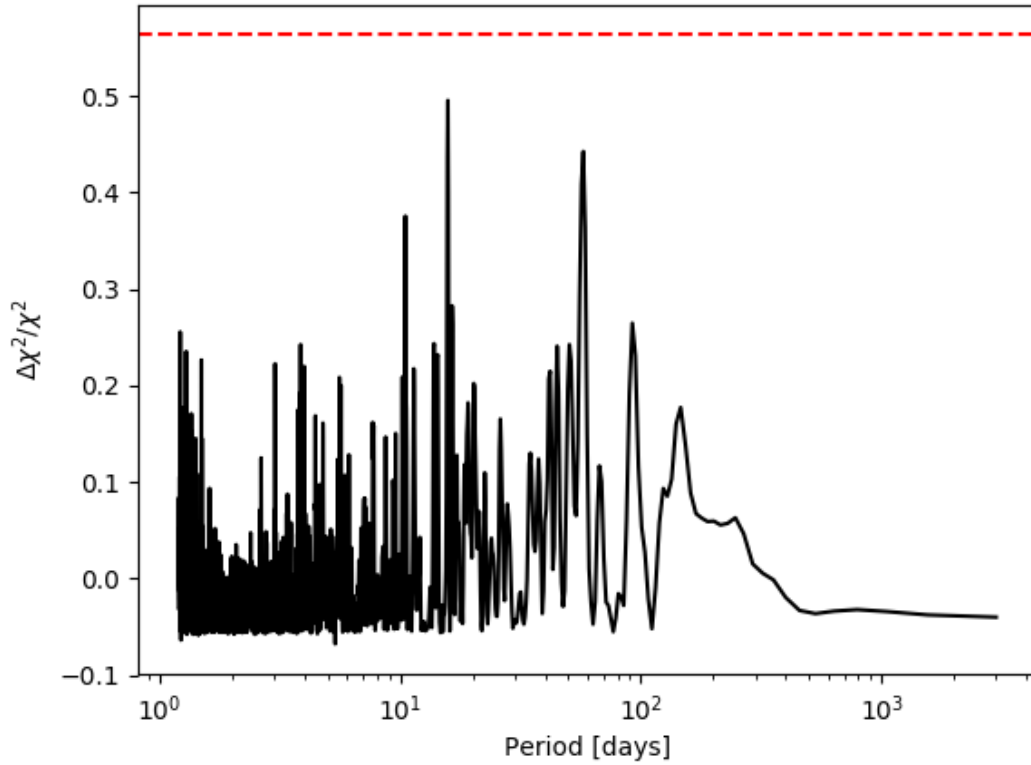


Figure 32. Periodogram search of the RVs showing no evidence for a second planet orbiting K2-111. Lines and annotations are similar to those in Fig. 12.

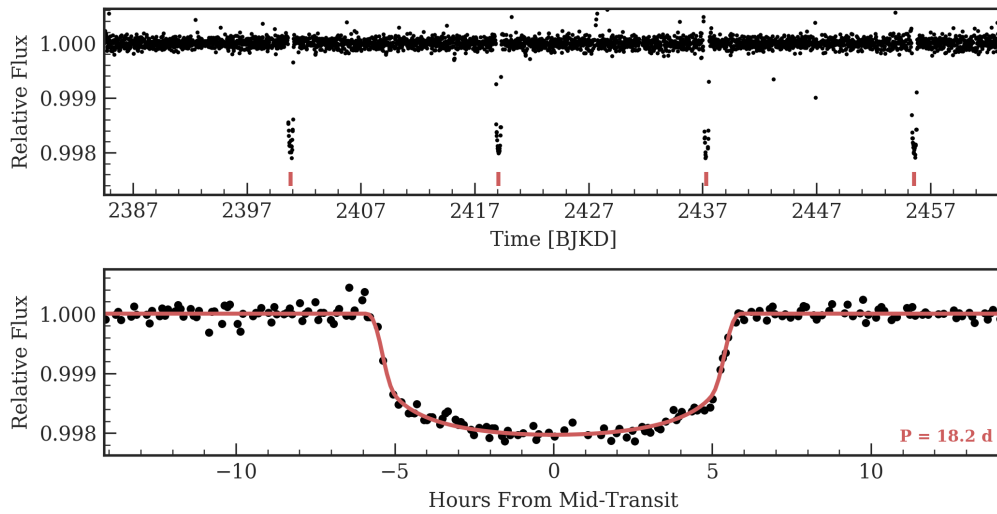


Figure 33. Time series (top) and phase-folded (bottom) light curve for the planet orbiting K2-99. Plot formatting is the same as in Fig. 10.

Table 16. K2-99 System Parameters

Parameter	Credible Interval	Maximum Likelihood	Units
RV Analysis – MCMC Step Parameters			
P_b	$\equiv 18.249$	$\equiv 18.249$	days
$T_{\text{conj},b}$	$\equiv 2457233.8255$	$\equiv 2457233.8255$	BJD _{TBD}
$\sqrt{e} \cos \omega_b$	$0.391^{+0.046}_{-0.053}$	0.405	
$\sqrt{e} \sin \omega_b$	$-0.36^{+0.13}_{-0.11}$	-0.36	
K_b	$56.2^{+3.7}_{-3.6}$	56.0	m s^{-1}
γ_{TULL}	408^{+12}_{-13}	407	m s^{-1}
γ_{HIRES}	91.2 ± 7.6	91.0	m s^{-1}
$\gamma_{\text{HARPS-N}}$	-2649^{+9}_{-10}	-2649.5	m s^{-1}
γ_{HARPS}	-2652 ± 6	-2652.3	m s^{-1}
γ_{FIES}	$-2756.4^{+6.3}_{-6.2}$	-2757.0	m s^{-1}
$\dot{\gamma}$	-1.93 ± 0.12	-1.94	$\text{m s}^{-1} \text{ day}^{-1}$
$\ddot{\gamma}$	$\equiv 0.0$	$\equiv 0.0$	$\text{m s}^{-1} \text{ day}^{-2}$
σ_{TULL}	5^{+25}_{-34}	16	m s^{-1}
σ_{HIRES}	$9.5^{+2.8}_{-2.3}$	8.1	m s^{-1}
$\sigma_{\text{HARPS-N}}$	-2^{+19}_{-17}	-7	m s^{-1}
σ_{HARPS}	11^{+10}_{-28}	11	m s^{-1}
σ_{FIES}	-1^{+18}_{-17}	-11	m s^{-1}
Orbital & Physical Parameters			
P_b	$\equiv 18.249$	$\equiv 18.249$	days
$T_{\text{conj},b}$	$\equiv 2457233.8255$	$\equiv 2457233.8255$	BJD _{TBD}
e_b	$0.283^{+0.072}_{-0.064}$	0.296	
ω_b	$-0.74^{+0.25}_{-0.19}$	-0.70	radians
K_b	$56.2^{+3.7}_{-3.6}$	56.0	m s^{-1}
M_b	287^{+23}_{-22}	286	M_{\oplus}
R_b/R_*	$0.04144^{+0.00061}_{-0.00032}$	0.04120	
ρ_b	0.83 ± 0.07	0.92	g cm^{-3}
R_b	$12.37^{+0.18}_{-0.10}$	12.00	R_{\oplus}
Priors			
Parameter	Prior		
e_b	< 0.99		

NOTE—

Reference epoch for $\dot{\gamma}, \ddot{\gamma}$: 2457550.6875529997

with a high (but not precisely determined) density ($12^{+12}_{-10} \text{ g cm}^{-3}$) suggesting a rocky composition. The larger mass for K2-36 c makes it more like typical sub-Neptunes, as its $2.2 R_{\oplus}$ radius suggests an appreciable H/He envelope.

A.24. K2-105

K2-105 is a late G dwarf in Field 5 with one transiting planet with a radius of $3.4 R_{\oplus}$ and an orbital period of 8 days. See Tables 1 and 2 for stellar properties and Table 3 for precise planet parameters. The planet was discovered by Narita et al. (2017) who estimated a mass upper limit of $90 M_{\oplus}$ ($3\text{-}\sigma$) based on eight RVs from Subaru/HDS gathered in three clusters. The planet is also

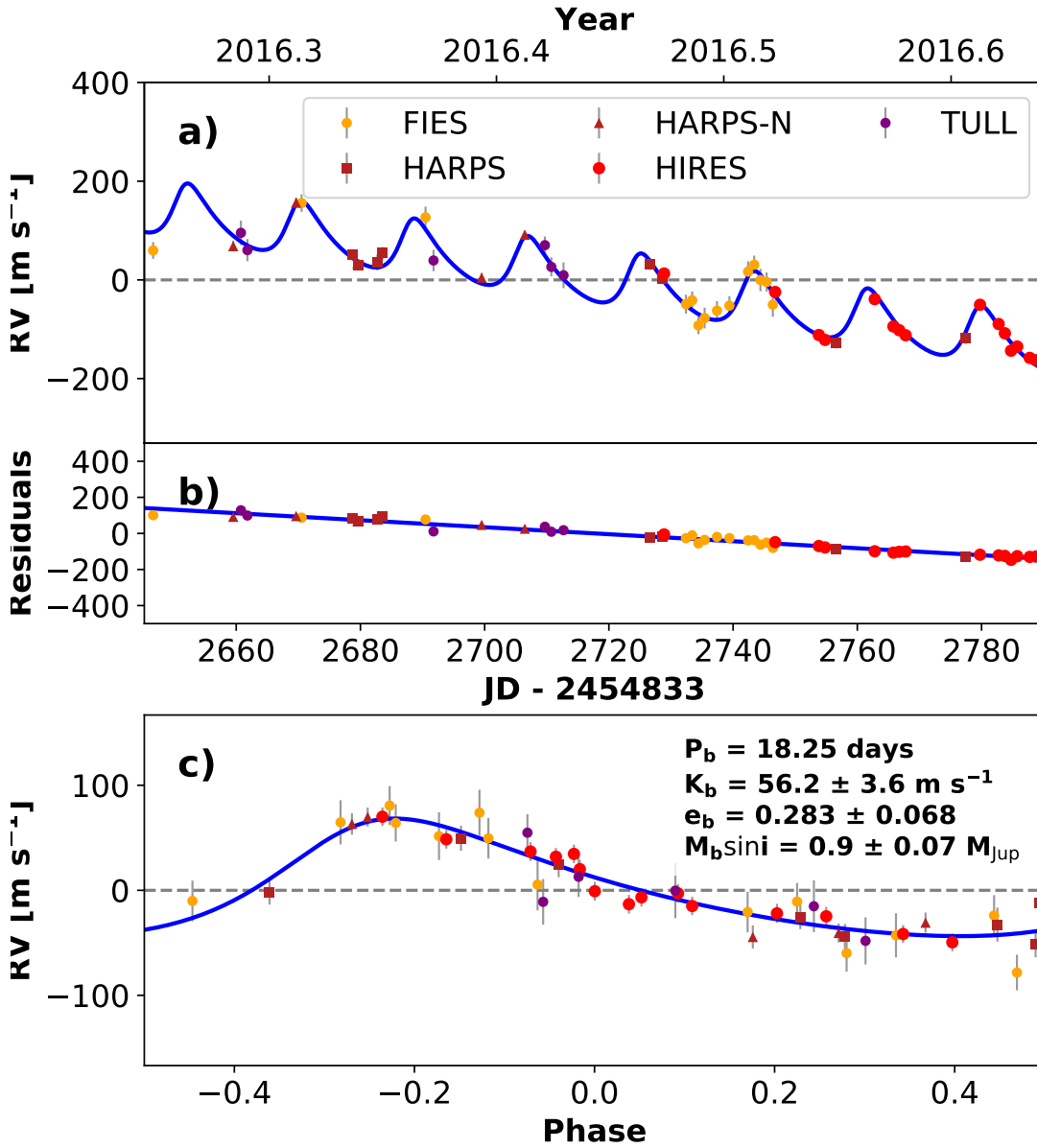


Figure 34. RVs and Keplerian model for K2-99. Symbols, lines, and annotations are similar to those in Fig. 11.

noted in the [Petigura et al. \(2018a\)](#) and [Mayo et al. \(2018\)](#) catalogs. HARPS-N transit spectroscopy hints at a misaligned orbit ([Bourrier et al. 2023](#)) and GIANO observations detect no sign of mass loss via the metastable Helium line ([Guilluy et al. 2023](#)). Our fit of the EVEREST light curve of the K2 photometry for K2-105 is shown in Fig. 49.

We acquired 31 RVs of K2-105 with HIRES, typically with an exposure meter setting of 80,000 counts. We modeled the system as a single planet in a circular orbit with the orbital period and phased fixed to the transit ephemeris. The results of this analysis are listed in Table 22 and the best fit model is shown in Fig. 50. We considered more complicated models but found insufficient evidence to justify inclusion of orbital eccentricity or a linear RV trend based on the AICc statistic. K2-105 b is a short-period planet with a size and density comparable to Neptune's.

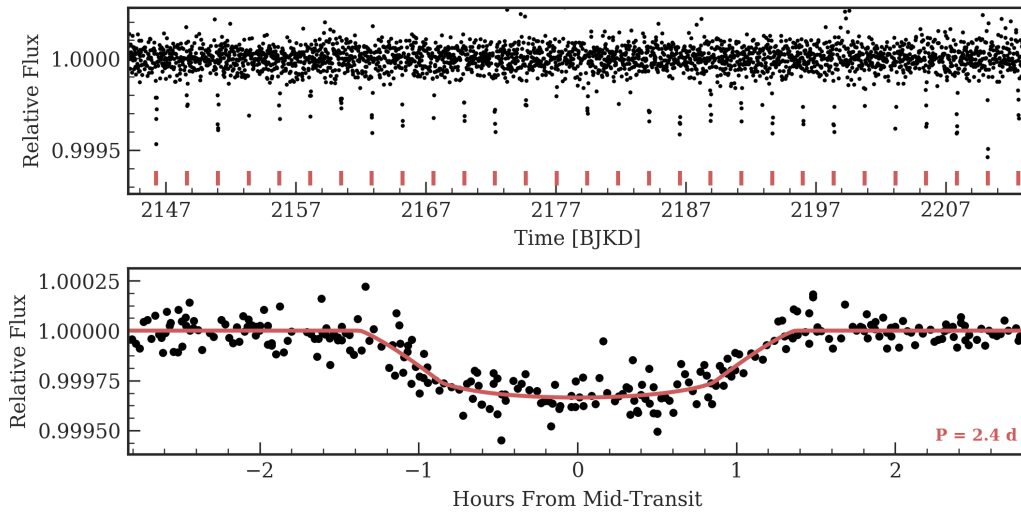


Figure 35. Time series (top) and phase-folded (bottom) light curve for the planet orbiting K2-265. Plot formatting is the same as in Fig. 10.

A.25. *K2-214*

K2-214 is a slightly evolved, solar-temperature star from Campaign 8 with one transiting planet with a $2.5 R_{\oplus}$ radius and an 8.5-day orbital period. See Tables 1 and 2 for stellar properties and Table 3 for precise planet parameters. The star is noted in the catalogs of Petigura et al. (2018a) and Mayo et al. (2018), and validated in the latter. Our fit of the EVEREST light curve of the K2 photometry for K2-214 is shown in Fig. 51.

We acquired 29 RVs of K2-214 with HIRES, typically with an exposure meter setting of 80,000 counts. We modeled the system as a single planet in a circular orbit whose period and phase are fixed to the transit ephemeris. The results of this analysis are listed in Table 23 and the adopted model is shown in Fig. 52. While the preferred model is a circular orbit with a trend, K2-214 b is poorly characterized by our HIRES measurements due to high jitter (see Table 23) and the planet is not detected in RVs. As a result, we adopt a circular model with no trend and provide the best-fit semiamplitude as an upper limit. This system does not have enough observations to meet our requirements for a GP analysis, thus more observations are needed to better understand K2-214.

A.26. *K2-220*

K2-220 is a G dwarf from Campaign 8 with one transiting planet with a $2.3 R_{\oplus}$ radius and a 13-day orbital period. See Tables 1 and 2 for stellar properties and Table 3 for precise planet parameters. The planet was noted in the catalogs by Petigura et al. (2018a) and Mayo et al. (2018), with validation in the latter.

Our fit of the EVEREST light curve of the K2 photometry for K2-220 is shown in Fig. 53. We acquired 28 RVs of K2-220 with HIRES, typically with an exposure meter setting of 80,000 counts. We modeled the system as a single planet in a circular orbit with the period and phase fixed to the transit ephemeris. The results of this analysis are listed in Table 24 and the best-fit model is shown in Fig. 54. We do not detect the Doppler signal from K2-220 b, but we can rule out a rocky

Table 17. K2-265 System Parameters

Parameter	Credible Interval	Maximum Likelihood	Units
RV Analysis – MCMC Step Parameters			
P_b	$\equiv 2.3691$	$\equiv 2.3691$	days
$T_{\text{conj},b}$	$\equiv 2456981.645$	$\equiv 2456981.645$	BJD _{TBD}
$\sqrt{e} \cos \omega_b$	$\equiv 0.0$	$\equiv 0.0$	
$\sqrt{e} \sin \omega_b$	$\equiv 0.0$	$\equiv 0.0$	
K_b	$2.38^{+0.70}_{-0.80}$	2.40	m s^{-1}
γ_{HIRES}	$-2.0^{+1.2}_{-1.5}$	-1.9	m s^{-1}
$\dot{\gamma}$	$\equiv 0.0$	$\equiv 0.0$	$\text{m s}^{-1} \text{ day}^{-1}$
$\ddot{\gamma}$	$\equiv 0.0$	$\equiv 0.0$	$\text{m s}^{-1} \text{ day}^{-2}$
σ_{HIRES}	$0.2^{+0.5}_{-4.3}$	1.9	m s^{-1}
η_3	17^{+15}_{-1}	15	days
η_2	$11.0^{+8.0}_{-2.0}$	9.0	days
η_4	$0.510^{+0.035}_{-0.082}$	0.529	
$\eta_{1,\text{HIRES}}$	$6^{+1.4}_{-0.5}$	5.6	m s^{-1}
Orbital & Physical Parameters			
P_b	$\equiv 2.3691$	$\equiv 2.3691$	days
$T_{\text{conj},b}$	$\equiv 2456981.645$	$\equiv 2456981.645$	BJD _{TBD}
e_b	$\equiv 0.0$	$\equiv 0.0$	
ω_b	$\equiv 0.0$	$\equiv 0.0$	radians
K_b	$2.38^{+0.70}_{-0.80}$	2.40	m s^{-1}
M_b	$4.6^{+1.4}_{-1.6}$	4.7	M_{\oplus}
R_b/R_*	$0.01683^{+0.00110}_{-0.00010}$	0.01660	
ρ_b	$5.2^{+1.5}_{-2.1}$	5.6	g cm^{-3}
R_b	$1.676^{+0.092}_{-0.031}$	1.668	R_{\oplus}
Priors			
Parameter	Prior		
$\eta_{1,\text{HIRES}}$	$\mathcal{U}(0, 1e + 100)$		
Numerical prior from photom. training on η_2, η_3, η_4			

composition based on a measured density of $0.0 \pm 1.6 \text{ g cm}^{-3}$. A gas-dominated composition is not surprising for a planet of this size.

A.27. K2-110

K2-110 is a late K dwarf from Campaign 6 with one transiting planet with a radius $2.5 R_{\oplus}$ and a period of 13 days. See Tables 1 and 2 for stellar properties and Table 3 for precise planet parameters.

K2-110 b was discovered by Osborn et al. (2017) who measured a mass of $16.7 \pm 3.2 M_{\oplus}$ and a density of $5.2 \pm 1.2 \text{ g cm}^{-3}$ based on 17 HARPS RVs and 11 HARPS-N RVs. The density is unusually high for a sub-Neptune planet. The planet was also noted in the catalogs by Mayo et al. (2018) and Petigura et al. (2018a). Bonomo et al. (2023b) report a mass of $15.9 \pm 2.7 M_{\oplus}$.

Our fit of the EVEREST light curve of the K2 photometry for K2-110 is shown in Fig. 55. We acquired 12 RVs of K2-110 with HIRES, typically with an exposure meter setting of 100,000 counts. We modeled the HIRES, HARPS-N, and HARPS RVs as a single planet in a circular orbit with the

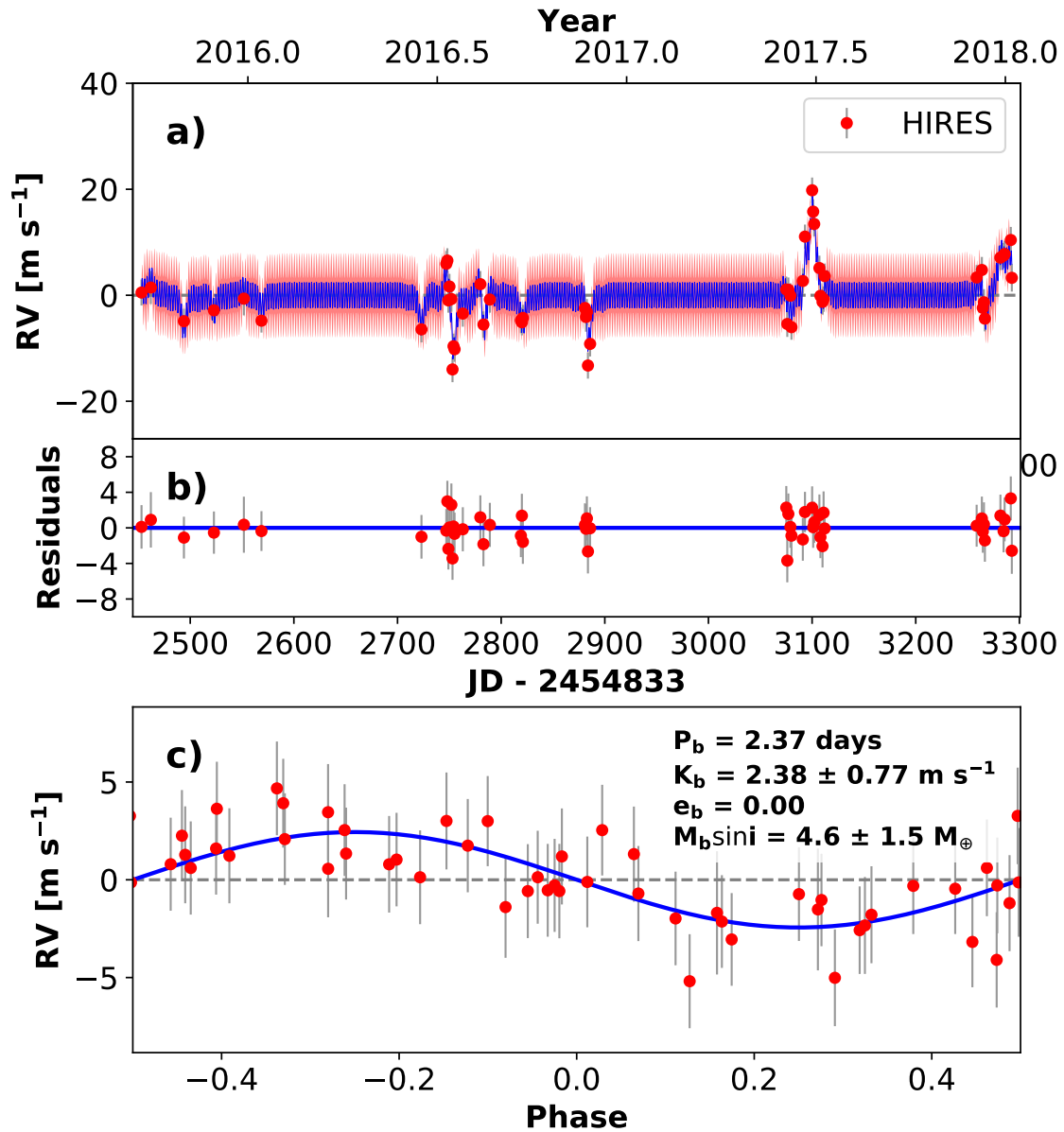


Figure 36. RVs and Keplerian model for K2-265. Symbols, lines, and annotations are similar to those in Fig. 11.

period and phase fixed to the transit ephemeris. We rejected more complicated models with orbital eccentricity and/or a linear RV trend based on the AICc statistic. The results of our analysis are listed in Table 25 and the best fit model is shown in Fig. 56. Our combined analysis confirms the previous results (Osborn et al. 2017; Bonomo et al. 2023b). K2-110 b has an unusually high density ($5.7^{+1.4}_{-1.2}$ g cm $^{-3}$) for its size.

A.28. WASP-47

WASP-47 has an extensive history that precedes and includes the K2 mission. The star is a slightly evolved, metal-rich, solar-temperature star. See Tables 1 and 2 for stellar properties and Table 3 for the precise planet parameters adopted in this paper. WASP-47b is a hot Jupiter discovered by Hellier et al. (2012) using ground-based photometry. They characterized the system using 19 RVs

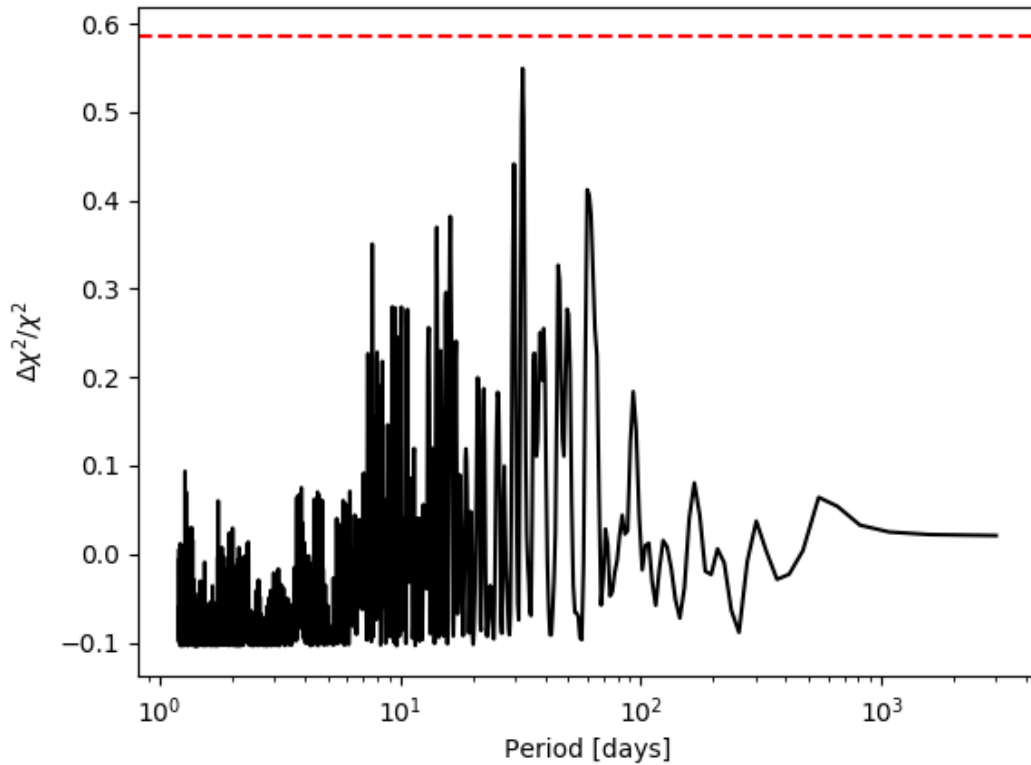


Figure 37. Periodogram search of the RVs showing no evidence for a second planet orbiting K2-265. The period with the most significant periodogram peak is at 32 d. Lines and annotations are similar to those in Fig. 12.

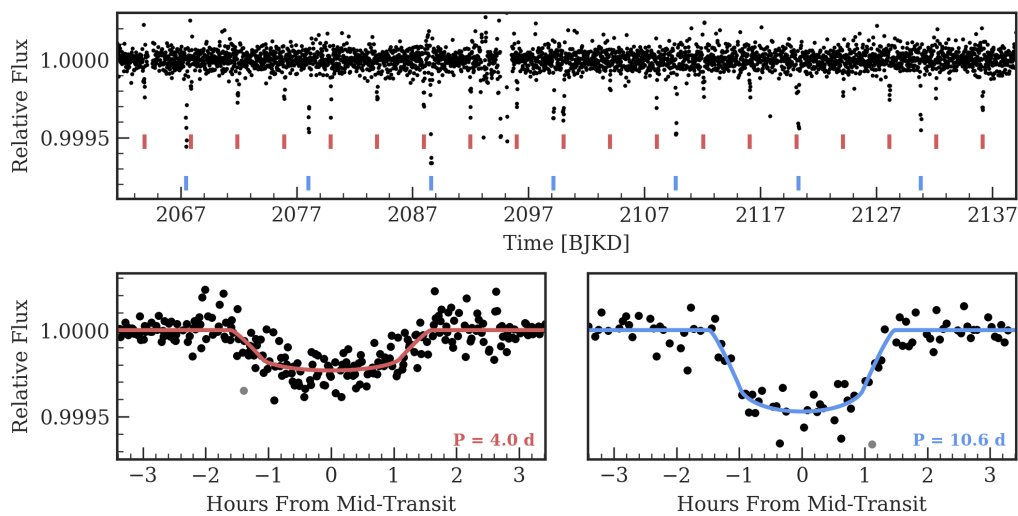


Figure 38. Time series (top) and phase-folded (bottom) light curve for the planet orbiting K2-38. Plot formatting is the same as in Fig. 10.

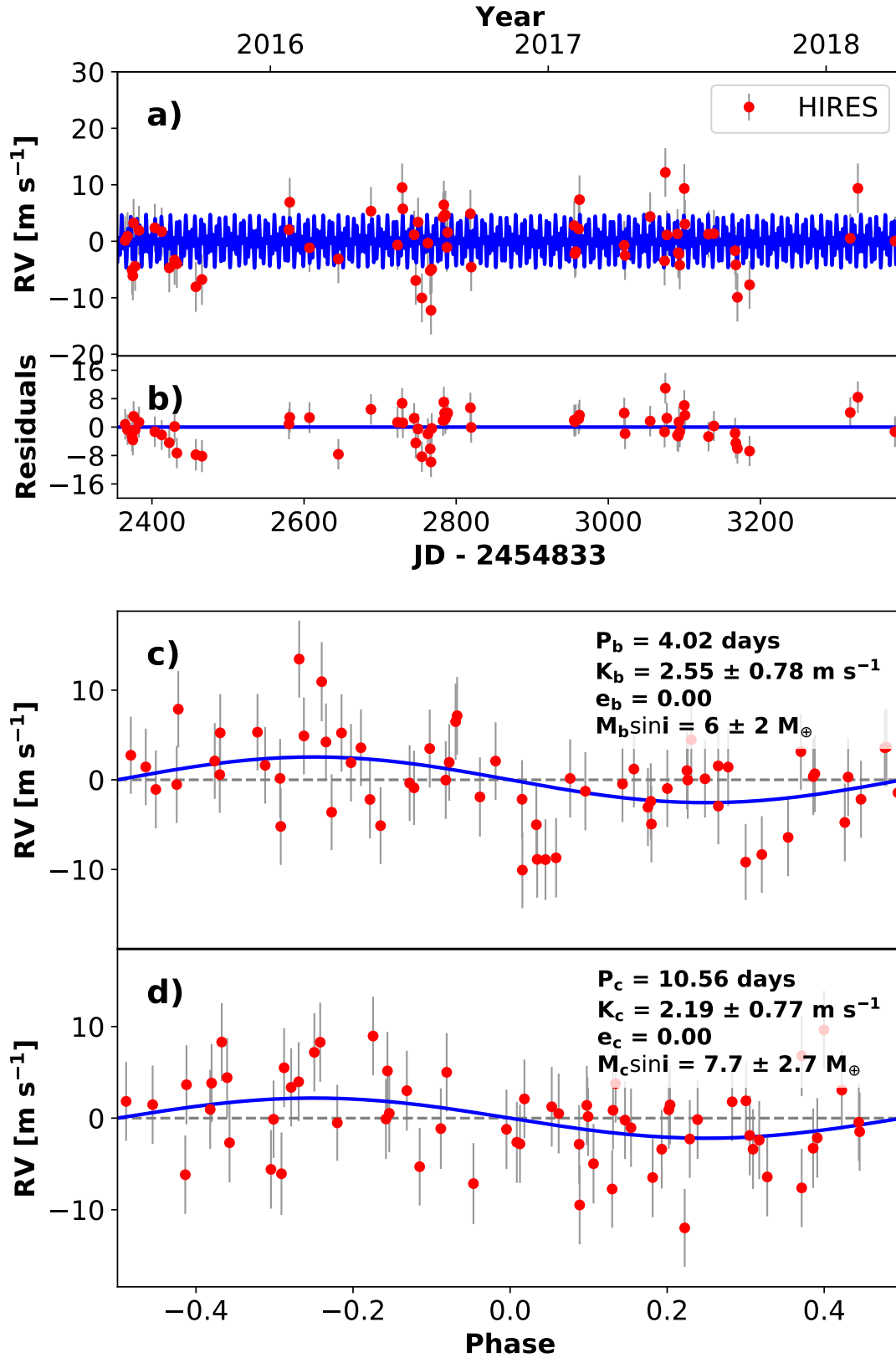


Figure 39. RVs and Keplerian model for K2-38. Symbols, lines, and annotations are similar to those in Fig. 11.

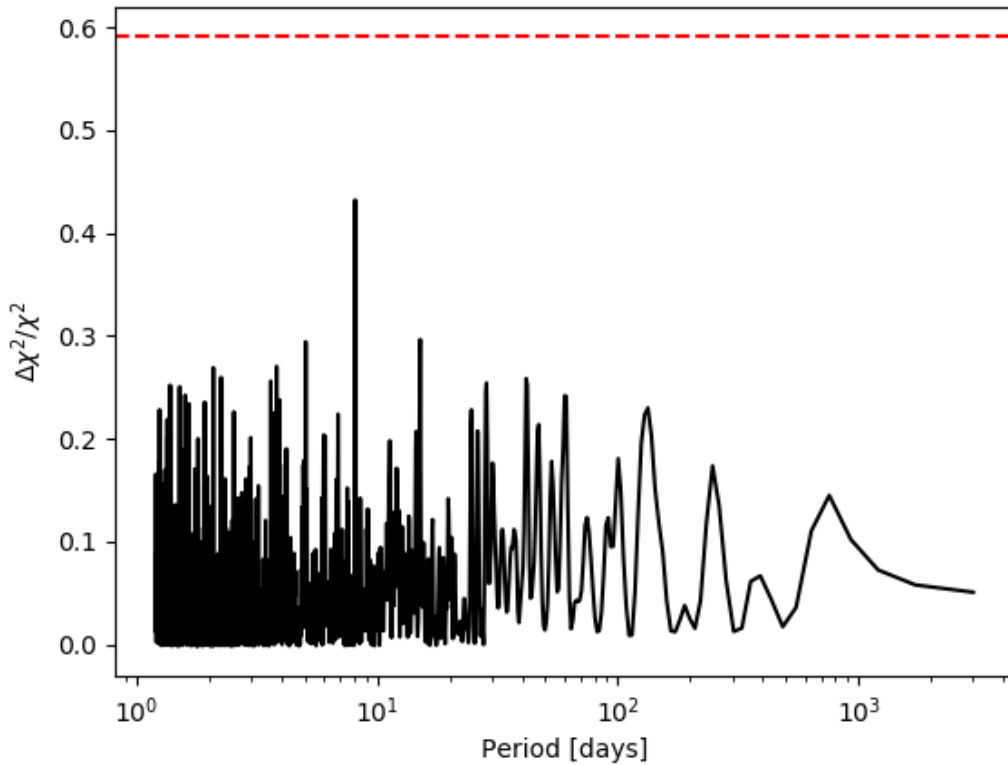


Figure 40. Periodogram search of the RVs showing no evidence for a second planet orbiting K2-38. Lines and annotations are similar to those in Fig. 12.

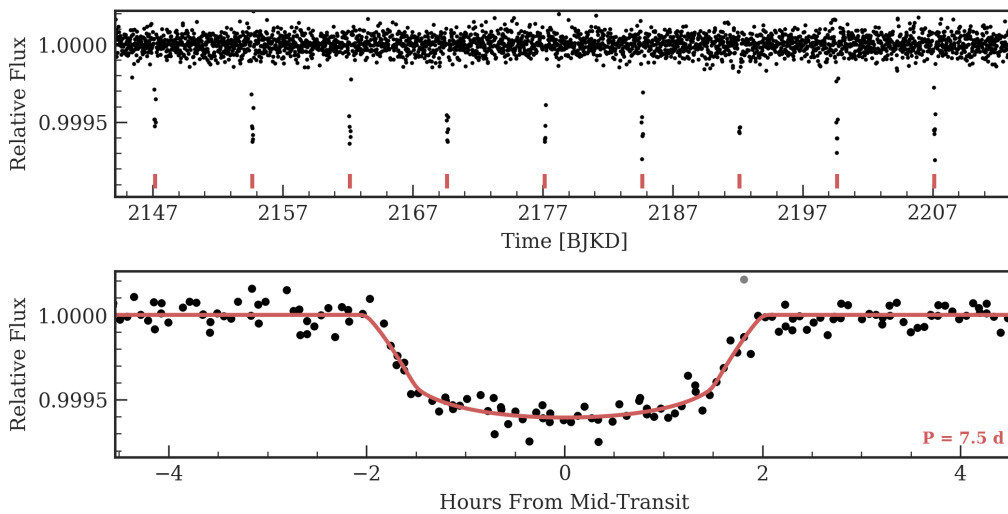


Figure 41. Time series (top) and phase-folded (bottom) light curve for the planet orbiting K2-73. Plot formatting is the same as in Fig. 10.

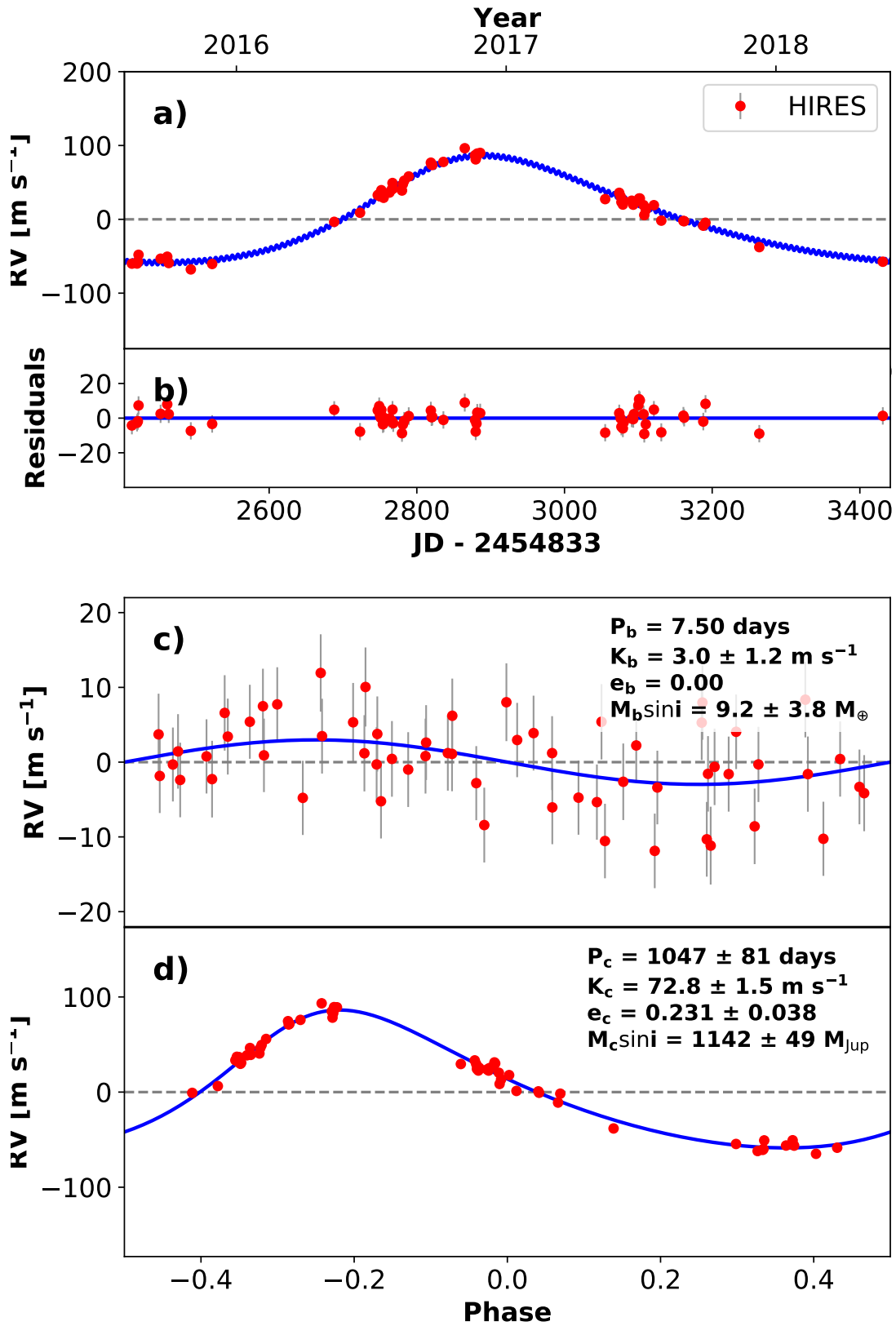


Figure 42. RVs and Keplerian model for K2-73. Symbols, lines, and annotations are similar to those in Fig. 11.

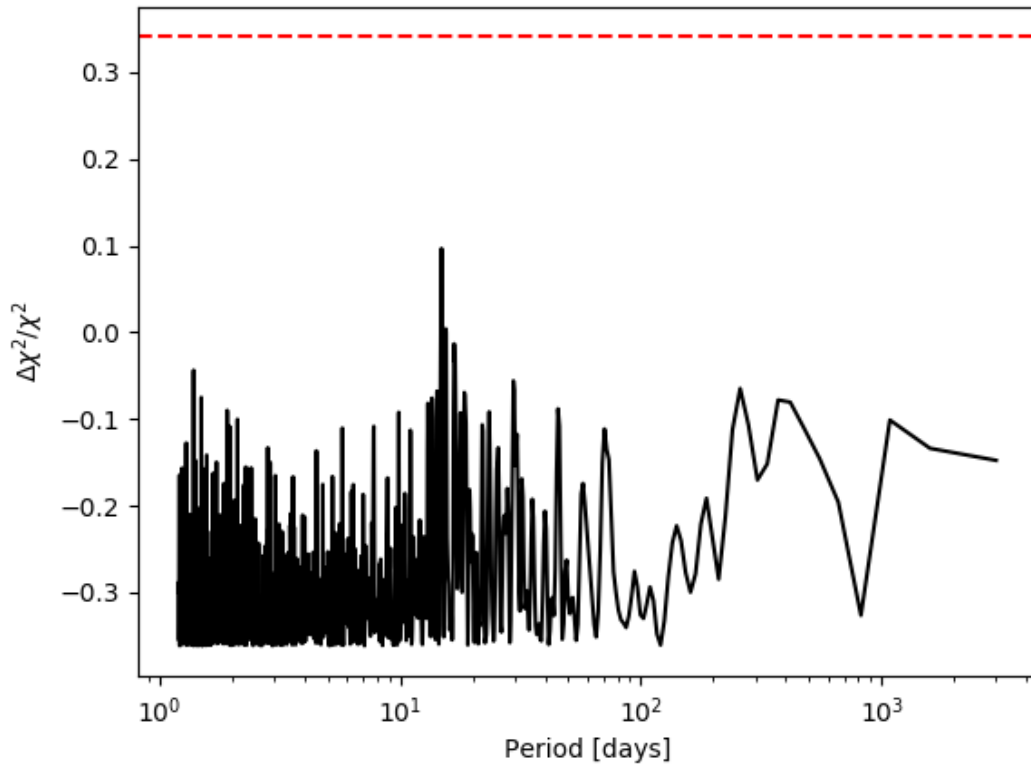


Figure 43. Periodogram search of the RVs showing no evidence for a second planet orbiting K2-73. Lines and annotations are similar to those in Fig. 12.

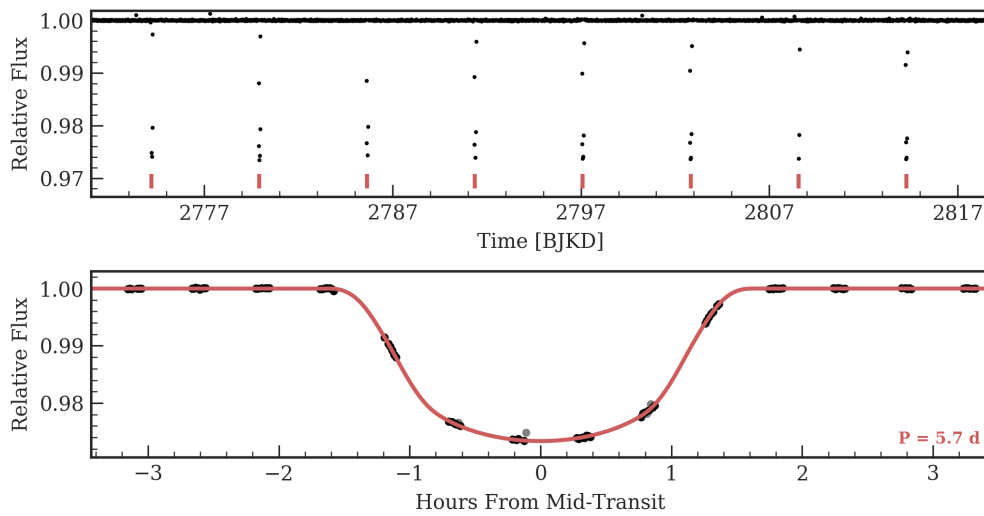


Figure 44. Time series (top) and phase-folded (bottom) light curve for the planet orbiting WASP-107. Plot formatting is the same as in Fig. 10.

Table 18. K2-38 System Parameters

Parameter	Credible Interval	Maximum Likelihood	Units
RV Analysis – MCMC Step Parameters			
P_b	$\equiv 4.0167$	$\equiv 4.0167$	days
$T_{\text{conj},b}$	$\equiv 2456896.8707$	$\equiv 2456896.8707$	BJD _{TBD}
$\sqrt{e} \cos \omega_b$	$\equiv 0.0$	$\equiv 0.0$	
$\sqrt{e} \sin \omega_b$	$\equiv 0.0$	$\equiv 0.0$	
K_b	2.55 ± 0.78	2.55	m s^{-1}
P_c	$\equiv 10.561$	$\equiv 10.561$	days
$T_{\text{conj},c}$	$\equiv 2456900.4751$	$\equiv 2456900.4751$	BJD _{TBD}
$\sqrt{e} \cos \omega_c$	$\equiv 0.0$	$\equiv 0.0$	
$\sqrt{e} \sin \omega_c$	$\equiv 0.0$	$\equiv 0.0$	
K_c	$2.19^{+0.76}_{-0.77}$	2.19	m s^{-1}
γ_{HIRES}	$-2.62^{+0.57}_{-0.56}$	-2.62	m s^{-1}
$\dot{\gamma}$	$\equiv 0.0$	$\equiv 0.0$	$\text{m s}^{-1} \text{ day}^{-1}$
$\ddot{\gamma}$	$\equiv 0.0$	$\equiv 0.0$	$\text{m s}^{-1} \text{ day}^{-2}$
σ_{HIRES}	$4.19^{+0.47}_{-0.41}$	4.02	m s^{-1}
Orbital & Physical Parameters			
P_b	$\equiv 4.0167$	$\equiv 4.0167$	days
$T_{\text{conj},b}$	$\equiv 2456896.8707$	$\equiv 2456896.8707$	BJD _{TBD}
e_b	$\equiv 0.0$	$\equiv 0.0$	
ω_b	$\equiv 0.0$	$\equiv 0.0$	radians
K_b	2.55 ± 0.78	2.55	m s^{-1}
M_b	6 ± 2	7	M_{\oplus}
R_b/R_*	$0.0142^{+0.0010}_{-0.0005}$	0.0147	
ρ_b	$9.3^{+3.4}_{-3.2}$	5.9	g cm^{-3}
R_b	$1.55^{+0.11}_{-0.05}$	1.82	R_{\oplus}
P_c	$\equiv 10.561$	$\equiv 10.561$	days
$T_{\text{conj},c}$	$\equiv 2456900.4751$	$\equiv 2456900.4751$	BJD _{TBD}
e_c	$\equiv 0.0$	$\equiv 0.0$	
ω_c	$\equiv 0.0$	$\equiv 0.0$	radians
K_c	$2.19^{+0.76}_{-0.77}$	2.19	m s^{-1}
M_c	7.7 ± 2.7	7.7	M_{\oplus}
R_c/R_*	$0.0201^{+0.0014}_{-0.0006}$	0.0196	
ρ_c	$3.9^{+1.6}_{-1.4}$	3.0	g cm^{-3}
R_c	$2.18^{+0.15}_{-0.07}$	2.40	R_{\oplus}
Priors			
Parameter	Prior		
None			

from CORALIE and measured a planet mass of $362 \pm 16 M_{\oplus}$. Neveu-VanMalle et al. (2016) added 26 CORALIE RVs and discovered an outer companion (WASP-47c) with a mass of $359 \pm 19 M_{\oplus}$ and an orbital period of 572 days.

Becker et al. (2015) searched the K2 photometry and discovered two additional transiting planets: WASP-47d with a period of 9 days and a radius of $3.6 R_{\oplus}$, and WASP-47e with a period of 0.8 days and a radius of $1.8 R_{\oplus}$. Note that the letters attached to the planets (b–e) follow their order of

Table 19. K2-73 System Parameters

Parameter	Credible Interval	Maximum Likelihood	Units
RV Analysis – MCMC Step Parameters			
P_b	$\equiv 7.4956$	$\equiv 7.4956$	days
$T_{\text{conj},b}$	$\equiv 2456987.6725$	$\equiv 2456987.6725$	BJD _{TBD}
$\sqrt{e} \cos \omega_b$	$\equiv 0.0$	$\equiv 0.0$	
$\sqrt{e} \sin \omega_b$	$\equiv 0.0$	$\equiv 0.0$	
K_b	3.0 ± 1.2	3.0	m s^{-1}
P_c	1000 ± 100	1000	days
$T_{\text{conj},c}$	2456905^{+62}_{-99}	2456905	BJD _{TBD}
$\sqrt{e} \cos \omega_c$	$0.397^{+0.065}_{-0.061}$	0.397	
$\sqrt{e} \sin \omega_c$	$-0.264^{+0.059}_{-0.053}$	-0.268	
K_c	$72.8^{+1.6}_{-1.4}$	72.5	m s^{-1}
γ_{HIRES}	$-22.2^{+2.7}_{-4.2}$	-22.2	m s^{-1}
$\dot{\gamma}$	$\equiv 0.0$	$\equiv 0.0$	$\text{m s}^{-1} \text{ day}^{-1}$
$\ddot{\gamma}$	$\equiv 0.0$	$\equiv 0.0$	$\text{m s}^{-1} \text{ day}^{-2}$
σ_{HIRES}	$-4.99^{+0.56}_{-0.65}$	-4.60	m s^{-1}
Orbital & Physical Parameters			
P_b	$\equiv 7.4956$	$\equiv 7.4956$	days
$T_{\text{conj},b}$	$\equiv 2456987.6725$	$\equiv 2456987.6725$	BJD _{TBD}
e_b	$\equiv 0.0$	$\equiv 0.0$	
ω_b	$\equiv 0.0$	$\equiv 0.0$	radians
K_b	3.0 ± 1.2	3.0	m s^{-1}
M_b	$9.2^{+3.8}_{-3.7}$	9.3	M_{\oplus}
R_b/R_*	$0.0227^{+0.0011}_{-0.0005}$	0.0230	
ρ_b	$2.8^{+1.3}_{-1.2}$	3.0	g cm^{-3}
R_b	$2.58^{+0.13}_{-0.06}$	2.68	R_{\oplus}
P_c	1000 ± 100	1000	days
$T_{\text{conj},c}$	2456905^{+62}_{-99}	2456905	BJD _{TBD}
e_c	$0.481^{+0.041}_{-0.037}$	0.230	
ω_c	$-0.59^{+0.16}_{-0.15}$	-0.59	radians
K_c	$72.8^{+1.6}_{-1.4}$	72.5	m s^{-1}
$M \sin i_c$	1142^{+53}_{-45}	1137	M_{\oplus}
Priors			
Parameter	Prior		
e_b	< 0.99		
e_c	< 0.99		

discovery, not orbital period order. [Becker et al. \(2015\)](#) also conducted the first TTV analysis of the system, finding planet masses of $341^{+73}_{-55} M_{\oplus}$ (WASP-47b), $< 22 M_{\oplus}$ (WASP-47e), and $15.2 \pm 7 M_{\oplus}$ (WASP-47d). For the K2 mission, the planets orbiting WASP-47 are included in the [Crossfield et al. \(2016\)](#), [Vanderburg et al. \(2016b\)](#), [Adams et al. \(2016\)](#), [Barros et al. \(2016\)](#), [Adams et al. \(2017\)](#), and [Wittenmyer et al. \(2018\)](#) catalogs.

Spurred by the high multiplicity and unusual system architecture, several teams pursued RV measurements of this system. First, [Dai et al. \(2015\)](#) reported 27 RVs from PFS. Their analysis did

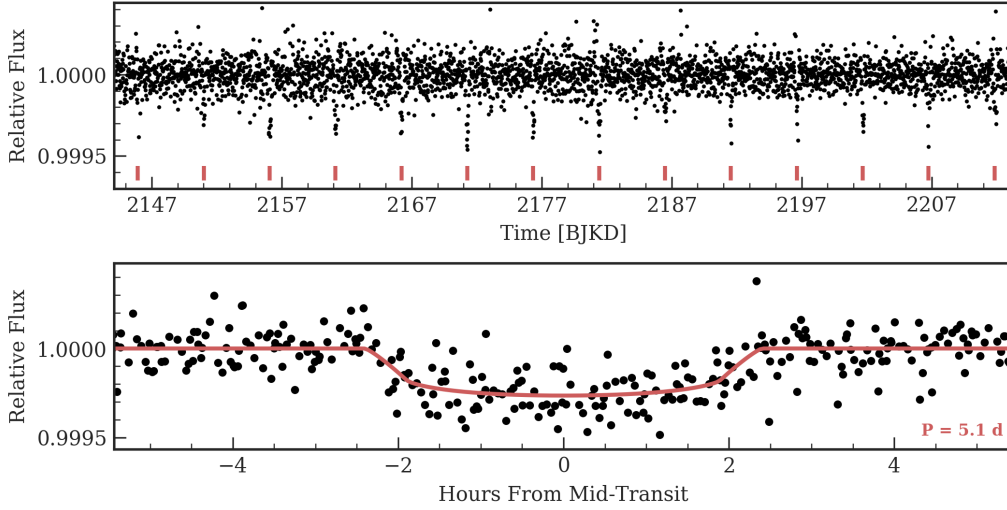


Figure 45. Time series (top) and phase-folded (bottom) light curve for the planet orbiting K2-66. Plot formatting is the same as in Fig. 10.

not include the prior CORALIE RVs and found masses of $12.2 \pm 3.7 M_{\oplus}$ (WASP-47e), $370 \pm 29 M_{\oplus}$ (WASP-47b), and $10.4 \pm 8.4 M_{\oplus}$ (WASP-47d).

Almenara et al. (2016) conducted a dynamical analysis based on transit times from K2 and RVs from Hellier et al. (2012) and Dai et al. (2015) and Neveu-VanMalle et al. (2016). They found masses of $364 \pm 9 M_{\oplus}$ (WASP-47b), $361^{+80}_{-54} M_{\oplus}$ ($M_P \sin i$; WASP-47c), $15.7 \pm 1.1 M_{\oplus}$, (WASP-47d), and $9.1^{+1.8}_{-2.9} M_{\oplus}$ (WASP-47e).

Sinukoff et al. (2017b) added 47 HIRES RVs. Combined with the previous CORALIE and PFS RVs, they measured masses of $356 \pm 12 M_{\oplus}$ (WASP-47b), $411 \pm 18 M_{\oplus}$ ($M_P \sin i$; WASP-47c), $12.8 \pm 2.7 M_{\oplus}$ (WASP-47d), and $9.1 \pm 1.2 M_{\oplus}$ (WASP-47e). A dynamical analysis by Weiss et al. (2017) considered all available RVs at the time of Sinukoff et al. (2017b) as well as transit times from K2. In particular, Weiss et al. (2017) found improved masses for WASP-47d ($13.6 \pm 2.0 M_{\oplus}$) compared to RV alone ($12.8 \pm 2.7 M_{\oplus}$) or TTVs alone ($16.1 \pm 3.8 M_{\oplus}$).

Vanderburg et al. (2017) added 69 HARPS-N RVs and performed a combined analysis with all available RVs. They found masses of $363.1 \pm 7.3 M_{\oplus}$ (WASP-47b), $398.2 \pm 9.3 M_{\oplus}$ ($M_P \sin i$; WASP-47c), $13.1 \pm 1.5 M_{\oplus}$ (WASP-47d), $6.83 \pm 0.66 M_{\oplus}$ (WASP-47e). Their analysis was the most precise RV-only analysis to date, which we update slightly here with new HIRES RVs.

Dai et al. (2019) incorporated parallax information from Gaia in a reanalysis of this system, including a Gaussian process to account for correlated noise. (They only list a mass for planet e, which is consistent with Vanderburg et al. (2017)) Sanchis-Ojeda et al. (2015) measured the obliquity of the giant planet, WASP-47b, using RV measurements from HIRES. They modeled the Rossiter-McLaughlin curve and found a projected obliquity of $\lambda = 0 \pm 24^\circ$, consistent with a spin orbit alignment. Most recently, Bryant & Bayliss (2022) used ESPRESSO RVs to measure planet e’s mass to be $6.77 \pm 0.57 M_{\oplus}$, consistent with our value below.

Kane et al. (2020) analyzed the K2 photometry to look for phase signatures for the planets to constrain their albedos. They determined that WASP-47b is potentially a “dark” planet with an

Table 20. K2-66 System Parameters

Parameter	Credible Interval	Maximum Likelihood	Units
RV Analysis – MCMC Step Parameters			
P_b	$\equiv 5.0694$	$\equiv 5.0694$	days
$T_{\text{conj},b}$	$\equiv 2456984.0075$	$\equiv 2456984.0075$	BJD _{TBD}
$\sqrt{e} \cos \omega_b$	$\equiv 0.0$	$\equiv 0.0$	
$\sqrt{e} \sin \omega_b$	$\equiv 0.0$	$\equiv 0.0$	
K_b	$5.9^{+1.3}_{-1.4}$	5.9	m s^{-1}
γ_{HIRES}	-1.6 ± 1.0	-2.0	m s^{-1}
$\dot{\gamma}$	$\equiv 0.0$	$\equiv 0.0$	$\text{m s}^{-1} \text{ day}^{-1}$
$\ddot{\gamma}$	$\equiv 0.0$	$\equiv 0.0$	$\text{m s}^{-1} \text{ day}^{-2}$
σ_{HIRES}	$5.89^{+1.30}_{-0.40}$	5.60	m s^{-1}
Orbital & Physical Parameters			
P_b	$\equiv 5.0694$	$\equiv 5.0694$	days
$T_{\text{conj},b}$	$\equiv 2456984.0075$	$\equiv 2456984.0075$	BJD _{TBD}
e_b	$\equiv 0.0$	$\equiv 0.0$	
ω_b	$\equiv 0.0$	$\equiv 0.0$	radians
K_b	$5.9^{+1.3}_{-1.4}$	5.9	m s^{-1}
M_b	$16^{+3.8}_{-4.1}$	16.5	M_{\oplus}
R_b/R_*	$0.01515^{+0.00110}_{-0.00030}$	0.01490	
ρ_b	$4.2^{+1.8}_{-0.7}$	3.6	g cm^{-3}
R_b	$\equiv 2.7545$	$\equiv 2.7545$	R_{\oplus}
Priors			
Parameter	Prior		
None			

albedo of 0.016 and WASP-47e shows early evidence of also having a low albedo. Planet e is also being targeted by JWST observations in GO-3615.

Our fit of the EVEREST light curve of the K2 photometry for WASP-47 is shown in Fig. 57. We acquired a total of 76 RVs of WASP-47 with HIRES, including those reported in Sinukoff et al. (2017b) and Sanchis-Ojeda et al. (2015). These HIRES observations typically had an exposure meter setting of 50,000 counts. We modeled the system as a four-planet system with the three transiting planets fixed in circular orbits and WASP-47c in an eccentric orbit. We searched for additional planets in the RVs and we found no evidence of a fifth planet (Fig. 59). The results of this analysis are listed in Table 26 and the best fit model is shown in Fig. 58. We found planet masses of $357 \pm 11 M_{\oplus}$ (WASP-47b), $395 \pm 13 M_{\oplus}$ ($M_P \sin i$; WASP-47c), $12.8 \pm 1.4 M_{\oplus}$ (WASP-47d), $7.38 \pm 0.72 M_{\oplus}$ (WASP-47e). Our results are consistent with the results from Vanderburg et al. (2017) to within 1σ .

A.29. K2-79

K2-79 is a slightly evolved, solar-temperature star in Field 4 with one transiting planet that has a radius of $3.7 R_{\oplus}$ and an orbital period of 11 days. See Tables 1 and 2 for stellar properties and Table 3 for precise planet parameters. K2-79 b is in the Crossfield et al. (2016) and Mayo et al. (2018)

Table 21. K2-36 System Parameters

Parameter	Credible Interval	Maximum Likelihood	Units
RV Analysis – MCMC Step Parameters			
P_b	$\equiv 1.4226$	$\equiv 1.4226$	days
$T_{\text{conj},b}$	$\equiv 2456827.963$	$\equiv 2456827.963$	BJD _{TBD}
$\sqrt{e} \cos \omega_b$	$\equiv 0.0$	$\equiv 0.0$	
$\sqrt{e} \sin \omega_b$	$\equiv 0.0$	$\equiv 0.0$	
K_b	4 ± 3	3.3	m s^{-1}
P_c	$\equiv 5.3408$	$\equiv 5.3408$	days
$T_{\text{conj},c}$	$\equiv 2456812.841$	$\equiv 2456812.841$	BJD _{TBD}
$\sqrt{e} \cos \omega_c$	$\equiv 0.0$	$\equiv 0.0$	
$\sqrt{e} \sin \omega_c$	$\equiv 0.0$	$\equiv 0.0$	
K_c	$11.4^{+3.4}_{-3.5}$	11.3	m s^{-1}
γ_{HIRES}	-0.5 ± 4.9	-1.4	m s^{-1}
$\gamma_{\text{HARPS-N}}$	$\equiv 13642.2773$	$\equiv 13642.2773$	m s^{-1}
$\dot{\gamma}$	$\equiv 0.0$	$\equiv 0.0$	$\text{m s}^{-1} \text{ day}^{-1}$
$\ddot{\gamma}$	$\equiv 0.0$	$\equiv 0.0$	$\text{m s}^{-1} \text{ day}^{-2}$
σ_{HIRES}	$8.9^{+3.4}_{-2.5}$	7.1	m s^{-1}
$\sigma_{\text{HARPS-N}}$	$\equiv 0.0$	$\equiv 0.0$	m s^{-1}
η_3	$13.9^{+7.5}_{-1.4}$	12.7	days
η_2	$27.8^{+5.2}_{-3.8}$	26.8	days
η_4	0.5 ± 0.1	0.5	
$\eta_{1,\text{HIRES}}$	$16.6^{+4.5}_{-4.2}$	15.9	m s^{-1}
$\eta_{1,\text{HARPS-N}}$	$\equiv 12.7507$	$\equiv 12.7507$	m s^{-1}
Orbital & Physical Parameters			
P_b	$\equiv 1.4226$	$\equiv 1.4226$	days
$T_{\text{conj},b}$	$\equiv 2456827.963$	$\equiv 2456827.963$	BJD _{TBD}
e_b	$\equiv 0.0$	$\equiv 0.0$	
ω_b	$\equiv 0.0$	$\equiv 0.0$	radians
K_b	4 ± 3	3.3	m s^{-1}
M_b	$5.1^{+4.5}_{-4.4}$	5.0	M_{\oplus}
ρ_b	12^{+12}_{-11}	10	g cm^{-3}
P_c	$\equiv 5.3408$	$\equiv 5.3408$	days
$T_{\text{conj},c}$	$\equiv 2456812.841$	$\equiv 2456812.841$	BJD _{TBD}
e_c	$\equiv 0.0$	$\equiv 0.0$	
ω_c	$\equiv 0.0$	$\equiv 0.0$	radians
K_c	$11.4^{+3.4}_{-3.5}$	11.3	m s^{-1}
M_c	26 ± 8	27	M_{\oplus}
ρ_c	$9.4^{+3.6}_{-3.3}$	8.4	g cm^{-3}
Priors			
Parameter	Prior		
$\eta_{1,\text{HIRES}}$	$\mathcal{U}(0, 1e + 100)$		
σ_{HIRES}	$\mathcal{U}(0, 1e + 100)$		
$\eta_{1,\text{HARPS-N}}$	$\mathcal{U}(0, 1e + 100)$		
$\sigma_{\text{HARPS-N}}$	$\mathcal{U}(0, 1e + 100)$		
Numerical prior from photom. training on η_2, η_3, η_4			

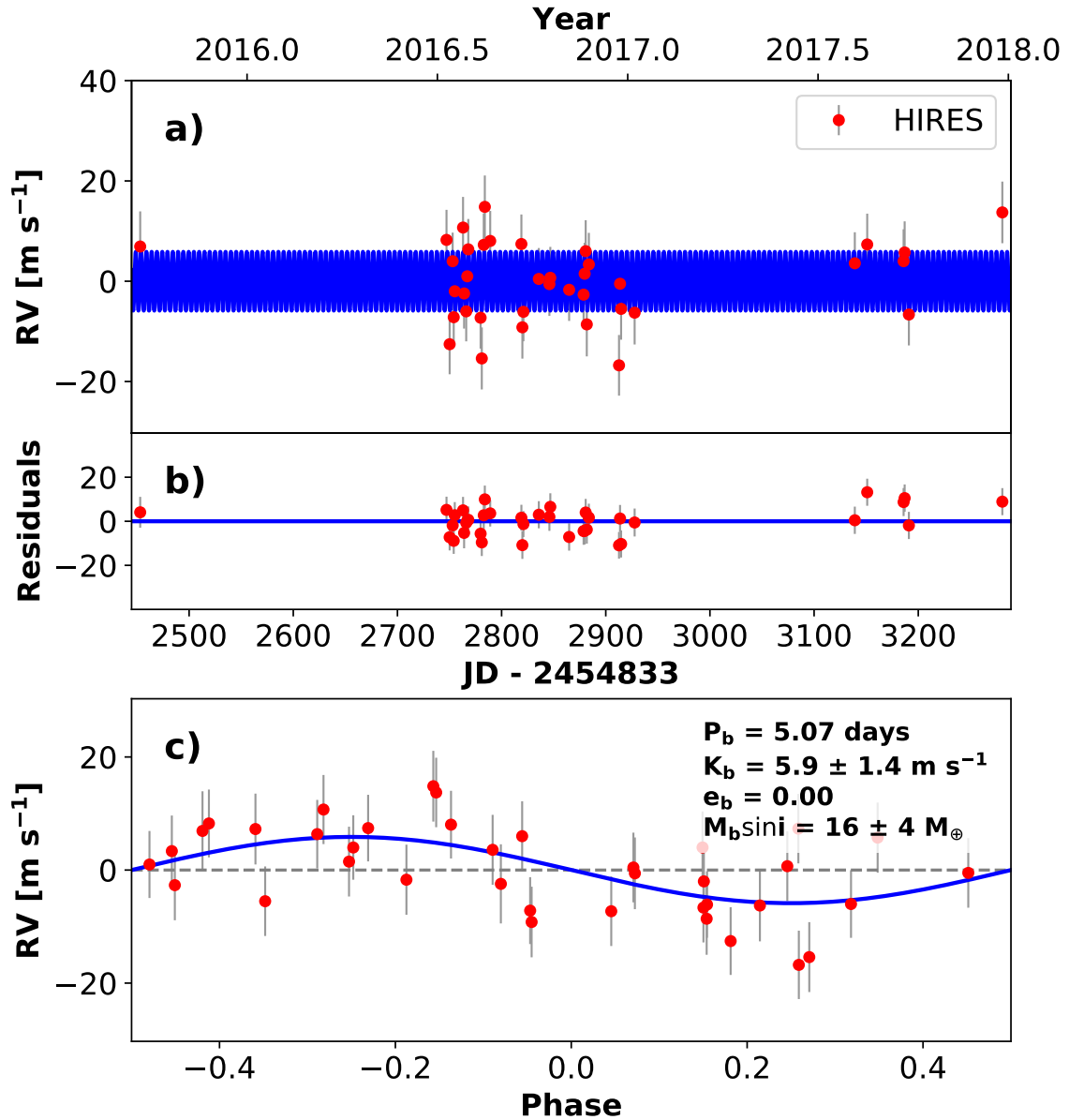


Figure 46. RVs and Keplerian model for K2-66. Symbols, lines, and annotations are similar to those in Fig. 11.

catalogs, the latter of which validated the planet. The planet’s mass has been previously measured to be 9–12 M_\oplus (Nava et al. 2022; Bonomo et al. 2023b).

Our fit of the EVEREST light curve of the K2 photometry for this star is shown in Fig. 60. We acquired 62 RVs with HIRES, typically with an exposure meter setting of 50,000 counts. We modeled the system as a single planet in a circular orbit with the orbital period and phase fixed to the transit ephemeris. Our model also included a linear RV trend which we justified based on $\Delta\text{AICc} = 4$ compared to a model without a trend. The results of this analysis are listed in Table 27 and the best-fit model is shown in Fig. 61. K2-79 b is a Neptune-sized planet whose Doppler signal we detected with 1- σ significance and has a low density (0.3 ± 0.4 g cm⁻³). The measurement of this signal was hampered by an unexpectedly high jitter for a star only modestly evolved and with low

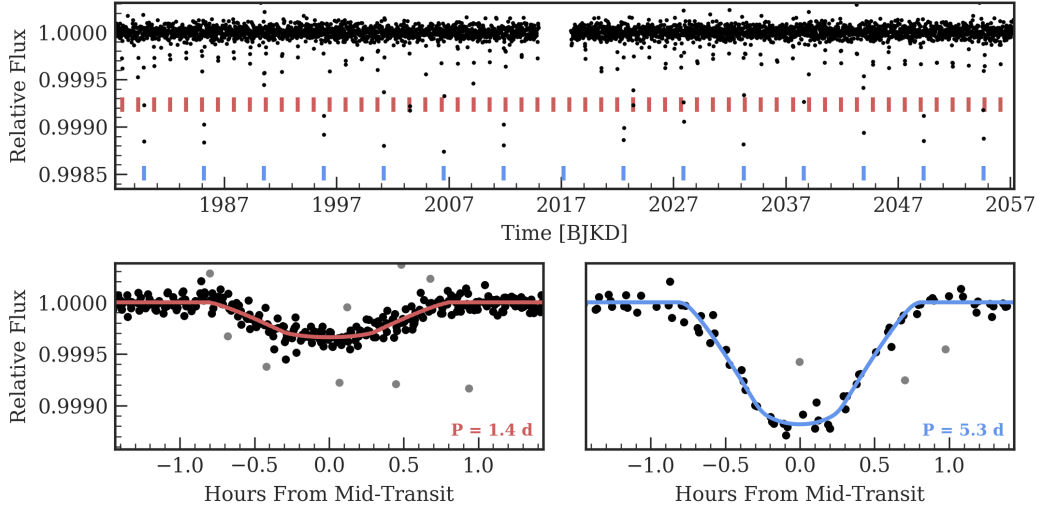


Figure 47. Time series (top) and phase-folded (bottom) light curve for the planet orbiting K2-36. Plot formatting is the same as in Fig. 10.

activity ($\log R'_{\text{HK}} = -5.129$). A search for additional planets found no significant signals in a ΔBIC periodogram. Our observations are consistent with the more precise measurements in the literature (Nava et al. 2022; Bonomo et al. 2023b).

A.30. K2-106

K2-106 is a slightly evolved, solar-temperature star from Campaign 8 with two transiting planets. The first planet has a radius of $1.8 R_{\oplus}$ with an ultra-short period of 0.8 days. The second planet has a size of $2.7 R_{\oplus}$ and a period of 13 days. See Tables 1 and 2 for stellar properties and Table 3 for precise planet parameters adopted in this paper. Our fit of the EVEREST light curve of the K2 photometry for K2-106 is shown in Fig. 63. The system was first reported as a candidate in Vanderburg et al. (2016b), and also in the catalogs by Petigura et al. (2018a) and Mayo et al. (2018). The system was first validated by Adams et al. (2017).

Sinukoff et al. (2017a) characterized the system by measuring planet masses of $9.0 \pm 1.6 M_{\oplus}$ for the USP and $< 24.4 M_{\oplus}$ (99.7% confidence) for the outer planet, based on 35 HIRES RVs. A later analysis by Guenther et al. (2017) measured masses of $8.36^{+0.96}_{-0.94} M_{\oplus}$ (K2-106 b) and $5.8^{+3.3}_{-3.0} M_{\oplus}$ (K2-106 c) based on RVs from PFS (13), HDS (3), FIES (6), HARPS-N (12), HARPS (20), as well as the earlier HIRES RVs. (Rodríguez Martínez et al. 2023) report masses of $8.5 \pm 1.0 M_{\oplus}$ and $5.9 \pm 3.3 M_{\oplus}$, Bonomo et al. (2023b) find $8.2 \pm 0.8 M_{\oplus}$ and $8.9 \pm 2.4 M_{\oplus}$, and Guenther et al. (2024) find $7.8 \pm 0.7 M_{\oplus}$ and $7.3 \pm 2.5 M_{\oplus}$.

We acquired 39 RVs of K2-106 with HIRES, including those previously reported in Sinukoff et al. (2017a). The observations have a typical exposure meter setting of 80,000 counts. We modeled the system as two planets in circular orbits with orbital periods and phases fixed to the transit ephemeris. We considered more complicated models with free eccentricities and/or a linear RV trend, but rejected those models based on the AIC statistic. Furthermore, we do not find evidence for a third planet in the system (Fig. 65). We binned each RV dataset into intervals of 1.4 hr. The results of our analysis are listed in Table 28 and the best-fit model is shown in Fig. 64. K2-106 b has a size and density

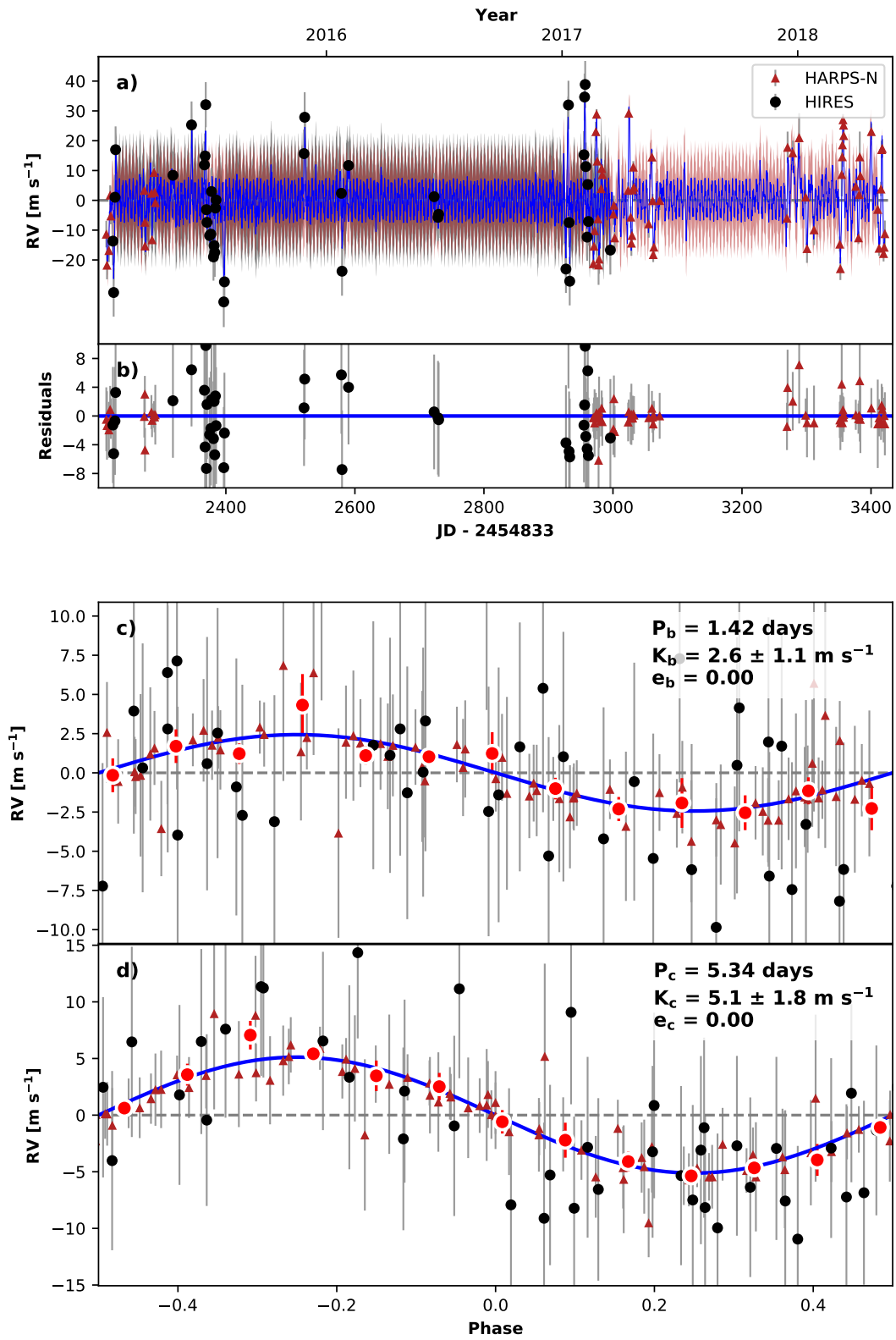


Figure 48. RVs and Keplerian model for K2-36. Symbols, lines, and annotations are similar to those in Fig. 11.

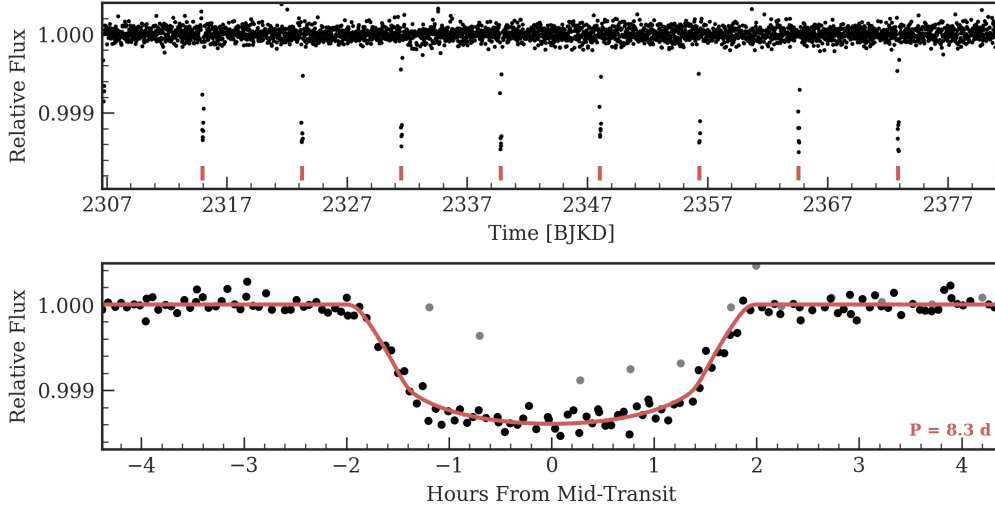


Figure 49. Time series (top) and phase-folded (bottom) light curve for the planet orbiting K2-105. Plot formatting is the same as in Fig. 10.

($7.3_{-1.3}^{+1.7} \text{ g cm}^{-3}$) consistent with a rocky super-Earth. The Doppler signal of the outer planet is only detected with $\sim 1\text{-}\sigma$ significance, but we can rule out a rocky composition based on the density estimate of $1.10_{-0.63}^{+0.67} \text{ g cm}^{-3}$. Our results are consistent with those of previous (and more recent) studies (Rodríguez Martínez et al. 2023; Bonomo et al. 2023b; Guenther et al. 2024).

A.31. K2-98

K2-98 is a late-F type star from Campaign 5 with $V \sin i = 5.6 \pm 1.0 \text{ km s}^{-1}$. The star hosts one transiting planet with radius of $4.9 R_{\oplus}$ and an orbital period of 10 days. See Tables 1 and 2 for stellar properties and Table 3 for precise planet parameters. The planet was discovered by Barragán et al. (2016) who measured a mass using 4 RVs from FIES, 4 from HARPS, and 4 from HARPS-N. The system is also in the catalogs of Petigura et al. (2018a) and Mayo et al. (2018).

Our fit of the EVEREST light curve of the K2 photometry for K2-98 is shown in Fig. 66. We acquired 6 RVs of K2-98 spanning 35 days with HIRES, typically with an exposure meter setting of 60,000. We modeled the RVs from HIRES, FIES, and HARPS as a single planet in a circular orbit with the orbital period and phase fixed to the transit ephemeris. Observations taken on the same night by the same telescope were binned in our analysis. The results of this analysis are listed in Table 29 and the best-fit model is shown in Fig. 67.

We note that Barragán et al. (2016) found a statistically significant mass of $32.1 \pm 8.1 M_{\oplus}$ while our analysis found $20_{-33}^{+21} M_{\oplus}$. The values are consistent, but the Barragán et al. (2016) uncertainty is much smaller. We attribute this discrepancy mainly to differences in modeling. Importantly, Barragán et al. (2016) did not include jitter (so far as we can tell) and required K to be $> 1 \text{ m s}^{-1}$ by including a uniform prior that forced K to be in the range $1\text{--}1000 \text{ m s}^{-1}$). We find that jitter is a critical part of the model; failure to include it can result in significantly underestimated uncertainties. Our model found large and poorly determined values for the jitter of each instrument (except for FIES), in part due to sparse measurements; see Table 29. Since each instrument only contributes 4–6 RVs to the analysis, we suggest that additional RVs of K2-98 would refine the mass measurement.

Table 22. K2-105 System Parameters

Parameter	Credible	Maximum	Units
	Interval	Likelihood	
RV Analysis – MCMC Step Parameters			
P_b	$\equiv 8.2673$	$\equiv 8.2673$	days
$T_{\text{conj},b}$	$\equiv 2457147.9887$	$\equiv 2457147.9887$	BJD _{TBD}
$\sqrt{e} \cos \omega_b$	$\equiv 0.0$	$\equiv 0.0$	
$\sqrt{e} \sin \omega_b$	$\equiv 0.0$	$\equiv 0.0$	
K_b	$5.1^{+1.4}_{-1.5}$	5.1	m s^{-1}
γ_{HIRES}	-1 ± 1	-1	m s^{-1}
$\dot{\gamma}$	$\equiv 0.0$	$\equiv 0.0$	$\text{m s}^{-1} \text{ day}^{-1}$
$\ddot{\gamma}$	$\equiv 0.0$	$\equiv 0.0$	$\text{m s}^{-1} \text{ day}^{-2}$
σ_{HIRES}	$5.1^{+1.2}_{-0.3}$	4.8	m s^{-1}
Orbital & Physical Parameters			
P_b	$\equiv 8.2673$	$\equiv 8.2673$	days
$T_{\text{conj},b}$	$\equiv 2457147.9887$	$\equiv 2457147.9887$	BJD _{TBD}
e_b	$\equiv 0.0$	$\equiv 0.0$	
ω_b	$\equiv 0.0$	$\equiv 0.0$	radians
K_b	$5.1^{+1.4}_{-1.5}$	5.1	m s^{-1}
M_b	$15.4^{+4.3}_{-4.5}$	15.5	M_{\oplus}
R_b/R_*	$0.0339^{+0.0003}_{-0.0015}$	0.0349	
ρ_b	$2.09^{+0.65}_{-0.59}$	2.07	g cm^{-3}
R_b	3.40 ± 0.10	3.40	R_{\oplus}
Priors			
Parameter	Prior		
None			

A.32. K2-3

K2-3 is an M0 dwarf star with 3 transiting planets with sizes of 2.1, 1.7, and 1.5 R_{\oplus} and orbital periods of 10.1, 24.6, and 44.6 d. The planetary system was discovered in [Crossfield et al. \(2015\)](#) as *K2*'s first multiplanet system, and is among the best studied *K2* systems to date. It also appears in the catalogs by [Montet et al. \(2015\)](#); [Foreman-Mackey et al. \(2015\)](#); [Vanderburg et al. \(2016b\)](#); [Crossfield et al. \(2016\)](#); [Barros et al. \(2016\)](#); [Sinukoff et al. \(2016\)](#); [Martinez et al. \(2017\)](#); [Kruse et al. \(2019\)](#). [Beichman et al. \(2016\)](#) refined the ephemerides and radii of the three planets with Spitzer transits and [Fukui et al. \(2016\)](#) refined the parameters of K2-3d with a ground-based transit.

Because the planets are desirable targets for transit spectroscopy, several groups have gathered RVs to measure planet masses. [Almenara et al. \(2015\)](#) measured 66 RVs from HARPS and determined that the masses of planets b, c, and d were 8.4 ± 2.1 , $2.1^{+2.1}_{-1.3}$, and $11.1 \pm 3.5 M_{\oplus}$, respectively. They cautioned that the RV semiamplitudes of planets c and d are likely affected by stellar activity. [Dai et al. \(2016\)](#) measured 31 RVs with PFS on Magellan and modeled the RVs with available HARPS data, giving planet masses of 7.7 ± 2.0 , < 12.6 , and $11.3^{+5.9}_{-5.8} M_{\oplus}$ for b, c, and d. [Damasso et al. \(2018\)](#) performed a RV analysis on a total of 132 HARPS and 197 HARPS-N measurements, including the Almenara sample. This HARPS analysis found that the masses of planets b and c are 6.6 ± 1.1

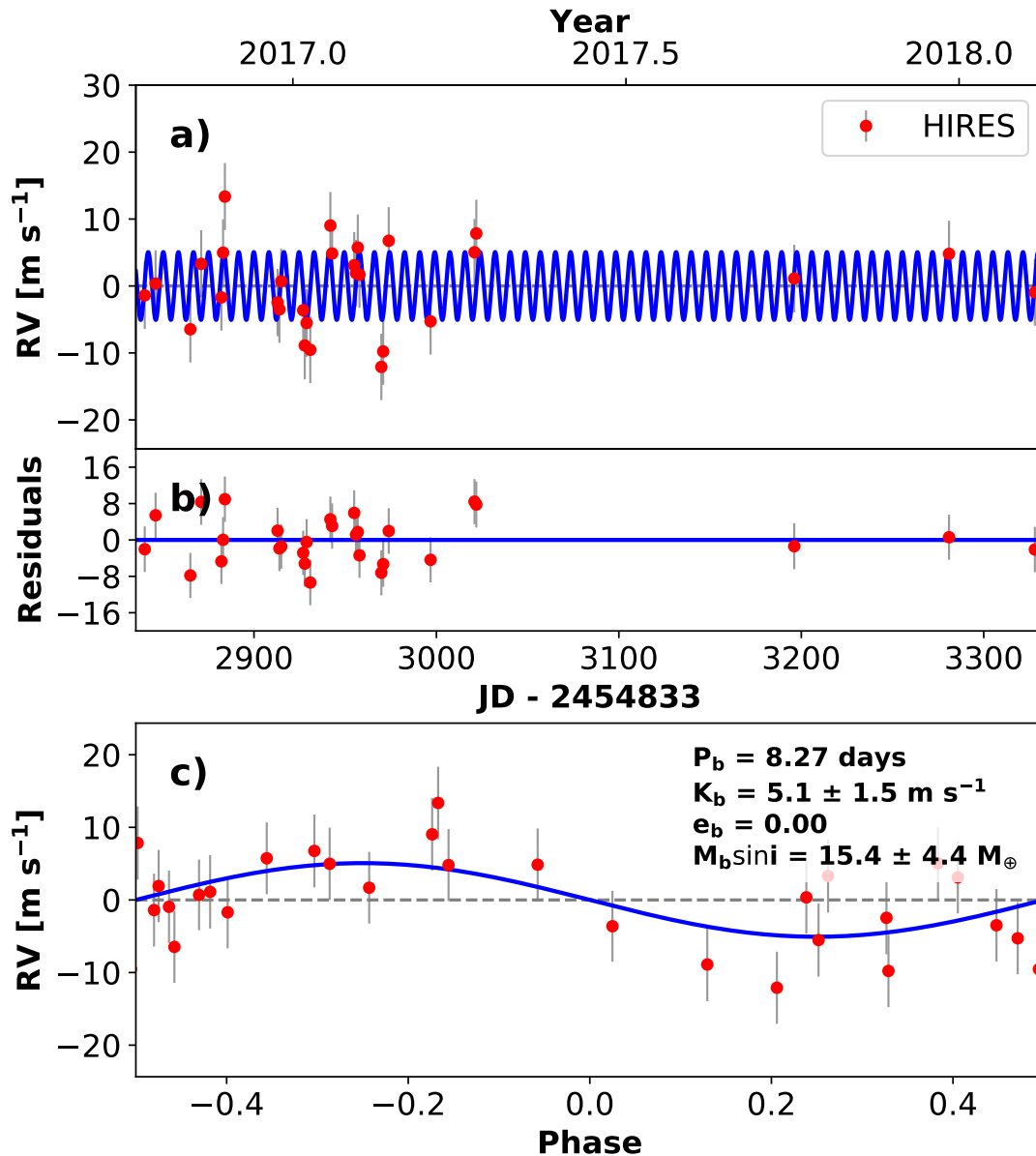


Figure 50. RVs and Keplerian model for K2-105. Symbols, lines, and annotations are similar to those in Fig. 11.

and $3.1^{+1.3}_{-1.2} M_\oplus$, respectively. They estimated the mass of planet d to be $2.7^{+1.2}_{-0.8} M_\oplus$ from a suite of injection-recovery tests. [Diamond-Lowe et al. \(2022\)](#) conduct a reanalysis of the system and measure masses of $5.1 \pm 0.6 M_\oplus$ and $2.7 \pm 0.9 M_\oplus$ for planets b and c, with again non-detection for planet d.

We acquired 50 RVs with HIRES, typically with an exposure meter setting of 80,000. We modeled the HIRES RVs and above HARPS and PFS data with a 3-planet model using a Gaussian process to describe stellar activity. The observations and analysis are described in [Kosiarek et al. \(2019b\)](#), whose results we adopt here. See Tables 1 and 2 for stellar properties and Table 3 for precise planet parameters.

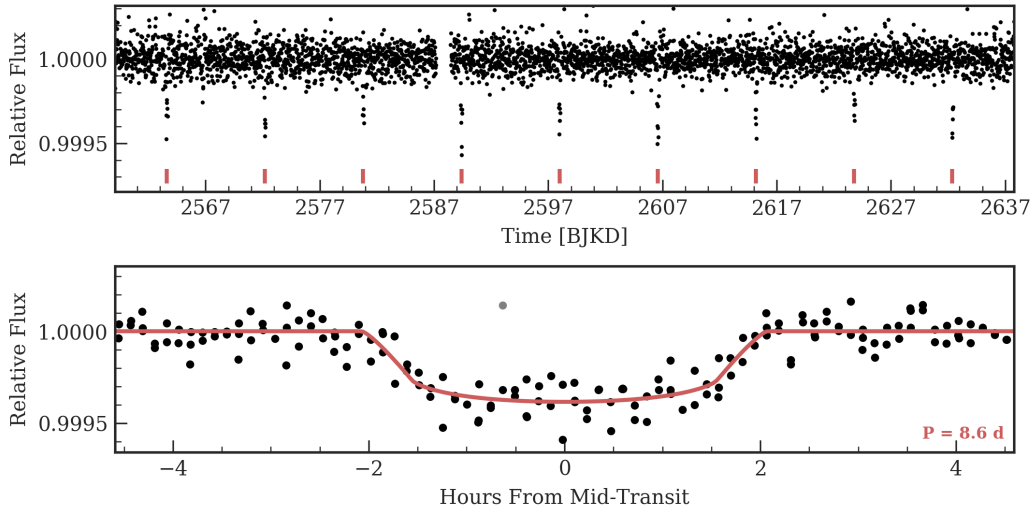


Figure 51. Time series (top) and phase-folded (bottom) light curve for the planet orbiting K2-214. Plot formatting is the same as in Fig. 10.

A.33. EPIC 213546283

EPIC 213546283 is a slightly evolved mid-G star in Field 7 with one transiting planet with a $3.3 R_{\oplus}$ radius in a 10-day orbital period. See Tables 1 and 2 for stellar properties and Table 3 for precise planet parameters. Our fit of the EVEREST light curve of the K2 photometry for EPIC 213546283 is shown in Fig. 68. The planet is listed in the catalogs of Petigura et al. (2018a) and Mayo et al. (2018), both of which list EPIC 213546283 b as a planet candidate. Livingston et al. (2018) estimated a false positive probability of 0.034 and designated the system as a planet candidate as well. Our measurements are not sufficient to confirm the planet but we do successfully rule out massive eclipsing binary false-positive scenarios, increasing the likelihood that this signal is planetary in origin.

We acquired 12 RVs of EPIC 213546283 with HIRES, typically with an exposure meter setting of 60,000 counts. We modeled the system as a single planet in a circular orbit with the orbital period and phase fixed to the transit ephemeris. The results of this analysis are listed in Table 30 and the best-fit model is shown in Fig. 69. We detected EPIC 213546283 b with $1\text{-}\sigma$ significance, which gives a density of $1 \pm 1 \text{ g cm}^{-3}$, consistent with similarly sized planets Neptune and Uranus.

The stellar rotation period of EPIC 213546283 was readily apparent from quasiperiodic variations in its non-detrended Everest light curve. Although this system did not meet our minimum number of observations requirement, we tried a GP model trained on Everest photometry. This model gave $K = 4 \pm 3 \text{ m s}^{-1}$.

A.34. K2-199

K2-199 is a K dwarf with two transiting planets with radii $1.8 R_{\oplus}$ and $2.9 R_{\oplus}$ and orbital periods of 3.2 and 7.4 days, respectively. See Tables 1 and 2 for stellar properties and Table 3 for precise planet parameters. The two planets are in the Petigura et al. (2018a) and Mayo et al. (2018) catalogs, the latter of which validated them. The planets' masses are reported by Akana Murphy et al. (2021) to be $6.9 \pm 1.8 M_{\oplus}$ and $12.4 \pm 2.3 M_{\oplus}$.

Table 23. K2-214 System Parameters

Parameter	Credible Interval	Maximum Likelihood	Units
RV Analysis – MCMC Step Parameters			
P_b	$\equiv 8.5966$	$\equiv 8.5966$	days
$T_{\text{conj},b}$	$\equiv 2457396.6009$	$\equiv 2457396.6009$	BJD _{TBD}
$\sqrt{e} \cos \omega_b$	$\equiv 0.0$	$\equiv 0.0$	
$\sqrt{e} \sin \omega_b$	$\equiv 0.0$	$\equiv 0.0$	
K_b	$1^{+1.7}_{-2.3}$	1.0	m s^{-1}
γ_{HIRES}	-0.6 ± 1.5	-0.6	m s^{-1}
$\dot{\gamma}$	$\equiv 0.0$	$\equiv 0.0$	$\text{m s}^{-1} \text{ day}^{-1}$
$\ddot{\gamma}$	$\equiv 0.0$	$\equiv 0.0$	$\text{m s}^{-1} \text{ day}^{-2}$
σ_{HIRES}	$7.2^{+1.7}_{-0.5}$	6.7	m s^{-1}
Orbital & Physical Parameters			
P_b	$\equiv 8.5966$	$\equiv 8.5966$	days
$T_{\text{conj},b}$	$\equiv 2457396.6009$	$\equiv 2457396.6009$	BJD _{TBD}
e_b	$\equiv 0.0$	$\equiv 0.0$	
ω_b	$\equiv 0.0$	$\equiv 0.0$	radians
K_b	$1^{+1.7}_{-2.3}$	1.0	m s^{-1}
M_b	$2.4^{+5.7}_{-7.3}$	3.3	M_{\oplus}
R_b/R_*	$0.018^{+0.002}_{-0.000}$	0.018	
ρ_b	$0.8^{+1.7}_{-2.7}$	1.3	g cm^{-3}
R_b	$\equiv 2.5122$	$\equiv 2.5122$	R_{\oplus}
Priors			
Parameter	Prior		
None			

Our fit of the EVEREST light curve of the K2 photometry for K2-199 is shown in Fig. 70. We acquired 45 RVs of K2-199 with HIRES, typically with an exposure meter setting of 60,000. We modeled the system as two planets in circular orbits with the orbital periods and phases fixed to the transit ephemerides. We rejected more complicated models with free eccentricities with/without a linear RV trend using the AICc statistic. A linear trend is slightly preferred ($\text{dAICc} = 2.5$) in the circular model, but because of the low significance we adopt the simpler no-trend model. The results of our analysis are listed in Table 31 and the best-fit model is shown in Fig. 71. We detected the Doppler signals of both planets with high significance, consistent with previous measurements (Akana Murphy et al. 2021). K2-199 b is a hot super-Earth with a high density consistent with a rocky composition. K2-199 c is a sub-Neptune with an intermediate density. Extending the baseline with more observations would help constrain a possible trend.

A.35. EPIC 245991048

EPIC 245991048 is a solar-type star in Field 12 with one transiting planet with a radius of $2.2 R_{\oplus}$ and an orbital period of 8 days. The planet does not appear in any catalogs to date, but was detected by our pipeline. Our observations are insufficient to validate the planet. See Tables 1 and 2 for stellar properties and Table 3 for precise planet parameters.

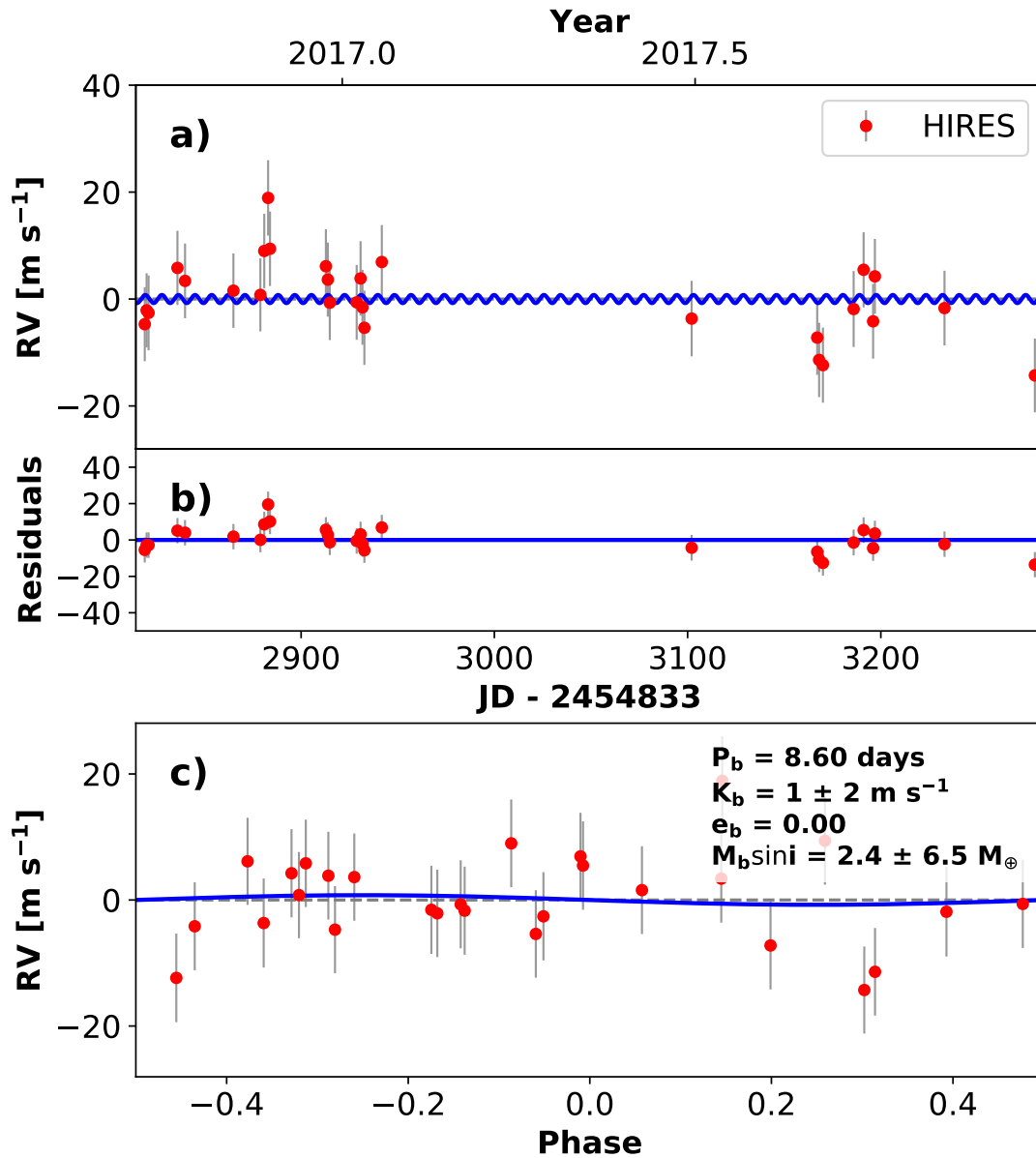


Figure 52. RVs and Keplerian model for K2-214. Symbols, lines, and annotations are similar to those in Fig. 11.

Our fit of the EVEREST light curve of K2 photometry for EPIC 245991048 is shown in Fig. 72. We acquired 16 RVs of EPIC 245991048 with HIRES, typically with an exposure meter setting of 80,000 counts. We modeled the system as a single planet in a circular orbit with an orbital period and phase fixed to the transit ephemeris. We rejected more complicated models with a free eccentricity and a linear RV trend based on the AICc statistic. The results of this analysis are listed in Table 32 and the best fit model is shown in Fig. 73. EPIC 245991048 b appears to be a sub-Neptune with an intermediate bulk density.

We tried a GP fit for this system but adopted a non-GP fit because of the small number of available RVs. A photometry-trained GP found $K_b = 2.3 \pm 1.9$ m s⁻¹, while an untrained GP found $K_b =$

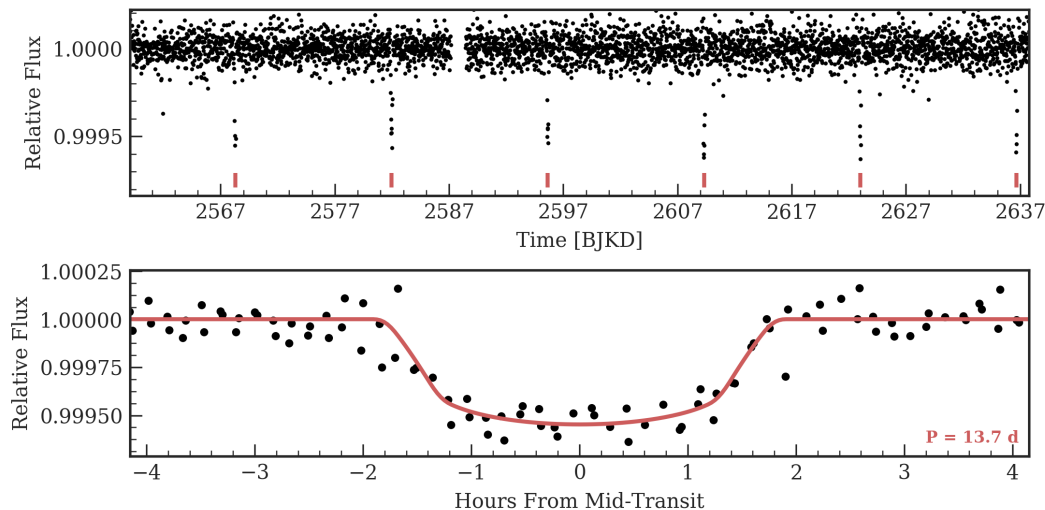


Figure 53. Time series (top) and phase-folded (bottom) light curve for the planet orbiting K2-220. Plot formatting is the same as in Fig. 10.

$1.5 \pm 2.3 \text{ ms}^{-1}$. Note that the median stellar rotation period parameter, η_3 , returned by the trained GP is different from the ≈ 50 day periodic signal seen in the residual plot of Figure 73.

A.36. K2-32

K2-32 is a K0 dwarf from Campaign 2 with three transiting planets with orbital periods near the 3:2:1 commensurability. The planets have sizes $5.1 R_{\oplus}$, $3 R_{\oplus}$, and $3.4 R_{\oplus}$, and orbital periods of 9 days, 21 days, and 32 days, respectively. See Tables 1 and 2 for stellar properties and Table 3 for precise planet parameters.

The planets were listed as candidates in Vanderburg et al. (2016b) and were subsequently confirmed in Sinukoff et al. (2016). Dai et al. (2016) obtained 43 RVs from HARPS and 6 RVs from PFS, measured a mass for the innermost planet, and obtained upper limits for planets c and d. Petigura et al. (2017b) added 31 HIRES observations and found masses of $16.5 \pm 2.7 M_{\oplus}$, $< 12.1 M_{\oplus}$ (95% confidence), and $10.3 \pm 4.7 M_{\oplus}$ for planets b, c, and d respectively. After our analysis was complete, Heller et al. (2019) applied a new transit least squares algorithm and detected a fourth transiting planet with a radius of $1 R_{\oplus}$ and an orbital period of 4.35 days, which would make the commensurability chain near 1:2:3:7. Our transit search did not recover this planet. With an expected RV semiamplitude of only 0.4 ms^{-1} , we do not expect it to contribute significantly to the Keplerian model. Lillo-Box et al. (2020) measure masses of planets b, c, d, and e of 15 ± 1.8 , 8.1 ± 2.4 , 6.7 ± 2.5 , and $2.1 \pm 1.2 M_{\oplus}$, respectively.

Our fit of the EVEREST light curve of the K2 photometry for K2-32 is shown in Fig. 74.

We acquired 64 RVs of K2-32 with HIRES, typically with an exposure meter setting of 60,000 counts. We modeled the system as three planets (b, c, d) in circular orbits with orbital periods and phases fixed to transit ephemerides and included the HARPS and PFS RVs from Dai et al. (2016) in our analysis. The results of this analysis are listed in Table 33 and the best-fit model is shown in Fig. 75. More complex models including eccentric orbits for each planet and a linear trend are strongly disfavored by an AICc comparison. We recovered planets b and d and find masses generally consistent

Table 24. K2-220 System Parameters

Parameter	Credible	Maximum	Units
	Interval	Likelihood	
RV Analysis – MCMC Step Parameters			
P_b	$\equiv 13.6819$	$\equiv 13.6819$	days
$T_{\text{conj},b}$	$\equiv 2457401.2729$	$\equiv 2457401.2729$	BJD _{TBD}
$\sqrt{e} \cos \omega_b$	$\equiv 0.0$	$\equiv 0.0$	
$\sqrt{e} \sin \omega_b$	$\equiv 0.0$	$\equiv 0.0$	
K_b	0.0 ± 1.2	0.0	m s^{-1}
γ_{HIRES}	$-0.72^{+0.76}_{-0.79}$	-0.72	m s^{-1}
$\dot{\gamma}$	$\equiv 0.0$	$\equiv 0.0$	$\text{m s}^{-1} \text{ day}^{-1}$
$\ddot{\gamma}$	$\equiv 0.0$	$\equiv 0.0$	$\text{m s}^{-1} \text{ day}^{-2}$
σ_{HIRES}	$3.4^{+1.0}_{-0.3}$	3.1	m s^{-1}
Orbital & Physical Parameters			
P_b	$\equiv 13.6819$	$\equiv 13.6819$	days
$T_{\text{conj},b}$	$\equiv 2457401.2729$	$\equiv 2457401.2729$	BJD _{TBD}
e_b	$\equiv 0.0$	$\equiv 0.0$	
ω_b	$\equiv 0.0$	$\equiv 0.0$	radians
K_b	0.0 ± 1.2	0.0	m s^{-1}
M_b	0.0 ± 4.0	0.0	M_{\oplus}
R_b/R_*	$\equiv 0.0215$	$\equiv 0.0215$	
ρ_b	-0.0 ± 1.6	0.0	g cm^{-3}
R_b	$\equiv 2.367$	$\equiv 2.367$	R_{\oplus}
Priors			
Parameter	Prior		
None			

with those in the literature (Petigura et al. 2017b; Lillo-Box et al. 2020). With the additional RVs we also measured a $\sim 2\sigma$ mass for planet c of $5.7^{+2.3}_{-2.4} M_{\oplus}$. At $\sim 0.4 \text{ m s}^{-1}$, the putative fourth planet at 4.35 days represents a challenge for next-generation EPRV instruments.

A.37. K2-108

K2-108 is mid-G star starting to ascend the subgiant branch in Campaign 5 with one transiting planet with a radius of $5.2 R_{\oplus}$ and an orbital period of 4.7 days. See Tables 1 and 2 for stellar properties and Table 3 for precise planet parameters. The planet is listed in the Petigura et al. (2018a) and Mayo et al. (2018) catalogs. K2-108 b was discovered and confirmed by Petigura et al. (2017b), whose solution we adopt here. They found a mass of $59.4 \pm 4.4 M_{\oplus}$ with a linear trend using 20 HIRES RVs. These RVs were mistakenly omitted from Petigura et al. (2017b), but are listed in Table 4.

A.38. K2-62

K2-62 is a late K dwarf in Field 3 with two transiting planets with orbital periods of 6.7 days and 16 days. Both planets have radii of about $2 R_{\oplus}$. See Tables 1 and 2 for stellar properties and Table

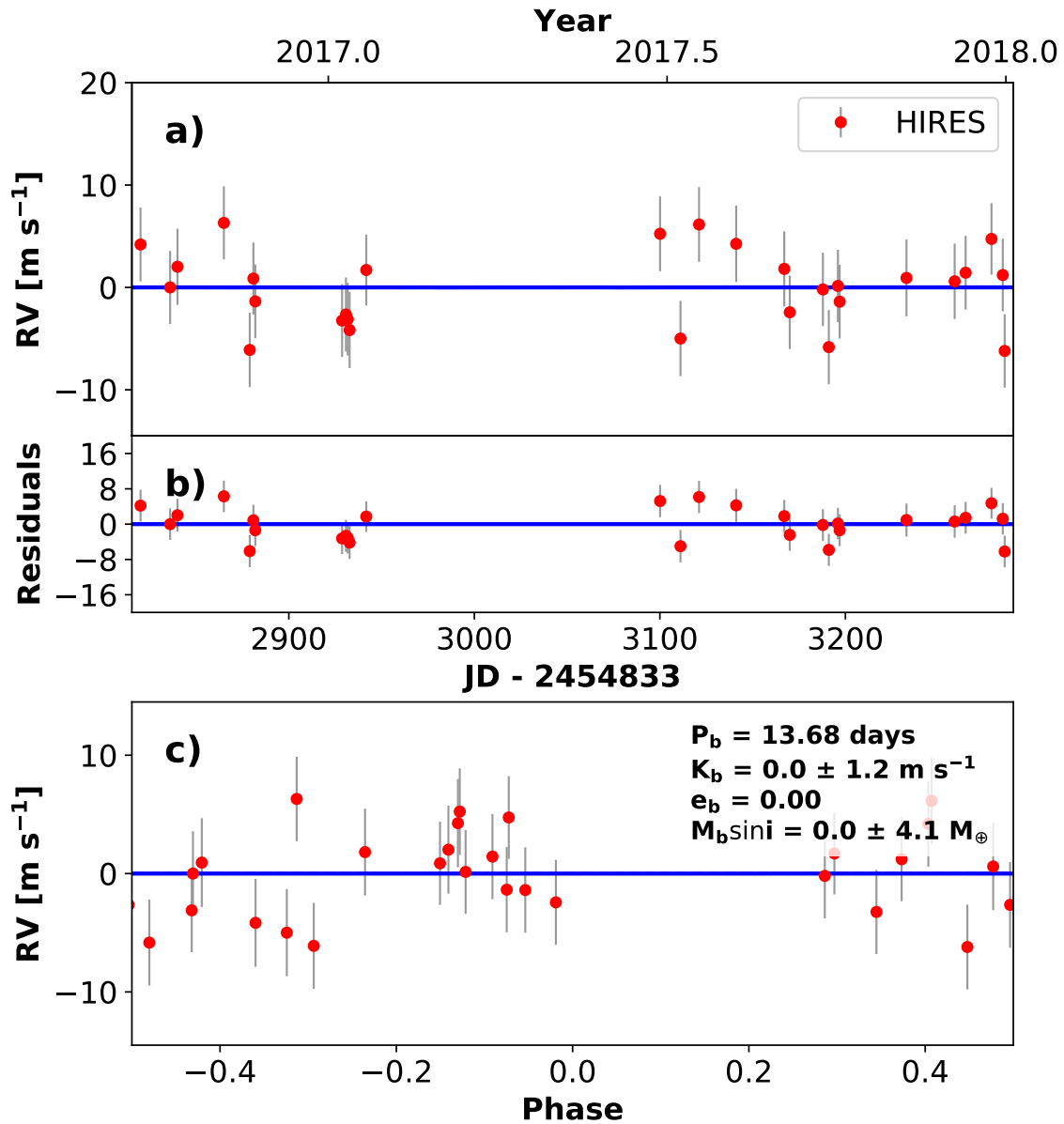


Figure 54. RVs and Keplerian model for K2-220. Symbols, lines, and annotations are similar to those in Fig. 11.

3 for precise planet parameters. The planets were validated by [Crossfield et al. \(2016\)](#) and appear in the [Vanderburg et al. \(2016b\)](#) and [Mayo et al. \(2018\)](#) catalogs.

Our fit of the EVEREST light curve of the K2 photometry for K2-62 is shown in Fig. 76. We acquired 20 RVs of K2-62 with HIRES, typically with an exposure meter setting of 60,000 counts. We modeled the system as two planets in circular orbits with orbital periods and phases fixed to the transit ephemerides. We adopted a model with a linear trend based on $\Delta\text{AICc} = 32$ compared to a flat model. Similarly, we rejected models with eccentric orbits. The results of our analysis are listed in Table 34 and the best fit model is shown in Fig. 77. Doppler signals from the two planets are not detected ($1\text{-}\sigma$ significance). The limits on density do not meaningfully constrain the compositions of these two planets.

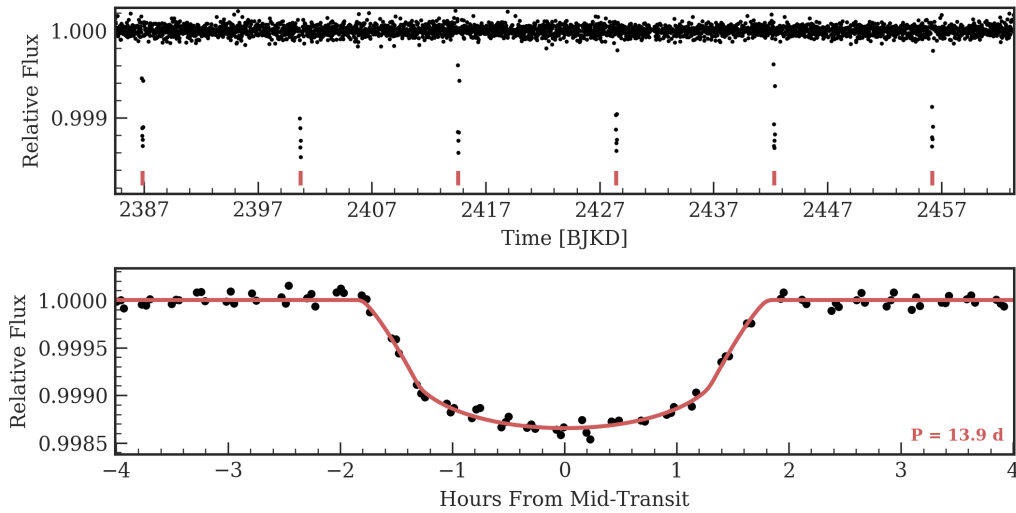


Figure 55. Time series (top) and phase-folded (bottom) light curve for the planet orbiting K2-110. Plot formatting is the same as in Fig. 10.

A.39. *K2-189*

K2-189 is a late-G/early-K dwarf from Campaign 6 with two transiting planets with radii of 1.5 and 2.5 R_{\oplus} and orbital periods of 2.6 and 6.7 days. See Tables 1 and 2 for stellar properties and Table 3 for precise planet parameters. The planets were validated by Mayo et al. (2018); Barros et al. (2016) and also appear in Petigura et al. (2018a).

Our fit of the EVEREST light curve of the K2 photometry for K2-189 is shown in Fig. 78. We acquired 17 RVs of K2-189 with HIRES, typically with an exposure meter setting of 60,000 counts. We modeled the system as two planets in circular orbits with orbital periods and phases fixed to the transit ephemerides. We rejected more complicated models with free eccentricity and/or a linear RV trend using the AICc statistic. The results of our analysis are listed in Table 35 and the best-fit model is shown in Fig. 79. Doppler signals from two planets are each detected with 1- σ significance, which weakly favors a high density and a rocky composition for the super-Earth K2-189 b and a low density and gas-dominated composition for K2-189 c.

A.40. *K2-10*

K2-10 is a G dwarf in Field 1 with one transiting planet with a radius of 3.6 R_{\oplus} and an orbital period of 19 days. See Tables 1 and 2 for stellar properties and Table 3 for precise planet parameters. The planet was discovered and validated by Montet et al. (2015). The planet also appears in the Crossfield et al. (2016), Vanderburg et al. (2016b), and Schmitt et al. (2016) catalogs. Van Eylen et al. (2016b) measured a mass of $27_{-16}^{+17} M_{\oplus}$ and a density of $2.6_{-1.6}^{+2.1} \text{ g cm}^{-3}$ based on 15 RVs from HARPS-N and 7 from FIES.

Our fit of the EVEREST light curve of the K2 photometry for K2-10 is shown in Fig. 80. We acquired 22 RVs of K2-10 with HIRES, typically with an exposure meter setting of 50,000. Using all of the available RVs, we modeled the system as one planet in a circular orbit with an orbital period and phase fixed to the transit ephemeris. We rejected more complicated models with free eccentricity and a linear RV trend using the AICc statistic. The results of our analysis are listed in Table 36 and

Table 25. K2-110 System Parameters

Parameter	Credible Interval	Maximum Likelihood	Units
RV Analysis – MCMC Step Parameters			
P_b	$\equiv 13.8637$	$\equiv 13.8637$	days
$T_{\text{conj},b}$	$\equiv 2457233.7386$	$\equiv 2457233.7386$	BJD _{TBD}
$\sqrt{e} \cos \omega_b$	$\equiv 0.0$	$\equiv 0.0$	
$\sqrt{e} \sin \omega_b$	$\equiv 0.0$	$\equiv 0.0$	
K_b	5.80 ± 0.99	6.00	m s^{-1}
γ_{HIRES}	-0.5 ± 1.4	-0.5	m s^{-1}
$\gamma_{\text{HARPS-N}}$	$-21637.2^{+1.8}_{-1.7}$	-21637.3	
γ_{HARPS}	$-21632.83^{+0.95}_{-0.94}$	-21632.83	m s^{-1}
$\dot{\gamma}$	$\equiv 0.0$	$\equiv 0.0$	$\text{m s}^{-1} \text{ day}^{-1}$
$\ddot{\gamma}$	$\equiv 0.0$	$\equiv 0.0$	$\text{m s}^{-1} \text{ day}^{-2}$
σ_{HIRES}	$4.6^{+1.4}_{-1.0}$	4.0	m s^{-1}
$\sigma_{\text{HARPS-N}}$	$4.0^{+2.6}_{-2.1}$	3.0	
σ_{HARPS}	3 ± 1	2.5	m s^{-1}
Orbital & Physical Parameters			
P_b	$\equiv 13.8637$	$\equiv 13.8637$	days
$T_{\text{conj},b}$	$\equiv 2457233.7386$	$\equiv 2457233.7386$	BJD _{TBD}
e_b	$\equiv 0.0$	$\equiv 0.0$	
ω_b	$\equiv 0.0$	$\equiv 0.0$	radians
K_b	5.80 ± 0.99	6.00	m s^{-1}
M_b	17 ± 3	17	M_{\oplus}
R_b/R_*	$0.0329^{+0.0011}_{-0.0005}$	0.0326	
ρ_b	6 ± 1	5.9	g cm^{-3}
R_b	$2.558^{+0.086}_{-0.036}$	2.524	R_{\oplus}
Priors			
Parameter	Prior		
σ_{HIRES}	$\mathcal{U}(0, 1e + 100)$		
σ_{HARPS}	$\mathcal{U}(0, 1e + 100)$		
$\sigma_{\text{HARPS-N}}$	$\mathcal{U}(0, 1e + 100)$		

the best-fit model is shown in Fig. 81. The planet mass and density from our analysis are consistent with and more precise than those in Van Eylen et al. (2016b).

A.41. EPIC 201357835 (K2-245)

K2-245 is a low-metallicity star ($[\text{Fe}/\text{H}] = -0.450 \pm 0.045$ dex) with nearly solar temperature in Field 10. It has one transiting planet with a radius of $3 R_{\oplus}$ and an orbital period of 12 days. See Tables 1 and 2 for stellar properties and Table 3 for precise planet parameters. Our fit of the EVEREST light curve of the K2 photometry for K2-245 is shown in Fig. 82. This system was first identified and validated as K2-245 by Livingston et al. (2018).

We acquired 7 RVs of K2-245 with HIRES, typically with an exposure meter setting of 60,000 counts. This star has low chromospheric activity with $\log R'_{\text{HK}} = -5.19$. We modeled the system as a single planet in a circular orbit with orbital period and phase fixed to the transit ephemerides. The results of this analysis are listed in Table 37 and the best-fit model is shown in Fig. 83. Our limited

Table 26. WASP-47 System Parameters

Parameter	Credible Interval	Maximum Likelihood	Units
RV Analysis – MCMC Step Parameters			
P_e	$\equiv 0.7896$	$\equiv 0.7896$	days
$T_{\text{conj},e}$	$\equiv 2456981.3436$	$\equiv 2456981.3436$	BJD _{TBD}
$\sqrt{e} \cos \omega_e$	$\equiv 0.0$	$\equiv 0.0$	
$\sqrt{e} \sin \omega_e$	$\equiv 0.0$	$\equiv 0.0$	
K_e	$4.85^{+0.46}_{-0.45}$	4.82	m s ⁻¹
P_b	$\equiv 4.1592$	$\equiv 4.1592$	days
$T_{\text{conj},b}$	$\equiv 2456982.9772$	$\equiv 2456982.9772$	BJD _{TBD}
$\sqrt{e} \cos \omega_b$	$\equiv 0.0$	$\equiv 0.0$	
$\sqrt{e} \sin \omega_b$	$\equiv 0.0$	$\equiv 0.0$	
K_b	$140.60^{+0.45}_{-0.44}$	140.60	m s ⁻¹
P_d	$\equiv 9.031$	$\equiv 9.031$	days
$T_{\text{conj},d}$	$\equiv 2456988.3079$	$\equiv 2456988.3079$	BJD _{TBD}
$\sqrt{e} \cos \omega_d$	$\equiv 0.0$	$\equiv 0.0$	
$\sqrt{e} \sin \omega_d$	$\equiv 0.0$	$\equiv 0.0$	
K_d	$4.05^{+0.44}_{-0.45}$	4.06	m s ⁻¹
P_c	$592.5^{+2.6}_{-2.5}$	592.3	days
$T_{\text{conj},c}$	$2455993.4^{+6.2}_{-7.1}$	2455993.8	BJD _{TBD}
$\sqrt{e} \cos \omega_c$	$-0.249^{+0.041}_{-0.039}$	-0.250	
$\sqrt{e} \sin \omega_c$	$0.486^{+0.022}_{-0.023}$	0.488	
K_c	31.13 ± 0.43	31.10	m s ⁻¹
γ_{PFS}	17.3 ± 2.1	17.3	m s ⁻¹
γ_{HIRES}	$9.81^{+0.81}_{-0.82}$	9.80	m s ⁻¹
$\gamma_{\text{HARPS-N}}$	-27040.4 ± 0.6	-27040.4	m s ⁻¹
γ_{CORALIE}	$-27079.9^{+2.5}_{-2.4}$	-27080.0	m s ⁻¹
$\dot{\gamma}$	$\equiv 0.0$	$\equiv 0.0$	m s ⁻¹ day ⁻¹
$\ddot{\gamma}$	$\equiv 0.0$	$\equiv 0.0$	m s ⁻¹ day ⁻²
σ_{PFS}	$6.4^{+1.7}_{-1.3}$	5.8	m s ⁻¹
σ_{HIRES}	$4.21^{+0.59}_{-0.52}$	4.00	m s ⁻¹
$\sigma_{\text{HARPS-N}}$	0.9 ± 0.6	0.3	m s ⁻¹
σ_{CORALIE}	7.6 ± 2.8	7.0	m s ⁻¹
Orbital & Physical Parameters			
P_e	$\equiv 0.7896$	$\equiv 0.7896$	days
$T_{\text{conj},e}$	$\equiv 2456981.3436$	$\equiv 2456981.3436$	BJD _{TBD}
e_e	$\equiv 0.0$	$\equiv 0.0$	
ω_e	$\equiv 0.0$	$\equiv 0.0$	radians
K_e	$4.85^{+0.46}_{-0.45}$	4.82	m s ⁻¹
M_e	$7.06^{+0.71}_{-0.69}$	7.03	M_{\oplus}
R_e/R_*	$0.0148^{+0.0015}_{-0.0005}$	0.0180	
ρ_e	$6.6^{+1.1}_{-1.6}$	3.4	g cm ⁻³
R_e	$1.79^{+0.18}_{-0.06}$	2.25	R_{\oplus}
P_b	$\equiv 4.1592$	$\equiv 4.1592$	days
$T_{\text{conj},b}$	$\equiv 2456982.9772$	$\equiv 2456982.9772$	BJD _{TBD}
e_b	$\equiv 0.0$	$\equiv 0.0$	
ω_b	$\equiv 0.0$	$\equiv 0.0$	radians
K_b	$140.60^{+0.45}_{-0.44}$	140.60	m s ⁻¹
M_b	357 ± 11	357	M_{\oplus}
R_b/R_*	$0.10137^{+0.00036}_{-0.00027}$	0.10124	
ρ_b	$1.065^{+0.035}_{-0.034}$	0.970	g cm ⁻³
R_b	$12.252^{+0.044}_{-0.033}$	12.640	R_{\oplus}
P_d	$\equiv 9.031$	$\equiv 9.031$	days
$T_{\text{conj},d}$	$\equiv 2456988.3079$	$\equiv 2456988.3079$	BJD _{TBD}
e_d	$\equiv 0.0$	$\equiv 0.0$	
ω_d	$\equiv 0.0$	$\equiv 0.0$	radians
K_d	$4.05^{+0.44}_{-0.45}$	4.06	m s ⁻¹
M_d	13.3 ± 1.5	13.3	M_{\oplus}

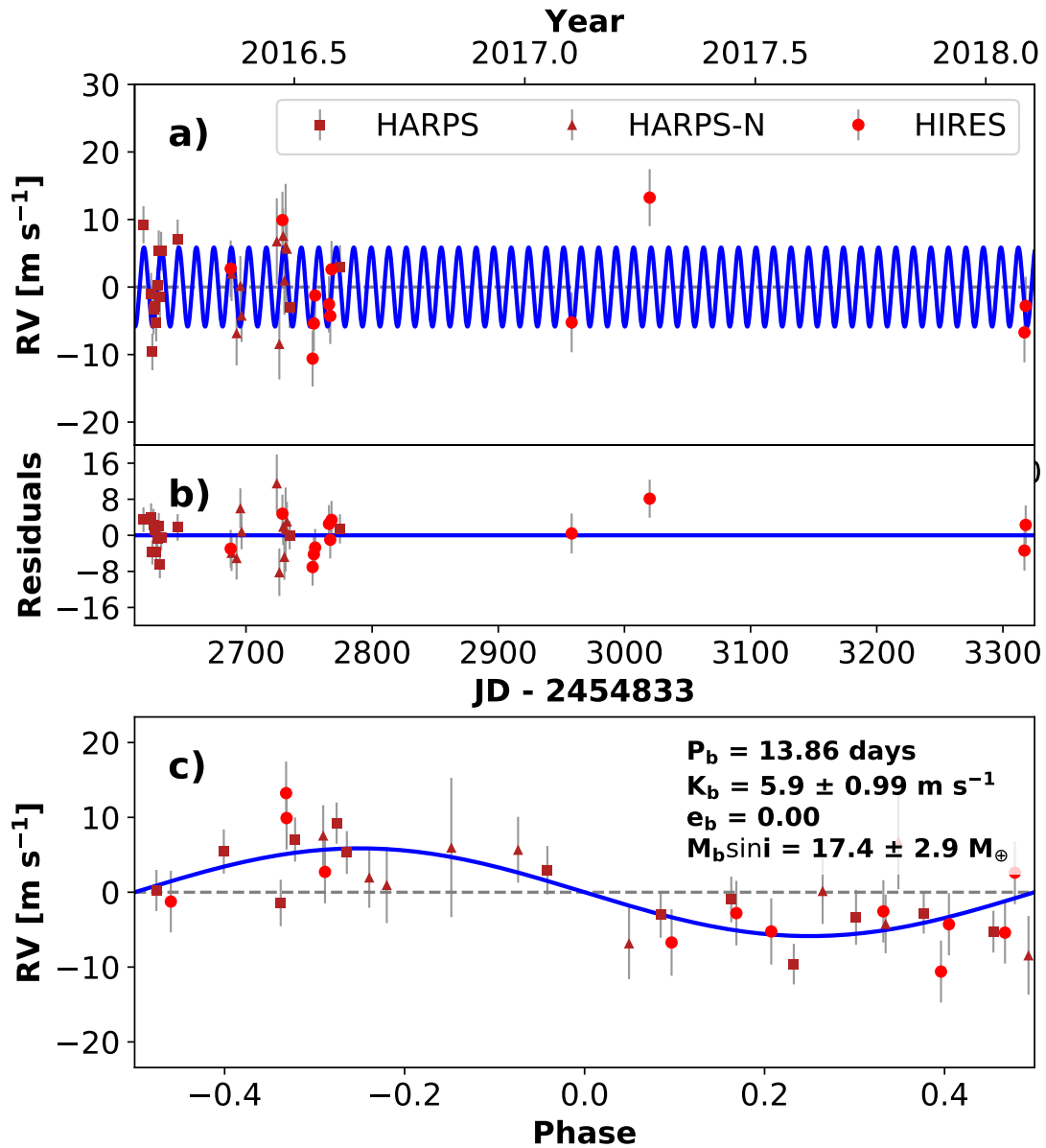


Figure 56. RVs and Keplerian model for K2-110. Symbols, lines, and annotations are similar to those in Fig. 11.

RVs do not measure a useful mass for this planet but we do successfully rule out massive eclipsing binary false-positive scenarios, increasing the likelihood that this signal is planetary in origin

A.42. K2-216

K2-216 is a chromospherically active ($\log R'_{\text{HK}} = -4.627$), late K dwarf in Field 8 with one transiting planet with a radius of $1.7 R_{\oplus}$ and an orbital period of 2.2 days. See Tables 1 and 2 for stellar properties and Table 3 for precise planet parameters. The star was validated by Mayo et al. (2018) and appears in the (Petigura et al. 2018a) catalog. Persson et al. (2018) reported that K2-216 b's mass is $8.0 \pm 1.6 M_{\oplus}$ based on 8 FIES RVs, 9 HARPS RVs, and 13 HARPS-N RVs. They accounted

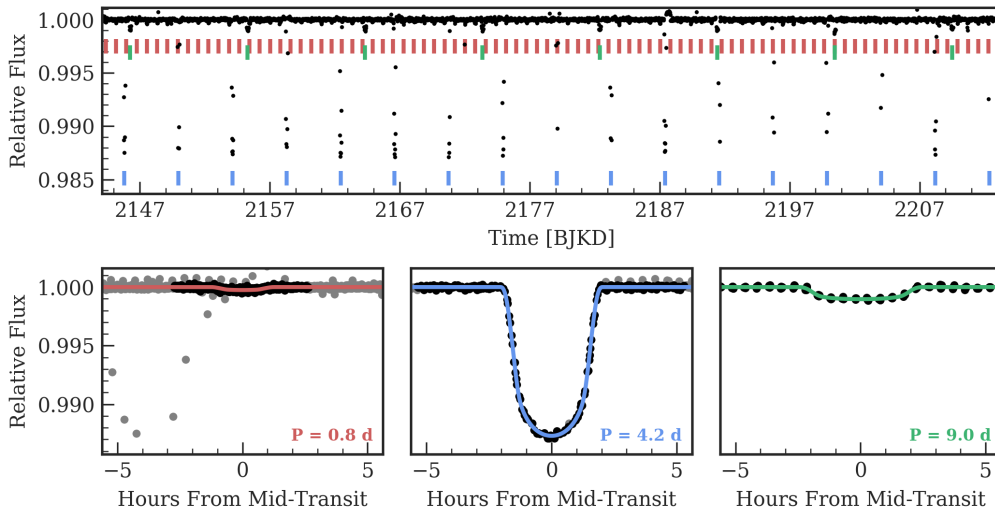


Figure 57. Time series (top) and phase-folded (bottom) light curve for the planet orbiting WASP-47. Plot formatting is the same as in Fig. 10.

for stellar activity using a floating-offset model and also computed a model with a Gaussian process that gave similar results.

Our fit of the EVEREST light curve of the K2 photometry for K2-216 is shown in Fig. 84. We acquired 31 RVs of K2-216 with HIRES, typically with an exposure meter setting of 60,000 counts. Since the star is active ($\log R'_{\text{HK}} = -4.594$) and our $N_{\text{obs, HIRES}} = 31$ measurements combined with RVs from the literature satisfies our prerequisites for a GP regression, we trained a GP on non-detrended Everest photometry (see Section 4.2.2) before using it to compute RV orbit posteriors. We modeled the system as a single planet in a circular orbit with the orbital period and phase fixed to the transit ephemeris. We rejected more complicated models including eccentricity and linear trends based on the AICc statistic. For comparison purposes, we also perform a RV orbit fit using an untrained GP. The trained hyperparameters are clearly peaked and restricted to a portion of the parameter space allowed by the priors, while in the untrained GP the posteriors for η_2 and η_3 extend over the entire allowable parameter space. Both cases yield consistent planet parameters.

Our GP analysis, combined with the higher precision HIRES RVs, yields a smaller mass than Persson et al. (2018). We find a $\sim 10\%$ smaller mass when considering models without a GP, which is consistent with the GP results given the uncertainties of the parameters. The results of our analysis are listed in Table 38 and the best fit model is shown in Fig. 85. K2-216 b is a short-period super-Earth with a density consistent with a rocky composition.

A.43. K2-280

K2-280 is a metal-rich ($[\text{Fe}/\text{H}] = 0.353 \pm 0.060$ dex), slightly evolved G star from Field 7 with one transiting planet with an orbital period of 20 days and a radius of $8.5 R_{\oplus}$. See Tables 1 and 2 for stellar properties and Table 3 for precise planet parameters. The object is listed as a planet candidate in the Petigura et al. (2018a) and Mayo et al. (2018) catalogs and Nowak et al. (2020) measure a planet mass of $37.1 \pm 5.6 M_{\oplus}$ and an eccentricity of 0.35. As described below, modeling of our HIRES

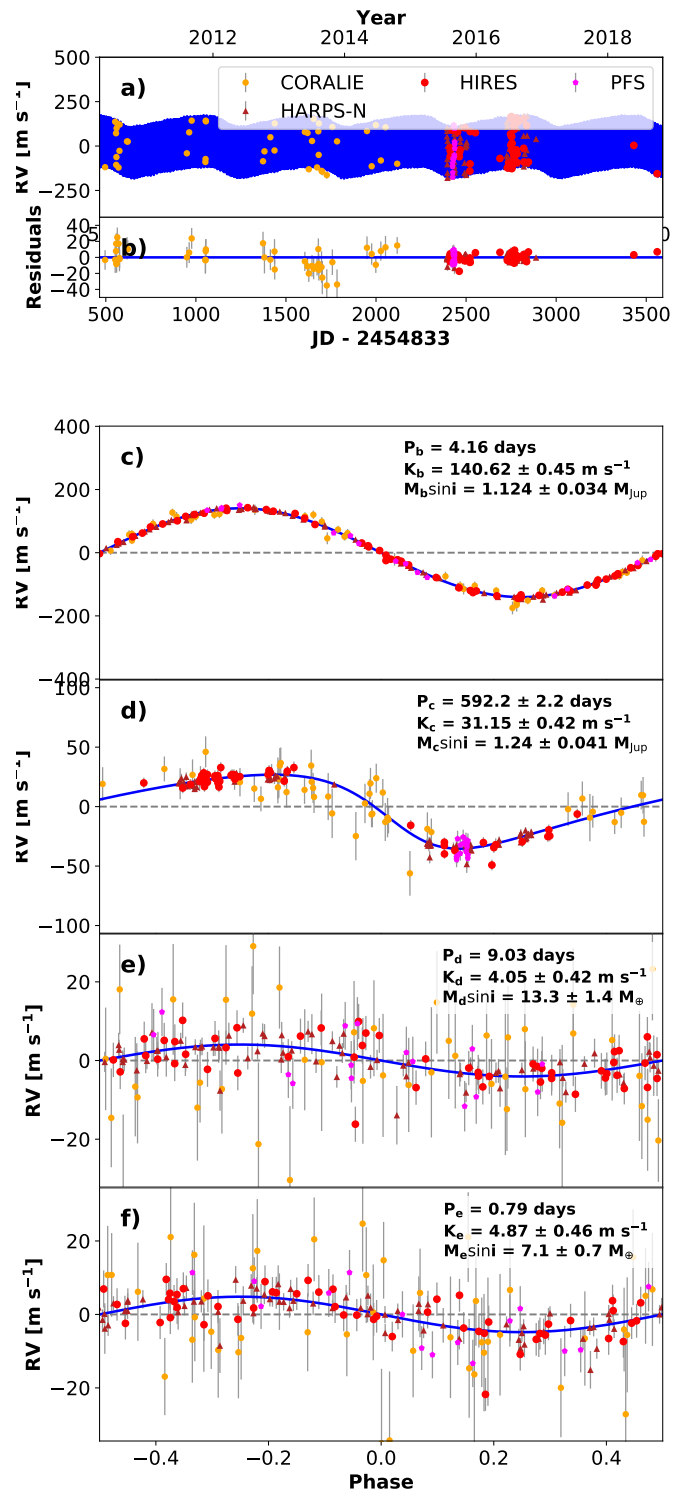


Figure 58. RVs and Keplerian model for WASP-47. Symbols, lines, and annotations are similar to those in Fig. 11.

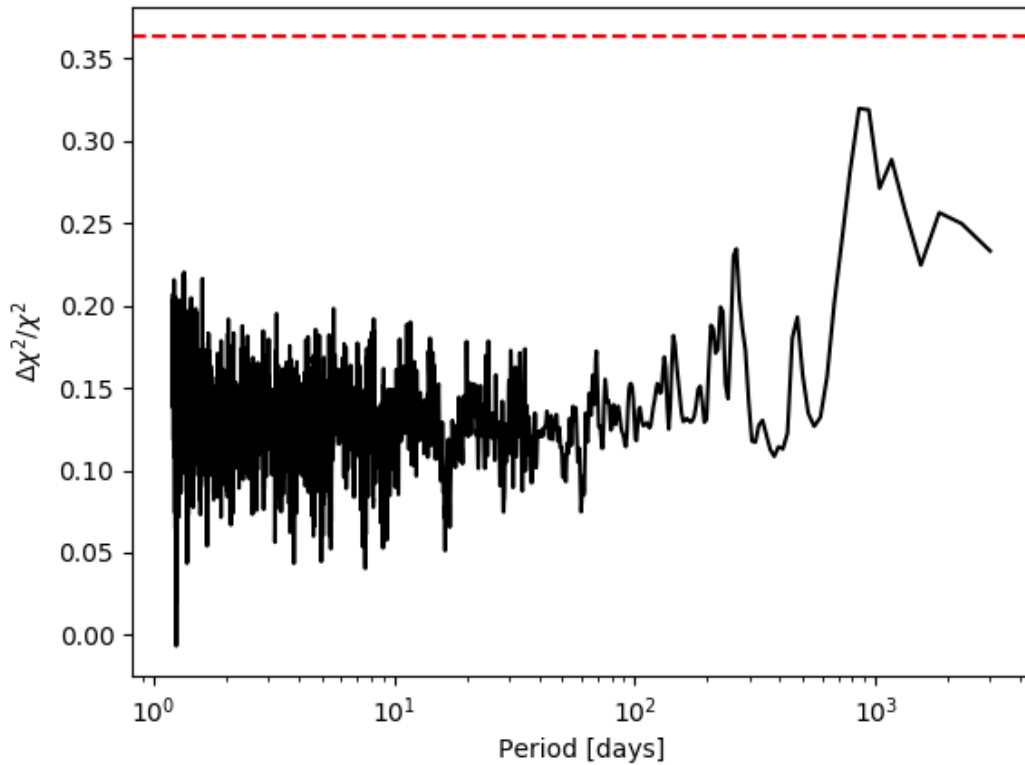


Figure 59. Periodogram search of the RVs showing no evidence for a fifth planet orbiting WASP-47. Lines and annotations are similar to those in Fig. 12.

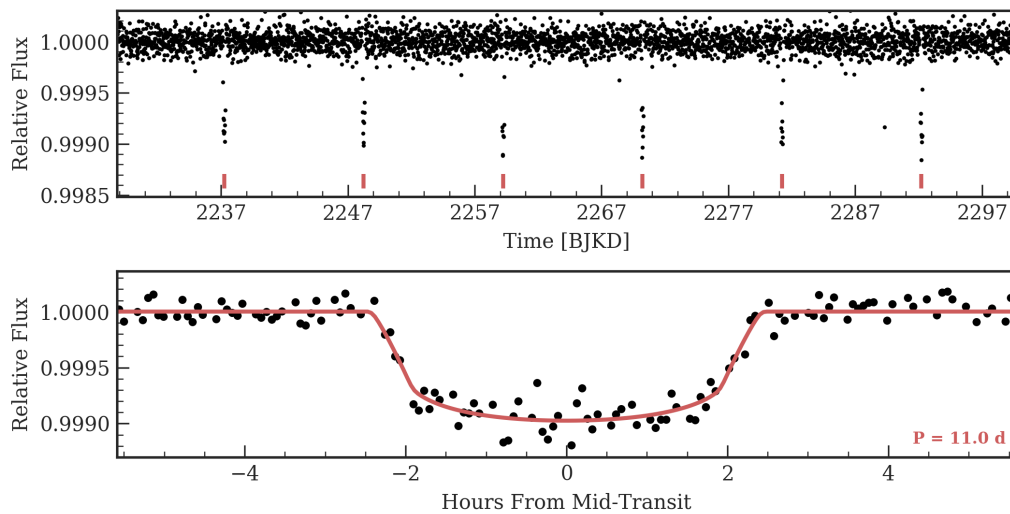


Figure 60. Time series (top) and phase-folded (bottom) light curve for the planet orbiting K2-79. Plot formatting is the same as in Fig. 10.

Table 27. K2-79 System Parameters

Parameter	Credible Interval	Maximum Likelihood	Units
RV Analysis – MCMC Step Parameters			
P_b	$\equiv 10.995$	$\equiv 10.995$	days
$T_{\text{conj},b}$	$\equiv 2457070.2428$	$\equiv 2457070.2428$	BJD_{TBD}
$\sqrt{e} \cos \omega_b$	$\equiv 0.0$	$\equiv 0.0$	
$\sqrt{e} \sin \omega_b$	$\equiv 0.0$	$\equiv 0.0$	
K_b	1.1 ± 1.2	1.1	m s^{-1}
γ_{HIRES}	0.8 ± 1.3	0.8	m s^{-1}
$\dot{\gamma}$	0.0087 ± 0.0034	0.0088	$\text{m s}^{-1} \text{ day}^{-1}$
$\ddot{\gamma}$	$\equiv 0.0$	$\equiv 0.0$	$\text{m s}^{-1} \text{ day}^{-2}$
σ_{HIRES}	$6.37^{+0.75}_{-0.65}$	6.10	m s^{-1}
Orbital & Physical Parameters			
P_b	$\equiv 10.995$	$\equiv 10.995$	days
$T_{\text{conj},b}$	$\equiv 2457070.2428$	$\equiv 2457070.2428$	BJD_{TBD}
e_b	$\equiv 0.0$	$\equiv 0.0$	
ω_b	$\equiv 0.0$	$\equiv 0.0$	radians
K_b	1.1 ± 1.2	1.1	m s^{-1}
M_b	3.8 ± 4.3	3.8	M_{\oplus}
R_b/R_*	$0.0289^{+0.0008}_{-0.0005}$	0.0286	
ρ_b	0.33 ± 0.37	0.40	g cm^{-3}
R_b	$3.99^{+0.11}_{-0.07}$	3.89	R_{\oplus}
Priors			
Parameter	Prior		
j_{itHIRES}	$\mathcal{U}(0, 1e + 100)$		

NOTE—

Reference epoch for $\dot{\gamma}, \ddot{\gamma}$: 2458061.964141

RVs also validates the planet. Our fit of the EVEREST light curve of the K2 photometry for K2-280 is shown in Fig. 86.

We acquired 16 RVs of K2-280 with HIRES, typically with an exposure meter setting of 80,000 counts. This star has low chromospheric activity with $\log R'_{\text{HK}} = -5.24$. We modeled the system as a single planet in a Keplerian orbit with the period and phase fixed to the transit ephemerides. We chose a model with a free eccentricity based on $\Delta\text{AICc} = 18$ compared to a model with a circular orbit. Using a similar comparison, we rejected a model with a linear RV trend. The results of this analysis include a significantly eccentric orbit as listed in Table 39 and shown in Fig. 87. We validated this planet with our 7σ radial velocity detection. (Livingston et al. (2018) had statistically validated the planet.) K2-280 b is a giant planet with a short-period, eccentric orbit, and our values are broadly consistent with those of Nowak et al. (2020).

A.44. K2-37

K2-37 is a late G dwarf with three transiting planets with sizes $1.6 R_{\oplus}$, $2.5 R_{\oplus}$, and $2.4 R_{\oplus}$ with orbital periods of 4.4 days, 6.4 days, and 14.1 days, respectively. See Tables 1 and 2 for stellar

Table 28. K2-106 System Parameters

Parameter	Credible Interval	Maximum Likelihood	Units
RV Analysis – MCMC Step Parameters			
P_b	$\equiv 0.5713$	$\equiv 0.5713$	days
$T_{\text{conj},b}$	$\equiv 2457393.4405$	$\equiv 2457393.4405$	BJD _{TBD}
$\sqrt{e} \cos \omega_b$	$\equiv 0.0$	$\equiv 0.0$	
$\sqrt{e} \sin \omega_b$	$\equiv 0.0$	$\equiv 0.0$	
K_b	6.6 ± 0.7	6.5	m s^{-1}
P_c	$\equiv 13.3392$	$\equiv 13.3392$	days
$T_{\text{conj},c}$	$\equiv 2457405.733$	$\equiv 2457405.733$	BJD _{TBD}
$\sqrt{e} \cos \omega_c$	$\equiv 0.0$	$\equiv 0.0$	
$\sqrt{e} \sin \omega_c$	$\equiv 0.0$	$\equiv 0.0$	
K_c	$1.44^{+0.79}_{-0.83}$	1.35	m s^{-1}
γ_{PFS}	0.0 ± 1.8	0.0	m s^{-1}
γ_{HIRES}	-1.9 ± 0.8	-1.9	m s^{-1}
γ_{HDS}	$1.9^{+8.4}_{-7.6}$	2.0	m s^{-1}
$\gamma_{\text{HARPS-N}}$	-15736 ± 1	-15736.0	m s^{-1}
γ_{HARPS}	$-15732.47^{+0.97}_{-0.93}$	-15732.43	m s^{-1}
γ_{FIES}	10.2 ± 2.2	10.2	m s^{-1}
$\dot{\gamma}$	$\equiv 0.0$	$\equiv 0.0$	$\text{m s}^{-1} \text{ day}^{-1}$
$\ddot{\gamma}$	$\equiv 0.0$	$\equiv 0.0$	$\text{m s}^{-1} \text{ day}^{-2}$
σ_{PFS}	$5.7^{+2.3}_{-1.7}$	5.0	m s^{-1}
σ_{HIRES}	$4.62^{+0.72}_{-0.58}$	4.37	m s^{-1}
σ_{HDS}	10^{+26}_{-7}	2	m s^{-1}
$\sigma_{\text{HARPS-N}}$	$1.7^{+1.5}_{-1.1}$	0.8	m s^{-1}
σ_{HARPS}	2.4 ± 1.1	2.1	m s^{-1}
σ_{FIES}	$0.01^{+2.47}_{-0.01}$	0.00	m s^{-1}
Orbital & Physical Parameters			
P_b	$\equiv 0.5713$	$\equiv 0.5713$	days
$T_{\text{conj},b}$	$\equiv 2457393.4405$	$\equiv 2457393.4405$	BJD _{TBD}
e_b	$\equiv 0.0$	$\equiv 0.0$	
ω_b	$\equiv 0.0$	$\equiv 0.0$	radians
K_b	6.6 ± 0.7	6.5	m s^{-1}
M_b	$8.03^{+0.88}_{-0.85}$	7.99	M_{\oplus}
R_b/R_*	$0.01676^{+0.00096}_{-0.00042}$	0.01650	
ρ_b	7 ± 1	7.614	g cm^{-3}
R_b	$1.87^{+0.11}_{-0.05}$	1.79	R_{\oplus}
P_c	$\equiv 13.3392$	$\equiv 13.3392$	days
$T_{\text{conj},c}$	$\equiv 2457405.733$	$\equiv 2457405.733$	BJD _{TBD}
e_c	$\equiv 0.0$	$\equiv 0.0$	
ω_c	$\equiv 0.0$	$\equiv 0.0$	radians
K_c	$1.44^{+0.79}_{-0.83}$	1.35	m s^{-1}
M_c	$5.0^{+2.8}_{-2.9}$	4.7	M_{\oplus}
R_c/R_*	$0.0269^{+0.0014}_{-0.0008}$	0.0264	
ρ_c	$0.98^{+0.59}_{-0.57}$	1.10	g cm^{-3}
R_c	$3.01^{+0.15}_{-0.09}$	2.90	R_{\oplus}
Priors			
Parameter	Prior		
σ_{HIRES}	$\mathcal{U}(0, 1e + 100)$		
σ_{PFS}	$\mathcal{U}(0, 1e + 100)$		
σ_{HDS}	$\mathcal{U}(0, 1e + 100)$		
σ_{FIES}	$\mathcal{U}(0, 1e + 100)$		
$\sigma_{\text{HARPS-N}}$	$\mathcal{U}(0, 1e + 100)$		
σ_{HARPS}	$\mathcal{U}(0, 1e + 100)$		

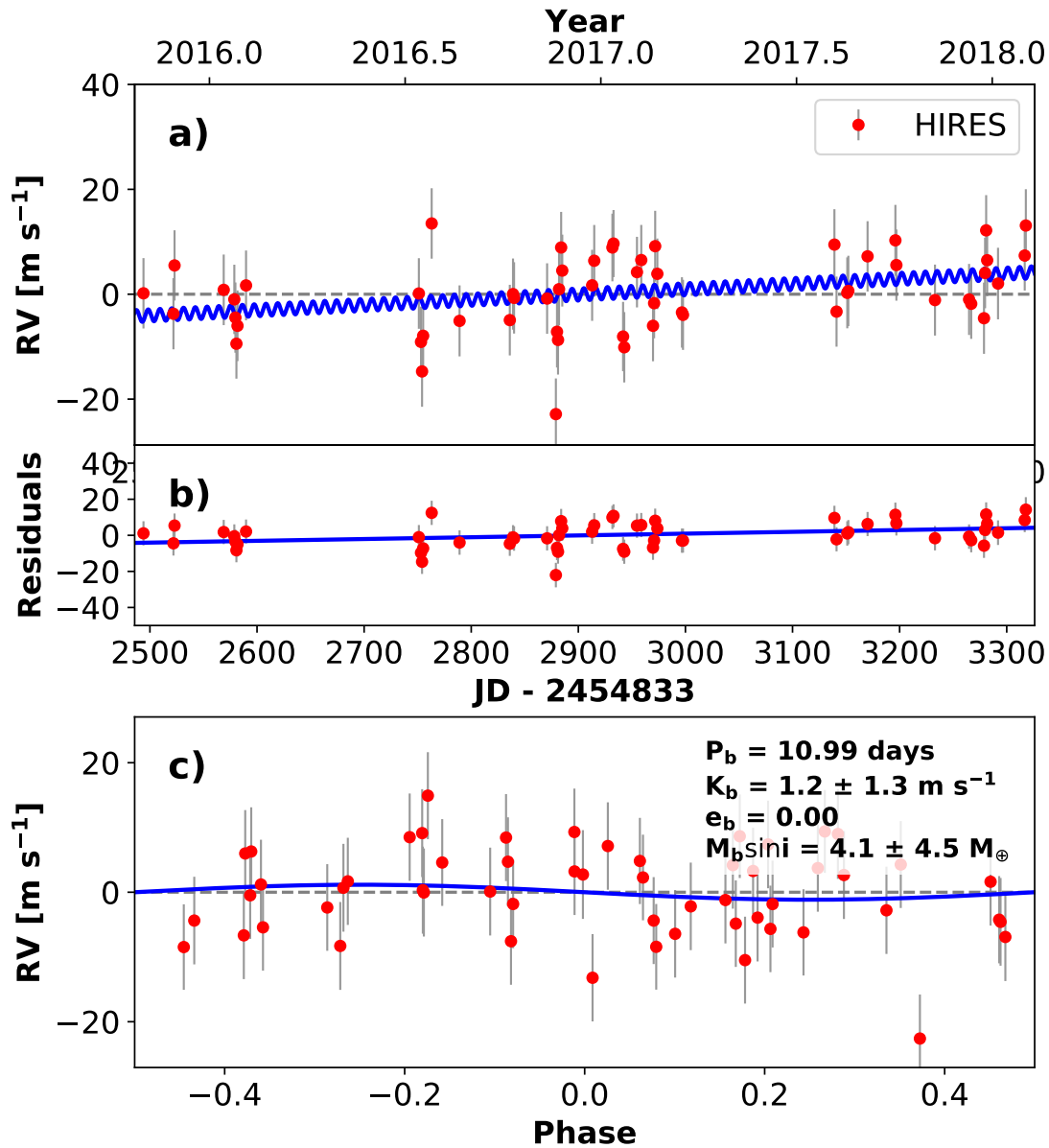


Figure 61. RVs and Keplerian model for K2-79. Symbols, lines, and annotations are similar to those in Fig. 11.

properties and Table 3 for precise planet parameters. The planets are validated and in the Crossfield et al. (2016), Vanderburg et al. (2016b), Sinukoff et al. (2016), and Wittenmyer et al. (2018) catalogs.

Our fit of the EVEREST light curve of the K2 photometry for K2-37 is shown in Fig. 88. We acquired 19 RVs of K2-37 with HIRES, typically with an exposure meter setting of 80,000 counts. We modeled the system as three planets in circular orbits with orbital periods and phases fixed to the transit ephemerides. We rejected more complicated models with noncircular orbits and/or a linear RV trend using the AICc statistic. The results of our analysis are listed in Table 40 and the best-fit model is shown in Fig. 89. The Doppler signals from planets b and c are not detected, while planet d is detected with $>2\text{-}\sigma$ significance. Continued monitoring of this multiplanet system is needed to constrain the properties of the two inner planets.

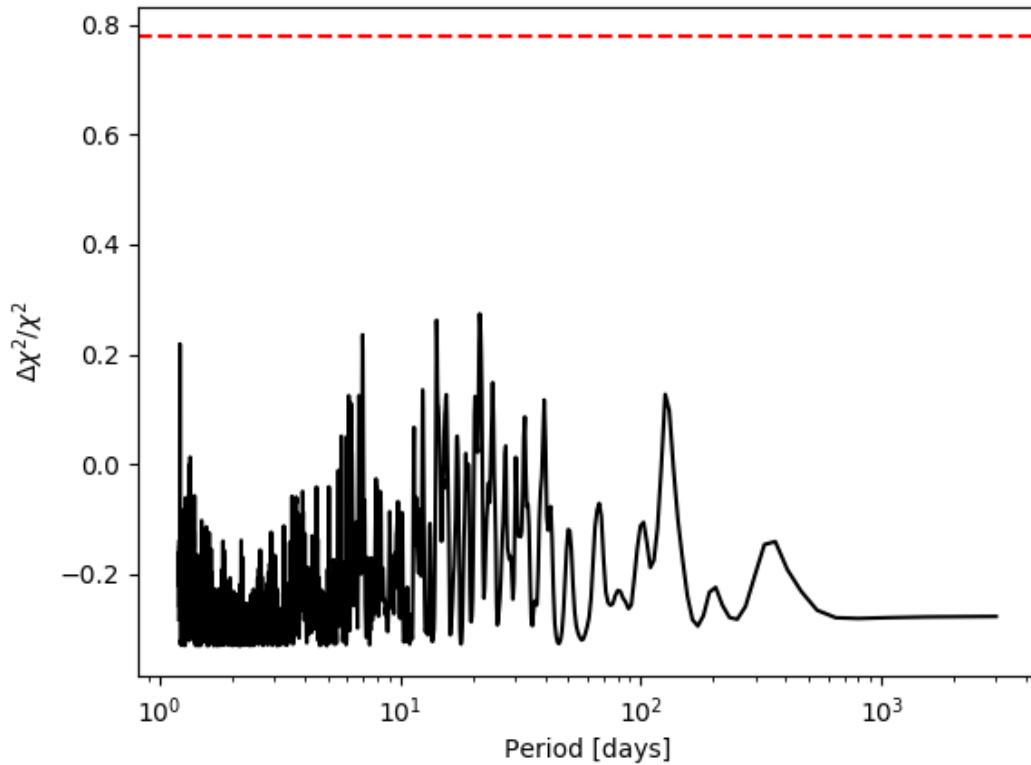


Figure 62. Periodogram search of the RVs showing no evidence for a second planet orbiting K2-79. Lines and annotations are similar to those in Fig. 12.

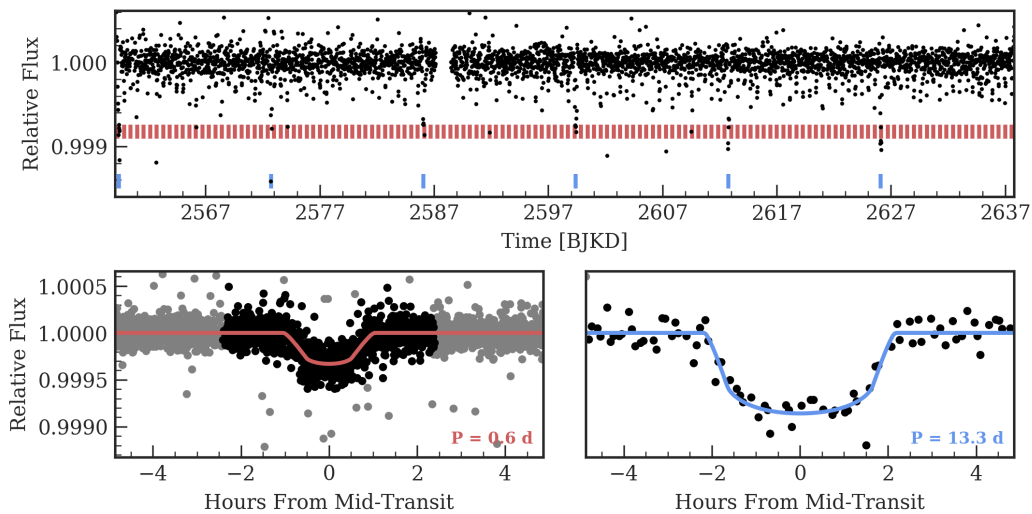


Figure 63. Time series (top) and phase-folded (bottom) light curve for the planets orbiting K2-106. Plot formatting is the same as in Fig. 10.

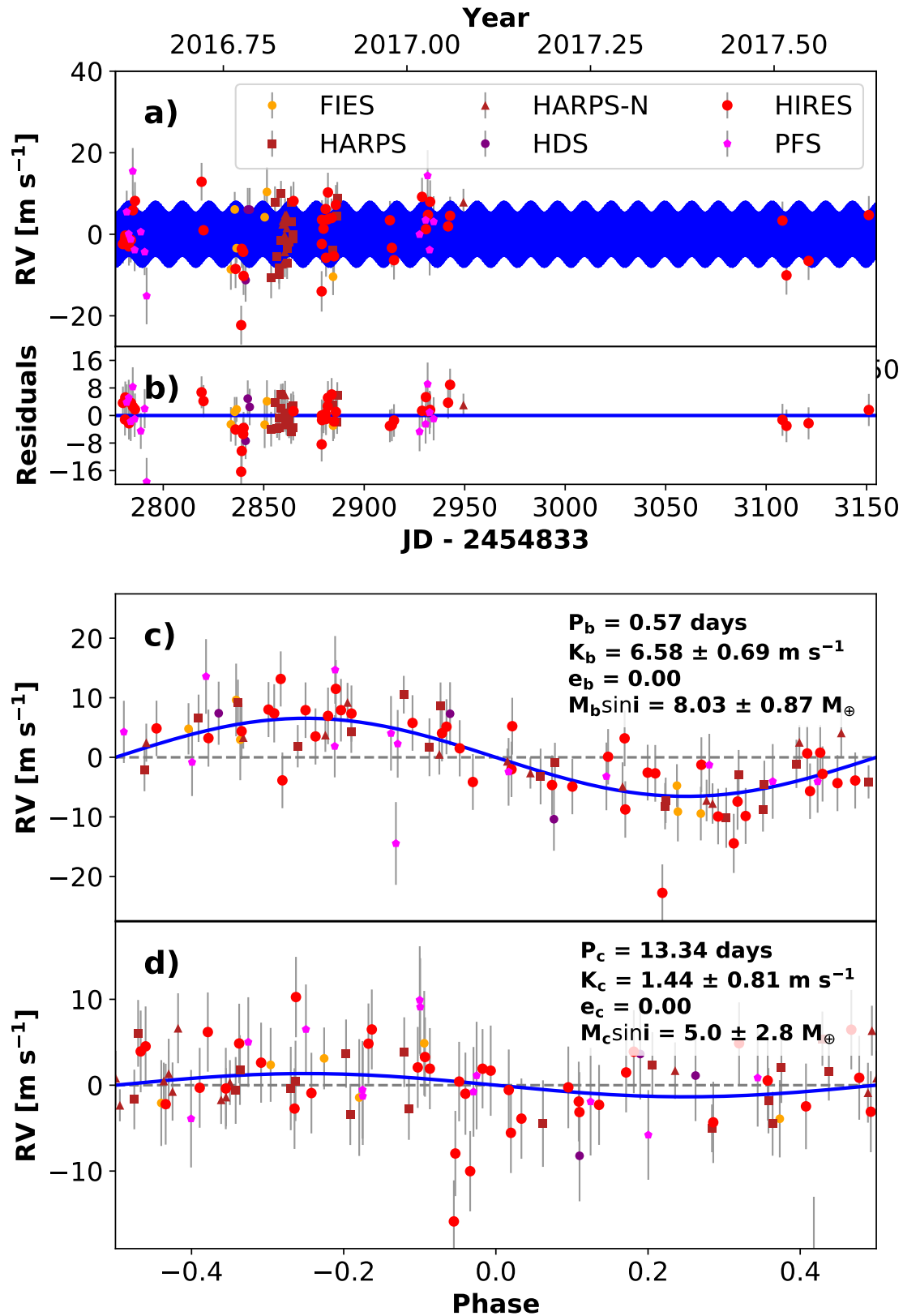


Figure 64. RVs and Keplerian model for K2-106. Symbols, lines, and annotations are similar to those in Fig. 11.

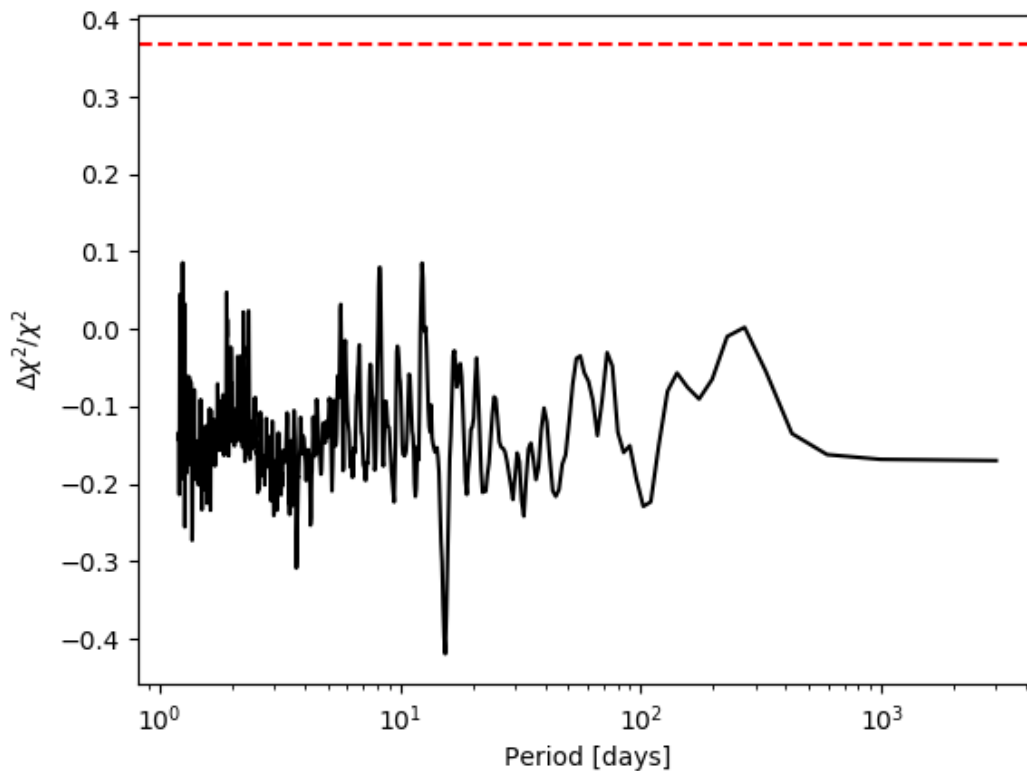


Figure 65. Periodogram search of the RVs showing no evidence for a third planet orbiting K2-106. Lines and annotations are similar to those in Fig. 12.

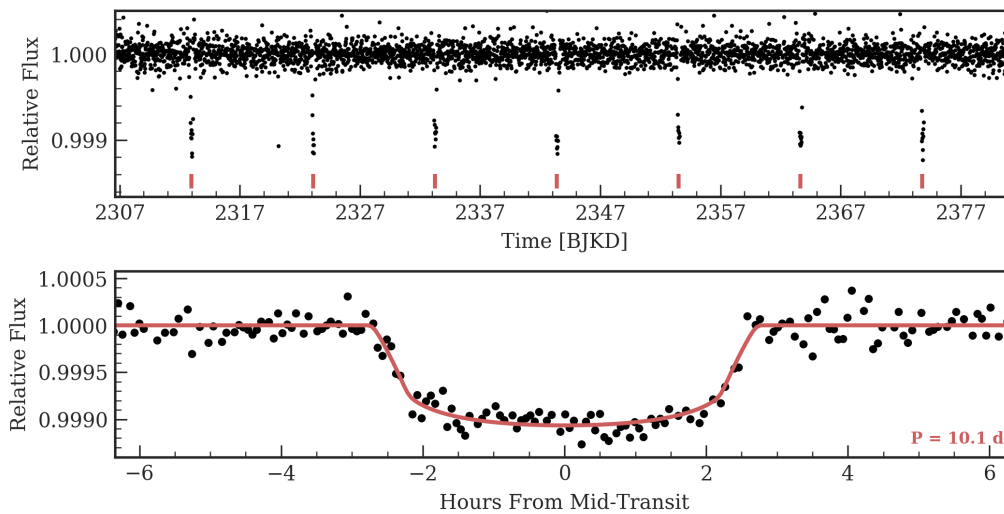


Figure 66. Time series (top) and phase-folded (bottom) light curve for the planet orbiting K2-98. Plot formatting is the same as in Fig. 10.

Table 29. K2-98 System Parameters

Parameter	Credible Interval	Maximum Likelihood	Units
RV Analysis – MCMC Step Parameters			
P_b	$\equiv 10.1369$	$\equiv 10.1369$	days
$T_{\text{conj},b}$	$\equiv 2457145.9796$	$\equiv 2457145.9796$	BJD _{TBD}
$\sqrt{e} \cos \omega_b$	$\equiv 0.0$	$\equiv 0.0$	
$\sqrt{e} \sin \omega_b$	$\equiv 0.0$	$\equiv 0.0$	
K_b	$5.6^{+5.8}_{-9.1}$	7.0	m s^{-1}
γ_{HIRES}	$0.9^{+8.9}_{-5.8}$	3.0	m s^{-1}
$\gamma_{\text{HARPS-N}}$	$76741.0^{+8.5}_{-9.4}$	76740.3	m s^{-1}
γ_{HARPS}	$76746.7^{+5.9}_{-6.7}$	76747.2	m s^{-1}
γ_{FIES}	$76612.3^{+6.3}_{-6.1}$	76612.1	m s^{-1}
$\dot{\gamma}$	$\equiv 0.0$	$\equiv 0.0$	$\text{m s}^{-1} \text{ day}^{-1}$
$\ddot{\gamma}$	$\equiv 0.0$	$\equiv 0.0$	$\text{m s}^{-1} \text{ day}^{-2}$
σ_{HIRES}	10^{+16}_{-7}	7	m s^{-1}
$\sigma_{\text{HARPS-N}}$	9^{+31}_{-9}	0	m s^{-1}
σ_{HARPS}	8^{+14}_{-7}	0	m s^{-1}
σ_{FIES}	5^{+13}_{-5}	0.0	m s^{-1}
Orbital & Physical Parameters			
P_b	$\equiv 10.1369$	$\equiv 10.1369$	days
$T_{\text{conj},b}$	$\equiv 2457145.9796$	$\equiv 2457145.9796$	BJD _{TBD}
e_b	$\equiv 0.0$	$\equiv 0.0$	
ω_b	$\equiv 0.0$	$\equiv 0.0$	radians
K_b	$5.6^{+5.8}_{-9.1}$	7.0	m s^{-1}
M_b	20^{+21}_{-33}	24	M_{\oplus}
R_b/R_*	$0.03015^{+0.00077}_{-0.00041}$	0.02990	
ρ_b	$0.9^{+1.0}_{-1.5}$	1.0	g cm^{-3}
R_b	$4.93^{+0.13}_{-0.07}$	5.11	R_{\oplus}
Priors			
Parameter	Prior		
σ_{HIRES}	$\mathcal{U}(0, 1e + 100)$		
σ_{FIES}	$\mathcal{U}(0, 1e + 100)$		
$\sigma_{\text{HARPS-N}}$	$\mathcal{U}(0, 1e + 100)$		
σ_{HARPS}	$\mathcal{U}(0, 1e + 100)$		

A.45. *K2-180*

K2-180 is a very metal poor ($[\text{Fe}/\text{H}] = -0.710 \pm 0.045$ dex) K dwarf from Campaign 5. It has one transiting planet with a radius of $2.4 R_{\oplus}$ and an orbital period of 8.9 days. See Tables 1 and 2 for stellar properties and Table 3 for precise planet parameters. The planet was validated by Mayo et al. (2018) and appears in the Petigura et al. (2018a) and Pope et al. (2016) catalogs. Korth et al. (2019) followed up this system with FIES and HARPS-N and measured a mass of $11.3 \pm 1.9 M_{\oplus}$ suggesting a rocky composition with a density of $5.6 \pm 1.9 \text{ g cm}^{-3}$.

Our fit of the EVEREST light curve of the K2 photometry for K2-180 is shown in Fig. 90. We acquired 26 RVs of K2-180 with HIRES, typically with an exposure meter setting of 50,000 counts. We modeled the system as a single planet in a circular orbit with an orbital period and phase fixed

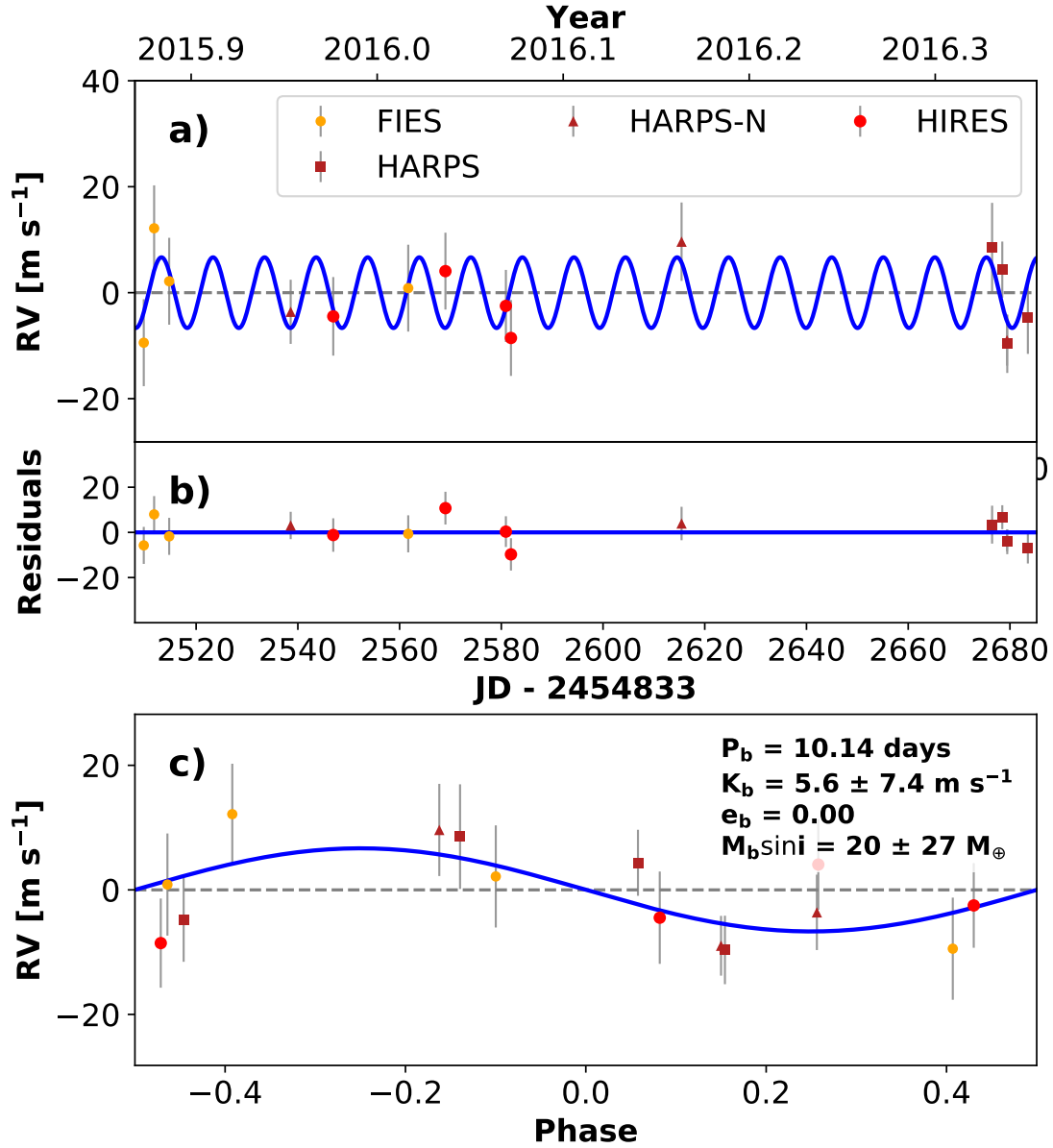


Figure 67. RVs and Keplerian model for K2-98. Symbols, lines, and annotations are similar to those in Fig. 11.

to the transit ephemeris. We rejected more complicated models with a noncircular orbit and/or a linear RV trend based on the AICc statistic. The results of our analysis are listed in Table 41 and the best-fit model is shown in Fig. 91. K2-180 b is a sub-Neptune with a low bulk density and orbits one of the most metal-poor planet hosts detected to date.

A.46. K2-27

K2-27 is a late G dwarf with one transiting planet with a radius of $4.7 R_{\oplus}$ and an orbital period of 6.8 days. See Tables 1 and 2 for stellar properties and Table 3 for precise planet parameters. The planet was noted in the catalogs of Crossfield et al. (2015), Vanderburg et al. (2016b), Schmitt et al. (2016), and Wittenmyer et al. (2018). Van Eylen et al. (2016b) measured a mass of $29.1^{+7.5}_{-7.4}$

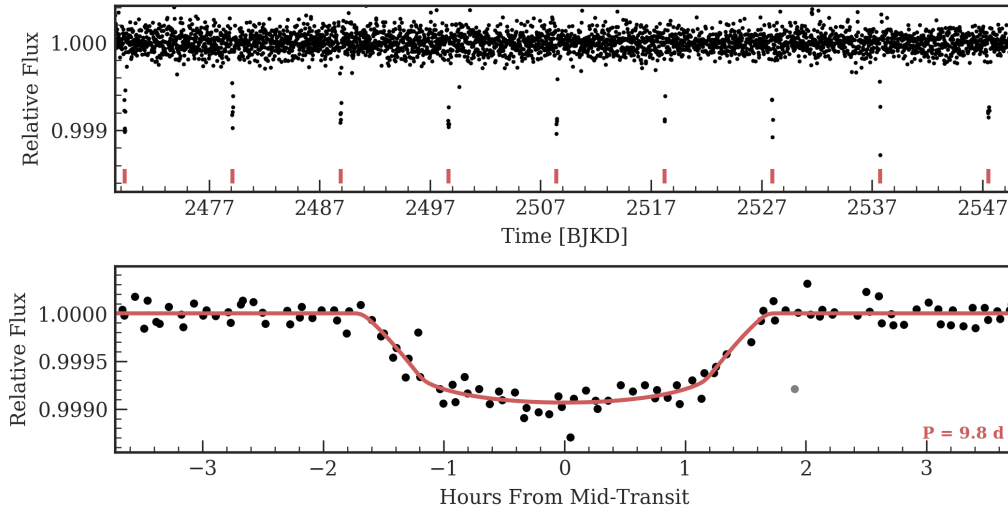


Figure 68. Time series (top) and phase-folded (bottom) light curve for the planet orbiting EPIC 213546283. Plot formatting is the same as in Fig. 10.

Table 30. EPIC 213546283 System Parameters

Parameter	Credible Interval	Maximum Likelihood	Units
RV Analysis – MCMC Step Parameters			
P_b	$\equiv 9.7706$	$\equiv 9.7706$	days
$T_{\text{conj},b}$	$\equiv 2457312.1249$	$\equiv 2457312.1249$	BJD _{TBD}
$\sqrt{e} \cos \omega_b$	$\equiv 0.0$	$\equiv 0.0$	
$\sqrt{e} \sin \omega_b$	$\equiv 0.0$	$\equiv 0.0$	
K_b	$2.7^{+2.9}_{-2.8}$	2.7	m s^{-1}
γ_{HIRES}	-2.0 ± 2.1	-2.0	m s^{-1}
$\dot{\gamma}$	$\equiv 0.0$	$\equiv 0.0$	$\text{m s}^{-1} \text{ day}^{-1}$
$\ddot{\gamma}$	$\equiv 0.0$	$\equiv 0.0$	$\text{m s}^{-1} \text{ day}^{-2}$
σ_{HIRES}	6^{+2}_{-1}	4.8	m s^{-1}
Orbital & Physical Parameters			
P_b	$\equiv 9.7706$	$\equiv 9.7706$	days
$T_{\text{conj},b}$	$\equiv 2457312.1249$	$\equiv 2457312.1249$	BJD _{TBD}
e_b	$\equiv 0.0$	$\equiv 0.0$	
ω_b	$\equiv 0.0$	$\equiv 0.0$	radians
K_b	$2.7^{+2.9}_{-2.8}$	2.7	m s^{-1}
M_b	8 ± 9	8.4	M_{\oplus}
R_b/R_*	$0.0285^{+0.0017}_{-0.0008}$	0.0289	
ρ_b	1.1 ± 1.2	1.0	g cm^{-3}
R_b	$3.41^{+0.21}_{-0.10}$	3.63	R_{\oplus}
Priors			
Parameter	Prior		
σ_{HIRES}	$\mathcal{U}(0, 1e + 100)$		

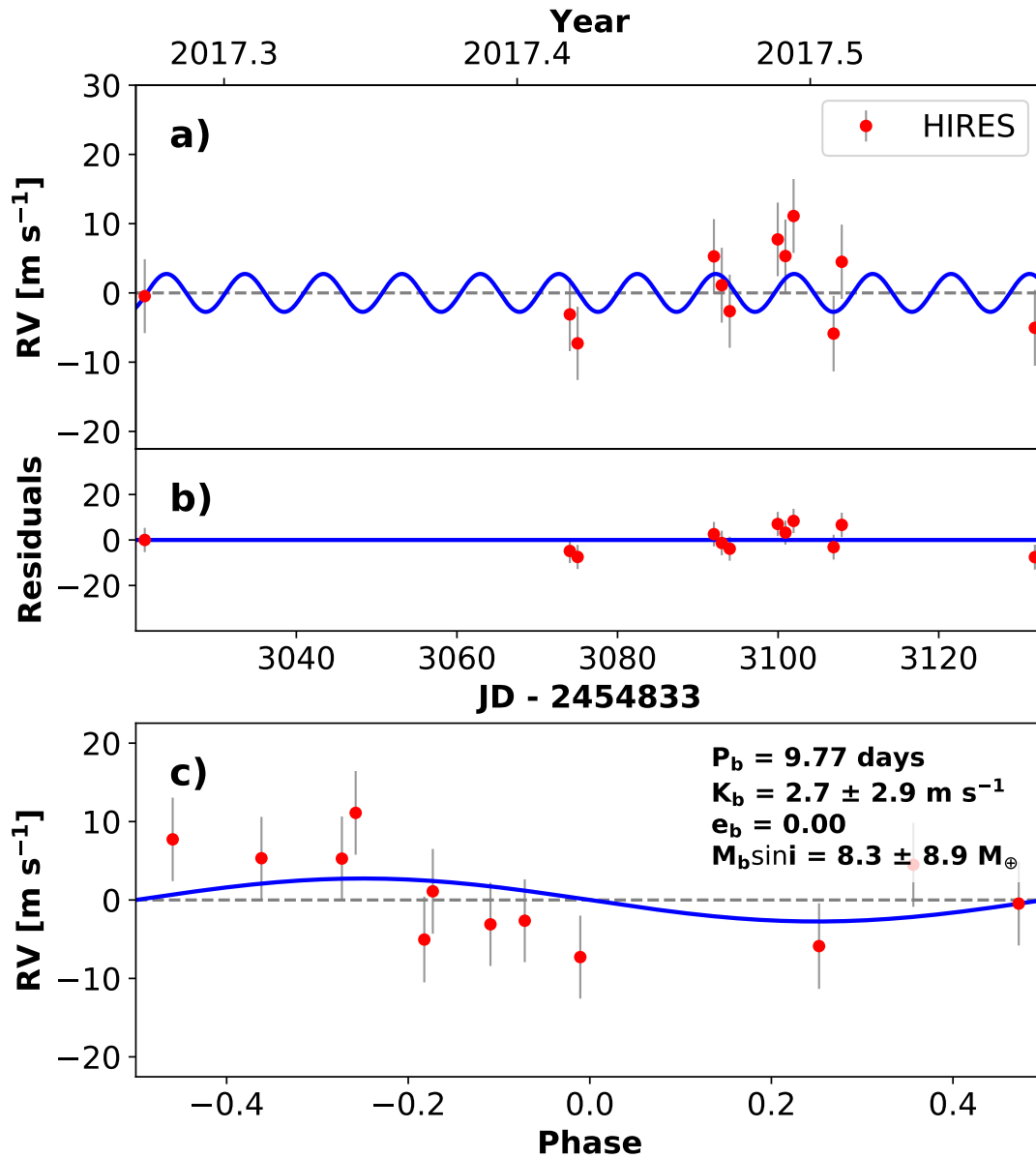


Figure 69. RVs and Keplerian model for EPIC 213546283. Symbols, lines, and annotations are similar to those in Fig. 11.

M_\oplus based on 6 HARPS and 19 from HARPS-N spectra. [Petigura et al. \(2017b\)](#) refined this mass measurement to $30.9 \pm 4.6 M_\oplus$ using an additional 15 HIRES spectra.

Our fit of the EVEREST light curve of the K2 photometry for K2-27 is shown in Fig. 92. Because we acquired only one additional RV of K2-27 with HIRES since [Petigura et al. \(2017b\)](#), our model only provides a slight update to their model. We modeled the system as a single planet with the period and phase fixed to the transit ephemeris. A model comparison based on the AICc statistic favors an eccentric orbit ($\Delta\text{AICc} = 7.04$) over a circular orbit. A linear trend is disfavored with a ΔAICc of 4.20. The results of our analysis are listed in Table 42 and the best-fit model is shown in Fig. 93. K2-27 b is an eccentric ($e = 0.24$) Neptune-sized planet with a density similar to Neptune.

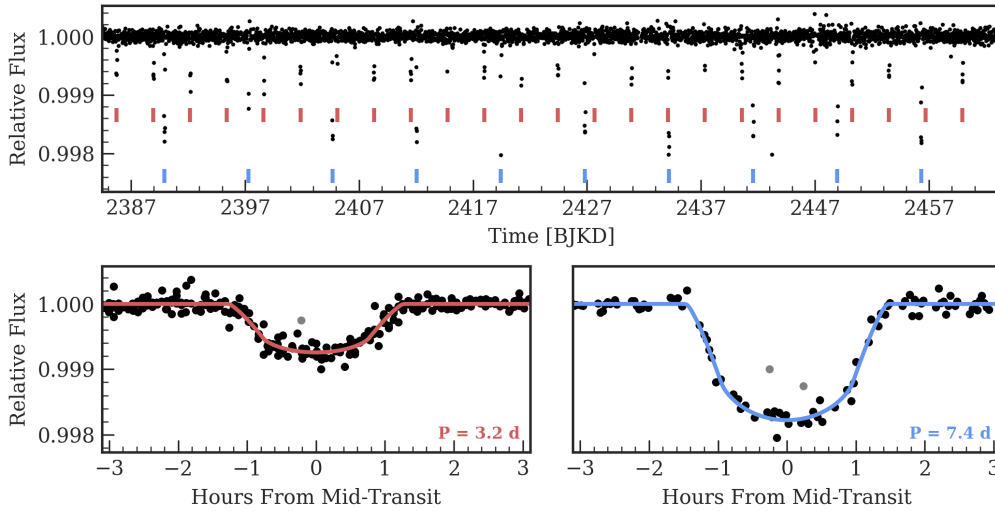


Figure 70. Time series (top) and phase-folded (bottom) light curve for the planet orbiting K2-199. Plot formatting is the same as in Fig. 10.

A.47. *K2-181*

K2-181 is a G dwarf in Field 5 with one transiting planet with radius of $2.3 R_{\oplus}$ and a 6.9-day orbital period. See Tables 1 and 2 for stellar properties and Table 3 for precise planet parameters. The planet is listed as a candidate in Barros et al. (2016) and Pope et al. (2016), was listed as confirmed in Mayo et al. (2018), but did not meet the validation criteria of Livingston et al. (2018) or Petigura et al. (2018a). Our fit of the EVEREST light curve of the K2 photometry for K2-181 is shown in Fig. 94.

We acquired 10 RVs of K2-181 with HIRES, typically with an exposure meter setting of 50,000 counts. We modeled the system as a single planet in a circular orbit with the orbital period and phase fixed to the transit ephemeris. The results of this analysis are listed in Table 43 and the best-fit model is shown in Fig. 95. We detected the Doppler signal at the $1\text{-}\sigma$ level, which is insufficient to place meaningful constraints on the density or composition. This system would benefit from continued RV monitoring.

A.48. *EPIC 245943455*

EPIC 245943455 is a G-dwarf from Field 12 with one transiting planet with a $4.1 R_{\oplus}$ radius and 6.3 day orbital period. See Tables 1 and 2 for stellar properties and Table 3 for precise planet parameters. Our fit of the EVEREST light curve of the K2 photometry for EPIC 245943455 is shown in Fig. 96. Dattilo et al. (2019) classify this object as a planet candidate. Our observations described below are insufficient to confirm the planet but we do successfully rule out massive eclipsing binary false-positive scenarios, increasing the likelihood that this signal is planetary in origin.

We acquired 9 RVs of EPIC 245943455 with HIRES, typically with an exposure meter setting of 50,000. We modeled the system as a single planet in a circular orbit with an orbital period and phase fixed to the transit ephemerides. The results of this analysis are listed in Table 44 and the best-fit model is shown in Fig. 97. Including a linear trend, curvature, or non-zero planet eccentricity is not warranted due to the small number of measurements and the ΔAICc between models. The RVs are

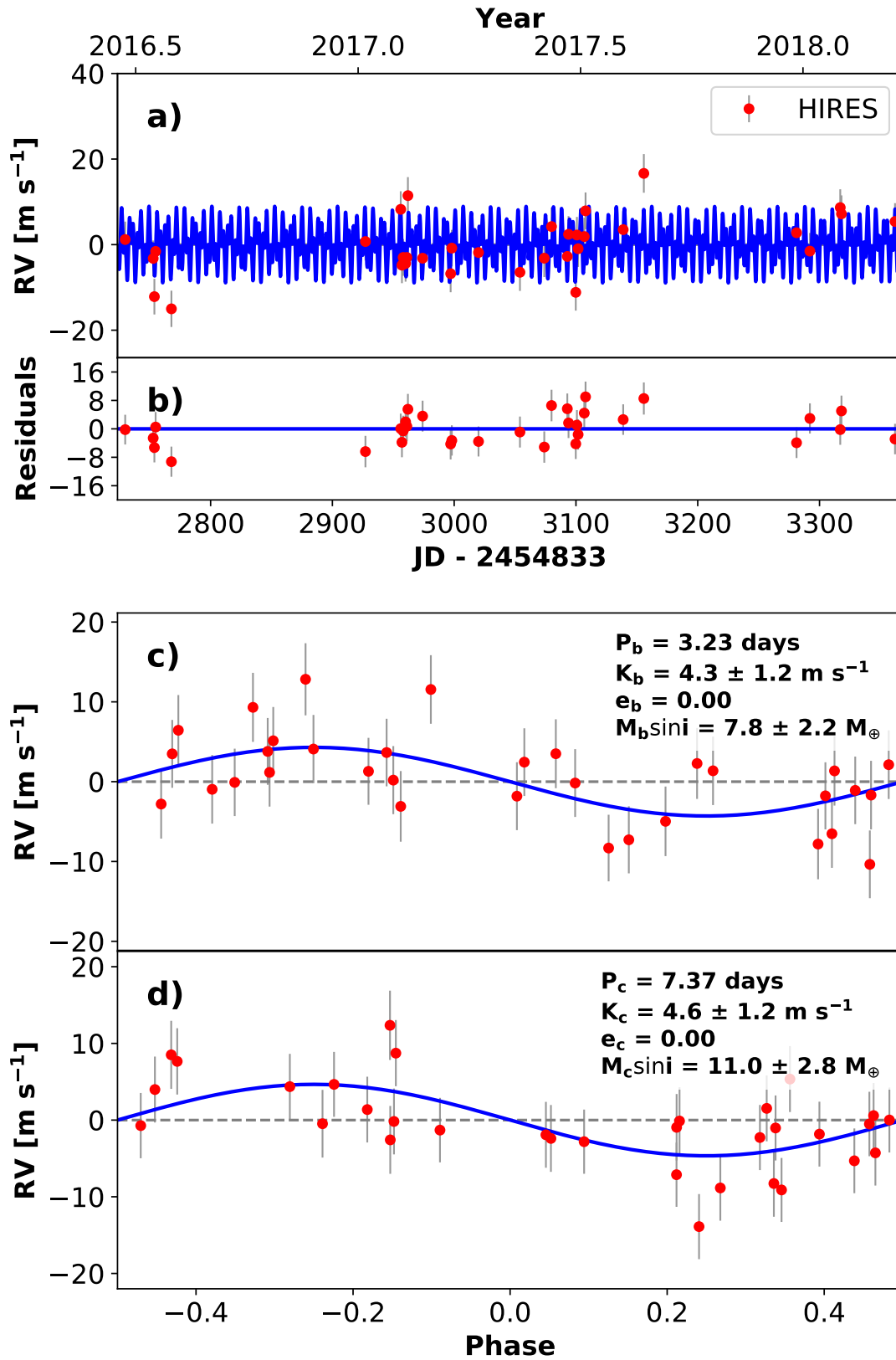


Figure 71. RVs and Keplerian model for K2-199. Symbols, lines, and annotations are similar to those in Fig. 11.

Table 31. K2-199 System Parameters

Parameter	Credible Interval	Maximum Likelihood	Units
RV Analysis – MCMC Step Parameters			
P_b	$\equiv 3.2253$	$\equiv 3.2253$	days
$T_{\text{conj},b}$	$\equiv 2457221.9649$	$\equiv 2457221.9649$	BJD _{TBD}
$\sqrt{e} \cos \omega_b$	$\equiv 0.0$	$\equiv 0.0$	
$\sqrt{e} \sin \omega_b$	$\equiv 0.0$	$\equiv 0.0$	
K_b	4 ± 1	4.0	m s^{-1}
P_c	$\equiv 7.3744$	$\equiv 7.3744$	days
$T_{\text{conj},c}$	$\equiv 2457222.9312$	$\equiv 2457222.9312$	BJD _{TBD}
$\sqrt{e} \cos \omega_c$	$\equiv 0.0$	$\equiv 0.0$	
$\sqrt{e} \sin \omega_c$	$\equiv 0.0$	$\equiv 0.0$	
K_c	$5.34^{+0.95}_{-0.94}$	5.35	m s^{-1}
γ_{HIRES}	-1.94 ± 0.71	-1.90	m s^{-1}
$\dot{\gamma}$	$\equiv 0.0$	$\equiv 0.0$	$\text{m s}^{-1} \text{ day}^{-1}$
$\ddot{\gamma}$	$\equiv 0.0$	$\equiv 0.0$	$\text{m s}^{-1} \text{ day}^{-2}$
σ_{HIRES}	$4.07^{+0.58}_{-0.49}$	3.83	m s^{-1}
Orbital & Physical Parameters			
P_b	$\equiv 3.2253$	$\equiv 3.2253$	days
$T_{\text{conj},b}$	$\equiv 2457221.9649$	$\equiv 2457221.9649$	BJD _{TBD}
e_b	$\equiv 0.0$	$\equiv 0.0$	
ω_b	$\equiv 0.0$	$\equiv 0.0$	radians
K_b	4 ± 1	4.0	m s^{-1}
M_b	$7.1^{+1.9}_{-1.8}$	7.2	M_{\oplus}
R_b/R_*	$0.0245^{+0.0018}_{-0.0006}$	0.0244	
ρ_b	$7.0^{+2.2}_{-2.1}$	6.7	g cm^{-3}
R_b	$1.74^{+0.13}_{-0.05}$	1.80	R_{\oplus}
P_c	$\equiv 7.3744$	$\equiv 7.3744$	days
$T_{\text{conj},c}$	$\equiv 2457222.9312$	$\equiv 2457222.9312$	BJD _{TBD}
e_c	$\equiv 0.0$	$\equiv 0.0$	
ω_c	$\equiv 0.0$	$\equiv 0.0$	radians
K_c	$5.34^{+0.95}_{-0.94}$	5.35	m s^{-1}
M_c	$12.6^{+2.3}_{-2.2}$	12.7	M_{\oplus}
R_c/R_*	$0.0377^{+0.0017}_{-0.0007}$	0.0370	
ρ_c	$3.54^{+0.74}_{-0.72}$	3.41	g cm^{-3}
R_c	$2.67^{+0.12}_{-0.05}$	2.74	R_{\oplus}
Priors			
Parameter	Prior		
j_{itHIRES}	$\mathcal{U}(0, 1e + 100)$		

few in number and cluster around the lower quadrature, making a definitive characterization of EPIC 245943455 b difficult. However, we can rule out high bulk densities.

A.49. K2-61

K2-61 is a G star with properties similar to the Sun from Campaign 3. The star has one transiting planet with a radius of $1.9 R_{\oplus}$ and an orbital period of 2.5 days. See Tables 1 and 2 for stellar properties and Table 3 for precise planet parameters. The planet was discovered and validated in

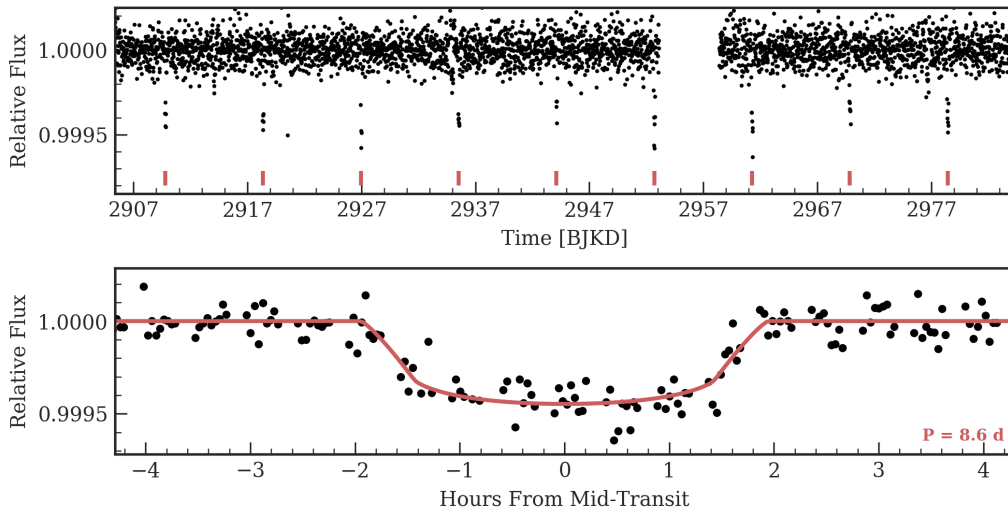


Figure 72. Time series (top) and phase-folded (bottom) light curve for the planet orbiting EPIC 245991048. Plot formatting is the same as in Fig. 10.

four catalog papers: Crossfield et al. (2016); Vanderburg et al. (2016b); Barros et al. (2016); Mayo et al. (2018). Our fit of the EVEREST light curve of the K2 photometry for K2-61 is shown in Fig. 98.

We acquired 7 RVs of K2-61 with HIRES, typically with an exposure meter setting of 50,000 counts. We modeled the system as a single planet in a circular orbit with the orbital period and phase fixed to the transit ephemeris. The results of this analysis are listed in Table 45 and the best-fit model is shown in Fig. 99. This small number of RVs provides only weak constraints, but rules out very high planet masses.

A.50. K2-121

K2-121 is an active ($\log R'_{\text{HK}} = -4.534$) K dwarf from Campaign 5 with one transiting planet with an orbital period of 5 days and a radius of $7.7 R_{\oplus}$. See Tables 1 and 2 for stellar properties and Table 3 for precise planet parameters. The star was characterized by Dressing et al. (2017). The planet appeared as a candidate in the catalog of Barros et al. (2016) and was subsequently validated in the Petigura et al. (2018a) and Mayo et al. (2018) catalogs. Our fit of the EVEREST light curve of the K2 photometry for K2-121 is shown in Fig. 100.

We acquired 18 RVs of K2-121 with HIRES, typically with an exposure meter setting of 40,000 counts. We modeled the system as a single planet in a circular orbit with the orbital period and phase fixed to the transit ephemeris. The results of this analysis are listed in Table 46 and the best-fit model is shown in Fig. 101. A model with eccentricity is only slightly disfavored with ΔAICc of just 1.46, but this may be from incomplete phase sampling. We find a high stellar jitter for this star (Table 46), likely due to the elevated chromospheric activity. We did not apply a Gaussian process model because of the small number of RVs. K2-121 b is a giant planet with Saturn-like radius and density.

Table 32. EPIC 245991048 System Parameters

Parameter	Credible Interval	Maximum Likelihood	Units
RV Analysis – MCMC Step Parameters			
P_b	$\equiv 8.5829$	$\equiv 8.5829$	days
$T_{\text{conj},b}$	$\equiv 2457742.7821$	$\equiv 2457742.7821$	BJD _{TBD}
$\sqrt{e} \cos \omega_b$	$\equiv 0.0$	$\equiv 0.0$	
$\sqrt{e} \sin \omega_b$	$\equiv 0.0$	$\equiv 0.0$	
K_b	$2.5^{+1.6}_{-1.7}$	2.6	m s^{-1}
γ_{HIRES}	-0.9 ± 1.3	-0.9	m s^{-1}
$\dot{\gamma}$	$\equiv 0.0$	$\equiv 0.0$	$\text{m s}^{-1} \text{ day}^{-1}$
$\ddot{\gamma}$	$\equiv 0.0$	$\equiv 0.0$	$\text{m s}^{-1} \text{ day}^{-2}$
σ_{HIRES}	$4.4^{+1.8}_{-1.3}$	4.0	m s^{-1}
Orbital & Physical Parameters			
P_b	$\equiv 8.5829$	$\equiv 8.5829$	days
$T_{\text{conj},b}$	$\equiv 2457742.7821$	$\equiv 2457742.7821$	BJD _{TBD}
e_b	$\equiv 0.0$	$\equiv 0.0$	
ω_b	$\equiv 0.0$	$\equiv 0.0$	radians
K_b	$2.5^{+1.6}_{-1.7}$	2.6	m s^{-1}
M_b	8.0 ± 5.0	8.0	M_{\oplus}
R_b/R_*	$0.0196^{+0.0013}_{-0.0002}$	0.0193	
ρ_b	$3.3^{+1.9}_{-2.6}$	3.7	g cm^{-3}
R_b	$2.33^{+0.15}_{-0.03}$	2.30	R_{\oplus}
Priors			
Parameter	Prior		
None			

A.51. *K2-18*

K2-18 was an exciting early K2 system from Campaign 1 because the M dwarf hosts a small transiting planet in or near the habitable zone, opening the door to possible characterization by transmission spectroscopy. The planet has a radius of $2.4 R_{\oplus}$ with an orbital period of 33 days. See Tables 1 and 2 for stellar properties and Table 3 for precise planet parameters. K2-18 b has been studied by Montet et al. (2015), Foreman-Mackey et al. (2015), Crossfield et al. (2016), Vanderburg et al. (2016b), Schmitt et al. (2016), Barros et al. (2016), Wittenmyer et al. (2018). Precise stellar properties of this star were determined by Martinez et al. (2017) and Dressing et al. (2019).

The original detection of K2-18 b was based on only two transits, leaving the transit ephemeris so uncertain that detailed characterization in the era of JWST would have been difficult because transit times with uncertainties of many hours to days. Benneke et al. (2017) improved the ephemeris by an order of magnitude by observing a single transit with *Spitzer* and removing an outlier from the analysis of the original K2 photometry.

The first mass measurement was performed by Cloutier et al. (2017) using 75 HARPS RVs. They found a mass for K2-18 b of $8.0 \pm 1.9 M_{\oplus}$ and a density of $3.3 \pm 1.2 \text{ g cm}^{-3}$, corresponding to a predominantly rocky planet with a significant gaseous envelope or an ocean planet with a water mass

Table 33. K2-32 System Parameters

Parameter	Credible Interval	Maximum Likelihood	Units
RV Analysis – MCMC Step Parameters			
P_b	$\equiv 8.992$	$\equiv 8.992$	days
$T_{\text{conj},b}$	$\equiv 2456909.9188$	$\equiv 2456909.9188$	BJD _{TBD}
$\sqrt{e} \cos \omega_b$	$\equiv 0.0$	$\equiv 0.0$	
$\sqrt{e} \sin \omega_b$	$\equiv 0.0$	$\equiv 0.0$	
K_b	$5.64^{+0.65}_{-0.66}$	5.70	m s^{-1}
P_c	$\equiv 20.6609$	$\equiv 20.6609$	days
$T_{\text{conj},c}$	$\equiv 2456961.4065$	$\equiv 2456961.4065$	BJD _{TBD}
$\sqrt{e} \cos \omega_c$	$\equiv 0.0$	$\equiv 0.0$	
$\sqrt{e} \sin \omega_c$	$\equiv 0.0$	$\equiv 0.0$	
K_c	$1.50^{+0.61}_{-0.63}$	1.51	m s^{-1}
P_d	$\equiv 31.7169$	$\equiv 31.7169$	days
$T_{\text{conj},d}$	$\equiv 2456903.786$	$\equiv 2456903.786$	BJD _{TBD}
$\sqrt{e} \cos \omega_d$	$\equiv 0.0$	$\equiv 0.0$	
$\sqrt{e} \sin \omega_d$	$\equiv 0.0$	$\equiv 0.0$	
K_d	3.11 ± 0.65	3.20	m s^{-1}
γ_{PFS}	-6.4 ± 3.7	-6.4	m s^{-1}
γ_{HIRES}	$-1.28^{+0.48}_{-0.49}$	-1.28	m s^{-1}
γ_{HARPS}	2.2 ± 1.2	2.2	m s^{-1}
$\dot{\gamma}$	$\equiv 0.0$	$\equiv 0.0$	$\text{m s}^{-1} \text{ day}^{-1}$
$\ddot{\gamma}$	$\equiv 0.0$	$\equiv 0.0$	$\text{m s}^{-1} \text{ day}^{-2}$
σ_{PFS}	$7.3^{+5.8}_{-2.8}$	4.8	m s^{-1}
σ_{HIRES}	$3.22^{+0.43}_{-0.37}$	3.00	m s^{-1}
σ_{HARPS}	$4.2^{+1.2}_{-0.9}$	4.0	m s^{-1}
Orbital & Physical Parameters			
P_b	$\equiv 8.992$	$\equiv 8.992$	days
$T_{\text{conj},b}$	$\equiv 2456909.9188$	$\equiv 2456909.9188$	BJD _{TBD}
e_b	$\equiv 0.0$	$\equiv 0.0$	
ω_b	$\equiv 0.0$	$\equiv 0.0$	radians
K_b	$5.64^{+0.65}_{-0.66}$	5.70	m s^{-1}
M_b	16.3 ± 1.9	16.5	M_{\oplus}
R_b/R_*	$0.0561^{+0.0011}_{-0.0005}$	0.0556	
ρ_b	$0.693^{+0.089}_{-0.088}$	0.650	g cm^{-3}
R_b	$5.037^{+0.097}_{-0.044}$	5.180	R_{\oplus}
P_c	$\equiv 20.6609$	$\equiv 20.6609$	days
$T_{\text{conj},c}$	$\equiv 2456961.4065$	$\equiv 2456961.4065$	BJD _{TBD}
e_c	$\equiv 0.0$	$\equiv 0.0$	
ω_c	$\equiv 0.0$	$\equiv 0.0$	radians
K_c	$1.50^{+0.61}_{-0.63}$	1.51	m s^{-1}
M_c	5.7 ± 2.4	5.8	M_{\oplus}
R_c/R_*	$0.0335^{+0.0015}_{-0.0007}$	0.0340	
ρ_c	1.1 ± 0.5	1.0	g cm^{-3}
R_c	$3.01^{+0.13}_{-0.06}$	3.17	R_{\oplus}
P_d	$\equiv 31.7169$	$\equiv 31.7169$	days
$T_{\text{conj},d}$	$\equiv 2456903.786$	$\equiv 2456903.786$	BJD _{TBD}
e_d	$\equiv 0.0$	$\equiv 0.0$	
ω_d	$\equiv 0.0$	$\equiv 0.0$	radians
K_d	3.11 ± 0.65	3.20	m s^{-1}
M_d	13.7 ± 2.9	13.9	M_{\oplus}
R_d/R_*	$0.0371^{+0.0024}_{-0.0008}$	0.0409	
ρ_d	$1.94^{+0.49}_{-0.47}$	1.40	g cm^{-3}
R_d	$3.33^{+0.22}_{-0.07}$	3.81	R_{\oplus}
Priors			
Parameter	Prior		
σ_{HIRES}	$\mathcal{U}(0, 1e + 100)$		
σ_{PFS}	$\mathcal{U}(0, 1e + 100)$		

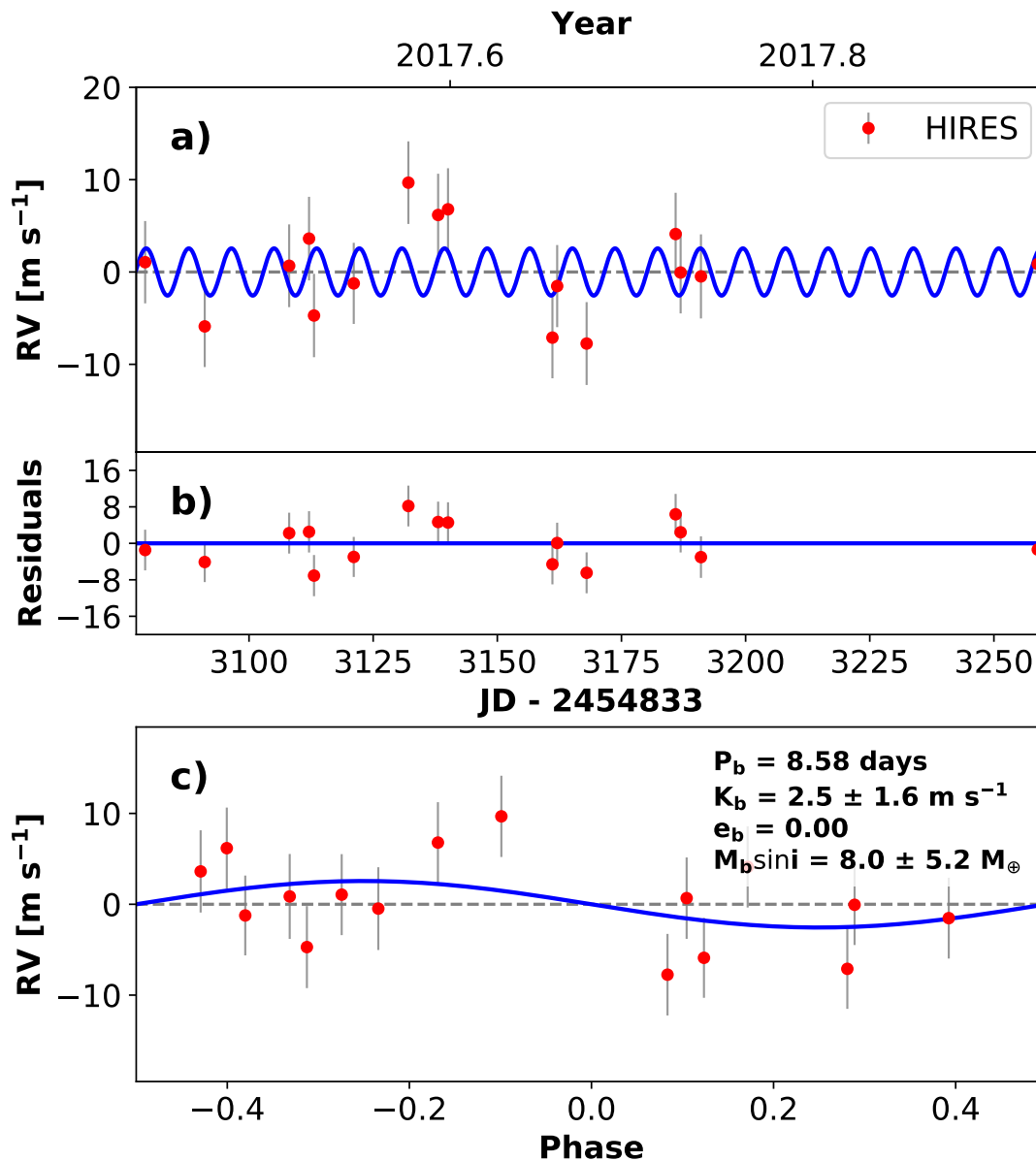


Figure 73. RVs and Keplerian model for EPIC 245991048. Symbols, lines, and annotations are similar to those in Fig. 11.

fraction $>50\%$. Their model also included a GP for stellar activity and favors a second, nontransiting planet with an 8.9 day orbital period and a mass of $m_c \sin i = 7.5 \pm 1.3 M_\oplus$.

The possible second non-transiting planet was considered by Sarkis et al. (2018) based on CARMENES RVs. They found that the signal varies in time and wavelength, and therefore interpreted it as being due to stellar activity. Their analysis found that the mass of planet b is $m_b = 8.4 \pm 1.4 M_\oplus$.

The system was revisited by Cloutier et al. (2019) with additional HARPS data. They investigated the effects of time-sampling and determined that the second signal is likely planetary. The revised radial velocity analysis gave planet masses of $m_b = 8.6 \pm 1.4 M_\oplus$ and $m_c \sin i = 5.6 \pm 0.8 M_\oplus$. Most

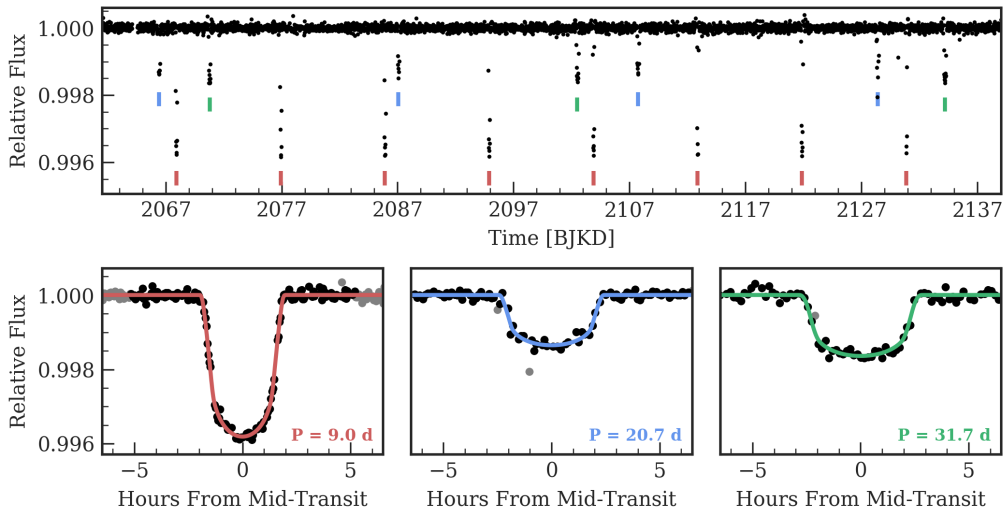


Figure 74. Time series (top) and phase-folded (bottom) light curve for the planet orbiting K2-32. Plot formatting is the same as in Fig. 10.

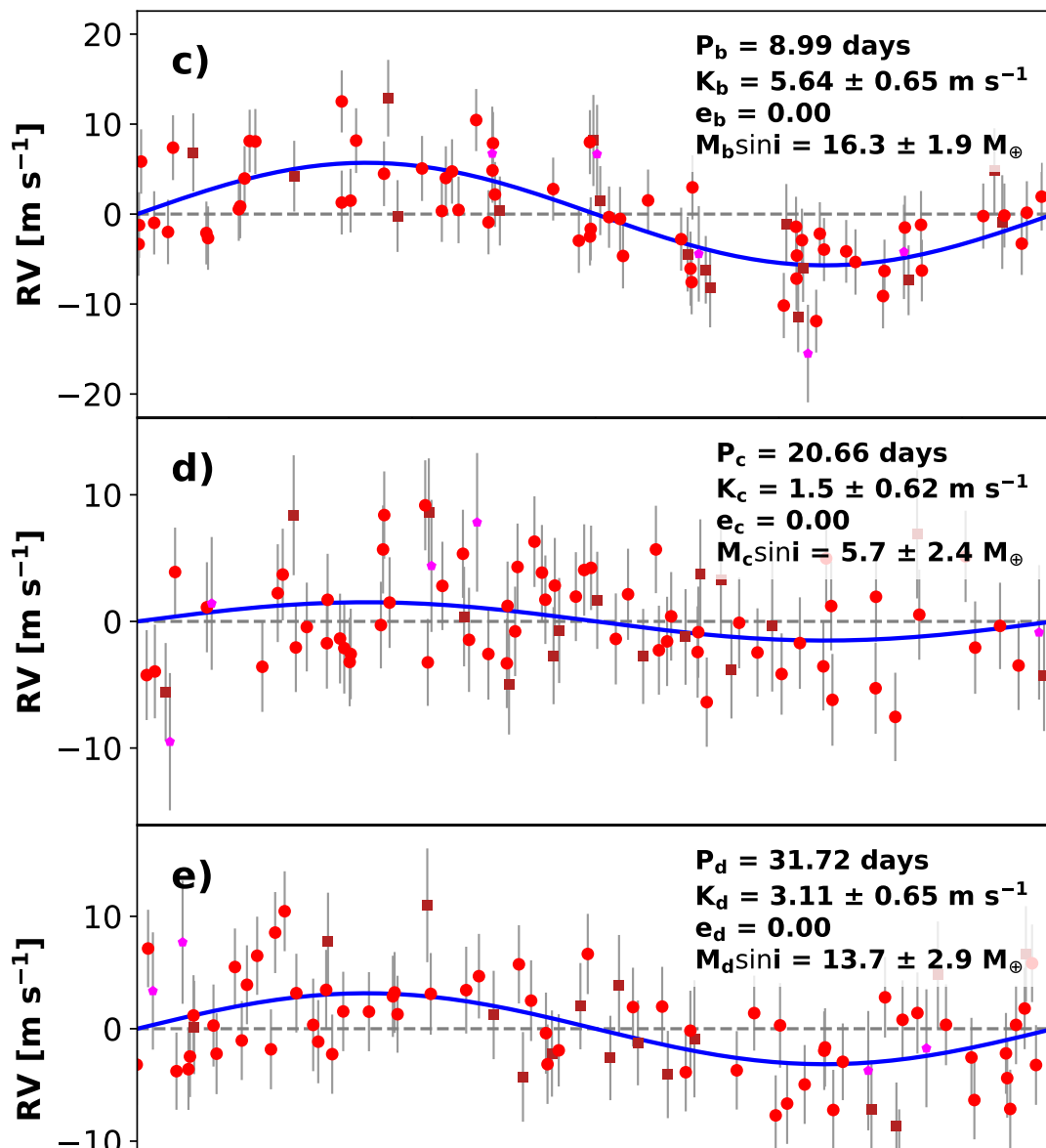
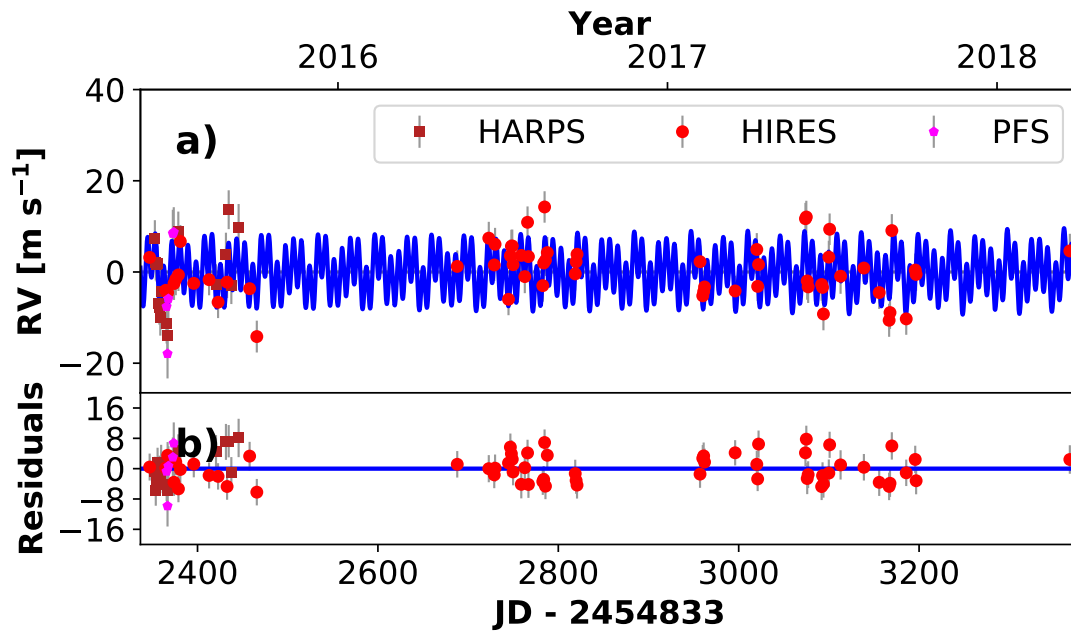
recently, Radica et al. (2022) reported a mass and minimum mass for planets b and c of 9.5 ± 1.7 and $6.9 \pm 1.0 M_{\oplus}$, respectively.

Further observations characterized the atmosphere of K2-18 b with the Hubble Space Telescope. Tsiaras et al. (2019) and Benneke et al. (2019) detected spectroscopic modulation in the planet's transmission spectrum. Initially interpreted as H_2O , subsequent *JWST* transmission spectroscopy revealed a curious atmospheric composition dominated by CH_4 and CO_2 (Madhusudhan et al. 2023). Madhusudhan et al. (2020) used the observed bulk and atmospheric properties of K2-18 b to constrain the interior structure. They investigated the mass fraction of H/He given different core compositions and determined that there are a wide range of acceptable compositions, ranging from an iron core with 6% H/He and 0.4% water by mass to a majority water planet with a minimal H_2 rich atmosphere. Additionally, dos Santos et al. (2020) constrained the atmospheric escape of K2-18 b through Lyman- α measurements and determined that the inferred rate allows for a volatile-rich atmosphere throughout its lifetime.

Our fit of the EVEREST light curve of the K2 photometry for K2-18 is shown in Fig. 102. We acquired 21 RVs of K2-18 with HIRES, typically with an exposure meter setting of 40,000 counts. We modeled the planet in a circular orbit with an orbital period and phase fixed to the transit ephemeris. Our fit includes both the HARPS and HIRES RVs along with a GP for stellar activity and the non-transiting planet found by Cloutier et al. (2017). The results are listed in Table 47 and the best-fit model is shown in Fig. 103. K2-18 b has a mass of $7.2 M_{\oplus}$ and density of 2.6 g cm^{-3} . Our results are consistent with those of previous studies.

A.52. K2-55

K2-55 is a K dwarf from Campaign 3 that hosts one Neptune-sized planet. This planet is cataloged in Crossfield et al. (2016); Vanderburg et al. (2016b); Schmitt et al. (2016); Barros et al. (2016); Martinez et al. (2017); Dressing et al. (2017); Wittenmyer et al. (2018); Kostov et al. (2019); Wittenmyer



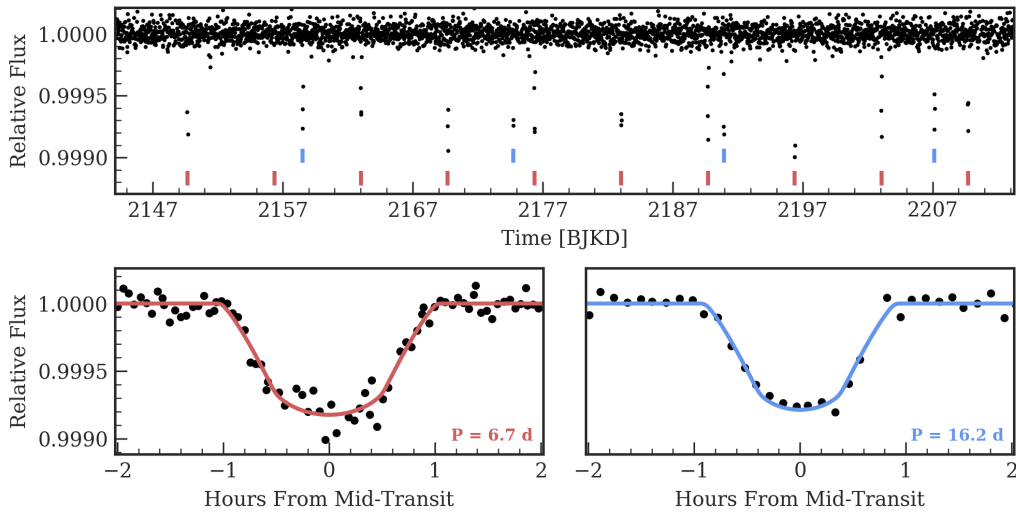


Figure 76. Time series (top) and phase-folded (bottom) light curve for the planet orbiting K2-62. Plot formatting is the same as in Fig. 10.

et al. (2020). Precise stellar parameters were determined in Martinez et al. (2017) and Wittenmyer et al. (2020).

Dressing et al. (2018) followed up this system with a Spitzer transit and 12 HIRES radial velocity measurements. We adopt their solution; see Tables 1 and 2 for stellar properties and Table 3 for the planet parameters. They found that a circular 1-planet model fits the data best, resulting in a planet mass of $M_b = 43.13^{+5.98}_{-5.80} M_{\oplus}$. This Neptune-sized planet is considerably denser ($2.8^{+0.8}_{-0.6} \text{ g cm}^{-3}$) than Uranus and Neptune in our own solar system, requiring a higher fraction of rocky material. Dressing et al. (2018) calculated that the planet is consistent with a 12% H/He envelope surrounding a rocky core using grids from Lopez & Fortney (2014).

A.53. K2-19

K2-19 (EPIC 201505350) is a late G dwarf with three transiting planets that have sizes of $7 R_{\oplus}$, $4 R_{\oplus}$, and $1.1 R_{\oplus}$ and orbital periods of 7.9 days, 11.9 days, and 2.5 days, respectively. See Tables 1 and 2 for stellar properties and Table 3 for precise planet parameters.

Planets b and c were discovered by Foreman-Mackey et al. (2015), who listed them as candidates, and were included in the Montet et al. (2015) catalog. Armstrong et al. (2015) independently discovered and validated planets b and c. K2-19 is also included in the catalogs of Vanderburg et al. (2016b), Crossfield et al. (2016), Barros et al. (2016) and Schmitt et al. (2016) (Planet Hunters). Sinukoff et al. (2016) later discovered the third transiting planet at 2.5 days (K2-19 d).

K2-19 was the first K2 system to show transit timing variations (TTVs). Using three ground-based transits, Barros et al. (2015) obtained photodynamical masses of $44 \pm 12 M_{\oplus}$ and $15.7 \pm 7.0 M_{\oplus}$. Their analysis also included 10 RVs from Sophie. Narita et al. (2015) also characterized the system using high-dispersion spectroscopy, AO imaging, and TTVs. Dai et al. (2016) used 61 PFS spectra with 5 m s^{-1} uncertainties as well as eight HARPS RVs with 3.8 m s^{-1} uncertainties to measure planet masses of $28.5^{+5.4}_{-5.0} M_{\oplus}$, $25.6 \pm 7.1 M_{\oplus}$, and $< 14.0 M_{\oplus}$ (95% confidence). A later analysis by Nespral et al. (2017) combining RVs from FIES, HARPS-N, and HARPS with TTVs found that including

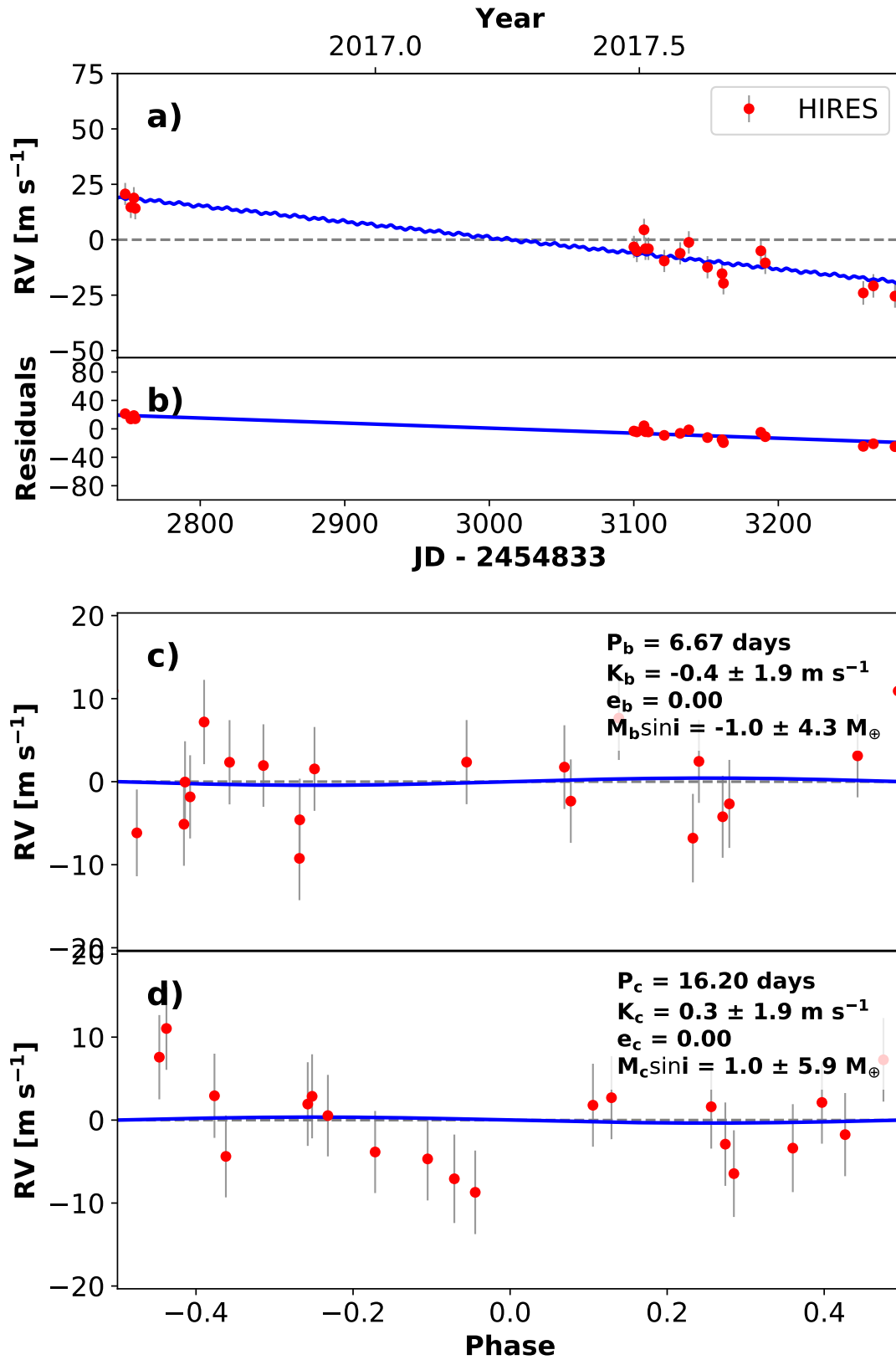


Figure 77. RVs and Keplerian model for K2-62. Symbols, lines, and annotations are similar to those in Fig. 11.

Table 34. K2-62 System Parameters

Parameter	Credible Interval	Maximum Likelihood	Units
RV Analysis – MCMC Step Parameters			
P_b	$\equiv 6.672$	$\equiv 6.672$	days
$T_{\text{conj},b}$	$\equiv 2456982.6852$	$\equiv 2456982.6852$	BJD _{TBD}
$\sqrt{e} \cos \omega_b$	$\equiv 0.0$	$\equiv 0.0$	
$\sqrt{e} \sin \omega_b$	$\equiv 0.0$	$\equiv 0.0$	
K_b	-0.4 ± 1.9	-0.4	m s^{-1}
P_c	$\equiv 16.197$	$\equiv 16.197$	days
$T_{\text{conj},c}$	$\equiv 2456991.5453$	$\equiv 2456991.5453$	BJD _{TBD}
$\sqrt{e} \cos \omega_c$	$\equiv 0.0$	$\equiv 0.0$	
$\sqrt{e} \sin \omega_c$	$\equiv 0.0$	$\equiv 0.0$	
K_c	0.3 ± 2.0	0.0	m s^{-1}
γ_{HIRES}	3.5 ± 1.5	3.5	m s^{-1}
$\dot{\gamma}$	$-0.0711^{+0.0084}_{-0.0085}$	-0.0711	$\text{m s}^{-1} \text{ day}^{-1}$
$\ddot{\gamma}$	$\equiv 0.0$	$\equiv 0.0$	$\text{m s}^{-1} \text{ day}^{-2}$
σ_{HIRES}	$6^{+2.3}_{-0.1}$	4.7	m s^{-1}
Orbital & Physical Parameters			
P_b	$\equiv 6.672$	$\equiv 6.672$	days
$T_{\text{conj},b}$	$\equiv 2456982.6852$	$\equiv 2456982.6852$	BJD _{TBD}
e_b	$\equiv 0.0$	$\equiv 0.0$	
ω_b	$\equiv 0.0$	$\equiv 0.0$	radians
K_b	-0.4 ± 1.9	-0.4	m s^{-1}
M_b	$-1.0^{+4.2}_{-4.3}$	-0.9	M_{\oplus}
R_b/R_*	$0.0260^{+0.0000}_{-0.0029}$	0.0282	
ρ_b	$-0.6^{+2.6}_{-2.8}$	-0.5	g cm^{-3}
R_b	$2.02^{+0.05}_{-0.17}$	2.14	R_{\oplus}
P_c	$\equiv 16.197$	$\equiv 16.197$	days
$T_{\text{conj},c}$	$\equiv 2456991.5453$	$\equiv 2456991.5453$	BJD _{TBD}
e_c	$\equiv 0.0$	$\equiv 0.0$	
ω_c	$\equiv 0.0$	$\equiv 0.0$	radians
K_c	0.3 ± 2.0	0.0	m s^{-1}
M_c	1.0 ± 6.0	1.0	M_{\oplus}
R_c/R_*	$\equiv 0.0255$	$\equiv 0.0255$	
ρ_c	$0.6^{+3.9}_{-3.7}$	0.6	g cm^{-3}
R_c	$\equiv 1.988$	$\equiv 1.988$	R_{\oplus}
Priors			
Parameter	Prior		
None			

NOTE—

 Reference epoch for $\dot{\gamma}, \ddot{\gamma}$: 2457847.4101299997

the TTVs resulted in a lower mass estimate than a fit to the RVs alone. Subsequent observations and joint TTV+RV modeling gave a detailed picture (Malavolta et al. 2017), and as more RVs were acquired the mass discrepancy between the RV and TTV determined masses was relieved (Borsato et al. 2019).

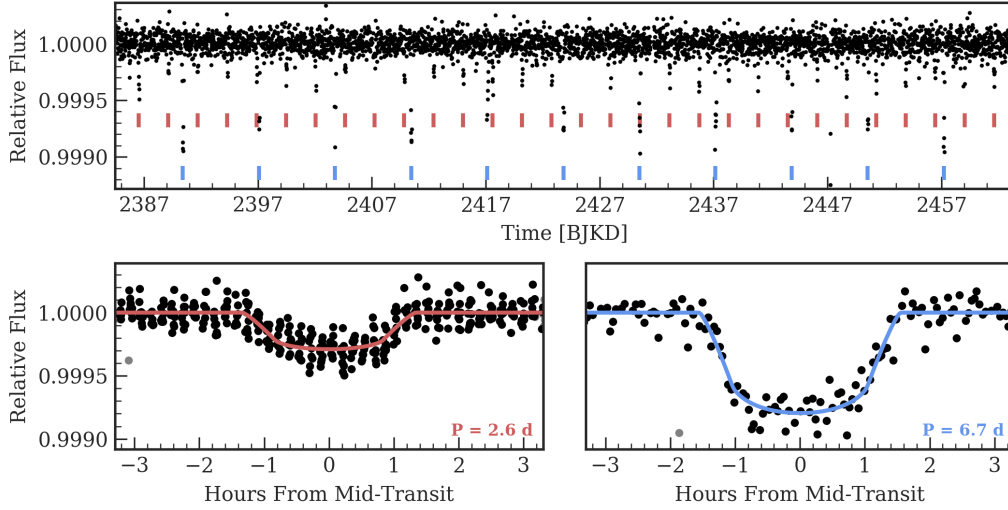


Figure 78. Time series (top) and phase-folded (bottom) light curve for the planet orbiting K2-189. Plot formatting is the same as in Fig. 10.

We acquired 51 RVs of K2-19 with HIRES, typically with an exposure meter setting of 60,000 counts. We adopted the Keplerian model as described in [Petigura et al. \(2020\)](#), which included these Keck-HIRES RVs and performed a photodynamical TTV analysis which included additional transit times from Spitzer and the Las Cumbres Observatory. The eccentricity for planets b and c was free, while that of planet d was fixed to a circular orbit. From their analysis, the authors derived masses of 32.4 ± 1.7 , 10.8 ± 0.6 , and $< 10 M_{\oplus}$ for planets b, c, and d, respectively. The masses and eccentricities were most constrained by the photodynamical analysis, as the RV precision was limited by $\approx 7 \text{ m s}^{-1}$ stellar jitter. This system is an intriguing test case for planet formation theories, as planet b has $\sim 50\%$ of its mass in the form of a gaseous envelope, and interestingly while K2-19 b and c are in a 3:2 commensurability, the planets are just 0.1% out of resonance ([Petigura et al. 2020](#)).

A.54. HIP 41378

HIP 41378 (K2-93, EPIC 211311380) is a bright late G dwarf observed in Campaigns 5 and 18. HIP 41378 hosts five transiting planets that were discovered and validated by [Vanderburg et al. \(2016\)](#) using observations from Campaign 5. The outermost planets had only a single transit measured and were then seen to transit again when revisited in Campaign 18, which reduced the period uncertainty to a set of discrete period solutions ([Becker et al. 2018](#); [Berardo et al. 2019](#)). The transiting planets (b, c, d, e, f) have orbital periods of 16, 32, 278, 369, and 542 days, and radii of 2.6, 2.7, 3.5, 4.9, and $9.2 R_{\oplus}$ respectively, adopting most likely solutions for the outer planets based on dynamical considerations. The outermost planet f does not show clear spectroscopic characteristics in *HST*/WFC3 transmission spectroscopy ([Alam et al. 2022](#)).

Our adopted stellar parameters are shown in Tables 1, 2 and 3. We adopted the solution by [Santerne et al. \(2019\)](#), who jointly modeled the radial velocities from PFS, HARPS, and HARSP-N, as well as 218 nightly HIRES observations from our team binned into 75 epochs, for a total of 464 RV epochs across the four instruments. They found masses of 6.89 ± 0.88 , 4.4 ± 1.1 , < 4.6 , 12 ± 5 , and $12 \pm 3 M_{\oplus}$, respectively. The ultra-low density inferred for HIP 41378 f, due to its Saturn-size

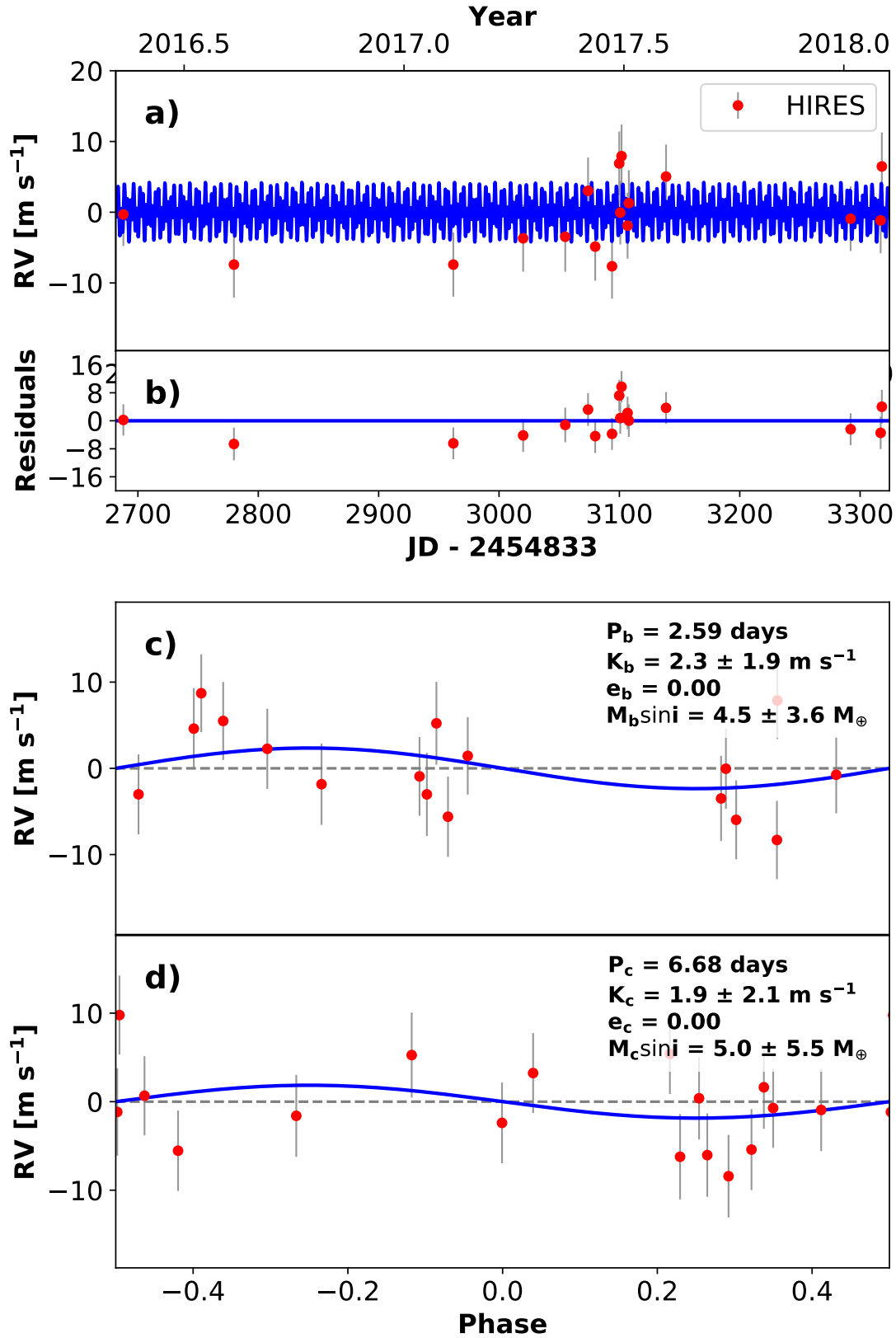


Figure 79. RVs and Keplerian model for K2-189. Symbols, lines, and annotations are similar to those in Fig. 11.

Table 35. K2-189 System Parameters

Parameter	Credible Interval	Maximum Likelihood	Units
RV Analysis – MCMC Step Parameters			
P_b	$\equiv 2.5881$	$\equiv 2.5881$	days
$T_{\text{conj},b}$	$\equiv 2457222.1466$	$\equiv 2457222.1466$	BJD _{TBD}
$\sqrt{e} \cos \omega_b$	$\equiv 0.0$	$\equiv 0.0$	
$\sqrt{e} \sin \omega_b$	$\equiv 0.0$	$\equiv 0.0$	
K_b	$2.3^{+1.8}_{-1.9}$	2.4	m s^{-1}
P_c	$\equiv 6.6793$	$\equiv 6.6793$	days
$T_{\text{conj},c}$	$\equiv 2457223.4182$	$\equiv 2457223.4182$	BJD _{TBD}
$\sqrt{e} \cos \omega_c$	$\equiv 0.0$	$\equiv 0.0$	
$\sqrt{e} \sin \omega_c$	$\equiv 0.0$	$\equiv 0.0$	
K_c	1.9 ± 2.1	1.9	m s^{-1}
γ_{HIRES}	-0.7 ± 1.5	-0.7	m s^{-1}
$\dot{\gamma}$	$\equiv 0.0$	$\equiv 0.0$	$\text{m s}^{-1} \text{ day}^{-1}$
$\ddot{\gamma}$	$\equiv 0.0$	$\equiv 0.0$	$\text{m s}^{-1} \text{ day}^{-2}$
σ_{HIRES}	$4.7^{+2.0}_{-1.0}$	4.0	m s^{-1}
Orbital & Physical Parameters			
P_b	$\equiv 2.5881$	$\equiv 2.5881$	days
$T_{\text{conj},b}$	$\equiv 2457222.1466$	$\equiv 2457222.1466$	BJD _{TBD}
e_b	$\equiv 0.0$	$\equiv 0.0$	
ω_b	$\equiv 0.0$	$\equiv 0.0$	radians
K_b	$2.3^{+1.8}_{-1.9}$	2.4	m s^{-1}
M_b	$4.5^{+3.5}_{-3.7}$	4.6	M_{\oplus}
R_b/R_*	$0.01575^{+0.00095}_{-0.00043}$	0.01569	
ρ_b	$8.6^{+8.5}_{-5.6}$	7.5	g cm^{-3}
R_b	$\equiv 1.4029$	$\equiv 1.4029$	R_{\oplus}
P_c	$\equiv 6.6793$	$\equiv 6.6793$	days
$T_{\text{conj},c}$	$\equiv 2457223.4182$	$\equiv 2457223.4182$	BJD _{TBD}
e_c	$\equiv 0.0$	$\equiv 0.0$	
ω_c	$\equiv 0.0$	$\equiv 0.0$	radians
K_c	1.9 ± 2.1	1.9	m s^{-1}
M_c	$5.0^{+5.5}_{-5.6}$	5.0	M_{\oplus}
R_c/R_*	$0.0260^{+0.0020}_{-0.0001}$	0.0254	
ρ_c	$2.1^{+2.6}_{-2.1}$	1.9	g cm^{-3}
R_c	$2.31^{+0.01}_{-0.18}$	2.44	R_{\oplus}
Priors			
Parameter	Prior		
None			

yet sub-Neptune mass, may be indicative of a small core surrounded by an extended envelope, or even a planetary ring system that deepens the transit (Akincanmi et al. 2020).

Santerne et al. (2019) also discovered an additional non-transiting planet at 62 days with a mass of $7.0 \pm 1.5 M_{\oplus}$ (assuming it is coplanar with the five transiting planets).

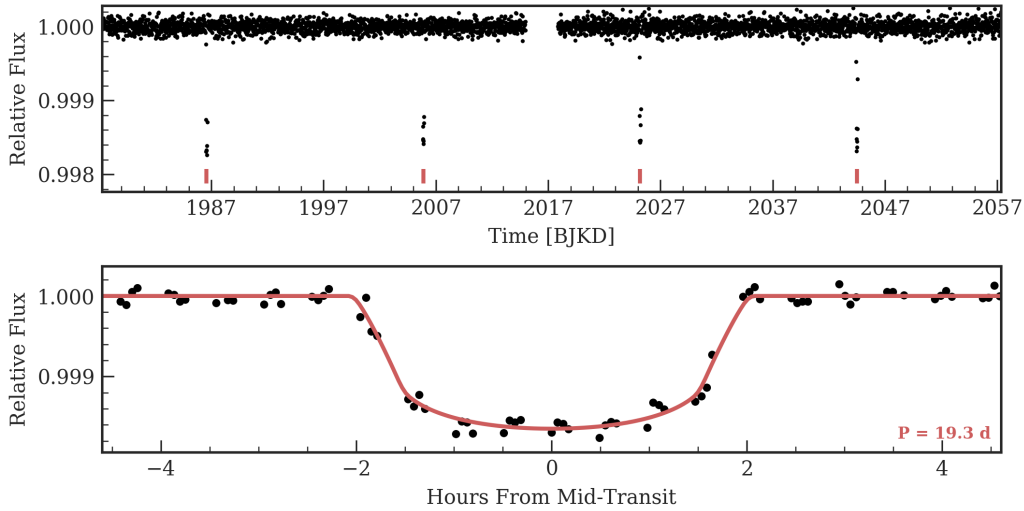


Figure 80. Time series (top) and phase-folded (bottom) light curve for the planet orbiting K2-10. Plot formatting is the same as in Fig. 10.

A.55. HD 89345 (K2-234)

HD 89345 (K2-234, EPIC 248777106) is a bright ($V = 9.4$, $K = 7.7$) G star in Campaign 14. It is a slightly evolved star that exhibits solar-like oscillations. Van Eylen et al. (2018b) and Yu et al. (2018) both discovered one warm sub-Saturn-sized planet ($R_b = 6.7 M_\oplus$) in an orbit of 11.8 days.

Van Eylen et al. (2018b) measured the mass of planet b ($M_b = 35.7 \pm 3.3 M_\oplus$) with 46 RV measurements from a combination of FIES, HARPS, and HARPS-N. They find an eccentric orbit to best fit the data ($e_b = 0.2$); however note that a circular orbit also reasonably fits the data given the small number of measurements. Yu et al. (2018) measured the mass of planet b ($M_b = 0.110 \pm 0.018 M_{Jup}$) with 12 HIRES and 9 APF radial velocity measurements. They also prefer an eccentric solution ($e_b = 0.22$), in line with other sub-Saturns (e.g., Petigura et al. 2017b).

The Yu et al. (2018) paper is based on data from this project and contains all of our HIRES measurements on this system. We refer to the transit fit shown in Yu et al. (2018) and report the planet parameters in Table 3. Because of the substantial data published in Van Eylen et al. (2018b), we performed an updated radial velocity fit for HD 89345 including all of the data published so far. This fit includes 12 HIRES (Yu et al. 2018), 21 APF (Yu et al. 2018, and this work), 16 FIES (Van Eylen et al. 2018b), 18 HARPS (Van Eylen et al. 2018b), and 12 HARPS-N measurements (Van Eylen et al. 2018b). The orbit of the planet is likely misaligned with its star’s rotation axis (Bourrier et al. 2023), and the planet reveals no signs of mass loss via transit spectroscopy of the metastable 1083 nm Helium line (Guilluy et al. 2023).

We modeled the system as a single-planet fit. We test additional parameters including a trend, curvature, and planet eccentricity. We adopt the inclusion of planet eccentricity ($\Delta AICc=20$) and reject the other models based on model comparison using the AICc statistic. The results of this analysis are listed in Table 48 and the best-fit model is shown in Fig. 104.

Table 36. K2-10 System Parameters

Parameter	Credible Interval	Maximum Likelihood	Units
RV Analysis – MCMC Step Parameters			
P_b	$\equiv 19.3055$	$\equiv 19.3055$	days
$T_{\text{conj},b}$	$\equiv 2456819.5794$	$\equiv 2456819.5794$	BJD _{TBD}
$\sqrt{e} \cos \omega_b$	$\equiv 0.0$	$\equiv 0.0$	
$\sqrt{e} \sin \omega_b$	$\equiv 0.0$	$\equiv 0.0$	
K_b	6.5 ± 2.0	6.0	m s^{-1}
γ_{HIRES}	1.1 ± 1.6	1.1	m s^{-1}
$\gamma_{\text{HARPS-N}}$	$8202.1^{+2.4}_{-3.1}$	8202.3	m s^{-1}
γ_{FIES}	$8061.9^{+5.1}_{-6.3}$	8062.4	m s^{-1}
$\dot{\gamma}$	$\equiv 0.0$	$\equiv 0.0$	$\text{m s}^{-1} \text{ day}^{-1}$
$\ddot{\gamma}$	$\equiv 0.0$	$\equiv 0.0$	$\text{m s}^{-1} \text{ day}^{-2}$
σ_{HIRES}	$6.2^{+1.9}_{-0.6}$	5.7	m s^{-1}
$\sigma_{\text{HARPS-N}}$	$1.9^{+4.0}_{-12.0}$	4.0	m s^{-1}
σ_{FIES}	0 ± 11	0	m s^{-1}
Orbital & Physical Parameters			
P_b	$\equiv 19.3055$	$\equiv 19.3055$	days
$T_{\text{conj},b}$	$\equiv 2456819.5794$	$\equiv 2456819.5794$	BJD _{TBD}
e_b	$\equiv 0.0$	$\equiv 0.0$	
ω_b	$\equiv 0.0$	$\equiv 0.0$	radians
K_b	6.5 ± 2.0	6.0	m s^{-1}
M_b	$25.2^{+8.9}_{-7.9}$	24.7	M_{\oplus}
R_b/R_*	$0.03724^{+0.00120}_{-0.00010}$	0.03690	
ρ_b	2.54 ± 1.00	2.00	g cm^{-3}
R_b	$3.773^{+0.020}_{-0.120}$	3.850	R_{\oplus}
Priors			
Parameter	Prior		
None			

Our mass measurement is consistent with estimates from both Yu et al. (2018) and Van Eylen et al. (2018b). With the inclusion of all RV measurements, we prefer an eccentric fit and find an eccentricity of 0.200 ± 0.042 .

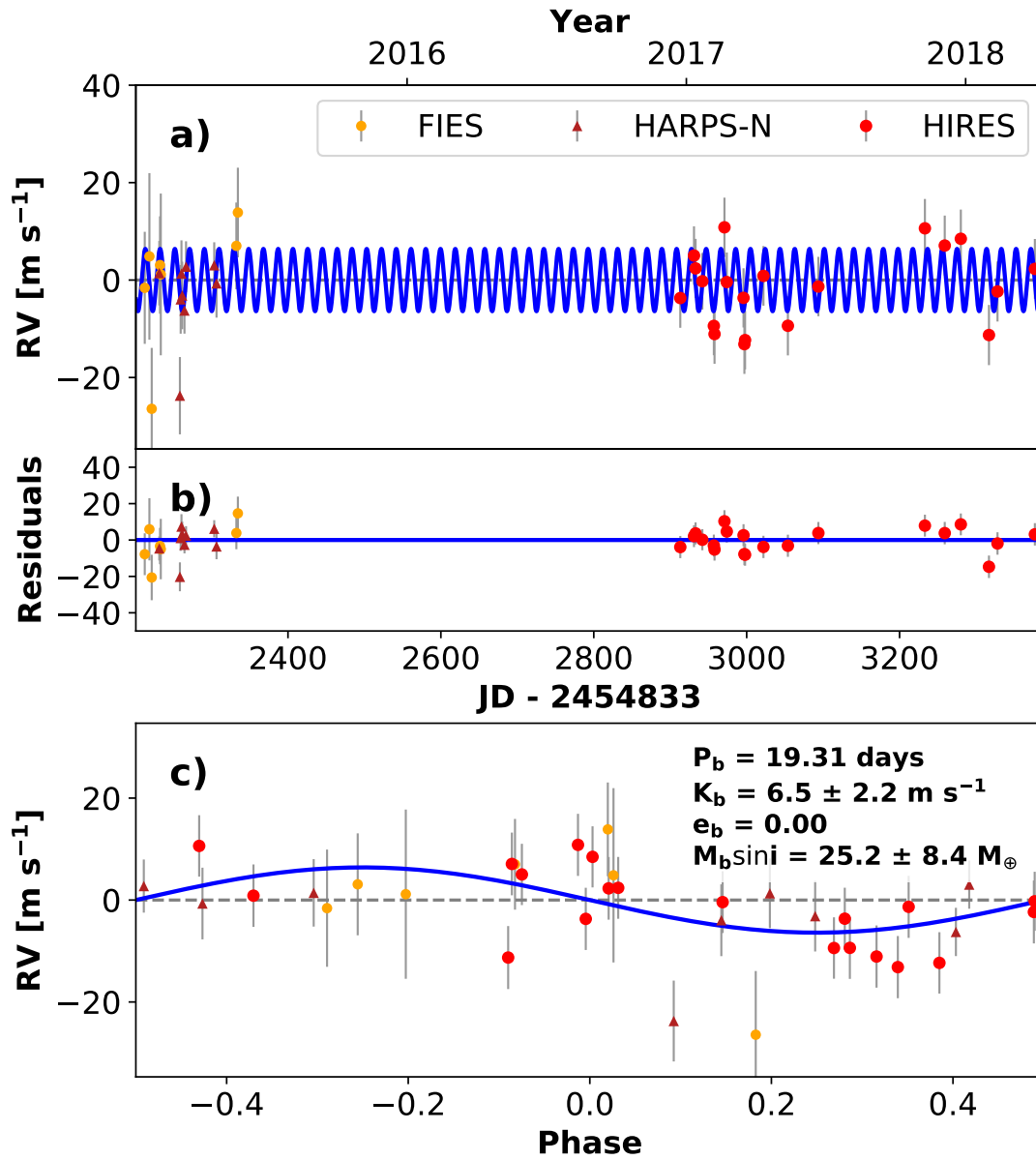


Figure 81. RVs and Keplerian model for K2-10. Symbols, lines, and annotations are similar to those in Fig. 11.

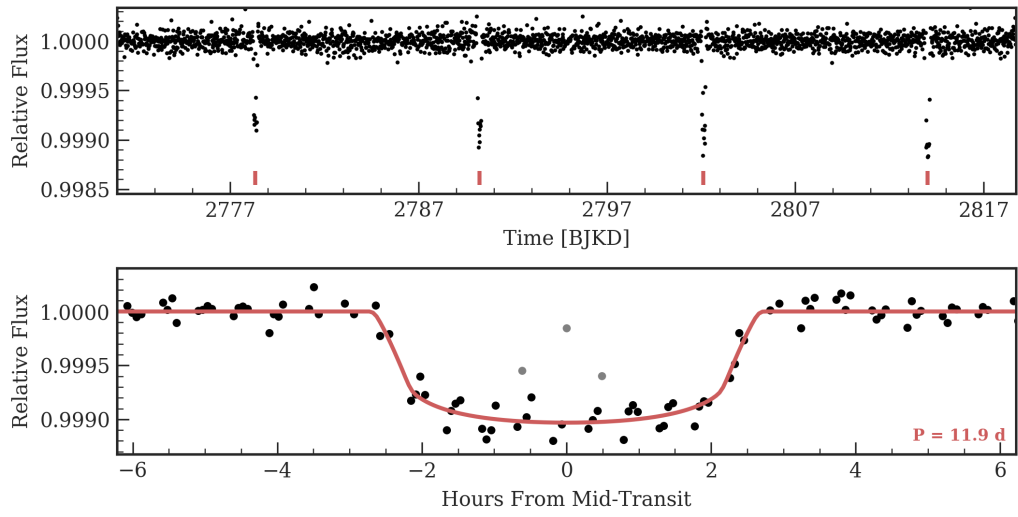


Figure 82. Time series (top) and phase-folded (bottom) light curve for the planet orbiting K2-245. Plot formatting is the same as in Fig. 10.

Table 37. EPIC 201357835 System Parameters

Parameter	Credible Interval	Maximum Likelihood	Units
RV Analysis – MCMC Step Parameters			
P_b	$\equiv 11.8938$	$\equiv 11.8938$	days
$T_{\text{conj},b}$	$\equiv 2457611.3378$	$\equiv 2457611.3378$	BJD_{TBD}
$\sqrt{e} \cos \omega_b$	$\equiv 0.0$	$\equiv 0.0$	
$\sqrt{e} \sin \omega_b$	$\equiv 0.0$	$\equiv 0.0$	
K_b	$5^{+7.8}_{-7.9}$	4.5	m s^{-1}
γ_{HIRES}	$-4.4^{+6.8}_{-6.7}$	-4.3	m s^{-1}
$\dot{\gamma}$	$\equiv 0.0$	$\equiv 0.0$	$\text{m s}^{-1} \text{ day}^{-1}$
$\ddot{\gamma}$	$\equiv 0.0$	$\equiv 0.0$	$\text{m s}^{-1} \text{ day}^{-2}$
σ_{HIRES}	7^{+10}_{-27}	9	m s^{-1}
Orbital & Physical Parameters			
P_b	$\equiv 11.8938$	$\equiv 11.8938$	days
$T_{\text{conj},b}$	$\equiv 2457611.3378$	$\equiv 2457611.3378$	BJD_{TBD}
e_b	$\equiv 0.0$	$\equiv 0.0$	
ω_b	$\equiv 0.0$	$\equiv 0.0$	radians
K_b	$5^{+7.8}_{-7.9}$	4.5	m s^{-1}
M_b	15 ± 26	15	M_{\oplus}
R_b/R_*	$0.0300^{+0.0017}_{-0.0001}$	0.0295	
ρ_b	$4.2^{+7.3}_{-7.2}$	4.1	g cm^{-3}
R_b	$2.67^{+0.07}_{-0.09}$	2.71	R_{\oplus}
Priors			
Parameter	Prior		
None			

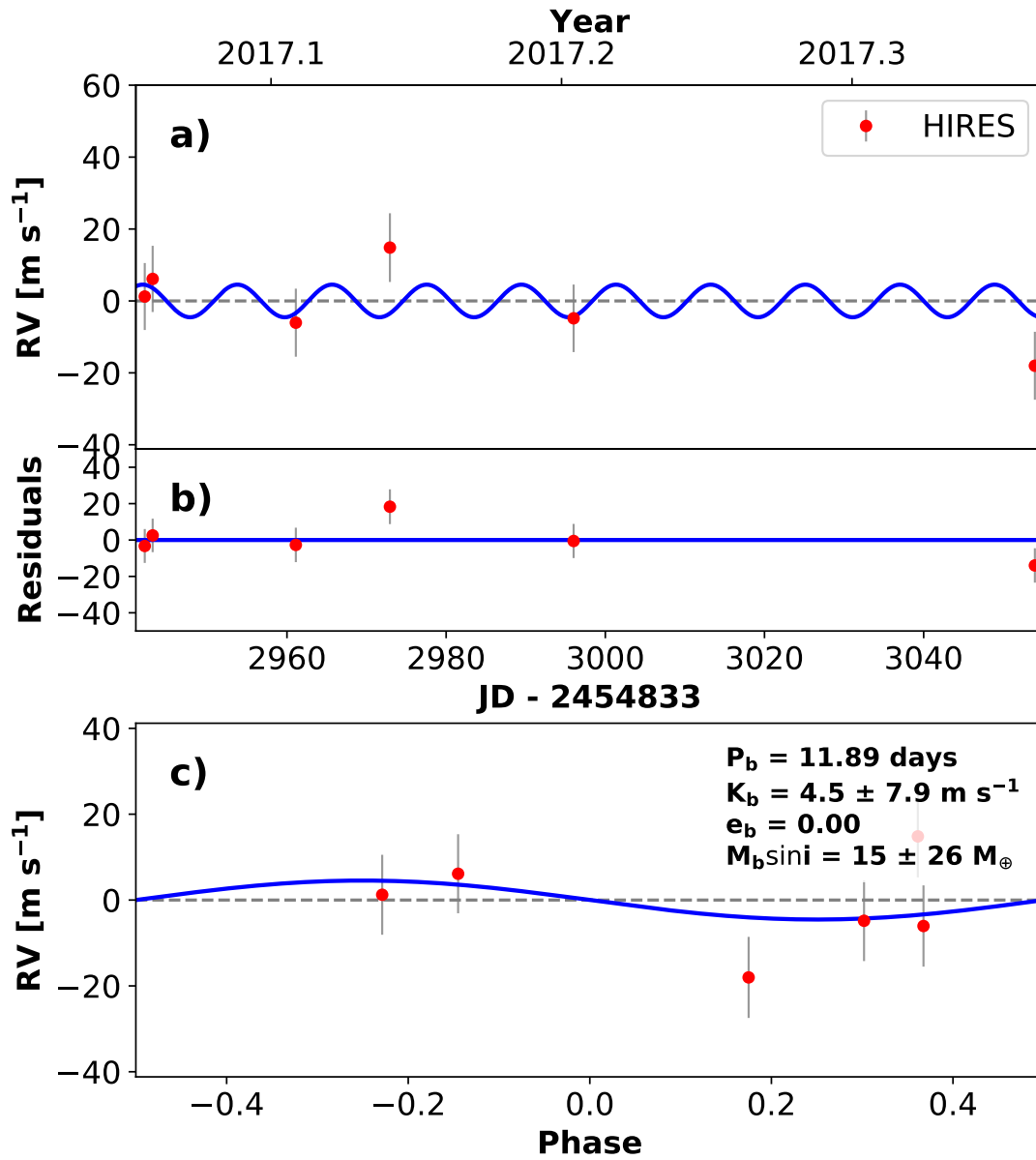


Figure 83. RVs and Keplerian model for K2-245. Symbols, lines, and annotations are similar to those in Fig. 11.

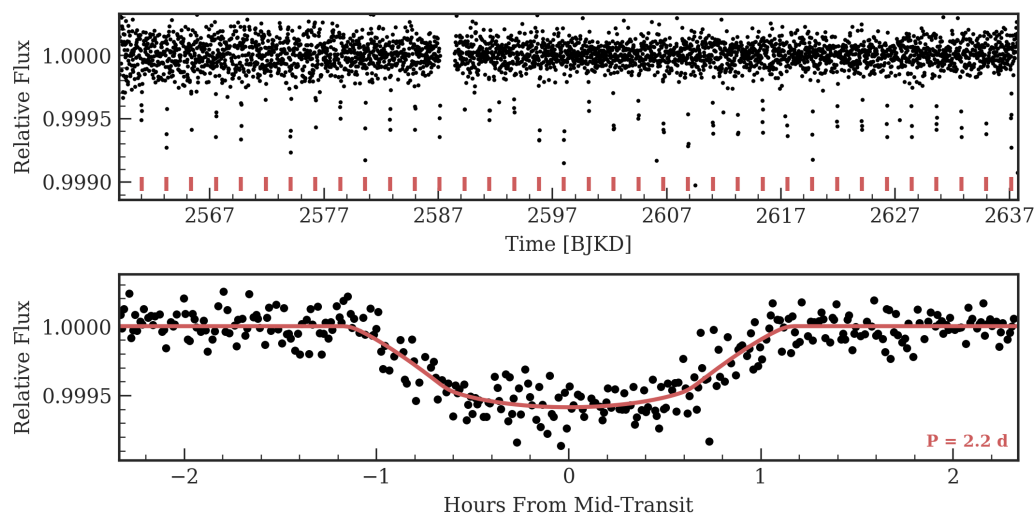


Figure 84. Time series (top) and phase-folded (bottom) light curve for the planet orbiting K2-216. Plot formatting is the same as in Fig. 10.

Table 38. K2-216 System Parameters

Parameter	Credible Interval	Maximum Likelihood	Units
RV Analysis – MCMC Step Parameters			
P_b	$\equiv 2.1748$	$\equiv 2.1748$	days
$T_{\text{conj},b}$	$\equiv 2457394.0417$	$\equiv 2457394.0417$	BJD _{TBD}
$\sqrt{e} \cos \omega_b$	$\equiv 0.0$	$\equiv 0.0$	
$\sqrt{e} \sin \omega_b$	$\equiv 0.0$	$\equiv 0.0$	
K_b	$3.77^{+0.80}_{-1.00}$	3.90	m s^{-1}
γ_{HIRES}	$-2.2^{+1.3}_{-1.1}$	-2.3	m s^{-1}
$\gamma_{\text{HARPS-N}}$	$-25911.1^{+2.4}_{-3.5}$	-25910.8	
γ_{HARPS}	$-25906^{+4.4}_{-3.7}$	-25906.2	m s^{-1}
$\gamma_{\text{FIES-POST}}$	-5 ± 4	-5	
γ_{FIES}	$1.4^{+4.0}_{-3.0}$	1.0	m s^{-1}
$\dot{\gamma}$	$\equiv 0.0$	$\equiv 0.0$	$\text{m s}^{-1} \text{ day}^{-1}$
$\ddot{\gamma}$	$\equiv 0.0$	$\equiv 0.0$	$\text{m s}^{-1} \text{ day}^{-2}$
σ_{HIRES}	$3.0^{+1.2}_{-5.8}$	3.0	m s^{-1}
$\sigma_{\text{HARPS-N}}$	$0.4^{+6.0}_{-3.0}$	-1.0	
σ_{HARPS}	0 ± 2	0	m s^{-1}
$\sigma_{\text{FIES-POST}}$	0^{+3}_{-2}	0	
σ_{FIES}	0 ± 2	0	m s^{-1}
η_3	$24.3^{+6.1}_{-2.8}$	23.5	days
η_2	$11.3^{+6.8}_{-3.5}$	10.1	days
η_4	$0.499^{+0.058}_{-0.077}$	0.506	
$\eta_{1,\text{HIRES}}$	$2.8^{+1.7}_{-1.2}$	2.5	m s^{-1}
$\eta_{1,\text{FIES}}$	$\equiv 0.0$	$\equiv 0.0$	m s^{-1}
$\eta_{1,\text{FIES-POST}}$	$\equiv 0.0$	$\equiv 0.0$	
$\eta_{1,\text{HARPS}}$	$5.5^{+9.2}_{-0.4}$	3.1	m s^{-1}
$\eta_{1,\text{HARPS-N}}$	$4.6^{+4.6}_{-2.5}$	4.2	
Orbital & Physical Parameters			
P_b	$\equiv 2.1748$	$\equiv 2.1748$	days
$T_{\text{conj},b}$	$\equiv 2457394.0417$	$\equiv 2457394.0417$	BJD _{TBD}
e_b	$\equiv 0.0$	$\equiv 0.0$	
ω_b	$\equiv 0.0$	$\equiv 0.0$	radians
K_b	$3.77^{+0.80}_{-1.00}$	3.90	m s^{-1}
M_b	$6.1^{+1.3}_{-1.7}$	6.3	M_{\oplus}
R_b/R_*	$\equiv 0.022$	$\equiv 0.022$	
ρ_b	$7^{+3.7}_{-0.5}$	5.5	g cm^{-3}
R_b	$\equiv 1.6599$	$\equiv 1.6599$	R_{\oplus}
Priors			
Parameter	Prior		
$\eta_{1,\text{FIES}}$	$\mathcal{U}(0, 1e + 100)$		
$\eta_{1,\text{FIES-POST}}$	$\mathcal{U}(0, 1e + 100)$		
$\eta_{1,\text{HARPS}}$	$\mathcal{U}(0, 1e + 100)$		
$\eta_{1,\text{HARPS-N}}$	$\mathcal{U}(0, 1e + 100)$		
$\eta_{1,\text{HIRES}}$	$\mathcal{U}(0, 1e + 100)$		
Numerical prior from photom. training on η_2, η_3, η_4			

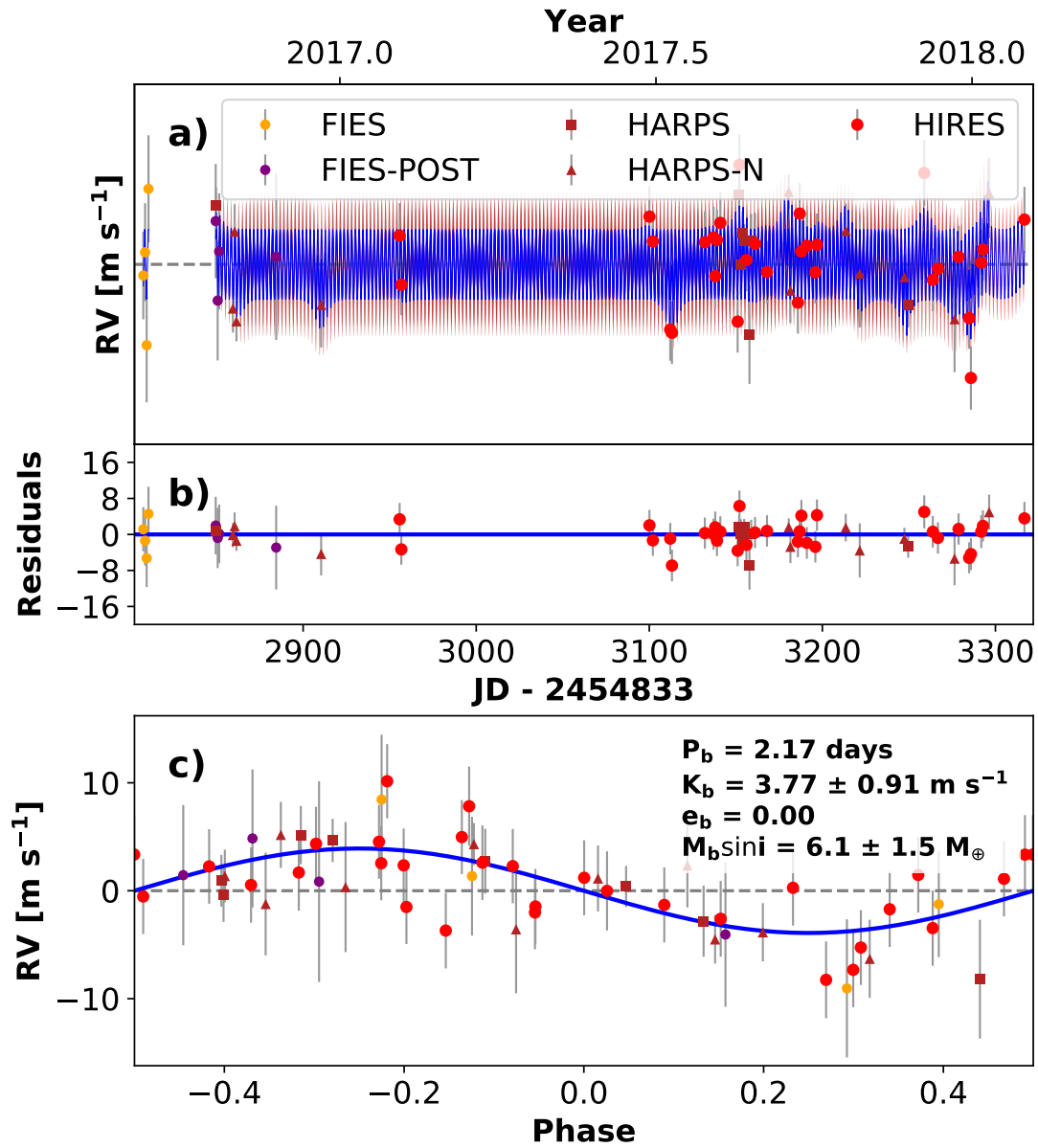


Figure 85. RVs and Keplerian model for K2-216. Symbols, lines, and annotations are similar to those in Fig. 11.

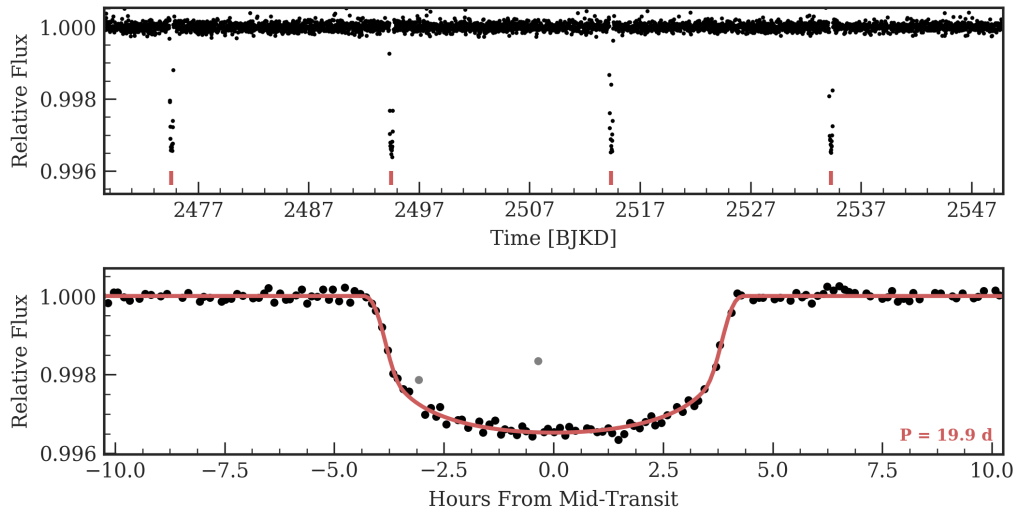


Figure 86. Time series (top) and phase-folded (bottom) light curve for the planet orbiting K2-280. Plot formatting is the same as in Fig. 10.

Table 39. K2-280 System Parameters

Parameter	Credible Interval	Maximum Likelihood	Units
RV Analysis – MCMC Step Parameters			
P_b	$\equiv 19.895$	$\equiv 19.895$	days
$T_{\text{conj},b}$	$\equiv 2457327.4761$	$\equiv 2457327.4761$	BJD _{TBD}
$\sqrt{e} \cos \omega_b$	-0.2 ± 0.1	-0.1	
$\sqrt{e} \sin \omega_b$	-0.6 ± 0.1	-0.7	
K_b	$11.9^{+1.7}_{-1.5}$	12.8	m s^{-1}
γ_{HIRES}	-1.5 ± 1.1	-2.0	m s^{-1}
$\dot{\gamma}$	$\equiv 0.0$	$\equiv 0.0$	$\text{m s}^{-1} \text{ day}^{-1}$
$\ddot{\gamma}$	$\equiv 0.0$	$\equiv 0.0$	$\text{m s}^{-1} \text{ day}^{-2}$
σ_{HIRES}	$2.9^{+1.1}_{-0.9}$	2.0	m s^{-1}
Orbital & Physical Parameters			
P_b	$\equiv 19.895$	$\equiv 19.895$	days
$T_{\text{conj},b}$	$\equiv 2457327.4761$	$\equiv 2457327.4761$	BJD _{TBD}
e_b	0.5 ± 0.1	0.5	
ω_b	$-1.90^{+0.14}_{-0.21}$	-1.77	radians
K_b	$11.9^{+1.7}_{-1.5}$	12.8	m s^{-1}
M_b	$49.0^{+6.5}_{-6.2}$	50.7	M_{\oplus}
R_b/R_*	$0.05362^{+0.00078}_{-0.00038}$	0.05340	
ρ_b	$0.643^{+0.088}_{-0.083}$	0.670	g cm^{-3}
R_b	$7.46^{+0.11}_{-0.05}$	7.45	R_{\oplus}
Priors			
Parameter	Prior		
e_b	< 0.99		
σ_{HIRES}	$\mathcal{U}(0, 1e + 100)$		

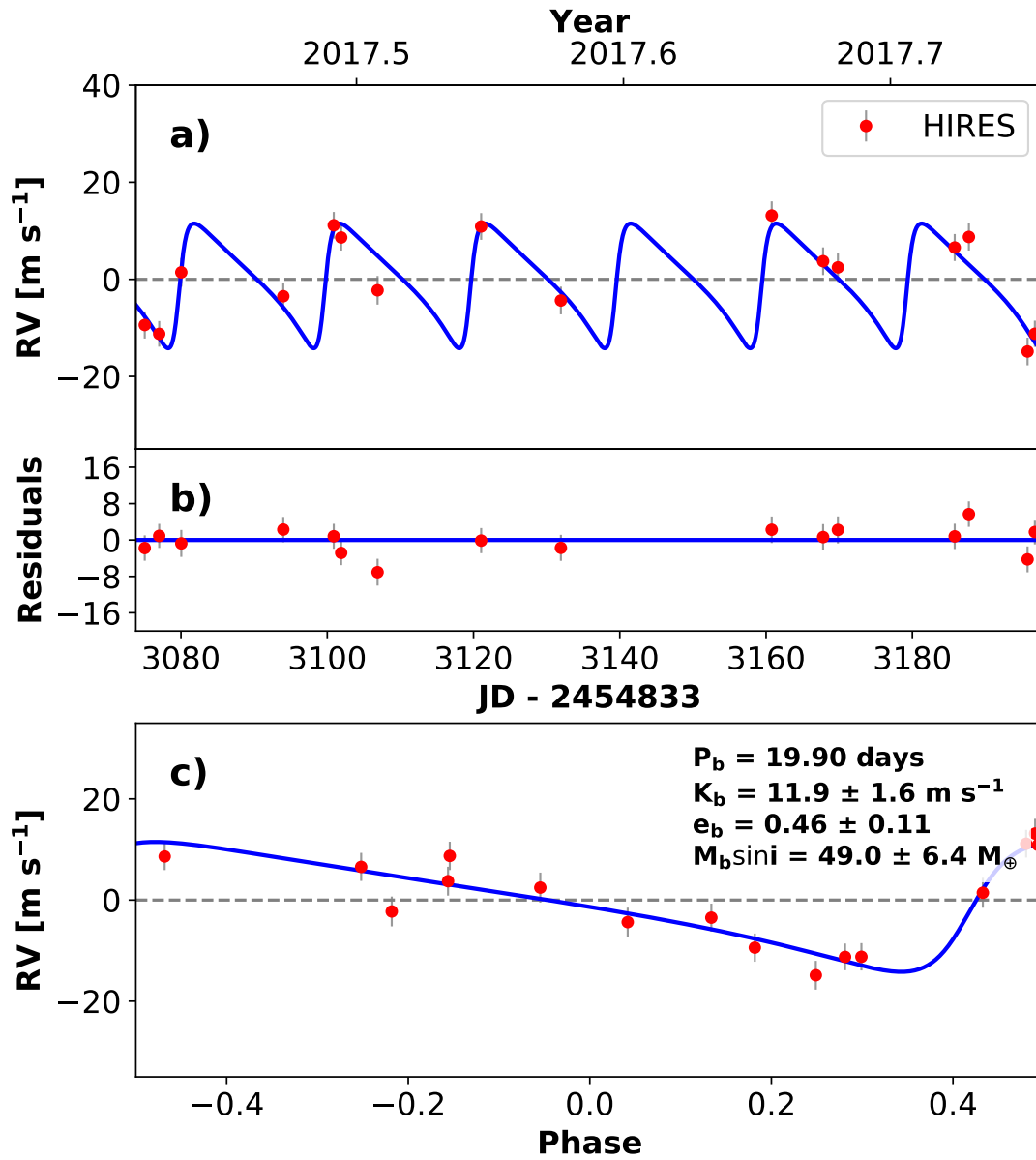


Figure 87. RVs and Keplerian model for K2-280. Symbols, lines, and annotations are similar to those in Fig. 11.

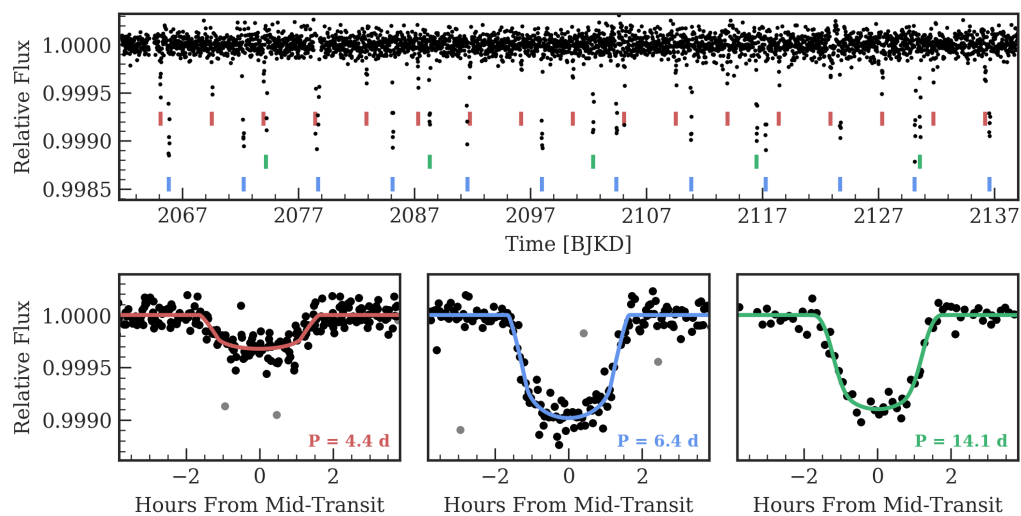
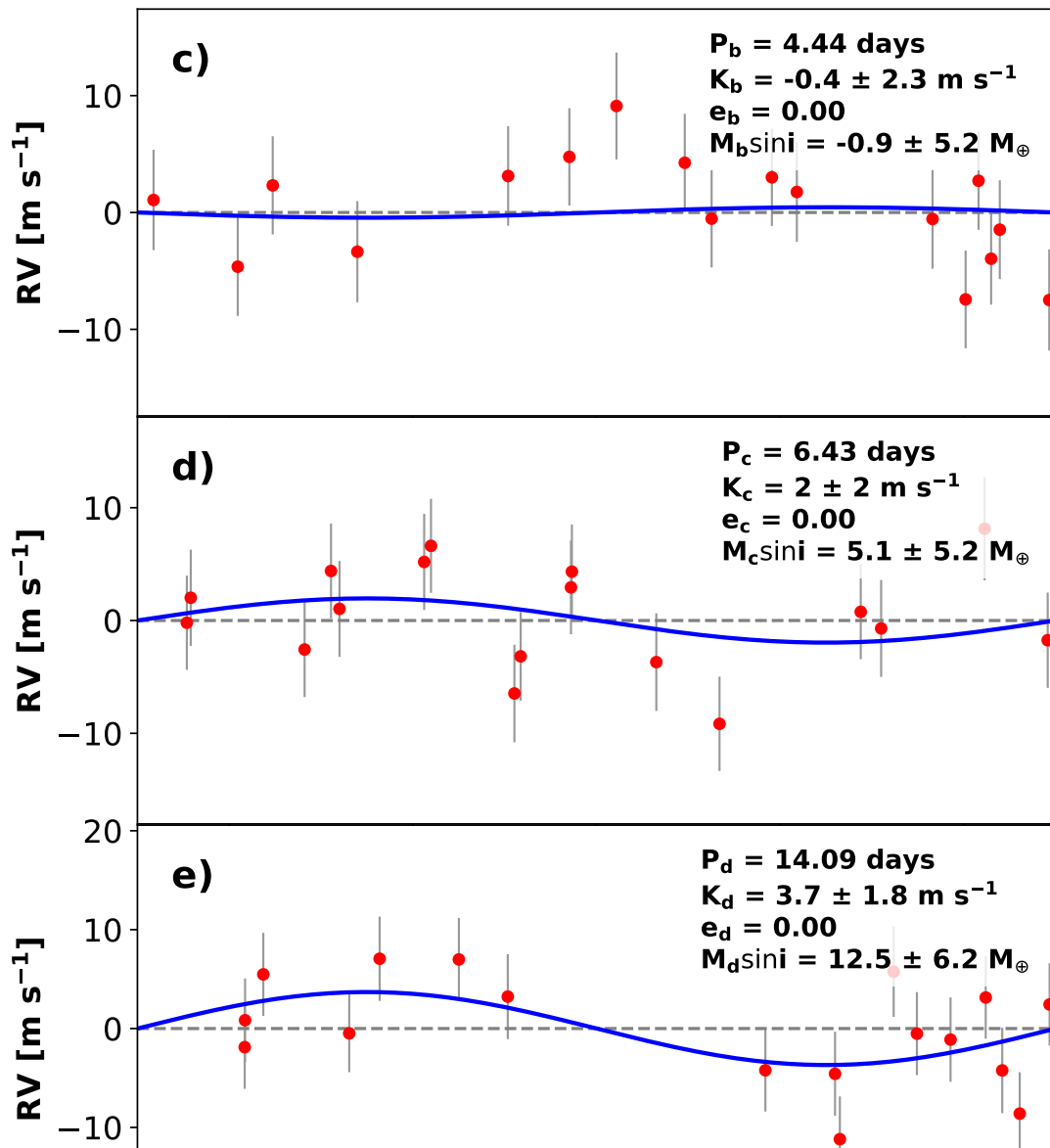
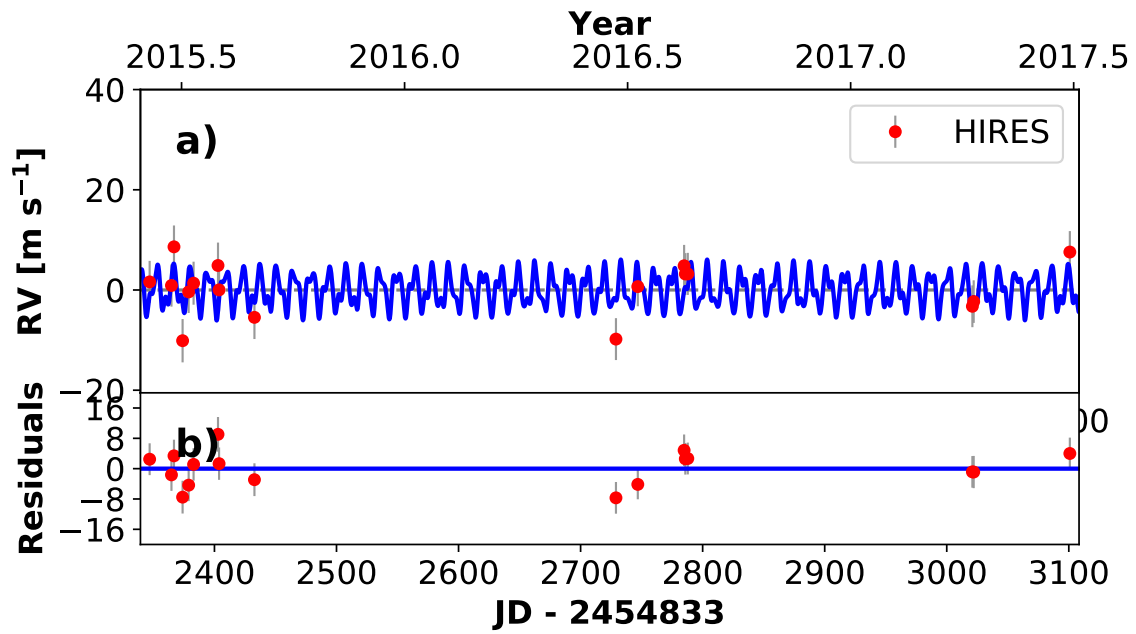


Figure 88. Time series (top) and phase-folded (bottom) light curve for the planet orbiting K2-37. Plot formatting is the same as in Fig. 10.

Table 40. K2-37 System Parameters

Parameter	Credible Interval	Maximum Likelihood	Units
RV Analysis – MCMC Step Parameters			
P_b	$\equiv 4.4434$	$\equiv 4.4434$	days
$T_{\text{conj},b}$	$\equiv 2456893.6753$	$\equiv 2456893.6753$	BJD _{TBD}
$\sqrt{e} \cos \omega_b$	$\equiv 0.0$	$\equiv 0.0$	
$\sqrt{e} \sin \omega_b$	$\equiv 0.0$	$\equiv 0.0$	
K_b	-0.4 ± 2.3	-0.4	m s^{-1}
P_c	$\equiv 6.4297$	$\equiv 6.4297$	days
$T_{\text{conj},c}$	$\equiv 2456898.8548$	$\equiv 2456898.8548$	BJD _{TBD}
$\sqrt{e} \cos \omega_c$	$\equiv 0.0$	$\equiv 0.0$	
$\sqrt{e} \sin \omega_c$	$\equiv 0.0$	$\equiv 0.0$	
K_c	2 ± 2	2	m s^{-1}
P_d	$\equiv 14.0923$	$\equiv 14.0923$	days
$T_{\text{conj},d}$	$\equiv 2456907.2331$	$\equiv 2456907.2331$	BJD _{TBD}
$\sqrt{e} \cos \omega_d$	$\equiv 0.0$	$\equiv 0.0$	
$\sqrt{e} \sin \omega_d$	$\equiv 0.0$	$\equiv 0.0$	
K_d	$3.7^{+1.9}_{-1.8}$	3.7	m s^{-1}
γ_{HIRES}	$-0.9^{+1.4}_{-1.3}$	-0.9	m s^{-1}
$\dot{\gamma}$	$\equiv 0.0$	$\equiv 0.0$	$\text{m s}^{-1} \text{ day}^{-1}$
$\ddot{\gamma}$	$\equiv 0.0$	$\equiv 0.0$	$\text{m s}^{-1} \text{ day}^{-2}$
σ_{HIRES}	$4.7^{+2.4}_{-0.3}$	3.8	m s^{-1}
Orbital & Physical Parameters			
P_b	$\equiv 4.4434$	$\equiv 4.4434$	days
$T_{\text{conj},b}$	$\equiv 2456893.6753$	$\equiv 2456893.6753$	BJD _{TBD}
e_b	$\equiv 0.0$	$\equiv 0.0$	
ω_b	$\equiv 0.0$	$\equiv 0.0$	radians
K_b	-0.4 ± 2.3	-0.4	m s^{-1}
M_b	-0.9 ± 5.2	-0.9	M_{\oplus}
R_b/R_*	$0.0165^{+0.0015}_{-0.0004}$	0.0163	
ρ_b	-2 ± 10	-2	g cm^{-3}
R_b	1.39 ± 0.10	1.40	R_{\oplus}
P_c	$\equiv 6.4297$	$\equiv 6.4297$	days
$T_{\text{conj},c}$	$\equiv 2456898.8548$	$\equiv 2456898.8548$	BJD _{TBD}
e_c	$\equiv 0.0$	$\equiv 0.0$	
ω_c	$\equiv 0.0$	$\equiv 0.0$	radians
K_c	2 ± 2	2	m s^{-1}
M_c	$5.1^{+5.1}_{-5.3}$	5.2	M_{\oplus}
R_c/R_*	$0.0287^{+0.0025}_{-0.0001}$	0.0281	
ρ_c	2 ± 2	2	g cm^{-3}
R_c	$2.41^{+0.09}_{-0.12}$	2.48	R_{\oplus}
P_d	$\equiv 14.0923$	$\equiv 14.0923$	days
$T_{\text{conj},d}$	$\equiv 2456907.2331$	$\equiv 2456907.2331$	BJD _{TBD}
e_d	$\equiv 0.0$	$\equiv 0.0$	
ω_d	$\equiv 0.0$	$\equiv 0.0$	radians
K_d	$3.7^{+1.9}_{-1.8}$	3.7	m s^{-1}
M_d	$12.5^{+6.3}_{-6.1}$	12.5	M_{\oplus}
R_d/R_*	$\equiv 0.0275$	$\equiv 0.0275$	
ρ_d	$\equiv 5.1906$	$\equiv 5.1906$	g cm^{-3}
R_d	$\equiv 2.3113$	$\equiv 2.3113$	R_{\oplus}
Priors			
Parameter	Prior		
None			



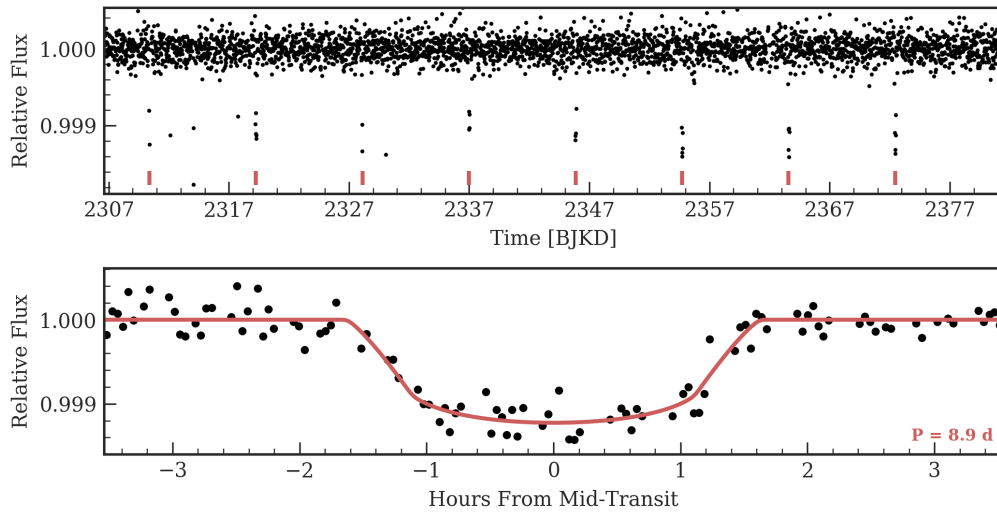


Figure 90. Time series (top) and phase-folded (bottom) light curve for the planet orbiting K2-180. Plot formatting is the same as in Fig. 10.

Table 41. K2-180 System Parameters

Parameter	Credible Interval	Maximum Likelihood	Units
RV Analysis – MCMC Step Parameters			
P_b	$\equiv 8.8656$	$\equiv 8.8656$	days
$T_{\text{conj},b}$	$\equiv 2457143.3945$	$\equiv 2457143.3945$	BJD _{TBD}
$\sqrt{e} \cos \omega_b$	$\equiv 0.0$	$\equiv 0.0$	
$\sqrt{e} \sin \omega_b$	$\equiv 0.0$	$\equiv 0.0$	
K_b	3.8 ± 0.9	3.8	m s^{-1}
γ_{HIRES}	$-1.63^{+0.92}_{-0.94}$	-1.60	m s^{-1}
$\gamma_{\text{HARPS-N}}$	-76614.5 ± 0.9	-76614.4	m s^{-1}
γ_{FIES}	$-76854.4^{+5.4}_{-5.2}$	-76854.0	m s^{-1}
$\dot{\gamma}$	$\equiv 0.0$	$\equiv 0.0$	$\text{m s}^{-1} \text{ day}^{-1}$
$\ddot{\gamma}$	$\equiv 0.0$	$\equiv 0.0$	$\text{m s}^{-1} \text{ day}^{-2}$
σ_{HIRES}	$3.80^{+0.89}_{-0.75}$	3.50	m s^{-1}
$\sigma_{\text{HARPS-N}}$	1 ± 1	0.0	m s^{-1}
σ_{FIES}	5^{+15}_{-4}	0	m s^{-1}
Orbital & Physical Parameters			
P_b	$\equiv 8.8656$	$\equiv 8.8656$	days
$T_{\text{conj},b}$	$\equiv 2457143.3945$	$\equiv 2457143.3945$	BJD _{TBD}
e_b	$\equiv 0.0$	$\equiv 0.0$	
ω_b	$\equiv 0.0$	$\equiv 0.0$	radians
K_b	3.8 ± 0.9	3.8	m s^{-1}
M_b	9.4 ± 2.2	9.4	M_{\oplus}
R_b/R_*	$0.0321^{+0.0016}_{-0.0008}$	0.0315	
ρ_b	5.2 ± 1.4	4.9	g cm^{-3}
R_b	$2.13^{+0.11}_{-0.05}$	2.19	R_{\oplus}
Priors			
Parameter	Prior		
σ_{HIRES}	$\mathcal{U}(0, 1e + 100)$		
σ_{FIES}	$\mathcal{U}(0, 1e + 100)$		
$\sigma_{\text{HARPS-N}}$	$\mathcal{U}(0, 1e + 100)$		

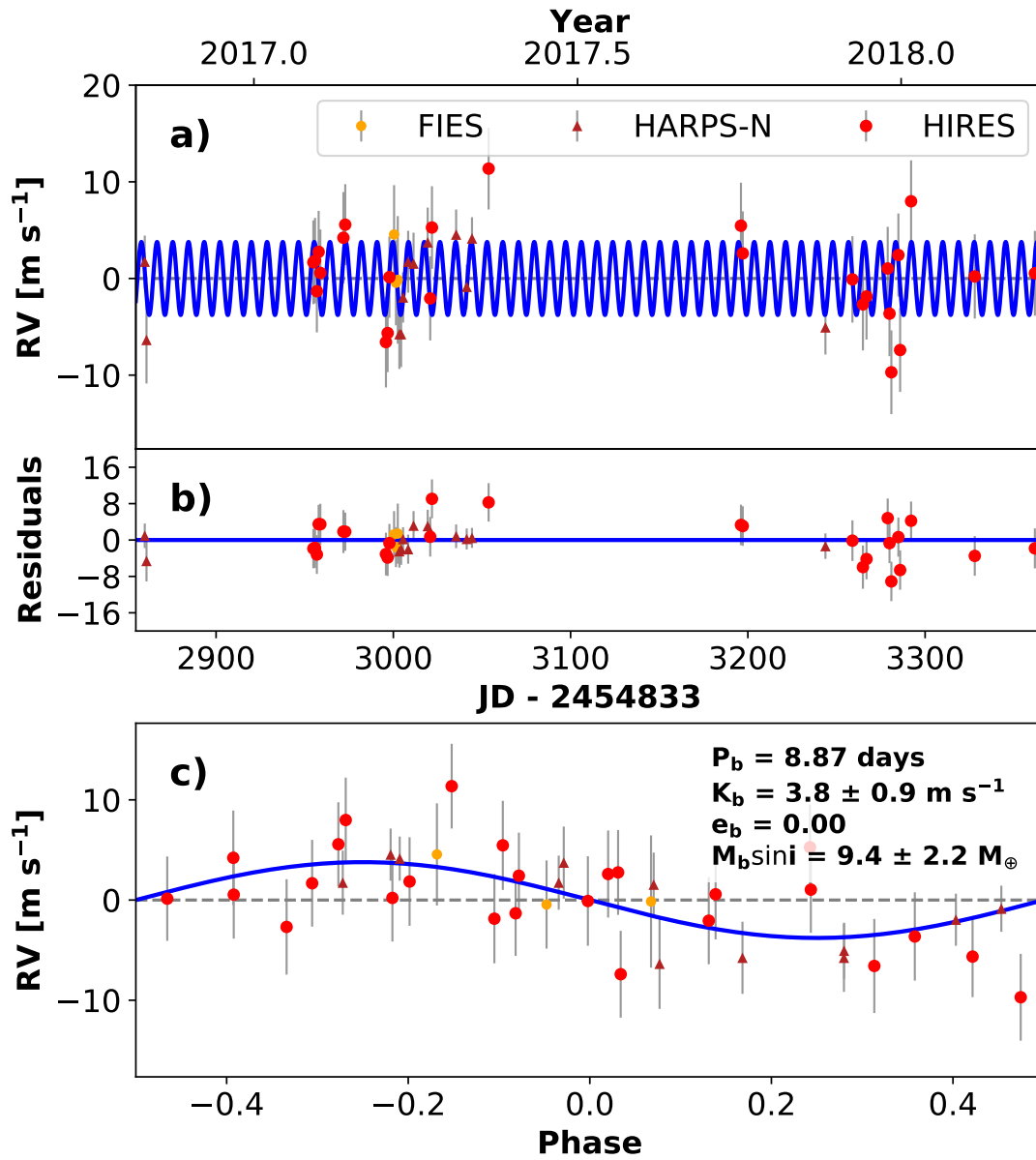


Figure 91. RVs and Keplerian model for K2-180. Symbols, lines, and annotations are similar to those in Fig. 11.

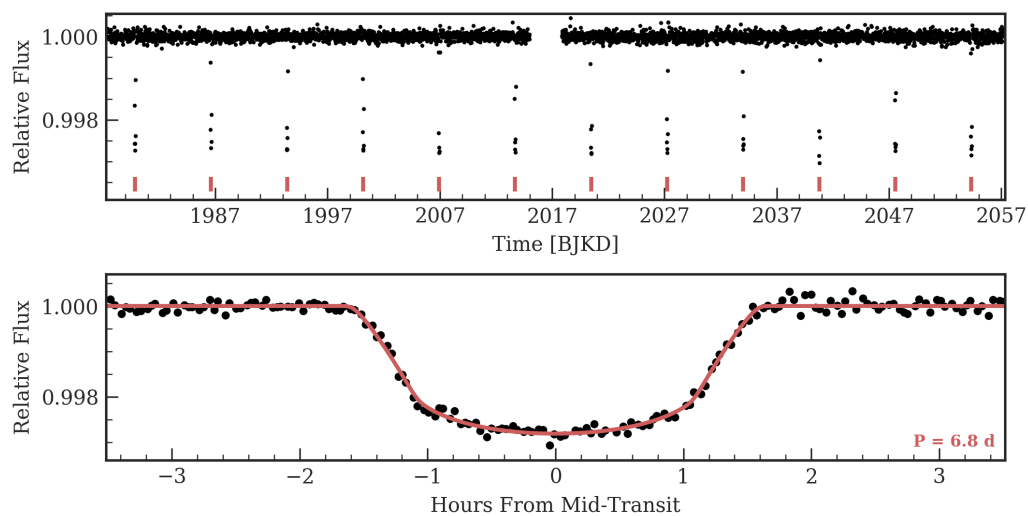


Figure 92. Time series (top) and phase-folded (bottom) light curve for the planet orbiting K2-27. Plot formatting is the same as in Fig. 10.

Table 42. K2-27 System Parameters

Parameter	Credible Interval	Maximum Likelihood	Units
RV Analysis – MCMC Step Parameters			
P_b	$\equiv 6.7713$	$\equiv 6.7713$	days
$T_{\text{conj},b}$	$\equiv 2456812.8447$	$\equiv 2456812.8447$	BJD _{TBD}
$\sqrt{e} \cos \omega_b$	$0.37^{+0.09}_{-0.14}$	0.39	
$\sqrt{e} \sin \omega_b$	$0.31^{+0.17}_{-0.22}$	0.30	
K_b	11.6 ± 1.4	11.6	m s^{-1}
γ_{HIRES}	$-3.8^{+1.3}_{-1.2}$	-3.8	m s^{-1}
$\gamma_{\text{HARPS-N}}$	$-37772.9^{+2.3}_{-2.6}$	-37772.0	
γ_{HARPS}	$-37775.4^{+1.6}_{-1.8}$	-37775.1	m s^{-1}
γ_{FIES}	-37980^{+19}_{-18}	-37980	m s^{-1}
$\dot{\gamma}$	$\equiv 0.0$	$\equiv 0.0$	$\text{m s}^{-1} \text{ day}^{-1}$
$\ddot{\gamma}$	$\equiv 0.0$	$\equiv 0.0$	$\text{m s}^{-1} \text{ day}^{-2}$
σ_{HIRES}	$4.1^{+1.3}_{-1.0}$	3.2	m s^{-1}
$\sigma_{\text{HARPS-N}}$	$5.0^{+3.3}_{-2.3}$	3.0	
σ_{HARPS}	$1.0^{+4.5}_{-1.0}$	0.0	m s^{-1}
σ_{FIES}	37^{+24}_{-13}	26	m s^{-1}
Orbital & Physical Parameters			
P_b	$\equiv 6.7713$	$\equiv 6.7713$	days
$T_{\text{conj},b}$	$\equiv 2456812.8447$	$\equiv 2456812.8447$	BJD _{TBD}
e_b	$0.249^{+0.075}_{-0.063}$	0.243	
ω_b	$0.69^{+0.41}_{-0.49}$	0.66	radians
K_b	11.6 ± 1.4	11.6	m s^{-1}
M_b	30.2 ± 3.6	30.5	M_{\oplus}
R_b/R_*	$0.0481^{+0.0013}_{-0.0006}$	0.0476	
ρ_b	1.53 ± 0.21	1.79	g cm^{-3}
R_b	$4.74^{+0.13}_{-0.06}$	4.54	R_{\oplus}
Priors			
Parameter	Prior		
e_b	< 0.99		
σ_{HIRES}	$\mathcal{U}(0, 1e + 100)$		
σ_{FIES}	$\mathcal{U}(0, 1e + 100)$		
σ_{HARPS}	$\mathcal{U}(0, 1e + 100)$		
$\sigma_{\text{HARPS-N}}$	$\mathcal{U}(0, 1e + 100)$		

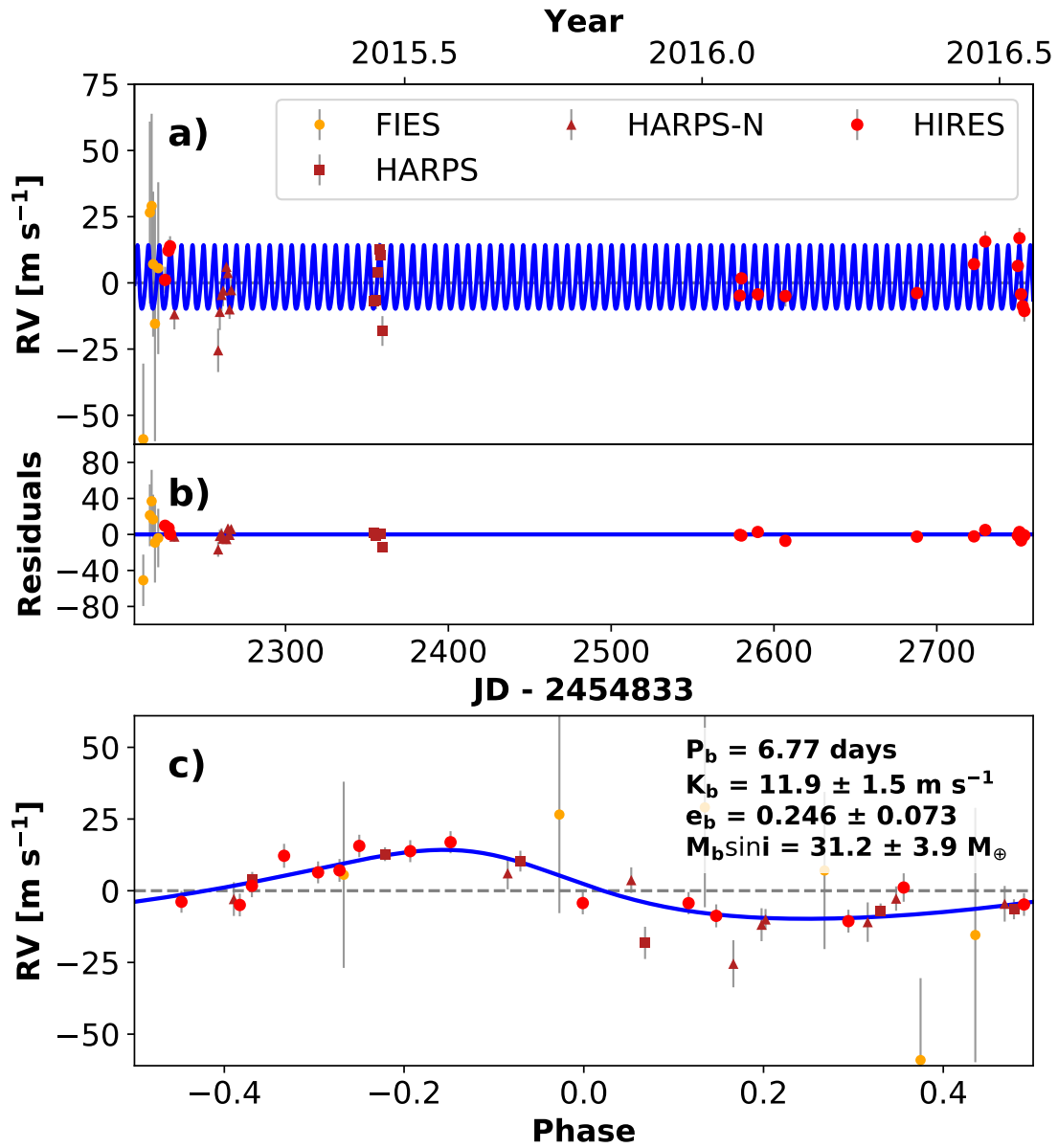


Figure 93. RVs and Keplerian model for K2-27. Symbols, lines, and annotations are similar to those in Fig. 11.

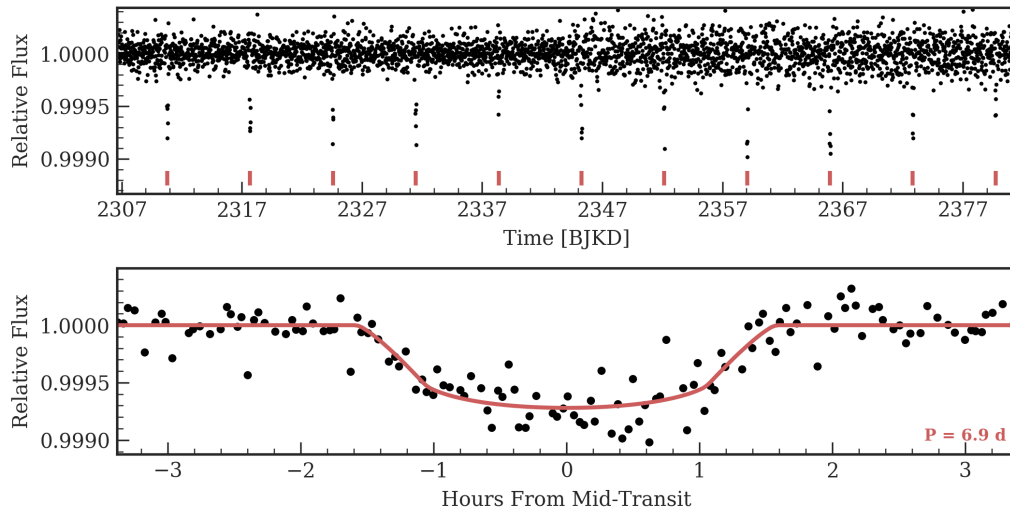


Figure 94. Time series (top) and phase-folded (bottom) light curve for the planet orbiting K2-181. Plot formatting is the same as in Fig. 10.

Table 43. K2-181 System Parameters

Parameter	Credible Interval	Maximum Likelihood	Units
RV Analysis – MCMC Step Parameters			
P_b	$\equiv 6.8941$	$\equiv 6.8941$	days
$T_{\text{conj},b}$	$\equiv 2457143.7948$	$\equiv 2457143.7948$	BJD _{TBD}
$\sqrt{e} \cos \omega_b$	$\equiv 0.0$	$\equiv 0.0$	
$\sqrt{e} \sin \omega_b$	$\equiv 0.0$	$\equiv 0.0$	
K_b	$4.1^{+6.3}_{-6.2}$	4.1	m s^{-1}
γ_{HIRES}	-0.7 ± 4.0	-1.0	m s^{-1}
$\dot{\gamma}$	$\equiv 0.0$	$\equiv 0.0$	$\text{m s}^{-1} \text{ day}^{-1}$
$\ddot{\gamma}$	$\equiv 0.0$	$\equiv 0.0$	$\text{m s}^{-1} \text{ day}^{-2}$
σ_{HIRES}	9^{+5}_{-23}	10	m s^{-1}
Orbital & Physical Parameters			
P_b	$\equiv 6.8941$	$\equiv 6.8941$	days
$T_{\text{conj},b}$	$\equiv 2457143.7948$	$\equiv 2457143.7948$	BJD _{TBD}
e_b	$\equiv 0.0$	$\equiv 0.0$	
ω_b	$\equiv 0.0$	$\equiv 0.0$	radians
K_b	$4.1^{+6.3}_{-6.2}$	4.1	m s^{-1}
M_b	12 ± 18	12	M_{\oplus}
R_b/R_*	$0.0248^{+0.0020}_{-0.0010}$	0.0250	
ρ_b	$3^{+5.3}_{-4.4}$	2.8	g cm^{-3}
R_b	$2.69^{+0.04}_{-0.25}$	2.86	R_{\oplus}
Priors			
Parameter	Prior		
None			

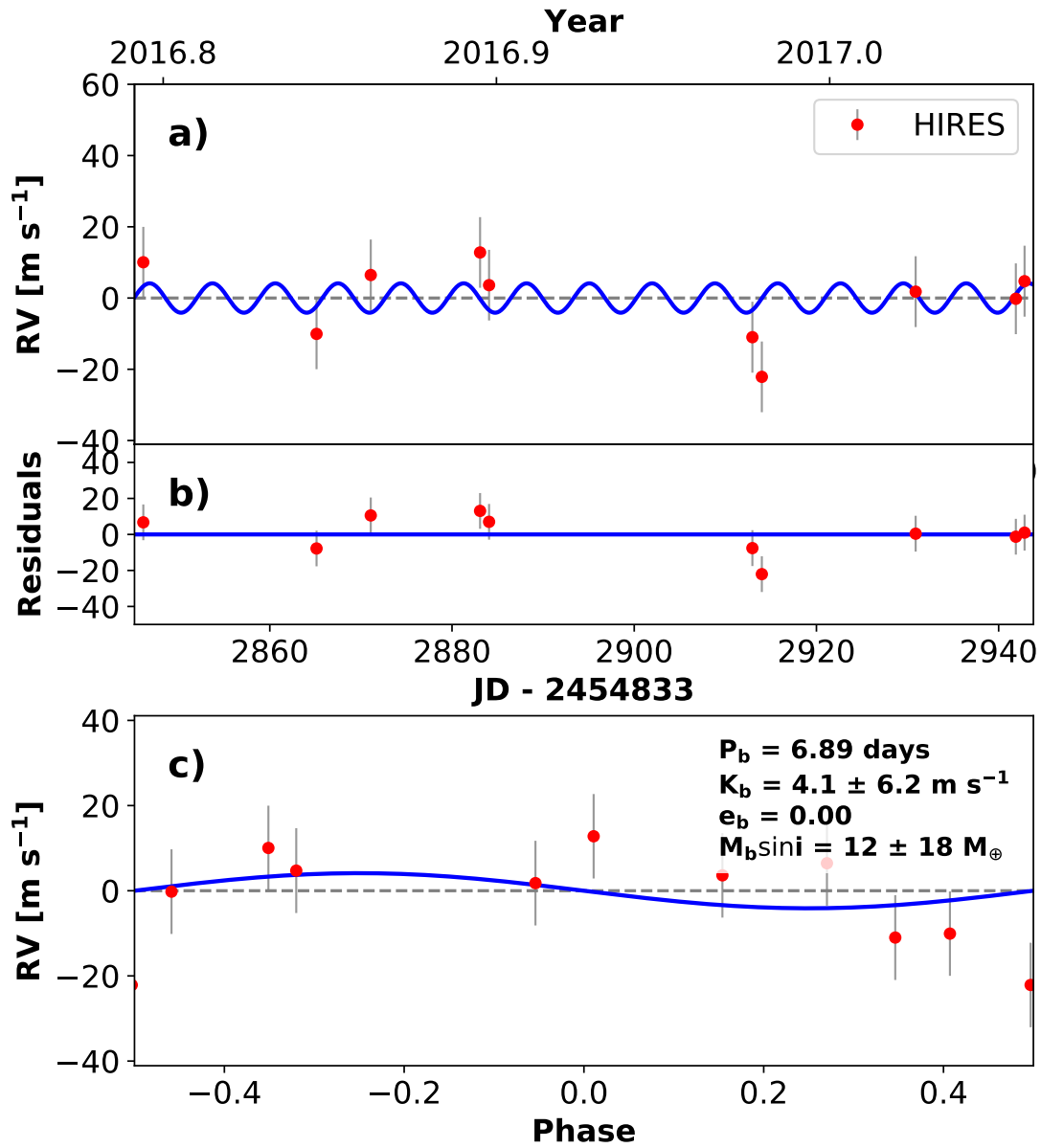


Figure 95. RVs and Keplerian model for K2-181. Symbols, lines, and annotations are similar to those in Fig. 11.

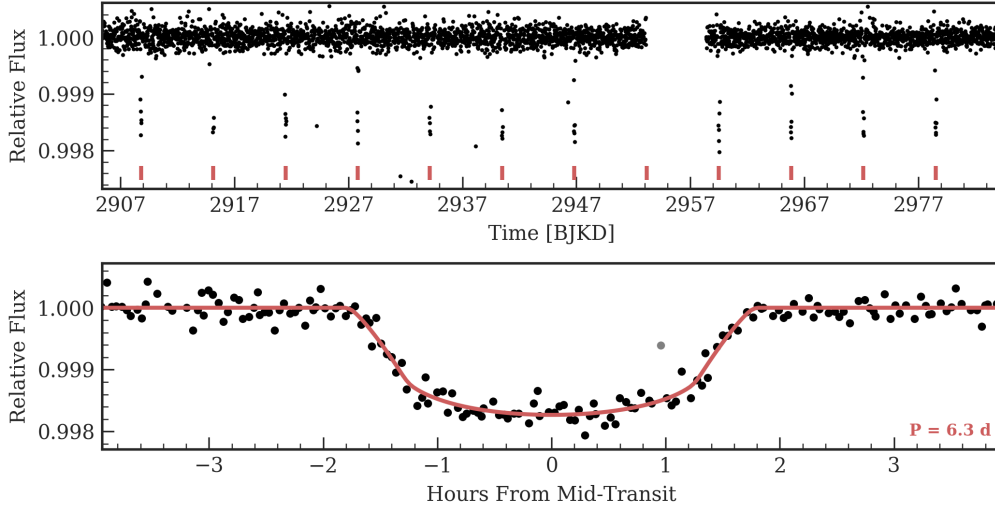


Figure 96. Time series (top) and phase-folded (bottom) light curve for the planet orbiting EPIC 245943455. Plot formatting is the same as in Fig. 10.

Table 44. EPIC 245943455 System Parameters

Parameter	Credible Interval	Maximum Likelihood	Units
RV Analysis – MCMC Step Parameters			
P_b	$\equiv 6.3393$	$\equiv 6.3393$	days
$T_{\text{conj},b}$	$\equiv 2457741.7946$	$\equiv 2457741.7946$	BJD _{TBD}
$\sqrt{e} \cos \omega_b$	$\equiv 0.0$	$\equiv 0.0$	
$\sqrt{e} \sin \omega_b$	$\equiv 0.0$	$\equiv 0.0$	
K_b	1.6 ± 1.7	1.6	m s^{-1}
γ_{HIRES}	0.2 ± 1.2	0.2	m s^{-1}
$\dot{\gamma}$	$\equiv 0.0$	$\equiv 0.0$	$\text{m s}^{-1} \text{ day}^{-1}$
$\ddot{\gamma}$	$\equiv 0.0$	$\equiv 0.0$	$\text{m s}^{-1} \text{ day}^{-2}$
σ_{HIRES}	$1.9^{+1.3}_{-1.0}$	1.3	m s^{-1}
Orbital & Physical Parameters			
P_b	$\equiv 6.3393$	$\equiv 6.3393$	days
$T_{\text{conj},b}$	$\equiv 2457741.7946$	$\equiv 2457741.7946$	BJD _{TBD}
e_b	$\equiv 0.0$	$\equiv 0.0$	
ω_b	$\equiv 0.0$	$\equiv 0.0$	radians
K_b	1.6 ± 1.7	1.6	m s^{-1}
M_b	4.4 ± 4.8	4.4	M_{\oplus}
R_b/R_*	$0.0379^{+0.0019}_{-0.0007}$	0.0371	
ρ_b	$0.39^{+0.44}_{-0.43}$	0.48	g cm^{-3}
R_b	$3.9^{+0.2}_{-0.1}$	3.7	R_{\oplus}
Priors			
Parameter	Prior		
σ_{HIRES}	$\mathcal{U}(0, 1e + 100)$		

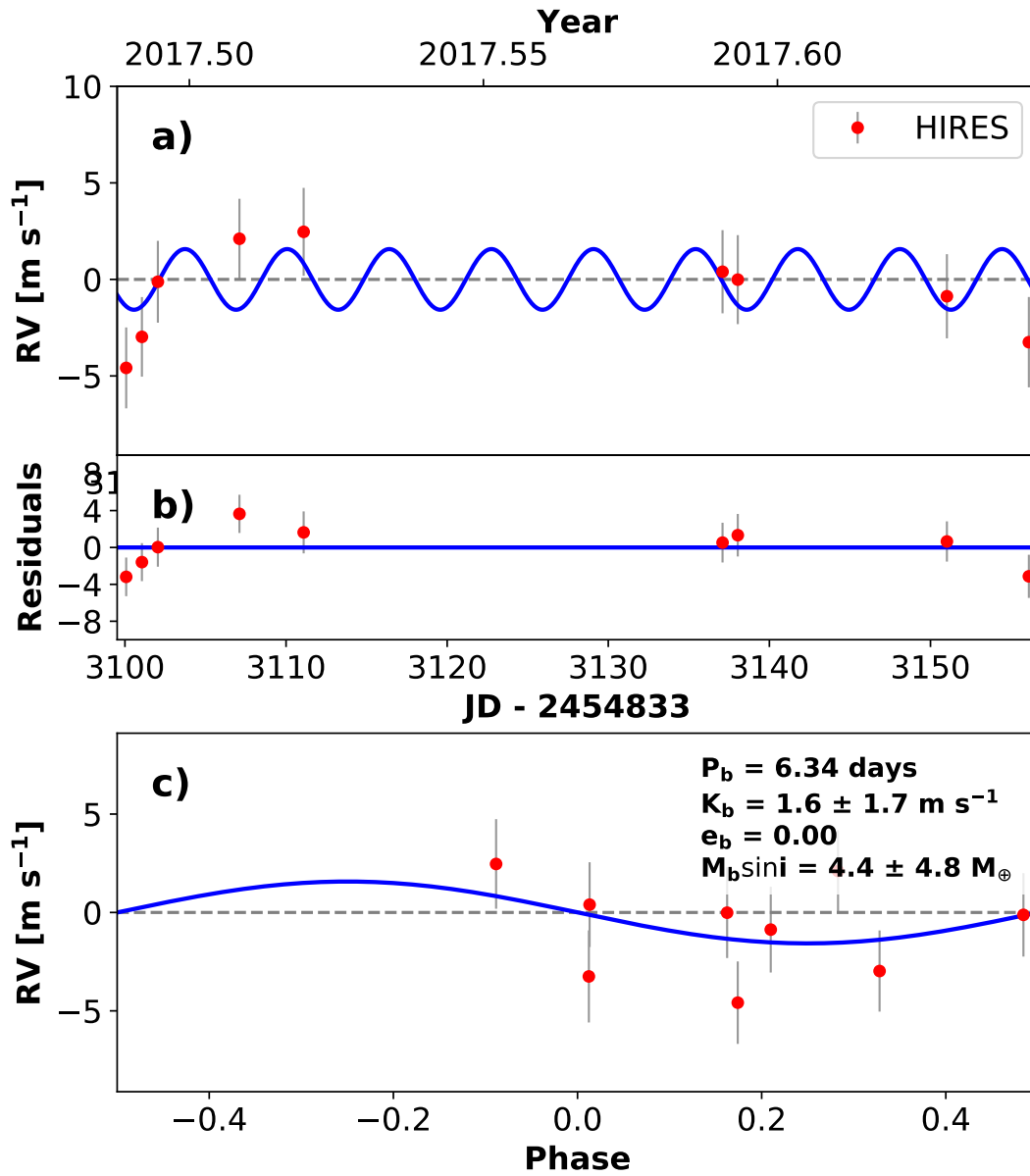


Figure 97. RVs and Keplerian model for EPIC 245943455. Symbols, lines, and annotations are similar to those in Fig. 11.

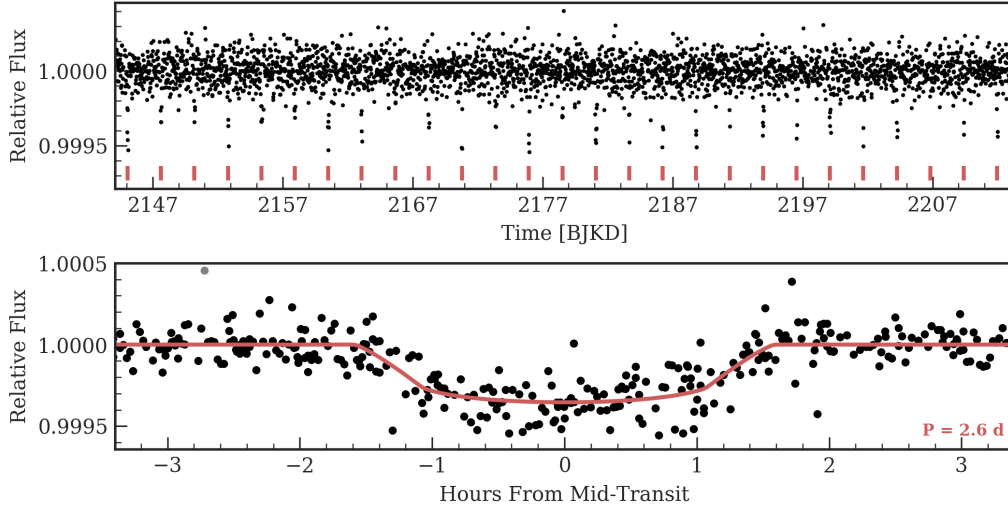


Figure 98. Time series (top) and phase-folded (bottom) light curve for the planet orbiting K2-61. Plot formatting is the same as in Fig. 10.

Table 45. K2-61 System Parameters

Parameter	Credible Interval	Maximum Likelihood	Units
RV Analysis – MCMC Step Parameters			
P_b	$\equiv 2.5734$	$\equiv 2.5734$	days
$T_{\text{conj},b}$	$\equiv 2456983.214$	$\equiv 2456983.214$	BJD _{TBD}
$\sqrt{e} \cos \omega_b$	$\equiv 0.0$	$\equiv 0.0$	
$\sqrt{e} \sin \omega_b$	$\equiv 0.0$	$\equiv 0.0$	
K_b	0.0 ± 3.7	0.1	m s^{-1}
γ^{HIRES}	-1.4 ± 3.1	-1.4	m s^{-1}
$\dot{\gamma}$	$\equiv 0.0$	$\equiv 0.0$	$\text{m s}^{-1} \text{ day}^{-1}$
$\ddot{\gamma}$	$\equiv 0.0$	$\equiv 0.0$	$\text{m s}^{-1} \text{ day}^{-2}$
σ^{HIRES}	$7.2^{+4.1}_{-2.3}$	4.8	m s^{-1}
Orbital & Physical Parameters			
P_b	$\equiv 2.5734$	$\equiv 2.5734$	days
$T_{\text{conj},b}$	$\equiv 2456983.214$	$\equiv 2456983.214$	BJD _{TBD}
e_b	$\equiv 0.0$	$\equiv 0.0$	
ω_b	$\equiv 0.0$	$\equiv 0.0$	radians
K_b	0.0 ± 3.7	0.1	m s^{-1}
M_b	$0.1^{+7.9}_{-7.8}$	0.2	M_{\oplus}
R_b/R_*	$0.01733^{+0.00098}_{-0.00048}$	0.01768	
ρ_b	0 ± 6	0	g cm^{-3}
R_b	$1.92^{+0.11}_{-0.05}$	1.92	R_{\oplus}
Priors			
Parameter	Prior		
σ^{HIRES}	$\mathcal{U}(0, 1e + 100)$		

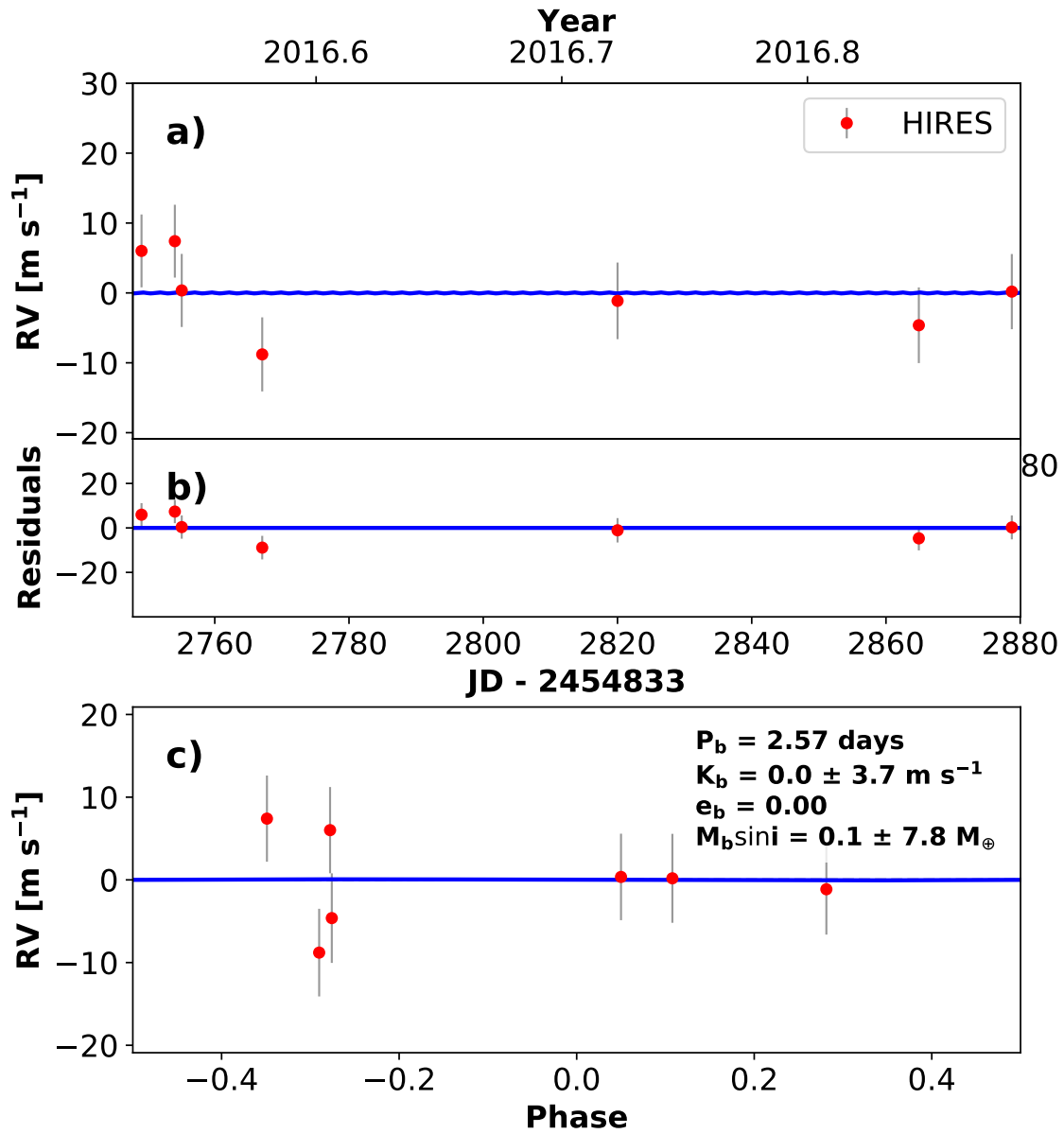


Figure 99. RVs and Keplerian model for K2-61. Symbols, lines, and annotations are similar to those in Fig. 11.

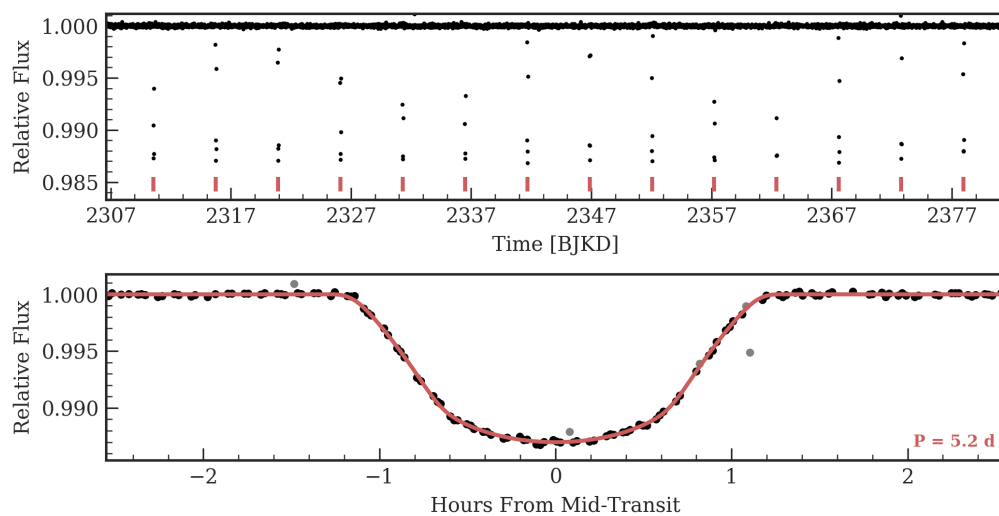


Figure 100. Time series (top) and phase-folded (bottom) light curve for the planet orbiting K2-121. Plot formatting is the same as in Fig. 10.

Table 46. K2-121 System Parameters

Parameter	Credible Interval	Maximum Likelihood	Units
RV Analysis – MCMC Step Parameters			
P_b	$\equiv 5.1857$	$\equiv 5.1857$	days
$T_{\text{conj},b}$	$\equiv 2457143.5607$	$\equiv 2457143.5607$	BJD_{TBD}
$\sqrt{e} \cos \omega_b$	$\equiv 0.0$	$\equiv 0.0$	
$\sqrt{e} \sin \omega_b$	$\equiv 0.0$	$\equiv 0.0$	
K_b	$24^{+4.8}_{-5.3}$	24.0	m s^{-1}
γ_{HIRES}	$2.2^{+3.8}_{-3.6}$	2.1	m s^{-1}
$\dot{\gamma}$	$\equiv 0.0$	$\equiv 0.0$	$\text{m s}^{-1} \text{ day}^{-1}$
$\ddot{\gamma}$	$\equiv 0.0$	$\equiv 0.0$	$\text{m s}^{-1} \text{ day}^{-2}$
σ_{HIRES}	$15.0^{+5.0}_{-1.0}$	13.0	m s^{-1}
Orbital & Physical Parameters			
P_b	$\equiv 5.1857$	$\equiv 5.1857$	days
$T_{\text{conj},b}$	$\equiv 2457143.5607$	$\equiv 2457143.5607$	BJD_{TBD}
e_b	$\equiv 0.0$	$\equiv 0.0$	
ω_b	$\equiv 0.0$	$\equiv 0.0$	radians
K_b	$24^{+4.8}_{-5.3}$	24.0	m s^{-1}
M_b	51^{+10}_{-11}	52	M_{\oplus}
R_b/R_*	$0.1013^{+0.0015}_{-0.0011}$	0.1016	
ρ_b	$0.76^{+0.25}_{-0.08}$	0.68	g cm^{-3}
R_b	$\equiv 7.1612$	$\equiv 7.1612$	R_{\oplus}
Priors			
Parameter	Prior		
None			

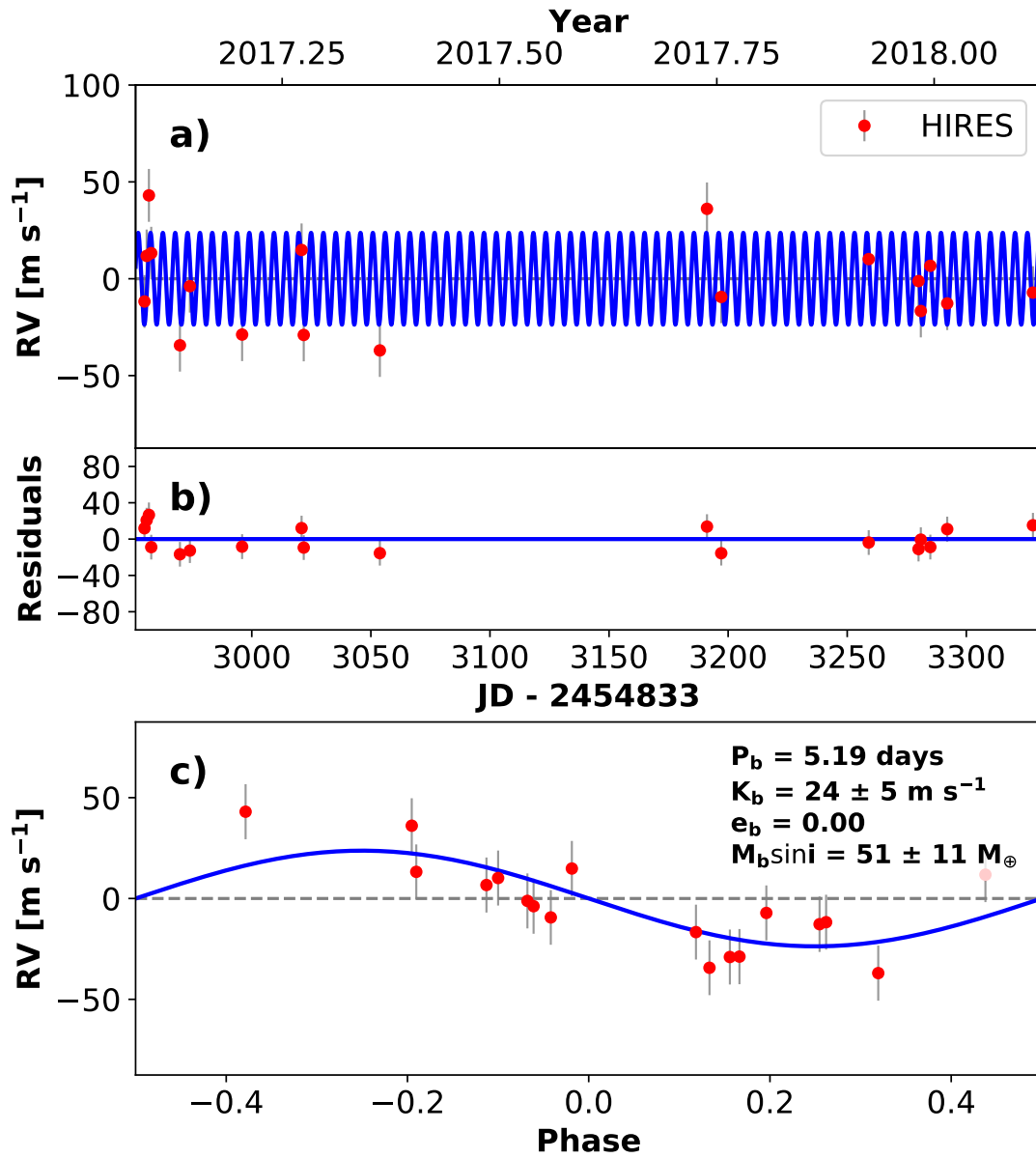


Figure 101. RVs and Keplerian model for K2-121. Symbols, lines, and annotations are similar to those in Fig. 11.

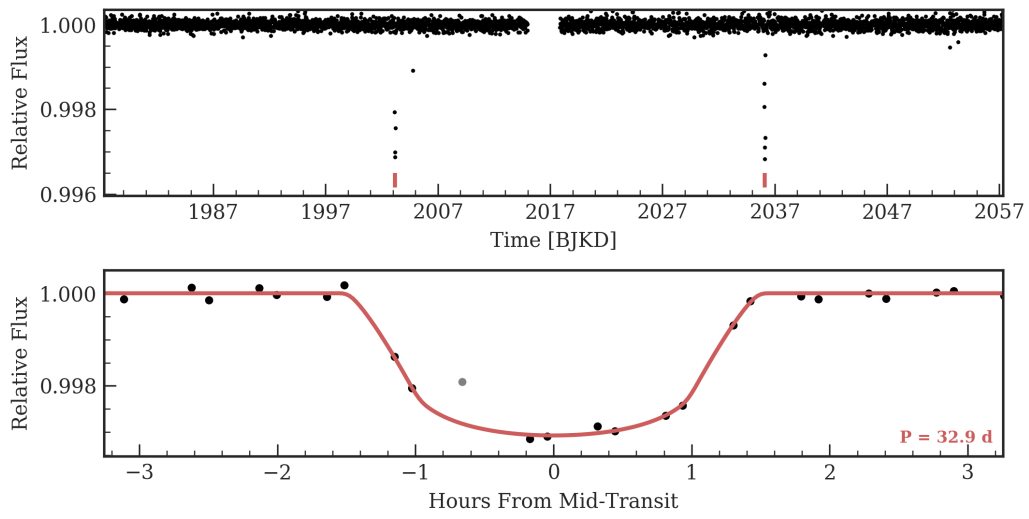


Figure 102. Time series (top) and phase-folded (bottom) light curve for the planet orbiting K2-18. Plot formatting is the same as in Fig. 10.

Table 47. K2-18 System Parameters

Parameter	Credible Interval	Maximum Likelihood	Units
RV Analysis – MCMC Step Parameters			
P_b	$\equiv 32.9411$	$\equiv 32.9411$	days
$T_{\text{conj},b}$	$\equiv 2456836.1719$	$\equiv 2456836.1719$	BJD _{TBD}
$\sqrt{e} \cos \omega_b$	$\equiv 0.0$	$\equiv 0.0$	
$\sqrt{e} \sin \omega_b$	$\equiv 0.0$	$\equiv 0.0$	
K_b	$3.13^{+0.44}_{-0.45}$	3.22	m s ⁻¹
P_c	$9.194^{+0.008}_{-0.007}$	9.194	days
$T_{\text{conj},c}$	$2456836.20^{+0.72}_{-0.75}$	2456836.20	BJD _{TBD}
$\sqrt{e} \cos \omega_c$	$\equiv 0.0$	$\equiv 0.0$	
$\sqrt{e} \sin \omega_c$	$\equiv 0.0$	$\equiv 0.0$	
K_c	3.33 ± 0.49	3.30	m s ⁻¹
γ_{HIRES}	-1.9 ± 1.6	-2.0	m s ⁻¹
γ_{HARPS}	$653.63^{+0.54}_{-0.47}$	653.67	m s ⁻¹
γ_{CARMENES}	$-4.0^{+6.1}_{-7.6}$	-3.4	m s ⁻¹
$\dot{\gamma}$	$\equiv 0.0$	$\equiv 0.0$	m s ⁻¹ day ⁻¹
$\ddot{\gamma}$	$\equiv 0.0$	$\equiv 0.0$	m s ⁻¹ day ⁻²
σ_{HIRES}	$5.1^{+1.3}_{-0.9}$	4.6	m s ⁻¹
σ_{HARPS}	$0.2^{+1.4}_{-1.6}$	0.7	m s ⁻¹
σ_{CARMENES}	$-0.0^{+0.3}_{-1.8}$	1.0	m s ⁻¹
η_3	490^{+250}_{-370}	180	days
η_2	340^{+330}_{-280}	20	days
η_4	$0.506^{+0.051}_{-0.056}$	0.500	
$\eta_{1,\text{HIRES}}$	$0.04^{+2.64}_{-0.04}$	0.00	m s ⁻¹
$\eta_{1,\text{CARMENES}}$	8^{+12}_{-4}	3	m s ⁻¹
$\eta_{1,\text{HARPS}}$	$0.001^{+0.324}_{-0.001}$	0.540	m s ⁻¹
Orbital & Physical Parameters			
P_b	$\equiv 32.9411$	$\equiv 32.9411$	days
$T_{\text{conj},b}$	$\equiv 2456836.1719$	$\equiv 2456836.1719$	BJD _{TBD}
e_b	$\equiv 0.0$	$\equiv 0.0$	
ω_b	$\equiv 0.0$	$\equiv 0.0$	radians
K_b	$3.13^{+0.44}_{-0.45}$	3.22	m s ⁻¹
M_b	$7.2^{+1.5}_{-1.4}$	7.5	M_{\oplus}
R_b/R_*	$0.0507^{+0.0016}_{-0.0009}$	0.0498	
ρ_b	$2.61^{+0.59}_{-0.53}$	2.51	g cm ⁻³
R_b	$2.461^{+0.078}_{-0.045}$	2.544	R_{\oplus}
P_c	$9.194^{+0.008}_{-0.007}$	9.194	days
$T_{\text{conj},c}$	$2456836.20^{+0.72}_{-0.75}$	2456836.20	BJD _{TBD}
e_c	$\equiv 0.0$	$\equiv 0.0$	
ω_c	$\equiv 0.0$	$\equiv 0.0$	radians
K_c	3.33 ± 0.49	3.30	m s ⁻¹
$M \sin i_c$	$5.0^{+1.1}_{-1.0}$	5.1	M_{\oplus}
Priors			
Parameter	Prior		
$\eta_{1,\text{CARMENES}}$	$\mathcal{U}(0, 1e + 100)$		
$\eta_{1,\text{HARPS}}$	$\mathcal{U}(0, 1e + 100)$		
$\eta_{1,\text{HIRES}}$	$\mathcal{U}(0, 1e + 100)$		
η_3	$\mathcal{U}(0, 809.230686)$		
η_2	$\mathcal{U}(0, 809.230686)$		
η_4	$\mathcal{N}(0.5, 0.05)$		
e_b	< 0.99		
e_c	< 0.99		

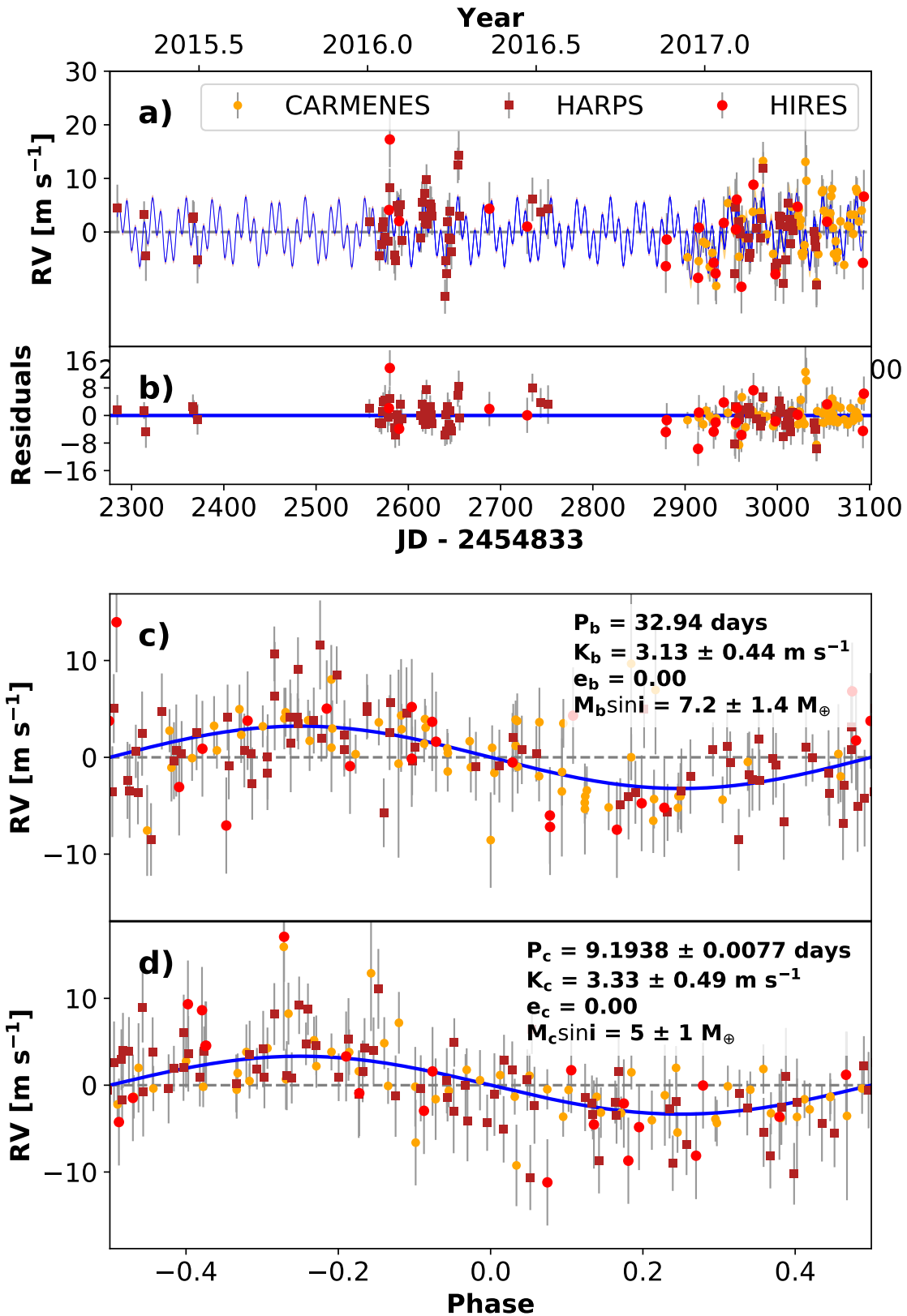


Figure 103. RVs and Keplerian model for K2-18. Symbols, lines, and annotations are similar to those in Fig. 11.

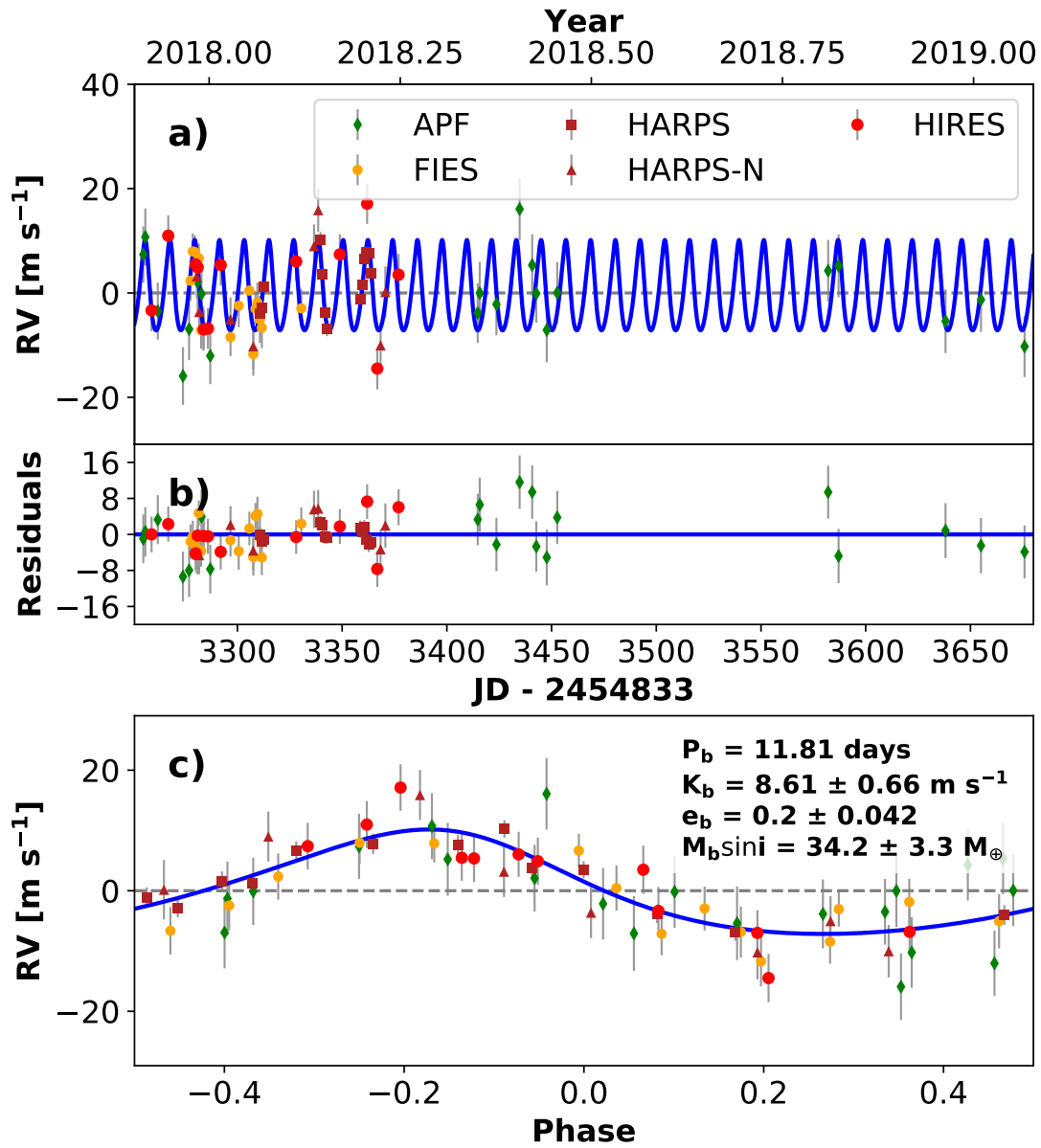


Figure 104. RVs and Keplerian model for HD 89345. Symbols, lines, and annotations are similar to those in Fig. 11.

Table 48. HD 89345 (K2-234) System Parameters

Parameter	Credible Interval	Maximum Likelihood	Units
RV Analysis – MCMC Step Parameters			
P_b	$\equiv 11.8147$	$\equiv 11.8147$	days
$T_{\text{conj},b}$	$\equiv 2457913.8041$	$\equiv 2457913.8041$	BJD _{TBD}
$\sqrt{e} \cos \omega_b$	$0.383^{+0.048}_{-0.066}$	0.389	
$\sqrt{e} \sin \omega_b$	$0.21^{+0.14}_{-0.17}$	0.21	
K_b	$8.59^{+0.67}_{-0.68}$	8.67	m s^{-1}
γ_{HIRES}	-2.8 ± 1.3	-2.9	m s^{-1}
$\gamma_{\text{HARPS-N}}$	2347 ± 2	2347	
γ_{HARPS}	$2354.23^{+0.56}_{-0.57}$	2354.23	m s^{-1}
γ_{FIES}	-2.4 ± 1.1	-2.0	m s^{-1}
γ_{APF}	$0.5^{+1.4}_{-1.3}$	0.5	m s^{-1}
$\dot{\gamma}$	$\equiv 0.0$	$\equiv 0.0$	$\text{m s}^{-1} \text{ day}^{-1}$
$\ddot{\gamma}$	$\equiv 0.0$	$\equiv 0.0$	$\text{m s}^{-1} \text{ day}^{-2}$
σ_{HIRES}	$4.2^{+1.3}_{-1.0}$	3.5	m s^{-1}
$\sigma_{\text{HARPS-N}}$	$5.2^{+2.2}_{-1.3}$	4.1	
σ_{HARPS}	$1.8^{+0.6}_{-0.4}$	1.4	m s^{-1}
σ_{FIES}	$1.7^{+1.4}_{-1.1}$	1.0	m s^{-1}
σ_{APF}	$5.1^{+1.4}_{-1.2}$	4.6	m s^{-1}
Orbital & Physical Parameters			
P_b	$\equiv 11.8147$	$\equiv 11.8147$	days
$T_{\text{conj},b}$	$\equiv 2457913.8041$	$\equiv 2457913.8041$	BJD _{TBD}
e_b	$0.200^{+0.045}_{-0.037}$	0.197	
ω_b	$0.49^{+0.32}_{-0.39}$	0.50	radians
K_b	$8.59^{+0.67}_{-0.68}$	8.67	m s^{-1}
M_b	$34.1^{+3.4}_{-3.3}$	34.6	M_{\oplus}
R_b/R_*	$0.0366^{+0.0022}_{-0.0008}$	0.0388	
ρ_b	$0.489^{+0.069}_{-0.078}$	0.467	g cm^{-3}
R_b	$7.20^{+0.43}_{-0.15}$	7.41	R_{\oplus}
Priors			
Parameter	Prior		
e_b	< 0.99		
σ_{HIRES}	$\mathcal{U}(0, 1e + 100)$		
σ_{APF}	$\mathcal{U}(0, 1e + 100)$		
σ_{FIES}	$\mathcal{U}(0, 1e + 100)$		
σ_{HARPS}	$\mathcal{U}(0, 1e + 100)$		
$\sigma_{\text{HARPS-N}}$	$\mathcal{U}(0, 1e + 100)$		